

# **Design, Synthesis and Biological Evaluation of the Novel MEK Inhibitor and Radioprotectors**

By

**Ying Cheng**

*Thesis  
Submitted to Flinders University  
for the degree of*

**Doctor of Philosophy**

College of Medicine and Public Health

April 2021

---

The research project was conducted under a cotutelle arrangement between Flinders University and the Institute of Radiation Medicine, Chinese Academy of Medical Sciences – Peking Union Medical College.

# CONTENTS

CONTENTS.....	I
LIST OF FIGURES.....	I
LIST OF TABLES.....	IV
LIST OF ABBREVIATIONS.....	V
SUMMARY.....	VIII
DECLARATION.....	XI
ACKNOWLEDGEMENTS.....	XII
LIST OF PUBLICATIONS.....	XIII
1. CHAPTER 1: INTRODUCTION AND LITERATURE REVIEW.....	1
1.1. Abstract.....	2
1.2. Introduction.....	2
1.3. Ras/Raf/MEK/ERK pathway and MEK inhibitors.....	6
1.4. MEK inhibitors approved by the US Food and Drug Administration (FDA)	
1.4.1. Trametinib (GSK1120212, JTP-74057).....	9
1.4.2. Cobimetinib (GDC-0973, XL518).....	11
1.4.3. Binimetinib (MEK162, ARRY-438162).....	12
1.4.4. Selumetinib (ARRY-142886; AZD6244).....	14
1.5. MEK inhibitors in clinical development.....	15
1.5.1. CI-1040 (PD184352).....	18

---

1.5.2.	PD-0325901 .....	18
1.5.3.	AZD-8330 (ARRY-424704) .....	18
1.5.4.	TAK-733 .....	19
1.5.5.	GDC-0623 .....	19
1.5.6.	Refametinib (RDEA-119, BAY-869766) .....	20
1.5.7.	Pimasertib (AS703026) .....	20
1.5.8.	RO4987655 (CH4987655) .....	21
1.5.9.	RO5126766 .....	21
1.5.10.	WX-554 .....	22
1.5.11.	HL-085 .....	22
1.6.	MEK Inhibitors in preclinical development .....	22
1.6.1.	ClnQ-03 .....	23
1.6.2.	G-573 .....	24
1.6.3.	PD184161 .....	24
1.6.4.	PD318088 .....	24
1.6.5.	PD98059 .....	24
1.6.6.	RO5068760 .....	25
1.6.7.	U0126 .....	25
1.6.8.	SL327 .....	25

---

1.7.	Radiotherapy and irradiation-induced small intestinal injury .....	25
1.8.	Radioprotectors .....	26
1.8.1	Aminothiols .....	27
1.8.2	Natural antioxidants .....	28
1.8.3	Other radioprotectors .....	29
1.9.	Conclusions .....	29
1.10.	Hypotheses .....	30
1.11.	Aims of this thesis .....	32
1.12.	Significance .....	33
1.13.	References .....	35
2.	CHAPTER 2: DESIGN, SYNTHESIS, AND CHARACTERIZATION OF A BENZOXAZOLE COMPOUND AS A NOVEL POTENTIAL MEK INHIBITOR .....	53
2.1.	Abstract .....	54
2.2.	Introduction .....	54
2.2.1	Cancer and RAS/RAF/MEK/ERK signaling pathway .....	54
2.2.2	Current progress with molecular structures of MEK inhibitors .....	56
2.3.	Material and methods .....	57
2.3.1.	Chemistry .....	57
2.3.2.	Design of KZ-001 .....	58
2.3.3.	Synthesis route of KZ-001 .....	59

---

2.3.4.	Preparation of KZ-001 .....	60
2.4.	Results and discussion.....	64
2.4.1.	KZ-001 as a new MEK inhibitor with a new core structure .....	64
2.4.2.	Binding mode of KZ-001 .....	64
2.4.3.	Characterization of KZ-001 .....	65
2.5.	Conclusions.....	68
2.6.	References.....	69
3.	CHAPTER 3: MEK INHIBITOR KZ-001 FOR THE TREATMENT OF RAS/RAF MUTANT CANCERS .....	73
3.1.	Abstract.....	74
3.2.	Introduction .....	75
3.3.	Materials and methods .....	77
3.3.1.	Cell lines and subculture.....	77
3.3.2.	Animals.....	77
3.3.3.	Cell-free kinase assay: Inhibition of MEK1 kinase.....	78
3.3.4.	Cell-free kinase assay: Inhibition of MEK2 kinase.....	78
3.3.5.	Cell-free kinase assay: Kinase selectivity assay .....	79
3.3.6.	Western blot analysis in A375, Colo-205, HT-29, Calu-6 cells .....	79
3.3.7.	Western blot analysis in tumor tissues.....	79
3.3.8.	Cell proliferation assay for single agent treatment .....	80

---

3.3.9.	Tumor cell apoptosis assay .....	80
3.3.10.	Cell cycle assay .....	81
3.3.11.	Pharmacokinetic (PK) studies .....	81
3.3.12.	Tumor xenografts.....	82
3.3.13.	<i>In vivo</i> efficacy of single drug treatment studies .....	82
3.3.14.	Statistical analyses .....	83
3.4.	Results and discussion.....	83
3.4.1.	KZ-001 is a potent and highly selective MEK inhibitor.....	84
3.4.2.	KZ-001 inhibits cellular ERK phosphorylation. ....	86
3.4.3.	KZ-001 shows high potency in single agent <i>in vitro</i> studies. ....	87
3.4.4.	KZ-001 induces apoptosis in Colo-205 and Calu-6 cells, but not A375 and HT-29 cells. ....	89
3.4.5.	KZ-001 induces cell cycle arrest in A375 cells. ....	91
3.4.6.	Pharmacokinetic evaluation of KZ-001 in ICR mouse via IV and PO administration.....	92
3.4.7.	The antitumor efficacy of KZ-001 in single agent administration using xenograft models.....	93
3.4.8.	The <i>in vivo</i> pharmacodynamic effects of KZ-001 in mice with A375, Calu-6, Colo-205 xenografts .....	95
3.5.	Conclusion .....	96
3.6	References .....	97

---

4. CHAPTER 4: SYNERGITIC EFFECTS OF KZ-001 COMBINED WITH COMMERCIAL ANTI-CANCER DRUGS .....	99
4.1. Abstract.....	100
4.2. Introduction .....	101
4.3. Materials and methods .....	102
4.3.1. Cell lines and subculture.....	102
4.3.2. <i>In vitro</i> combination drug treatment study .....	103
4.3.3. <i>In vivo</i> efficacy studies of combination drug treatments .....	103
4.3.4. Statistical analyses .....	104
4.4. Results and discussion.....	105
4.4.1. The combination of KZ-001 and vemurafenib shows synergistic effects in BRAF mutant cell lines <i>in vitro</i> .....	105
4.4.2. The combination of KZ-001 and docetaxel shows synergistic effects against BRAF and KRAS mutant cell lines <i>in vitro</i> .....	105
4.4.3. The effect of the combination of KZ-001 with vemurafenib on the treatment of A375 tumor xenografts <i>in vivo</i> .....	106
4.4.4. Effects of combination treatments with KZ-001 and vemurafenib on Colo-205 tumor xenografts <i>in vivo</i> .....	107
4.4.5. Effects of combination treatments with KZ-001 and docetaxel on Calu-6 tumor xenografts <i>in vivo</i> .....	108
4.5. Conclusion .....	109

---

4.6 References .....	110
<b>5. CHAPTER 5: DESIGN, SYTHESIS, AND CHARATERIZATION OF NEOVEL RADIOPROTECTORS .....</b>	<b>113</b>
5.1 Abstract .....	114
5.2 Introduction.....	115
5.3 Materials and methods .....	117
5.3.1 Chemistry .....	117
5.3.2 Animals and ethics approval and consent to participate.....	117
5.3.3 Novel compounds design for radioprotection .....	117
5.3.4 Synthesis of XH-101 .....	118
5.3.5 Synthesis of XH-102.....	120
5.3.6 Synthesis of XH-103.....	121
5.3.7 Synthesis of XH-105.....	123
5.3.8 30-day survival rate experiments .....	124
5.4 Results and discussion .....	124
5.4.1 New compounds design, synthesis, and characterization .....	124
5.4.2 Characterization of XH-101 .....	125
5.4.3 Characterization of XH-102 .....	126
5.4.4 Characterization of XH-103 .....	128
5.4.5 Characterization of XH-105 .....	130

---

5.4.6 30-day survival rate .....	131
5.5 Conclusion.....	132
5.6 References .....	134
6. CHAPTER 6: THE PROTECTIVE EFFECTS OF XH-105 AGAINST RADIATION-INDUCED INTESTINAL INJURY .....	137
6.1 Abstract .....	138
6.2 Introduction .....	138
6.3 Materials and methods .....	140
6.3.1 Animals .....	140
6.3.2 Ethics approval and consent to participate.....	140
6.3.3 Irradiation and treatment.....	140
6.3.4 Histological analysis .....	141
6.3.5 Immunohistochemistry analysis .....	142
6.3.6 TUNEL assay .....	142
6.3.7 Isolation of intestinal crypt cells .....	142
6.3.8 Western Blot analysis .....	143
6.3.9 Immunofluorescence analysis.....	143
6.3.10 Statistical analysis .....	143
6.4 Results .....	144
6.4.1 XH-105 improves the survival rate of mice after TBI .....	144

---

6.4.2 XH-105 reduces the damages of intestinal morphology after TBI .....	145
6.4.3 XH-105 enhances Lgr5 <sup>+</sup> ISC survival and maintains the regeneration of intestinal cells after TBI .....	146
6.4.4 XH-105 decreases apoptosis of the small intestine after TBI .....	148
6.4.5 XH-105 attenuates DNA damage of the small intestine after TBI.....	149
6.4.6 XH-105 protects the small intestine against radiation-induced injury at least in part via the p53 signaling pathway .....	150
6.5 Conclusion.....	151
6.6 Acknowledgement .....	151
6.7 References .....	153
 7. CHAPTER 7: PROTECTIVE EFFECT OF HL-008 AGAINST H <sub>2</sub> O <sub>2</sub> AND BETA-AMYLOID-INDUCED NEUROTOXICITY.....	 158
7.1 Abstract .....	159
7.2 Introduction.....	160
7.3 Materials and methods .....	161
7.3.1 Chemicals and medium .....	161
7.3.2 Cell culture and treatment.....	162
7.3.3 Cell viability assay .....	162
7.3.4 MTT assay for determining protection of PC-12 cells against H <sub>2</sub> O <sub>2</sub> cytotoxicity.....	162

---

7.3.5 MTT assay for determining protection of PC-12 cells against A $\beta$ <sub>1-42</sub> cytotoxicity.....	163
7.3.6 Neurite outgrowth assay .....	163
7.3.7 Statistical analysis .....	163
7.4 Results and discussion.....	164
7.4.1 HL-008 shows no cytotoxicity in PC-12 cells and HEK293 cells.....	164
7.4.2 Neuroprotection of HL-008 against H <sub>2</sub> O <sub>2</sub> -induced cytotoxicity.....	164
7.4.3 Neuroprotection of HL-008 against A $\beta$ <sub>1-42</sub> -induced cytotoxicity .....	166
7.4.4 HL-008 enhances neurite outgrowth.....	167
7.5 Conclusion.....	169
7.6 References .....	170
8. CHAPTER 8: CONCLUSION AND FUTURE DIRECTION.....	173
8.1 Conclusion and major findings.....	174
8.2 Future directions.....	177
8.2.1 Combination of KZ-001 with CDK4/6 inhibitors for the treatment of RAS mutant colorectal cancers.....	177
8.2.2 Triple therapy (KZ-001 + BRAF inhibitors + EGFR inhibitors) for the treatment of BRAF mutant colorectal cancers .....	178
8.2.3 Combination of KZ-001 with anti-PD-1 or anti-PD-L1 to improve tumor immunity.....	179
8.2.4 KZ-001 for the inhibition of reperfusion injury.....	180

---

8.2.5 Apoptosis-related and neuroinflammation-related mechanism study of HL-008 .....	180
8.2.6 Combination of KZ-001 with XH-105 to enhance tumor cell radiosensitivity .....	181
8.3 References .....	182
APPENDICES .....	185

## LIST OF FIGURES

Figure 1-1 Distributions of cases and deaths for the ten most common cancers in 2018 ....	3
Figure 1-2 MEK inhibitors in clinical study.....	16
Figure 1-3 MEK inhibitors in preclinical study .....	23
Figure 1-4 Molecular structures of aminothiols .....	27
Figure 1-5 Molecular structures of natural antioxidants.....	27
Figure 2-1 Representative generic structure of MEK inhibitors and its interaction with MEK1 kinase.....	59
Figure 2-2 Synthesis route of KZ-001 .....	60
Figure 2-3 KZ-001 structure overlay with AZD6244 with the co-crystal structure of MEK1 (PDB code: 4U7Z) as the model.....	65
Figure 2-4 <sup>1</sup> H NMR spectrum of KZ-001 .....	66
Figure 2-5 <sup>13</sup> C NMR spectra of KZ-001 .....	66
Figure 2-6 MS spectrum of KZ-001.....	67
Figure 2-7 HRMS-TOF spectrum of KZ-001 .....	67
Figure 2-8 HPLC spectrum of KZ-001.....	67
Figure 3-1 Dose-dependent inhibition of MEK1 and MEK2 activity in the presence of KZ-001 and AZD6244 using the Z'-LYTE kinase assay kit with ATP concentration at 45 μM and the radiometric assay with ATP concentration at 10 μM, respectively.....	85
Figure 3-2 Western blot analyses of dose-dependent effects of KZ-001 on phosphorylation of MEK1/2 and ERK1/2 and MEK1/2 and ERK1/2 expression levels in different cancer cell lines .....	87
Figure 3-3 Dose-response of A375, Colo-205, HT-29, Calu-6, and A431 cell lines on survival rate following treatment with KZ-001 and AZD6244.....	89
Figure 3-4 KZ-001 induced apoptosis in Calu-6, A375, HT-29, and Colo-205 cells.....	90
Figure 3-5 KZ-001 induced cell cycle arrests in A375 cells. Cells were treated for 24 h with 10 nM or 10 μM KZ-001, or vehicle.....	91
Figure 3-6 Concentration-Time curves of KZ-001 after single dosing by IV and PO.....	92

---

Figure 3-7 Tumor growths and body weight change of A375 xenografts in vivo in single drug treatments..	94
Figure 3-8 Tumor growths and body weight change of Colo-205 xenografts in vivo in single drug treatment..	94
Figure 3-9 Tumor growths and body weight change of Calu-6 xenografts in vivo in single drug treatment.	95
Figure 3-10 Western blot analyses of effects of KZ-001 on phosphorylation of ERK1/2 and ERK1/2 expression levels for tissue lysates obtained from A375, Calu-6 and Colo-205 xenografts.....	96
Figure 4-1 Fa-CI curves of BRAF mutant cell lines treated with KZ-001 combined with vemurafenib.....	105
Figure 4-2 Fa-CI curves of BRAF and KRAS mutant cell lines treated with KZ-001 combined with the cytotoxic drug docetaxel.....	106
Figure 4-3 Synergistic effect of KZ-001 combined with vemurafenib on BRAF-mutant A375 tumor xenografts.....	107
Figure 4-4 Synergistic effects of KZ-001 combined with vemurafenib on BRAF mutant Colo-205 xenografts. ....	108
Figure 4-5 Synergistic effects of KZ-001 combined with docetaxel on KRAS-mutant tumor Calu-6 xenografts. ....	108
Figure 5-1 Design concepts of new compounds .....	118
Figure 5-2 Molecular structures of four new compounds.....	118
Figure 5-3 Synthesis route of XH-101.....	119
Figure 5-4 Synthesis route of XH-102.....	120
Figure 5-5 Synthesis route of XH-103.....	122
Figure 5-6 Synthesis route of XH-105.....	123
Figure 5-7 <sup>1</sup> H NMR spectrum of XH-101.....	125
Figure 5-8 MS spectrum of XH-101..	126
Figure 5-9 <sup>13</sup> C NMR spectrum of XH-101.....	126
Figure 5-10 <sup>1</sup> H NMR spectrum of XH-102.....	127

---

Figure 5-11 MS spectrum of XH-102..	127
Figure 5-12 <sup>13</sup> C NMR spectrum of XH-102 (101 MHz, CDCl <sub>3</sub> ).....	128
Figure 5-13 <sup>1</sup> HNMR spectrum of XH-103.....	129
Figure 5-14 MS spectrum of XH-103..	129
Figure 5-15 <sup>13</sup> C NMR (101 MHz, CDCl <sub>3</sub> ) spectrum of XH-103.....	130
Figure 5-16 <sup>1</sup> HNMR Spectra of XH-105.....	131
Figure 5-17 LC-MS Spectra of XH-105.....	131
Figure 5-18 30-day survival rate studies under 7.2 Gy TBI..	132
Figure 6-1 XH-105 improved survival of mice after 9.0 Gy TBI..	144
Figure 6-2 XH-105 protected the intestinal morphology of mice after 9.0Gy TBI.....	145
Figure 6-3 XH-105 enhanced proliferation and differentiation ability of the Lgr5 <sup>+</sup> small intestine after 9.0 Gy TBI.....	147
Figure 6-4 XH-105 decreased apoptosis of the small intestine after 9.0 Gy TBI. ....	149
Figure 6-5 XH-105 attenuated DNA damage of mice after 9.0 Gy TBI.....	150
Figure 6-6 XH-105 decreased the expression of p53 and Bax of the small intestine after 9.0 Gy TBI.....	151
Figure 7-1 Relative cell viability (%) of PC-12 cells and HEK293 cells determined by MTT assay following 48 h treatment with increasing concentrations of HL-008.....	164
Figure 7-2 Protective effects of HL-008 against dose-related H <sub>2</sub> O <sub>2</sub> -induced cytotoxicity in PC-12 cells.....	166
Figure 7-3 Neuroprotection activity of HL-008 against Aβ <sub>1-42</sub> (1 μM) induced cytotoxicity measured by MTT assay following 48 h treatment.....	167
Figure 7-4 Effect of different concentrations of HL-008 on neurite outgrowth in PC-12 cell..	169

## LIST OF TABLES

Table 1-1 New cases and deaths for 36 cancers and all cancers combined in 2018 [1].....	5
Table 1-2 Preclinical and clinical data for approved MEK inhibitors .....	7
Table 1-3 MEK inhibitors in clinical trials.....	17
Table 1-4 MEK inhibitors in preclinical development.....	23
Table 3-1 LC/MS/MS mobile phase gradients.....	82
Table 3-2 Group setting of mice in single drug studies .....	83
Table 3-3 Inhibitory activity of KZ-001 (10 $\mu$ M) against a panel of protein kinases.....	85
Table 3-4 IC <sub>50</sub> values of a panel of cancer cell lines exposed to KZ-001 and AZD6244 ....	89
Table 3-5 Plasma concentration and PK parameters of KZ-001 .....	93
Table 4-1 Group setting of mice in drug combination studies.....	104
Table 5-1 Group setting of mice.....	124
Table 6-1 Group setting of mice.....	141

## LIST OF ABBREVIATIONS

ALK	Anaplastic lymphoma kinase
BBB	Blood brain barrier
BCA	Bicinchoninic acid
BnBr	Benzyl bromide
CDK4/6	Cyclin-dependent kinase 4 and 6
DAB	3,3'-Diaminobenzidine tetrahydrochloride hydrate
DIPEA	N,N-Diisopropylethylamine
DSBs	Double-strand breaks
EDCI	N-(3-Dimethylaminopropyl)-N'-ethylcarbodiimide hydrochloride
EGFR	Epidermal growth factor receptor
ESI-MS	Electrospray ionization mass spectrometry
FDA	Food and Drug Administration
FGFR3	Fibroblast growth factor receptor 3
H&E	Hematoxylin-eosin
HOBt	1-Hydroxybenzotriazole
HPLC	High Performance Liquid Chromatography
HRMS	High Resolution Mass Spectrum
IC <sub>50</sub>	50% inhibitory concentration

---

IESCs	Intestinal epithelial stem cells
ISCs	Intestinal stem cells
LiHMDS	Hexamethyldisilamide
MEK1	Mitogen-activated protein kinase kinase 1
MEK2	Mitogen-activated protein kinase kinase 2
MHC	Major histocompatibility complex
MS	Mass spectrum
mTOR	Mechanistic target of rapamycin
MTS	3-(4,5-dimethylthiazol-2-yl)-5-(3-carboxymethoxyphenyl)-2-(4-sulfophenyl)-2H-tetrazolium)
MTT	3-(4,5-dimethylthiazol-2-yl)-2,5-diphenyltetrazolium bromide
NMR	Nuclear magnetic resonance
PBS	Phosphate buffered saline
PDGFR $\alpha$	Platelet-derived growth factor receptor A
PD-L1	Programmed cell death ligand 1
PI	Propidium iodide
PK	Pharmacokinetics
PKA	Protein kinase A
p-TsOH	p-Toluenesulfonic acid
r.t.	room temperature

---

RAS	Rat sarcoma virus
RIGS	Radiation-induced gastrointestinal syndrome
ROS	Reactive oxygen stress
STAT3	Signal transducer and activator of transcription 3
TBI	Total body irradiation
TGI	Tumor growth inhibition
TLC	Thin layer chromatography
TrkA	Tropomyosin receptor kinase A
TrkB	Tropomyosin receptor kinase B
TrkC	Tropomyosin receptor kinase C
TUNEL	Termination deoxynucleotidyl transferase dUTP nick end labeling

---

## SUMMARY

Signalling pathway dysregulation is associated with tumorigenesis. Aggressive tumour behaviour is often related with resistance to commonly used anti-cancer drugs. Cancer treatments commonly apply radio-therapy despite frequent negative side effects, including intestinal injury. The RAS/RAF/MEK/ERK signalling pathway plays a key role in regulating cell proliferation and apoptosis. This signalling pathway is deregulated in approximately one third of malignant tumours. Mutations in RAS/RAF occur in approximately 30% of malignancies and are associated with aggressive cancer behaviours and poor prognosis. To address these problems, this research consisted of two parts: 1) development and efficacy evaluation of a novel MEK inhibitor and 2) development of a series of novel compounds and evaluation of their intestinal radio-protective action and neuroprotective activity.

Based on the previously reported X-ray structure, AZD6244, a drug in phase III clinical trials, was chosen as a positive control and as a lead compound for further activity enhancement research to overcome the shortcomings of existing MEK inhibitors. As a result, a novel benzoxazole compound (KZ-001) was developed and the research determined that it is a highly potent and selective MEK 1/2 inhibitor, suitable for the potential treatment of cancer.

*In vitro*, KZ-001 showed approximately 27-fold and 12-fold greater inhibition of MEK1 and MEK2 kinase compared to AZD6244, respectively. Kinase selectivity studies showed that KZ-001 is a highly selective MEK1/2 inhibitor. Using the MTT- or MTS assay, KZ-001 had a 26- to 32-fold higher anti-proliferation activity in BRAF mutant cancer cell lines and 17-fold higher anti-proliferation activity in KRAS mutant cancer cell lines compared to AZD6244. *In vivo* xenograft models confirmed higher tumour growth inhibition activity of KZ-001 and the body weights of treated animals did not change significantly.

Like other known MEK inhibitors, KZ-001 inhibited the MAPK signalling pathway. KZ-001 completely blocked ERK phosphorylation in BRAF- and KRAS- mutant cell lines. The FITC

---

Annexin V apoptosis assay demonstrated early apoptosis in Calu-6 and COLO 205 cell populations but not in A375 and HT-29 cells. Measurement of DNA content in A375 cells showed a significant increase of G1 phase cells and a decrease of S and G2 phase, and caused cell cycle delay of A375 cells at the G0/G1 phase.

In pharmacokinetic studies, KZ-001 showed good oral absorption and clearance from the blood stream. To determine its potential for clinical application, the synergistic effect of KZ-001 with other drug agents was investigated both *in vitro* and *in vivo* (xenograft models). KZ-001 exhibited synergistic anti-cancer effects in combination with the BRAF inhibitor vemurafenib and a microtubule-stabilizing chemotherapeutic agent docetaxel. Results obtained strongly suggest that KZ-001 is a very promising new anti-cancer drug for treatment of RAS/RAF mutant tumours.

Radiation-induced intestinal injury is one of the major side effects in patients receiving radiation therapy. There is no specific clinical treatment for radiation enteritis. This study aimed to find ROS-scavengers by rationale compound design for the treatment of radiation injury and neurodegenerative diseases.

Four compounds were designed which were expected to cleave into polyphenol and aminothiols *in vivo* to mitigate radiation injury. The 30-day survival experiments in C57BL/6J mice investigated radio-protective effects. Further research focused on the compound XH-105 because of its superior radio-protective effect compared to the other three compounds. XH-105 was administered by gavage to C57BL/6J mice one hour prior to total body irradiation (TBI) and survival rate was monitored. Survival rates of Lgr5<sup>+</sup> ISCs, Ki67<sup>+</sup> cells and villi<sup>+</sup> enterocytes were determined histologically and lysozyme were identified and activity quantified by immunohistochemistry. DNA damage and cellular apoptosis in intestinal tissues were also evaluated. After TBI, XH-105 significantly enhanced survival rates, attenuated structural damage of the small intestine, decreased the rate of apoptosis, reduced DNA damage, maintained cell regeneration and promoted crypt proliferation and differentiation compared to vehicle-treated mice. XH-105 also reduced the expression of

---

Bax and p53 in the small intestine. These data suggest that XH-105 protects against radiation-induced intestinal injury by inhibiting the p53-dependent apoptosis pathway.

Oxidative stress plays a central role in the common pathophysiology of neurodegenerative diseases. In Alzheimer's disease, the aggregation of A $\beta$  could induce ROS. HL-008, as an aminothiols compound, might be able to eliminate ROS in cell microenvironment. In this study, HL-008 showed no toxicity to PC-12 cells and protected PC-12 cells against H<sub>2</sub>O<sub>2</sub>-induced cytotoxicity. Moreover, this study showed that pretreatment with HL-008 could increase cell viability after exposure to A $\beta$ <sub>1-42</sub>. Furthermore, all investigated concentrations of HL-008 enhanced neurite outgrowth in a dose-dependent manner.

In summary, this project developed a novel MEK inhibitor for the treatment of RAS/RAF mutant cancers and a set of radioprotectors for the mitigation of radiotherapy-induced intestinal injury. In addition, one radioprotector could potentially be used for the treatment of neurodegenerative diseases.

---

## DECLARATION

I certify that this thesis does not incorporate without acknowledgment any material previously submitted for a degree or diploma in any university; and that to the best of my knowledge and belief it does not contain any material previously published or written by another person except where due reference is made in the text.

Signed.....Ying Cheng.....

Date.....April 2021.....

---

## ACKNOWLEDGEMENTS

The research project was conducted under a cotutelle arrangement between Flinders University and Institute of Radiation Medicine, Chinese Academy of Medical Sciences – Peking Union Medical College. The PhD thesis would not have been possible without the support of both institutions and numerous people.

Firstly, I would like to express my sincere gratitude and appreciation to my main supervisors, Prof. Hongqi Tian, and Prof. Wei Zhang, co-supervisor AProf. Kirsten Heimann, for their helpful guidance and continuous support during this project. Their kind support and encouragement, both academically and in general life, helped me overcoming all the hardship throughout my PhD study. They guided me throughout my research and writing of this thesis, and provided funding for the research. It is their support that makes my PhD experience productive. Their inspiration and contributions are priceless and will be beneficial to my whole life. They deserve the best respects, and I am lucky to have these best supervisors.

Secondly, I would like to thank the members of Flinders Centre for Marine Bioproducts Development (CMBD). In particular, Dr. Biju Balakrishnan for giving me induction for the tissue culture; Mr. Peng Su for helping me with HPLC analysis and great help for general life; Ms Kushari Burns who efficiently manages and facilitates all work in our laboratory and department; along with Ms. Jane Keane who gave me kind support. I would like to thank Prof. Chris Franco, AProf. Munish Puri, Dr. Renu Abraham and Dr. Siti Mubarakah for lab induction. I would like to thank Dr. Jingjing Wang and Dr. Xuan Luo for kindly offering help during my experiments. I would also thank Dr. Zhen Guo for her great help whenever I experienced hardship, and thank Wanling Cai, Renao Bai, Dr. Trung Nguyen, Jos Lum and other CMBD staff and students for their help and friendship.

I acknowledge with many thanks Prof. Scott Smid for his help with my cells and induction to his laboratory and Prof. Colin Raston for providing chemistry lab facilities.

Last but not least, I would like to thank my family members, for truly believing in me and for providing me with great support. Without their support and tremendous encouragement, I certainly could not have reached this far.

---

## LIST OF PUBLICATIONS

### Journal Articles:

#### Published:

1. **Cheng Y.**; Wang X.; Xia X.; Zhang W.; Tian H.\*. A benzoxazole compound as a novel MEK inhibitor for the treatment of RAS/RAF mutant cancer. *International Journal of Cancer*, 2019, 145(2): 586-596.
2. **Cheng Y.**<sup>#</sup>; Dong Y.<sup>#</sup>; Hou Q.; Wu J. ; Tian H\*. Li D.\*. The protective effects of XH-105 against radiation-induced Intestinal Injury. *Journal of Cellular and Molecular Medicine*, 2019, 23: 2238-2247.
3. Dong Y.<sup>#</sup>; **Cheng Y.**<sup>#</sup>; Hou Q.; Wu, J.; Li D\*.; Tian H\*.. The protective effect of new compound XH-103 on radiation-induced GI syndrome, *Oxidative Medicine and Cellular Longevity*, Volume 2018, Article ID 3920147. <https://doi.org/10.1155/2018/3920147>.
4. Li Y.<sup>#</sup>; **Cheng Y.**<sup>#</sup>; Zhang M.; He X.; Kong L.; Zhou K.; Zhou Y.; Li L.; Tian H.<sup>\*</sup>; Song X.\*; Cui Y.<sup>\*</sup>. Development of a new compound with increased antitumor activity by cotargeting MEK and Pim-1 in colorectal cancer. *Iscience*, 2020, 23 (7), 101254.
5. **Cheng Y.**; Tian H.\*. Current development status of MEK inhibitors. *Molecules*, 2017, 22, 1551.

#### Manuscript accepted:

1. Liu Y.<sup>#</sup>; **Cheng Y.**<sup>#</sup>; Zhang W.\*; Tian H.\*. Neuroprotective effect of a new free radical scavenger HL-008 against ischemia-reperfusion injury in MCAO rats. *Neuroscience*, 2021.

#### Patents:

1. Tian, H. \*; **Cheng, Y.**; Zhang, Q., Zhu, Z.; Wang, Y.. Amino mercaptan compound and preparation method therefor and use thereof in protection against radiation. PCT/CN2017/100158.

- 
2. Tian, H. \*; **Cheng, Y.**; Zhang, Q.; Zhu, Z.; Wang, Y.; Fan S.. A new type of compound with radiation protection function, preparation method and use thereof, **China Patent Granted No.:** ZL201610723925.8.
  3. Tian H.\*; **Cheng Y**; Zhang Q.; Zhu Z.; Wang Y.. Amino mercaptan compound and preparation method therefor and use thereof in protection against radiation, **China Patent Application No.:** 201610802313.8.
  4. Tian H.\*; Zhu Z.; Zhang Q.; **Cheng Y.**.. A new type of compound with radiation protection function, preparation method and use thereof, **China Patent Granted No.:** ZL 201610829269.X.

**Conference abstract:**

1. **Cheng Y.**<sup>#</sup>; Dong Y.<sup>#</sup>; Hou Q.; Wu J.; Tian H.\*; Li D.\*. **2018**, 'The protective effects of XH-105 against radiation-induced Intestinal Injury'. The 3<sup>rd</sup> global Chinese congress of radiation research. Tianjin, China.

# 1. CHAPTER 1: INTRODUCTION AND LITERATURE REVIEW

Part of this literature review (From Section 1.3 - Section 1.6) has been published in *Molecules*, Year 2018, Vol. 22, 1551, Page 1-20, and the development status was updated at the end of year 2020.

## 1.1. Abstract

Cancer incidence and mortality are rapidly increasing worldwide. The RAS/RAF/MEK/ERK pathway is deregulated in approximately one third of malignant tumors. Mitogen-activated protein kinase kinase (MEK) inhibitors could block this pathway and inhibit tumor proliferation. The current development status of MEK inhibitors, including preclinical data and progress made in clinical studies, is summarized in this review. Different MEK inhibitors, possessing specific physicochemical properties and bioactivity characteristics, may provide different options for patients seeking treatment for cancer. Moreover, the combination of MEK inhibitors with other therapies—such as chemotherapy, targeted therapy, and immunotherapy—may be a promising approach for clinical use.

Though remarkable progress has been made in the field of cancer treatment, radiotherapy and chemotherapy remain important in cancer treatment. While better disease control is achieved with radiotherapy dose escalation, common usual side effects are acute toxicity and damage of healthy tissue. It is therefore important to develop radioprotectors to mitigate irradiation injury. The most widely studied radioprotectors are summarized here. Radioprotectors in different categories possess their own properties, showing different extent of activity and toxicity. Combined treatment with antimetabolite compounds and natural anti-oxidants may be a promising direction for the development of radioprotectors.

**KEYWORDS:** MEK inhibitors; targeted therapy; combination treatment; approved drug; clinical study; preclinical study; radioprotectors; anti-oxidants.

## 1.2. Introduction

Cancer incidence and mortality are rapidly increasing world-wide, and cancer is expected as the sole most important barrier to increasing life expectancy globally. According to the latest statistics, it is estimated that there were 18.1 million new cases and 9.6 million cancer deaths worldwide in 2018 [1]. These findings were also supported by the World Health Organization [2]. Bray et al. (2018) reported the distribution of all-cancer incidence and mortality (Table 1-1). Of all cancer types, lung cancer ranks as the leading cause of incidence and mortality. An estimated 2.1 million new lung cancer cases (nearly 11.6% of the total new cases) and 1.8 million deaths (nearly 18.4% of cancer deaths) were estimated in 2018, respectively (Figure 1-1).

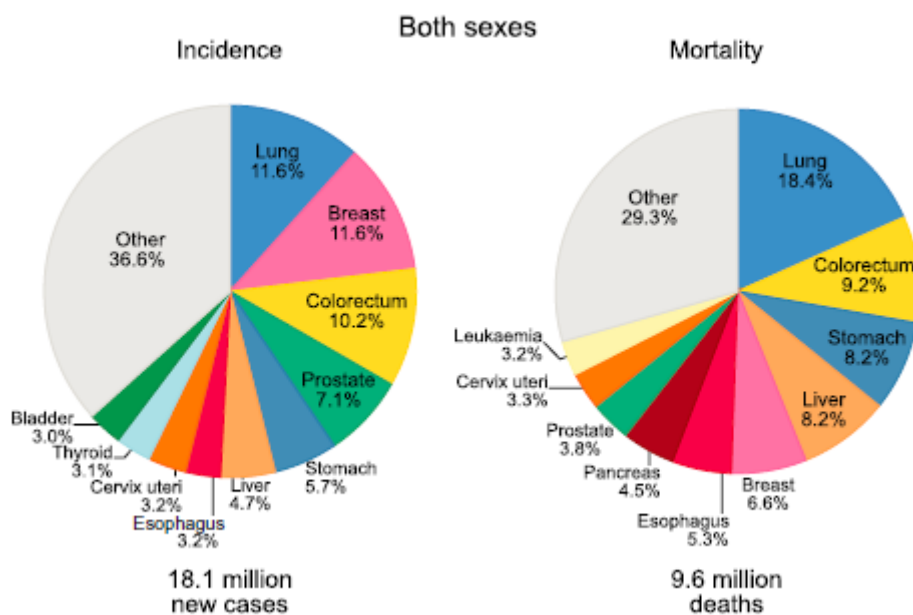


**Figure 1-1 Distributions of cases and deaths for the ten most common cancers in 2018 [1]**

The mitogen-activated protein kinase (MAPK) signaling pathway plays critical roles in the regulation of diverse cellular activities, including cell proliferation, survival, differentiation, and motility [3]. Dysregulation of the MAPK pathway occurs in more than one-third of all malignancies. The classical MAPK pathway consists of Ras (a family of related small G-proteins which are expressed in all animal cell lineages and organs), Raf (a family of three serine/threonine-specific protein kinases that are related to retroviral oncogenes), MEK (mitogen-activated protein kinase kinase), and ERK (extracellular signal-regulated kinases), sequentially relaying proliferative signals generated at the cell surface receptors into the nucleus through cytoplasmic signaling. MEK inhibitors target the Ras/Raf/MEK/ERK signaling pathway, inhibiting cell proliferation and inducing apoptosis, hence offering potential in clinical use for cancer treatment, especially for those cancers induced by RAS/RAF dysfunction [4].

Owing to the widespread activation of this pathway in numerous neoplasms, MEK inhibitors have been in the process of development and study as a type of monotherapy or combination therapy with other targeted and cytotoxic drugs in a variety of clinical situations. More recently, combination treatment with immune checkpoint inhibitors has emerged as an efficacious treatment for some cancers, expanding the efficacy of this class of agents [5].

---

This review summarizes recent progress in the development of MEK inhibitors, complementary to an earlier review [6-17] but with a greater focus on those compounds that have been approved or are in clinical stages of development. A brief summary of compounds undergoing preclinical studies is also provided.

**Table 1-1 New cases and deaths for 36 cancers and all cancers combined in 2018 [1]**

<b>CANCER SITE</b>	<b>NO. OF NEW CASES (% OF ALL SITES)</b>	<b>NO. OF DEATHS (% OF ALL SITES)</b>	<b>CANCER SITE</b>	<b>NO. OF NEW CASES (% OF ALL SITES)</b>	<b>NO. OF DEATHS (% OF ALL SITES)</b>
Lung	2,093,876 (11.6)	1,761,007 (18.4)	Ovary	295,414 (1.6)	184,799 (1.9)
Breast	2,088,849 (11.6)	626,679 (6.6)	Melanoma of skin	287,723 (1.6)	60,712 (0.6)
Prostate	1,276,106 (7.1)	358,989 (3.8)	Gallbladder	219,420 (1.2)	165,087 (1.7)
Colon	1,096,601 (6.1)	551,269 (5.8)	Larynx	177,422 (1.0)	94,771 (1.0)
Nonmelanoma of skin	1,042,056 (5.8)	65,155 (0.7)	Multiple myeloma	159,985 (0.9)	106,105 (1.1)
Stomach	1,033,701 (5.7)	782,685 (8.2)	Nasopharynx	129,079 (0.7)	72,987 (0.8)
Liver	841,080 (4.7)	781,631 (8.2)	Oropharynx	92,887 (0.5)	51,005 (0.5)
Rectum	704,376 (3.9)	310,394 (3.2)	Hypopharynx	80,608 (0.4)	34,984 (0.4)
Esophagus	572,034 (3.2)	508,585 (5.3)	Hodgkin lymphoma	79,990 (0.4)	26,167 (0.3)
Cervix uteri	569,847 (3.2)	311,365 (3.3)	Testis	71,105 (0.4)	9,507 (0.1)
Thyroid	567,233 (3.1)	41,071 (0.4)	Salivary glands	52,799 (0.3)	22,176 (0.2)
Bladder	549,393 (3.0)	199,922 (2.1)	Anus	48,541 (0.3)	19,129 (0.2)
Non-Hodgkin lymphoma	509,590 (2.8)	248,724 (2.6)	Vulva	44,235 (0.2)	15,222 (0.2)
Pancreas	458,918 (2.5)	432,242 (4.5)	Kaposi sarcoma	41,799 (0.2)	19,902 (0.2)
Leukemia	437,033 (2.4)	309,006 (3.2)	Penis	34,475 (0.2)	15,138 (0.2)
Kidney	403,262 (2.2)	175,098 (1.8)	Mesothelioma	30,443 (0.2)	25,576 (0.3)
Corpus uteri	382,069 (2.1)	89,929 (0.9)	Vagina	17,600 (0.1)	8,062 (0.1)
Lip, oral cavity	354,864 (2.0)	177,384 (1.9)	All sites excluding skin	17,036,901	9,489,872
Brain, nervous system	296,851 (1.6)	241,037 (2.5)	<b>ALL sites</b>	<b>18,078,957</b>	<b>9,555,027</b>

### **1.3. Ras/Raf/MEK/ERK pathway and MEK inhibitors**

Signal transduction occurs when an extracellular signaling molecule activates a specific receptor located on the cell surface. In turn, this receptor triggers a biochemical chain of events inside the cell and creates a response. The Ras/Raf/MEK/ERK pathway is one of the critical pathways involved in signal transduction, which results in the control of cell proliferation, survival, and differentiation [18, 19] and plays a role in the development of multiple cancers including melanoma, non-small cell lung cancer (NSCLC), etc. MEK1 and MEK2 are closely related and participate in the Ras/Raf/MEK/ERK signal transduction cascade. Blockage of the pathway with MEK1/2 inhibitors could result in the clinical benefits for treatment of cancers with RAS/RAF dysfunction. Therefore, efforts have focused in past decades on the development of MEK1/2 inhibitors. The first MEK inhibitor, PD098059, was reported in 1995 [20], since then a number of MEK inhibitors have progressed to clinical stages of development. More recently, the combination of MEK- with BRAF (A member of the Raf kinase family of growth signal transduction protein kinases)-inhibitors and/or other therapies has provided a new treatment option for multiple cancers.

### **1.4. MEK inhibitors approved by the US Food and Drug Administration (FDA)**

Four MEK inhibitors, including trametinib, cobimetinib, binimetinib and selumetinib, were approved by the FDA and the European Medicines Agency (EMA). Preclinical and clinical data for these four compounds are summarized in Table 1-2.

**Table 1-2 Preclinical and clinical data for approved MEK inhibitors**

Item	Trametinib	Cobimetinib	Binimetinib	Selumetinib
Structure				
BCS <sup>1</sup> class	BCS II (high permeability, low solubility)	BCS I (high permeability, high solubility)	BCS IV (low permeability, low solubility)	N/A
Salt form	dimethyl sulfoxide solvate (1:1)	hemifumarate	Non-solvated	hyd-sulfate
Molecule weight (free base)	615.4	531.32	441.23	457.68
In vitro (enzyme) [21, 22]	MEK <sup>2</sup> kinase	MEK1 IC <sub>50</sub> = 0.95 nM MEK2 IC <sub>50</sub> = 199 nM	MEK1 IC <sub>50</sub> = 12 nM MEK2 IC <sub>50</sub> = 46 nM	MEK1 IC <sub>50</sub> = 10-14 nM N/A
In vitro (cell potency) [23, 24]	A375	0.74 nM	5 nM	34.4±9.3nM N/A
In vivo efficacy (xenograft) [21, 22]		TGI <sup>4</sup> = 60% @ 0.1 mpk; 14 days	TGI = 87% @ 3 mg/kg, 21days, QD <sup>5</sup>	TGI = 102.5% @ 30mg/kg, 14 days, BID N/A
	A375	TGI = 102% @ 0.3 mpk; 14 days; TGI = 118% @ 3 mpk; 14 days	TGI = 106% @ 5 mg/kg, 21 days, QD	TGI = 105% @ 100mg/kg, 14 days, BID
Pharmacokinetics [25, 26]	C <sub>max</sub> <sup>6</sup>	2.7 μM (3 mg/kg, mice) 0.47 μM (3 mg/kg, rats)	0.997 μM (30 mg/kg, male rats)	6.8 μg/mL(30 mg/kg, male mice) 55 μg/mL (50mg/kg BID, male mice)
	T <sub>max</sub> <sup>7</sup>	4 h (mice, 3 mg/kg, 14 days, repeat) 4 h (rats, 1 mg/kg, 21days, repeat)	2 h (30 mg/kg, male rats)	2 h (30 mg/kg, male mice) 3.8 h (50mg/kg BID, male mice) 1 h (50mg/kg BID, female mice)
	T <sub>1/2</sub> <sup>8</sup>	3.8 h (mice) 5.5 h (rats)	5.56 h (30 mg/kg, male rats)	5.72 h (30 mg/kg, male mice) 5 h (monkey, 5mg/kg)
	protein binding rate	97.40% (human)	98.8% (5 μM, dog) 93.5% (5 μM, human)	97% (human)

Item	Trametinib	Cobimetinib	Binimetinib	Selumetinib	
Structure					
Toxicokinetics (rats) [23, 24]	$T_{max}$	4 h (male rats, 0.1667mg/kg, week 4)	N/A	1h (10 mg/kg, male mice, day 27)	0.67 h (5 mg/kg, BID, week 26)
	$C_{max}$	10.1 ng/mL (male rats, 0.1667 mg/kg, week 4)	39.9 ng/mL (male rats, 3 mg/kg, day 22)	5.85 µg/mL (male mice, 10 mg/kg, day 27)	6.1 µg/mL (5 mg/kg, BID, week 26)
	$AUC_{0-t}$ <sup>9</sup>	188 ng·h/mL (male rats, 0.1667 mg/kg, week 4)	244 ng·h/mL (male rats, 3 mg/kg, day 22)	39 µg/mL (male mice, 10 mg/kg, day 27)	26.6µg/mL (5 mg/kg, BID, week 26)
Clinical PK [27, 28]	MTD <sup>10</sup>	3 mg/day (QD)	60 mg/day, QD, 21/7 100 mg/day, QD, 14/14	60 mg, BID	25 mg/m <sup>2</sup> [29]
	$T_{max}$	1.5 h (2 mg, QD)	2.4 h (60 mg, QD)	1.5 h (45 mg, BID)	1.0 h (25 mg/m <sup>2</sup> ) [29]
	$C_{max}$	22.2 ng/mL (2 mg, QD)	273 ng/mL (60 mg, QD)	241 ng/mL (45 mg, BID)	886 ng/mL (25 mg/m <sup>2</sup> ) [29]
	$T_{1/2}$	4–5 d (2 mg, QD)	43.6 h (60 mg, QD)	7.4 h (45 mg, BID)	6.2 h (25 mg/m <sup>2</sup> ) [29]
	CL/F <sup>11</sup>	5.4 L/h (2 mg, QD)	13.8 L/h (60 mg, QD)	20 h/L(45 mg, BID)	N/A
	AUC	370 ng·h/mL (0-t, day 15, 2 mg, QD)	4340 ng·h/mL (60 mg, QD)	964 ng·h /mL	2520 ng·hr/mL [29]
	period/cycle	21 days/7 days off	21 days/7 days off	21 days/cycle	28 days/cycle
	absolute bioavailability	72% (2 mg, QD)	46% (20 mg, QD)	54%	N/A
	recommended dose	2 mg, QD	60 mg, QD	45 mg, BID	25 mg/m <sup>2</sup>
Adverse reactions [27, 28]	rash, diarrhea, fatigue, peripheral edema, nausea, and dermatitis acneiform	gastrointestinal disorders, rash, pyrexia, increased blood CPK <sup>12</sup> , chorioretinopathy	rash, nausea, vomiting, diarrhoea, peripheral oedema, and fatigue	acneiform rash, gastrointestinal effects, and asymptomatic creatine kinase elevation	

<sup>1</sup> BSC: biopharmaceutics classification system. <sup>2</sup> MEK: mitogen-activated protein kinase kinase. <sup>3</sup> IC<sub>50</sub>: half maximal inhibitory concentration. <sup>4</sup> TGI: tumor growth inhibition. <sup>5</sup> QD: once a day. <sup>6</sup> C<sub>max</sub>: peak concentration. <sup>7</sup> T<sub>max</sub>: peak time. <sup>8</sup> T<sub>1/2</sub>: elimination half-life. <sup>9</sup> AUC<sub>0-t</sub>: Area under the plasma drug concentration-time curve. <sup>10</sup> MTD: maximum tolerated dose. <sup>11</sup> CL/F: apparent plasma clearance. <sup>12</sup> CPK: creatine phosphokinase.

---

#### 1.4.1. Trametinib (GSK1120212, JTP-74057)

Trametinib (GSK1120212, JTP-74057) was the first MEK inhibitor approved by the FDA (May, 2013) for treatment of melanoma. It is an allosteric, non-ATP-competitive inhibitor with sub-nanomolar activity against purified MEK1 and MEK2 kinases (half maximal inhibitory concentration (IC<sub>50</sub>) of 0.7 nM [21] and 0.9 nM, respectively) and its chemical structure is shown in Table 1-2..

In a preclinical study, trametinib showed high efficacy in xenograft models. For the HT-29 xenograft model, oral administration of trametinib demonstrated efficacy in inhibiting tumor growth at a dose of either 0.3 mg/kg or 1 mg/kg once daily (QD) for 14 days, and could block tumor growth almost completely at a dose of 1 mg/kg [30]. Similar findings were observed in an A549 (KRAS (proto-oncogene corresponding to the oncogene first identified in Kirsten rat sarcoma virus) mutant cell line) xenograft model with tumor growth inhibition of 92% and 87% at 5.0 mg/kg and 2.5 mg/kg, respectively [31].

In a clinical study, single agent treatment with trametinib resulted in a statistically significant and clinically meaningful improvement in progression-free survival (PFS) compared to standard chemotherapy [32]. In a global multi-center, randomized, open-label and controlled trial, 322 melanoma patients with the BRAF V600E or V600K-mutant were allocated on a ratio of 2:1 into either the trametinib group or conventional chemotherapy group (dacarbazine or paclitaxel), respectively. It was reported that trametinib resulted in an improved overall response rate (22% *versus* 8%) and progression-free survival (4.8 *versus* 1.5 months) when compared to the group receiving cytotoxic treatment [33]. Rash, diarrhea, and peripheral edema were the main adverse events, but those were manageable. A phase I/Ib study evaluating trametinib plus docetaxel or pemetrexed in patients with advanced KRAS-mutant NSCLC showed that the primary endpoint of overall response rate (ORR) was met for both combinations [34] (ClinicalTrials.gov number, NCT01192165).

The FDA initially approved the combination of trametinib and dabrafenib for patients with unresectable or metastatic melanoma with BRAF V600E or V600K mutations in January 2014, based on the results of median PFS extended from 8.8 months to 11.0 months when compared with dabrafenib monotherapy in a multi-center phase III trial [25, 35]. The EMA approved this combination a year later for adults with unresectable or metastatic melanoma

---

with the BRAF V600 mutation. MEK and BRAF inhibitors hence presented a new treatment method for metastatic melanoma [36].

For BRAF-mutant NSCLC, the FDA awarded the breakthrough therapy designation for combination of trametinib and dabrafenib in 2015, and approved this combination in June 2017 [37] following the EMA's approval in April the same year [38]. Breakthrough therapy designation refers to a drug where preliminary clinical evidence suggests significant improvement in the treatment of a serious condition over available therapies on a clinically significant endpoint(s) (<https://www.fda.gov/regulatory-information/food-and-drug-administration-safety-and-innovation-act-fdasia>). The approval of this combination was based on results from a three-cohort, multicenter, non-randomized, open-label study of patients with stage IV NSCLC. In this phase II trial, 36 treatment-naïve patients and 57 previously treated patients were assigned to the combination regimen with trametinib and dabrafenib, and 78 previously treated patients received the single agent dabrafenib. The results showed that there was an overall response rate (ORR) of more than 60%, with median PFS of longer than 9 months in the combination group, while there was an ORR of 27% with PFS of 5.5 months in the dabrafenib group [39]. In summary, the combination of MEK and BRAF inhibitors has provided a new treatment option for BRAF-mutant NSCLC [40]. On April 30, 2018, FDA approved the adjuvant treatment of trametinib plus dabrafenib for the BRAF V600-Mutant melanoma and approved the combination drugs (trametinib + dabrafenib) for the treatment of BRAF-positive anaplastic thyroid cancer the following month.

Recently, combination treatments of MEK with programmed cell death protein 1 (PD-1) inhibitors [41-43] has shown promise. Preclinical and translational data demonstrated that BRAF inhibitors and MEK inhibitors altered the tumor microenvironment in favor of immunotherapy and enhanced the efficacy of immune checkpoint inhibition with anti-PD-1 agents [44, 45]. Trametinib, in combination with dabrafenib and pembrolizumab, was developed by Merck Sharp & Dohme Corp. and Novartis for the treatment of melanoma in a phase II study. Based on a manageable toxicity profile in patients with BRAF<sup>V600</sup>-mutant melanoma in a phase I study, the ongoing phase II study will further evaluate safety and efficacy of this triple-combination treatment as a first-line therapy for BRAF-mutant melanoma.

The development of triple regimens on the above approved combination with either pembrolizumab or spartalizumab (PDR 001) are ongoing by Merck Sharp & Dohme and

---

Novartis, respectively, for the treatment of melanoma. A trial to assess the triple-combination treatment with trametinib, dabrafenib, and the anti-programmed death-ligand 1 (PD-L1) antibody durvalumab in 26 patients with BRAF-mutated advanced melanoma was conducted. A 69% ORR was obtained and 16 of 18 responding patients had continuous responses [46].

Apart from melanoma and NSCLC, trametinib as a single agent or in combination with dabrafenib has also been tested in other types of cancers. As reported by the American Society of Clinical Oncology (ASCO) recently, a two-arm phase II study with either trametinib or 5-fluorouracil/capecitabine in refractory advanced biliary cancer was stopped due to the lack of efficacy in the trametinib arm. In contrast, a combination with dabrafenib was shown to be well tolerated in BRAF-mutated papillary thyroid carcinoma in one randomized phase II trial.

#### **1.4.2. Cobimetinib (GDC-0973, XL518)**

The second approved MEK inhibitor was cobimetinib (GDC-0973, XL518), which was developed by Exelixis and Genentech (Roche). The compound was awarded the status of orphan drug by the FDA in 2014 for malignant melanoma with the BRAF V600 mutation, and was then approved for combination treatment with vemurafenib for unresectable or metastatic melanoma with a BRAF V600E or V600K mutation in November 2015.

The chemical structure of cobimetinib is shown in Table 1-2. Cobimetinib is a potent and highly selective MEK inhibitor, with a biochemical  $IC_{50}$  of 0.9 nM against MEK1 [22]. It also showed broad efficacy *in vivo* in xenograft models with BRAF- and KRAS-mutated cell lines [47]. Preclinical studies demonstrated that this agent was effective in inhibiting the growth of many tumor cells bearing a BRAF mutation. In preclinical studies, cobimetinib was associated with sustained ERK/MAPK inhibition in tumor tissues, with minimal drug exposure in the brain.

In a phase III trial, median PFS was 12.3 months for cobimetinib plus vemurafenib *versus* 7.2 months for vemurafenib alone, and these data supported the use of this combination as a standard first-line approach to improve survival in patients with advanced BRAF<sup>V600</sup> mutant melanoma [48].

Currently, there are many ongoing clinical studies for cobimetinib combined with other targeted therapies, for example, combination treatments of cobimetinib with GDC-0941 (a phosphoinositol 3 kinase (PI3K) inhibitor) or GDC-0994 (an ERK1/2 inhibitor) for metastatic

---

solid tumors (ClinicalTrials.gov number, NCT02457793) and the combination with idasanutlin (p53-MDM2 inhibitor) and venetoclax (BCL-2 inhibitor) for the treatment of leukemia.

The combination of cobimetinib with immunotherapy is also an intensively investigated topic. A phase Ib dose-escalation and dose-expansion study (ClinicalTrials.gov number, NCT01988896) achieved longer PFS, with a median of 12.0 months in the combination treatment group of cobimetinib with atezolizumab compared to monotherapy with either atezolizumab or cobimetinib [49]. An updated phase Ib study (ClinicalTrials.gov number, NCT01656642) showed that cobimetinib + atezolizumab + vemurafenib in BRAF<sup>V600</sup> mutant metastatic melanoma had a manageable safety profile and promising antitumor activity [50]. The phase III trial (ClinicalTrials.gov number, NCT02908672) that evaluated first-line combination treatment with vemurafenib plus cobimetinib and atezolizumab in BRAF<sup>V600</sup> mutation-positive advanced or metastatic melanoma (IMspire150) showed that progression-free survival as assessed by study investigator was significantly prolonged with atezolizumab *versus* control (15.1 vs 10.6 months; hazard ratio [HR] 0.78; 95% CI 0.63-0.97;  $p=0.025$ ) [51]. Cobimetinib, in combination with atezolizumab and regorafenib, was used for the treatment of colorectal cancer in a phase III trial (ClinicalTrials.gov number, NCT02788279).

The clinical study results of activity and safety of cobimetinib and atezolizumab in colorectal cancer (CRC) showed that the treatment is well tolerated at the maximum of administered doses. In addition, patients with MSS CRC responded to the combination of cobimetinib and atezolizumab, which provides support for the continued evaluation of the combination [52] (ClinicalTrials.gov number, NCT01988896).

#### **1.4.3. Binimetinib (MEK162, ARRY-438162)**

Binimetinib (MEK162, ARRY-438162) was approved by the FDA in 2018 for combination treatment with encorafenib for unresectable or metastatic melanoma with a BRAF<sup>V600E</sup> or <sup>V600K</sup> mutation. Binimetinib was approved based on a randomized phase III trial (COLUMBUS; NCT 01909453) in 577 patients with BRAF<sup>V600E</sup> or <sup>V600K</sup> mutation-positive unresectable or metastatic melanoma. The trial outcome showed that the median PFS was 14.9 months for patients receiving binimetinib plus encorafenib and 7.3 months for the vemurafenib monotherapy arm (hazard ratio 0.54, 95% CI: 0.41, 0.71, two-sided  $p<0.0001$ ). Common adverse events (AEs) included fatigue, nausea, vomiting, diarrhea, abdominal pain, and arthralgia [53, 54].

---

Binimetinib is an orally bioavailable, highly selective, non-ATP-competitive MEK inhibitor that has the potential to treat a range of malignant diseases. Binimetinib, 5-((4-bromo-2-fluorophenyl)amino)-4-fluoro-*N*-(2-hydroxyethoxy)-1-methyl-1*H*-benzo[*d*]imidazole-6-carboxamide (Table 1-2), was discovered by Array BioPharm., and was then co-developed by Array BioPharm/Novartis. In preclinical studies, binimetinib either alone or in combination with other agents showed significant antitumor activities in cell lines and animal models [55].

An open-label and non-randomized phase II study assessed the safety and efficacy of single-agent binimetinib treatment in adult patients with locally advanced and unresectable or metastatic malignant cutaneous melanoma, harboring BRAF V600E or NRAS (a member of the RAS gene family) mutations (ClinicalTrials.gov number, NCT01320085). The resulting data supported clinical activity of binimetinib in patients with NRAS-mutated and BRAF-mutated metastatic melanoma. Binimetinib was the first targeted therapy to show activity in patients with NRAS-mutated melanoma and offered a potential option for types of cancer with few effective treatments [55, 56].

Another randomized phase III, open label, multi-center, two-arm study was designed to compare the efficacy of binimetinib *versus* dacarbazine in patients with advanced unresectable or metastatic NRAS mutation-positive melanoma (NEMO, NCT01763164). The data showed that the ORR was 15% *versus* 7% and median PFS was 2.8 months (95% CI 2.8–3.6) *versus* 1.5 months (1.5–1.7) in the binimetinib group and dacarbazine group, respectively (hazard ratio 0.62 (95% CI (confidence interval) 0.47–0.80); one-sided  $p < 0.001$ ) [57]. PFS by binimetinib was statistically higher, this was not clinically significant (2.8 *versus* 1.5 months), leading to the withdrawal of a new drug application (NDA) application for binimetinib as a mono-therapy for NRAS-mutated melanoma from the FDA.

Other plans for binimetinib combinations with immunotherapy (e.g., with pembrolizumab in treating patients with locally advanced or metastatic triple-negative breast cancer; with pembrolizumab in advanced NSCLC; with pembrolizumab and encorafenib for the treatment of malignant melanoma; with encorafenib and nivolumab in treating patients with microsatellite-stable BRAF<sup>V600E</sup> metastatic colorectal cancer; with nivolumab, LGX818, and ipilimumab for the treatment of metastatic melanoma, etc.) are also underway.

---

Combination treatment with the CDK4/6 inhibitor palbociclib (PD-0332991) and the MEK inhibitor binimetinib (MEK162) for the treatment for advanced KRAS mutant non-small cell lung cancer (ClinicalTrials.gov number, NCT03170206) is also undergoing clinical trials.

#### **1.4.4. Selumetinib (ARRY-142886; AZD6244)**

Selumetinib (AZD6244) is an effective, highly selective, non-ATP-competitive MEK1 inhibitor which was developed by Array BioPharma and then licensed to AstraZeneca. The molecular structure is shown in Table 1-2. On April 10, 2020, the FDA approved selumetinib for pediatric patients with neurofibromatosis type 1 (NF1) who have symptomatic, inoperable plexiform neurofibromas (PN) [58]. The approval was based on the open-label, multi-center, single-arm trial in pediatric patients with NF1 and a measurable target PN that could not be surgically removed without risk of substantial morbidity (SPRINT, NCT01362803). The ORR was 66% (n=33; 95% CI: 51, 79), and 100% partial response was achieved. The most common adverse reactions were rash, vomiting, abdominal pain, diarrhea, nausea, dry skin, fatigue, musculoskeletal pain, fever, acne, stomatitis, headache, paronychia, and pruritus [59].

In 2004, Array BioPharma and AstraZeneca co-developed selumetinib for clinical study with several phase I and II clinical trials carried out in monotherapy for solid tumors [60-64]. Unfortunately, it was discontinued in phase II trials due to failure to improve on outcomes for temozolomide for progression-free survival outcomes (median time to event 78 and 80 days, respectively; hazard ratio, 1.07; 80% confidence interval, 0.86–1.32) [65].

Randomized phase II studies that compared selumetinib with conventional cytotoxic chemotherapy for a wide array of malignancies have also been performed. Selumetinib showed no superiority when compared with temozolomide in patients with chemotherapy-naïve melanoma, or pemetrexed in patients with NSCLC who had not responded to first-line and second-line therapies, or capecitabine in patients with pancreatic cancer and colorectal cancer. Nevertheless, antitumor activity of selumetinib was detected in each of these comparative studies.

Several clinical trials on selumetinib in combination with other cancer drugs have been conducted. A phase Ib study of a combination treatment with selumetinib and cyclosporine A (CsA) in patients with advanced solid tumors with an expansion cohort in metastatic colorectal cancer (mCRC) showed that the combination therapy appeared to be well

---

tolerated, with evidence of activity in mCRC (ClinicalTrials.gov number, NCT02188264) [66]. Selumetinib in combination with sorafenib in advanced hepatocellular carcinoma (HCC) is also under study (ClinicalTrials.gov number, NCT01029418) [67]. A randomized Phase II study for KRAS-mutated NSCLC did show very promising results for selumetinib plus docetaxel *versus* docetaxel, with significant improvement in median PFS (5.3 *versus* 2.1 months,  $p = 0.014$ ) and objective response rate (ORR) (37% *versus* 0%,  $p < 0.0001$ ). The overall survival benefit was 9.4 *versus* 5.2 months ( $p = 0.21$ ), but with high toxicity. Efficacy could, however, not be repeated in a multi-national phase III clinical trial. A total of 510 KRAS-mutated NSCLC patients were randomized 1:1 to receive selumetinib + docetaxel or placebo + docetaxel. The result showed that addition of selumetinib to docetaxel did not improve progression-free survival compared with docetaxel alone (ClinicalTrials.gov number, NCT01933932) [68]. Combination therapy with selumetinib plus dacarbazine has also been compared with placebo plus dacarbazine for a first-line treatment in patients with BRAF mutated melanoma in a phase II study. While markedly improved PFS was observed with the addition of selumetinib to the therapeutic regimen, no overall survival benefit was demonstrated.

Recently, a phase I trial with pediatric patients with recurrent or refractory low-grade glioma has been reported. In this study, 25 subjects received a median of 13 cycles (range: 1–26). Fourteen (37%) completed all protocol treatments (26 cycles ( $n = 13$ ), 13 cycles ( $n = 1$ )) with at least stable disease; 2-year progression-free survival at the recommended phase II dose (RP2D) was  $69 \pm 9.8\%$  SE (standard error) [69]. The study showed that selumetinib had promising antitumor activity in children with low-grade glioma. In the early phase II result, selumetinib was effective in treating children with recurrent/refractory low-grade glioma (LGG), including those with neurofibromatosis type 1 (NF-1)-associated LGG and pilocytic astrocytomas (PA) harboring BRAF<sup>V600E</sup> mutation or BRAF-KIAA 1549 fusion. Larger prospective studies are necessary to validate efficacies of this agent in treating children with LGG harboring specific molecular aberrations in the future [70].

### **1.5. MEK inhibitors in clinical development**

To our knowledge, there are 11 MEK inhibitors currently explored in clinical studies. The MEK inhibitors in clinical trials—including their efficacy, therapeutic indications, sponsors, and status—are shown in Table 1-3, while their chemical structures are presented in Figure 1-2.

The compound properties, efficacy, and clinical studies undertaken are comprehensively reviewed one by one below.

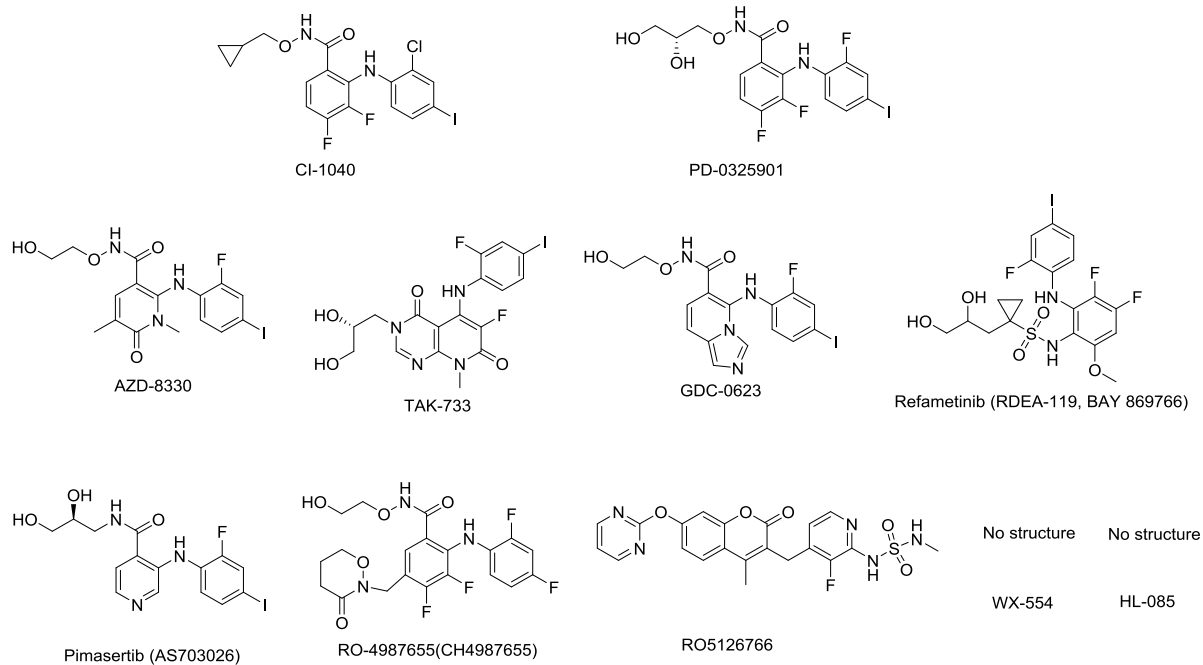


**Figure 1-2 MEK inhibitors in clinical study.**

**Table 1-3 MEK inhibitors in clinical trials**

<b>MEK Inhibitor</b>	<b>Target</b>	<b>IC<sub>50</sub></b>	<b>Indications</b>	<b>Company</b>	<b>Clinical Phase</b>
CI-1040 (PD184352) [71]	MEK1/2	2.3 nM	breast cancer, colorectal cancer, lung cancer, and pancreatic cancer	Pfizer	Phase II
PD0325901 [71]	MEK1/2	0.33 nM	melanoma, colonic neoplasms, breast neoplasms, carcinoma, NSCLC <sup>1</sup>	Pfizer	Phase II
AZD8330 [72]	MEK1/2	7 nM	advanced solid tumors	AstraZeneca	Phase I
TAK-733 [73]	MEK1/2	3.2 nM	advanced non-hematologic malignancies, advanced metastatic melanoma	Millennium Pharmaceutical, Inc./Takeda Pharmaceutical Company Limited	Phase I
GDC-0623 [53]	MEK1/2	0.13 nM	metastatic solid tumors	Genentech	Phase I
Refametinib (RDEA119; BAY 869766) [74]	MEK1/2	19 nM/47 nM	hepatocellular cancer, melanoma, colorectal cancer	Ardea Biosciences/Bayer	Phase II
Pimasertib (AS703026) [75]	MEK1/2	5–11 nM	colorectal cancer, multiple myeloma	Merck and Co.	Phase II
RO4987655 (CH4987655) [76]	MEK1	42 nM	neoplasms	Hoffman-La Roche	Phase I
RO5126766 [76]	RAF/MEK1/2	160 nM	neoplasms	Hoffmann-La Roche	Phase I
WX-554 [77]	MEK1/2	4.7 nM /10.7 nM	advanced solid tumors	Wilex, AG. Germany	Phase I/II (terminated)
HL-085 [78]	MEK1	1.9–10 nM	no data	Binjiang Pharma	Phase I

<sup>1</sup> NSCLC: non-small-cell lung cancer; <sup>2</sup> BRAF: a human gene that encodes a protein called B-Raf; <sup>3</sup> NRAS: a member of the RAS gene family.

---

### 1.5.1. CI-1040 (PD184352)

CI-1040 was the first MEK inhibitor evaluated at clinical stage by Pfizer/Warner-Lambert [71]. This compound presented a novel series of benzhydroxamate esters derived from their MEK inhibitor precursor anthranilic acids. CI-1040 was developed in phase II for breast cancer, colorectal cancer, lung cancer, and pancreatic cancer, but exhibited poor exposure due to poor solubility and rapid clearance [79], likely leading to insufficient antitumor activity in two phase II studies completed in 2003 [80] (ClinicalTrials.gov number, NCT00034827, NCT00033384). Hence, to resolve the problems of this compound, a second compound PD-0325901 was developed for clinical trial.

### 1.5.2. PD-0325901

PD-0325901 is a derivative of the MEK inhibitor CI-1040. The hydroxamate side chain of CI-1040 was optimized to improve solubility and exposure in oral administration (PO) by Pfizer/Warner-Lambert. PO or intravenous injection (IV) of PD-0325901 induced in a dose-dependent decrease in phosphorylation of MAPK (pMAPK) in liver and lung caused by MEK inhibition. Inhibition of pMAPK in liver was generally comparable between the routes of administration, whereas inhibition of pMAPK in lung was longer lasting when IV-administered possibly due to higher PD-0325901 plasma maximum concentration ( $C_{max}$ ) [60, 81].

PD-0325901 failed in its phase II clinical trials for the treatment of KRAS mutant NSCLC, as it did not meet its primary efficacy end-point (ClinicalTrials.gov number, NCT00174369) [82]. A phase I/II study for the treatment of melanoma, colonic neoplasms and breast neoplasms was terminated in 2007 due to musculoskeletal, neurological and ocular toxicity (ClinicalTrials.gov number, NCT 00147550) [83]. Furthermore, the combination of PD-325901 with the CDK4/6 inhibitor palbociclib for the same indication is still ongoing to date (ClinicalTrials.gov number, NCT 02022982). A phase II study in adolescents and adults with neurofibromatosis type-1 (NF1) was completed in August, 2018 (ClinicalTrials.gov number, NCT 02196471). Recently, an additional phase IIb trial in adult and pediatric patients with NF1-associated inoperable plexiform neurofibromas (PNs) that are causing significant morbidity is ongoing, and estimated to be completed in mid-2022 (ClinicalTrials.gov number, NCT03962543). There are two more phase I or I/II studies ongoing in colorectal cancer or KRAS mutated malignancies (ClinicalTrials.gov number, NCT02510001, NCT02039336); both are combination treatments.

### 1.5.3. AZD-8330 (ARRY-424704)

AZD-8330 is an orally active, selective MEK inhibitor with potential antineoplastic activity. The structural core for this compound is 6-oxo-1,6-dihydropyridazine, which presents a different class of MEK inhibitors [84]. AZD-8330 is a non-ATP-competitive MEK1/2 inhibitor, with an  $IC_{50}$  of 7 nM [85].

---

AZD-8330 was employed as a single agent, and the results from a phase I clinical trial for the treatment of solid tumors (ClinicalTrials.gov number, NCT00454090) showed that commonly reported toxicities included acneiform dermatitis, fatigue, diarrhea, and vomiting. Four patients experienced dose-limiting toxicities: mental status changes (40 mg QD; 2/9 patients and 60 mg QD; 1/3) and rash (20 mg BID; 1/9). The maximum tolerated dose was defined as 20 mg BID. The exposure of AZD-8330 increased approximately proportionally with dosage across a dose range of 0.5–60 mg QD. Phosphorylated ERK levels in peripheral blood mononuclear cells were measured and target inhibition was confirmed. AZD-8330 demonstrated a manageable toxicity profile with fewer class-effect AEs compared with other MEK inhibitors [86]. No further clinical studies have been reported recently.

#### **1.5.4. TAK-733**

TAK-733 is an orally bioavailable, non-ATP-competitive small-molecule inhibitor of MEK1/2 with potential antineoplastic activity. TAK-733 is a highly potent and selective MEK allosteric site inhibitor with an IC<sub>50</sub> of 3.2 nM. TAK-733 demonstrated potent enzymatic and cell activity inhibition with an EC<sub>50</sub> (concentration for 50% of maximal effect) of 1.9 nM against ERK phosphorylation in cells [73]. TAK-733 reveals broad antitumor activity in mouse xenograft models of human cancer including models of melanoma, colorectal, NSCLC, pancreatic and breast cancer.

A phase I clinical study (ClinicalTrials.gov number, NCT00948467) of TAK-733 was developed by Millennium Pharmaceuticals Inc., and the results from the dose-escalation phase I showed that the maximum tolerated dose was 16 mg, QD, irrespective of body weight. Common drug-related AEs included dermatitis acneiform, diarrhea, and increased blood creatine phosphokinase. TAK-733 demonstrated a generally manageable toxicity profile and limited antitumor activity [87]. No further investigations have been published recently.

#### **1.5.5. GDC-0623**

GDC-0623, with the chemical name of (1-(5-((2-fluoro-4-iodophenyl)amino)imidazo[1,5-a]pyridin-6-yl)-2-(2-hydroxyethoxy)ethan-1-one), is a potent, orally active, selective non-ATP-competitive MEK inhibitor (MEK1, Ki = 0.13 nM, + ATP). It was developed by Genentech, and has a novel structure of imidazopyridine [53]. GDC-0623 has broad potency in cell-based assays, particularly in both KRAS and BRAF mutant cancer cell lines, with corresponding efficacy in xenograft tumor models. It exhibited higher activity in KRAS mutant tumors than BRAF mutant tumors [88]. In preclinical pharmacokinetics and efficacy assessments, GDC-0623 showed low clearance and a low volume of distribution. The results of safety, tolerability, and pharmacokinetics from its phase I study were published in 2014 (ClinicalTrials.gov number, NCT01106599).

---

### **1.5.6. Refametinib (RDEA-119, BAY-869766)**

Refametinib, discovered by Ardea Biosciences and developed by Bayer, is a potent and orally bioavailable, non-ATP-competitive inhibitor with a low ability to accumulate in brain and other neural tissues. The  $IC_{50}$  of refametinib against MEK1 was 19 nM [74]. It was selected for clinical development due to its potency and favorable pharmacokinetic profile.

Several phase I, I/II, or II clinical trials had been conducted for single or combination therapy. One phase I/II study concluded that refametinib plus gemcitabine was well tolerated, with a promising objective response rate [89]. One phase II clinical study (ClinicalTrials.gov number, NCT01204177) of the combination therapy with refametinib and sorafenib for the treatment of RAS-mutated hepatocellular carcinoma (HCC) has been carried out as a first line systemic treatment due to the high prevalence of constitutive activation of MAPK pathway in HCC. The results showed efficacy benefits; among 70 enrolled patients, 4 patients had confirmed partial response and 22 patients had stable disease for 10 months or more [90]. However, this combination was poorly tolerated, with several severe AEs reported and almost all patients required dose modifications due to drug toxicity. Since the previous phase II study, another phase II study with refametinib or refametinib in combination with sorafenib in patients with RAS-mutated HCC (ClinicalTrials.gov number, NCT01915589 and NCT01915602) was performed involving 1,318 patients in Asian patients exhibited a robust clinical response compared with patients with wild-type RAS. The results showed that the ORR and disease control rate (DCR) were 0%, 56.3% respectively in the refametinib treatment group, while the ORR and DCR were 6.3%, 43.8%, respectively in refametinib plus sorafenib treatment group. Therefore, either monotherapy or combination therapy in a large number of patients harboring RAS mutation was not pursued further [91].

### **1.5.7. Pimasertib (AS703026)**

Pimasertib, developed by Merck KGaA and known as AS703026 or MSC1936369B, is a selective, orally bioavailable, non-ATP-competitive MEK1/2 inhibitor with potent antitumor activity in cell lines and xenograft models with constitutive activation of the MAPK pathway. Its structure, including (2-fluoro-4-iodophenyl) amino, core structure pyridine, and side chain (*S*)-*N*-(2,3-dihydroxypropyl) acetamide, is different from other MEK inhibitors. The first-in-human trial reported pharmacokinetics (PK) and pharmacodynamics (PD) of pimasertib in patients with advanced solid tumors. Pimasertib exhibited a favorable PK profile in patients with solid tumors, by inhibiting phosphorylation of ERK in peripheral blood mononuclear cell (PBMC) [92, 93]. Pimasertib showed clinical activity in a dose-dependent manner. Sustained responses were observed mostly in BRAF or NRAS-mutated melanoma [75, 94]. Currently, a few phase I/II studies are ongoing to evaluate efficacy of pimasertib in advanced or metastatic solid tumors including ovarian cancer, NRAS-mutated cutaneous

---

melanoma, ovarian cancer, breast cancer, NSCLC, hepatocellular carcinoma, metastatic colorectal cancer, and pancreatic adenocarcinoma. A randomized phase II trial compared the combination of pimasertib with the PI3K inhibitor SAR245409 in previously treated unresectable borderline or low-grade ovarian cancer involved 65 patients and showed that ORR was 9.4% in the combination therapy *versus* 12.1% in the monotherapy, exceeding 50% of patients in both therapy arms discontinued the trials. Hence, the study was terminated early because of low ORR and high rate of discontinuation [95]. Another phase II comparison trial of pimasertinib *versus* dacarbazine (DTIC) in N-RAS mutated cutaneous melanoma (ClinicalTrials.gov number, NCT01693068) conducted in 194 patients showed that PFS was significantly improved with pimasertib *versus* DTIC (median 13 *versus* 7 weeks); however no improvement of OS was observed. Moreover, serious adverse events (SAEs) were more frequent in the pimasertinib cohort [96].

#### **1.5.8. RO4987655 (CH4987655)**

RO4987655, possessing a unique 3-oxo-oxazinane ring structure at the 5-position of the benzamide core structure [76], was developed by Hoffman–La Roche. RO4987655 is an orally active small molecule, targeting MEK1 with potential antineoplastic activity. It was designed based on the X-ray crystal structure information of the target enzyme, followed by multi-dimensional optimization including metabolic stability, physicochemical properties, and safety profiles.

RO4987655 exhibited slow dissociation from the MEK1 enzyme, remarkable antitumor efficacy both in monotherapy and combination therapy *in vivo*, desirable metabolic stability, and insufficient MEK inhibition in mouse brain, implying few central nervous system (CNS)-related side effects in humans.

An excellent PK profile and clear target inhibition in PBMC were demonstrated in one phase I study with healthy volunteers [97], and also showed manageable toxicity, a favorable PK/PD profile, and promising preliminary antitumor activity with heavily pretreated patients [85, 98, 99], which has been further investigated in specific populations of patients with RAS and/or RAF mutation-driven tumors (ClinicalTrials.gov number, NCT00817518).

#### **1.5.9. RO5126766**

RO5126766, known as CH5126766, is a dual Raf/MEK inhibitor specifically targeting the kinase activities of Raf and MEK, resulting in blocking target gene transcription, the transcription of which is linked to malignant transformation of cells. RO5126766, bearing a sulfamide moiety instead of aniline in coumarin, was identified as a clinical compound with enhanced inhibitory activity, satisfactory PK/PD profiles, and manageable toxicity [100]. More studies are needed to further

---

clarify the safety and efficacy of this agent, as well as this novel class of MEK-RAF inhibitors in various cancers.

#### **1.5.10. WX-554**

WX-554 is a selective, noncompetitive MEK1/2 inhibitor entering preliminary human studies. Phase I pharmacokinetic and pharmacodynamic study showed that WX-554 was well tolerated, with the recommended phase II fixed dose being 75 mg twice weekly [77]. Unfortunately, two dose-escalation phase I/II studies in patients with advanced solid tumors were terminated for business reasons [101] (ClinicalTrials.gov number, NCT01859351, NCT01581060).

#### **1.5.11. HL-085**

HL-085 is an orally active, selective MEK inhibitor with significant inhibitory activity against MEK kinase and an  $IC_{50}$  value of 1.9–10 nM. *In vitro*,  $IC_{50}$  values in tumor cell lines were 0.41–6.2 nM in A375, 0.1–7.8 nM in COLO 205 and 0.88–2.9 nM in HT29, respectively. Oral administration of HL-085 (1 mg/kg, QD, 21 days) in BRAF-mutant COLO 205 and A375 xenograft models showed high tumor growth inhibition (TGI) (70–76% and 60–70%, respectively). HL-085 is effective in inhibiting tumor proliferation in other tumor cells as well. Currently, HL-085 is investigated in a phase I clinical study. A first-in-human phase I/II study (ClinicalTrials.gov number, NCT 03973151) in Chinese patients with NRASm advanced melanoma showed that tumor shrinkage was achieved in ten out of 33 enrolled patients. Four patients had confirmed partial response (PR), and 6 patients achieved stable disease (SD) status with 66.7% over 14 weeks. The median PFS was 17.4 weeks, and confirmed best ORR was 33.3% with a DCR 83.3%. This study demonstrated that HL-085 is well tolerated with manageable side-effects and promising anti-cancer activity in the treatment of NRASm advanced melanoma [102].

### **1.6. MEK Inhibitors in preclinical development**

There are several MEK inhibitors in preclinical development (Table 1-4) and the structures are shown in Figure 1-3.

**Table 1-4 MEK inhibitors in preclinical development**

MEK Inhibitor	Target	IC <sub>50</sub>	Current Sponsor
ClnQ-03	MEK1/2	5/10 μM	No data
G-573	MEK	No data	Genentech
PD184161	MEK	10–100 nM	Pfizer
PD318088	MEK1	No data	Pfizer Global Research & Development
PD98059	MEK1	2 μM	No data
RO5068760	MEK1	0.025 ± 0.012 μM	Hoffmann-La Roche, Inc.
U0126	MEK1/2	0.07 μM/0.06 μM	No data
SL327	MEK1/2	0.18 μM/0.22 μM	No data

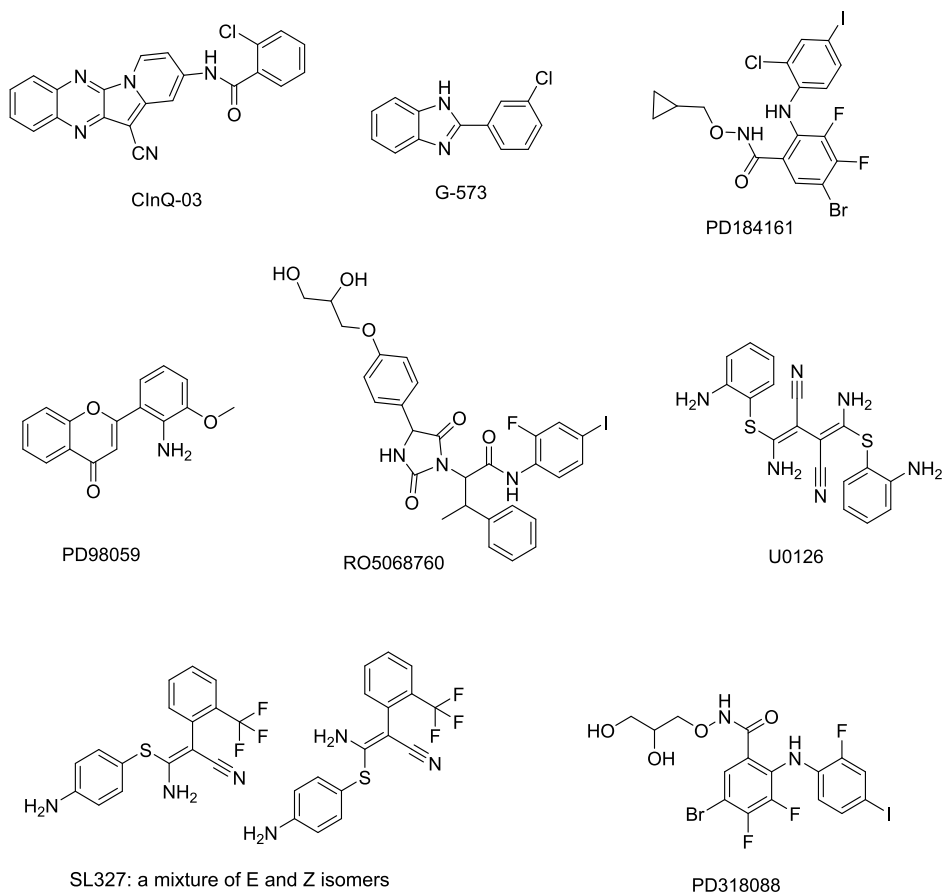


**Figure 1-3 MEK inhibitors in preclinical study**

**1.6.1. ClnQ-03**

---

ClnQ-03 is a novel and specific MEK inhibitor both *in vitro* and *in vivo*. ClnQ-03 has a distinctive chemical structure compared to other MEK inhibitors, such as PD318088, PD184352, PD0325901, and selumetinib. The compound has similar binding affinity and displays almost the same binding mode with known inhibitors. ClnQ-03 binds deeply in the binding pocket in a manner similar to the crystal ligand; docking and experimental data suggest that ClnQ-03 shows an ability to inhibit MEK1/2.

A xenograft mouse model indicated that administration of ClnQ-03 at 1 or 5 mg/kg for 11 days suppressed colon cancer cell growth significantly without toxicity. Furthermore, ClnQ-03 decreased phosphorylation levels of ERKs in a cell-based assay, which was consistent with *in vivo* results. Based on these findings, ClnQ-03 is being considered and developed as a novel MEK inhibitor [103].

#### **1.6.2. G-573**

G-573 is a potent and selective allosteric inhibitor of MEK. Structural and functional analysis illustrates that G-573 forms a strong hydrogen bond with MEK kinase. G-573 inhibited ERK phosphorylation in HCT116 tumor with IC<sub>50</sub> value estimated to be 0.406 μM, and ED<sub>50</sub> values in HCT116 and H2122 mouse xenograft models were estimated to be 4.6 and 1.9 mg/kg/day, respectively [104].

#### **1.6.3. PD184161**

PD184161 is an orally-active MEK inhibitor which inhibited MEK activity more effectively (IC<sub>50</sub> = 10–100 nM) in a time- and concentration-dependent manner than PD098059 or U0126. Structurally, PD184161 is an analog of CI-1040 but distinct from PD098059 and U0126. It joins the mechanistic class of agents that inhibit the downstream phosphorylation of ERK through their direct effects on MEK. Unlike PD098059 and U0126, PD184161 exhibits increased solubility and oral bioavailability. It showed antitumor effects against HCC *in vitro* and *in vivo*, correlated with suppression of MEK activity. PD184161 is, however, unable to suppress MEK activity in HCC xenografts in the long term [105, 106].

#### **1.6.4. PD318088**

PD318088, another analog of CI-1040 with a biarylamine structure, is a novel non-ATP-competitive MEK1 inhibitor. The compound binds adjacent to the ATP binding site. Its potency in inhibiting MEK1 activation is not affected by ATP concentration, suggesting that PD318088 does not compete with ATP [107].

#### **1.6.5. PD98059**

---

PD98059 is a potent and selective non-ATP-competitive MEK1 inhibitor by binding to the ERK-specific MAP kinase MEK, therefore preventing phosphorylation of ERK1/2 (p44/p42 MAPK) by MEK1/2. PD98059 can interact with GST-MEK1 or partially activated MEK, but does not inhibit the MAPK homologues JNK and P38 (D.R. Alessi and P. Cohen, personal communication) [108]. In addition, PD98059 efficiently inhibited MEK in a selective manner, but not other kinases such as RAF kinase, cAMP (cyclic Adenosine monophosphate)-dependent kinase, protein kinase C, v-Src (a gene found in Rous sarcoma virus), epidermal growth factor (EGF) receptor kinase, and PI3K [109, 110].

#### **1.6.6. RO5068760**

RO5068760, is a potent, highly selective, non-ATP-competitive MEK1/2 inhibitor. *In vitro*, RO5068760 inhibited MEK1 kinase activity potently with an  $IC_{50}$  of  $0.025 \pm 0.012 \mu\text{mol/L}$  in a RAF/MEK/ERK cascade assay. It also showed significant efficacy in a broad spectrum of tumors via the activation of aberrant MAPK pathway. RO5068760 showed superior efficacy in tumors harboring the BRAF V600E mutation [111]. The assessment study of target suppression in healthy volunteers showed a peak time ( $t_{\text{max}}$ ) of two hours and biphasic disposition with reaction half-time ( $T_{1/2}$ ) of 5~9 h. The inhibition of phosphorylation of ERK was relatively modest, with mean maximal suppression of 55% [112].

#### **1.6.7. U0126**

U0126 is a potent and selective non-competitive MEK inhibitor, inhibiting MEK1 and MEK2 ( $IC_{50}$  values of 70 nM and 60 nM, respectively). It inhibited ERK phosphorylation up to 80% in astrocytes. Surprisingly, U0126 also caused profound depletion of ATP in glucose-deprived cells, leading to death by necrosis [113]. The antiviral potential of U0126 was also reported, not only in cell culture *in vitro*, but also in mouse models *in vivo* [114].

#### **1.6.8. SL327**

SL327 is a homolog of U0126 and is a mixture of E and Z isomers. SL327 inhibited MEK1 and MEK2, with  $IC_{50}$  values of 0.18  $\mu\text{M}$  and 0.22  $\mu\text{M}$ , respectively. *In vivo*, the study showed that the combination of SL327 with sunitinib malate induced significant additive suppression of doxorubicin-resistant anaplastic thyroid carcinoma (ATC) tumor growth [115].

### **1.7. Radiotherapy and irradiation-induced small intestinal injury**

---

Though remarkable progress has been made in the area of cancer treatment, radiotherapy and chemotherapy remain an important component of cancer treatment. Approximately 50% of patients undergo chemotherapy during the course of cancer treatment [116]. Skin cancers (squamous and basal cell carcinomas), prostate- and cervix carcinomas, lymphomas, and head and neck carcinomas are example cancers treated with radiotherapy. Better cancer control by radiotherapy dose escalation is accompanied by significant toxicity and damage of healthy tissues [117]. The main symptoms of radiation-induced intestinal damage include anorexia, vomiting, diarrhea, dehydration, systemic infection, and in extreme cases, septic shock and death [118].

Ionizing radiation from radiotherapy results in the generation of reactive free radicals which may damage DNA, RNA, protein, and cell membranes. The damage of DNA and RNA thus block their ability to divide and proliferate further [119]. Molecular events that lead to normal tissue injury are complex and include oxidative stress, inflammation, senescence, pro-fibrogenic cytokines, etc. [120].

The small intestine is one of the most sensitive organs to irradiation. The epithelium of the small intestine consists of repeated finger-like invagination called crypts associated with numerous protrusion/villi. The small intestine epithelia act as a barrier against the penetration of pathogens. The renewal of small intestine is regulated by intestine stem cells (ISCs) located near the bottom of the epithelial crypt. There are around four to six ISCs per crypt in differentiated Paneth cells. The function of Paneth cells is to secrete antibacterial compounds [121].

Active ISCs govern epithelial renewal and rapidly divide to progenitor cells in the transit-amplifying region. The ISCs renewal signaling cascades have been characterized, including Wnt, bone morphogenic protein, Notch, Ephrin, JAK/STAT1, PTEN, AKT and PI3K [122].

### **1.8. Radioprotectors**

To reduce the side effects caused by radiotherapy, radioprotectors have emerged as a significant need in clinic applications. Several radioprotectors have been proven to reduce radiation damage to normal tissues, including amino thiols, natural antioxidants and other radioprotective agents.

### 1.8.1 Aminothiols

Aminothiols have been widely studied, including cystein, cystamine, amifostine, PrC-210, 2-aminoethyl isothiurea, cysteamine thiosulfate (WR-2721, WR-3689), and thiazodine derivatives (See Figure 1-4). Their molecular structures either include –SH, or contain groups that can be cleaved to –SH. A structure review showed that amino and thiol groups are typically separated by less than three carbon atoms. As a result, amino groups carry a positive charge which is beneficial for binding to DNA [123].

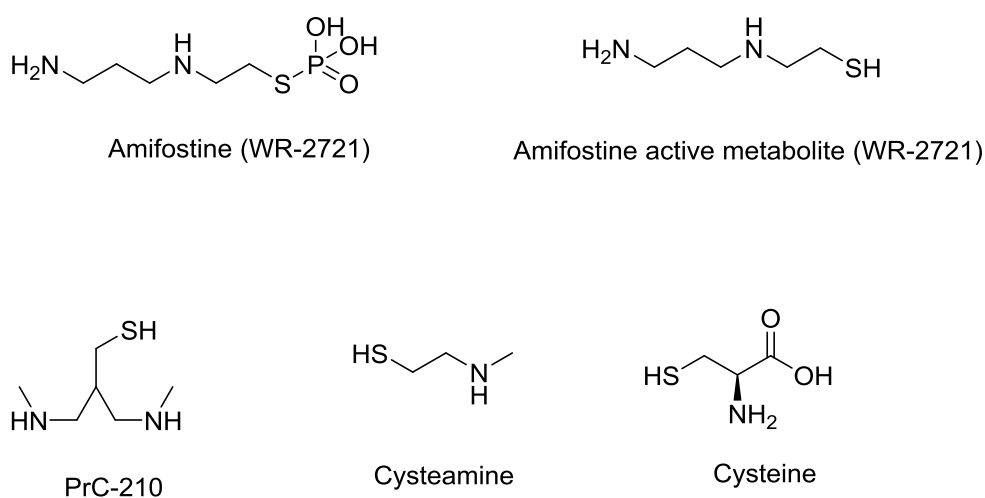


**Figure 1-4 Molecular structures of aminothiols**

To date, amifostine is the only chemical drug of this group approved by the FDA for protecting against the toxicity of radiotherapy in cancer patients. Amifostine (WR-2721:  $\text{H}_2\text{N}(\text{CH}_2)_3\text{NH}(\text{CH}_2)_2\text{SPO}_3\text{H}_2$ ) is a powerful radiation-protecting drug, initially developed by the Walter Reed Army Medical Center. This compound is a free radical scavenger and an organic thiol phosphate prodrug. *In vivo*, Amifostine can be cleaved into the –SH form (WR-1065:  $\text{H}_2\text{N}(\text{CH}_2)_3\text{NH}(\text{CH}_2)_2\text{SH}$ ). The mechanism of amifostine radioprotection includes scavenging of secondary radicals generated by radiation exposure [124]. Furthermore, a meta-analysis proved that amifostine did not have tumor-protective effects [125]. However, the efficacy of this compound is limited by its high toxicity and undesirable side effects [126]. In a phase III clinical study, 16/39 patients (41%) amifostine was discontinued due to severe adverse effects, hence this study was terminated [127].

Fahl et al. designed and synthesized a new compound PrC-210, which has: (1) a free thiol ROS scavenging group; (2) a short, flexible alkyl backbone with two (+) charged amines; and (3) a side chain that displaces the thiol away from the alkyl backbone and DNA helix [128]. Cheryl et al. evaluated PrC-210 in rat and mouse models and demonstrated that oral PrC-210 by gavage 30-90 min before irradiation provided 100% survival in rats and mice under 9.0 Gy of whole-body irradiation. No detectable nausea/vomiting or hypotension side effects were observed in the preclinical models [129].

### 1.8.2 Natural antioxidants

Natural antioxidants exist widely in plants and fruits and play an important role in radioprotection. A series of antioxidants are shown in Figure 1-5. Since natural antioxidants are affordable as well as less toxic, they attract a lot of attention. Efficacies are slightly weaker than determined for amifostine or synthesized compounds. Among the natural antioxidants, flavonoids and polyenes are the most promising and widely studied. Vitamins A, C, and E, and beta-carotene are polyenes. Catecholic acid, resveratrol, epicatechin, quercetin, genistein, and baicalein are flavonoids.

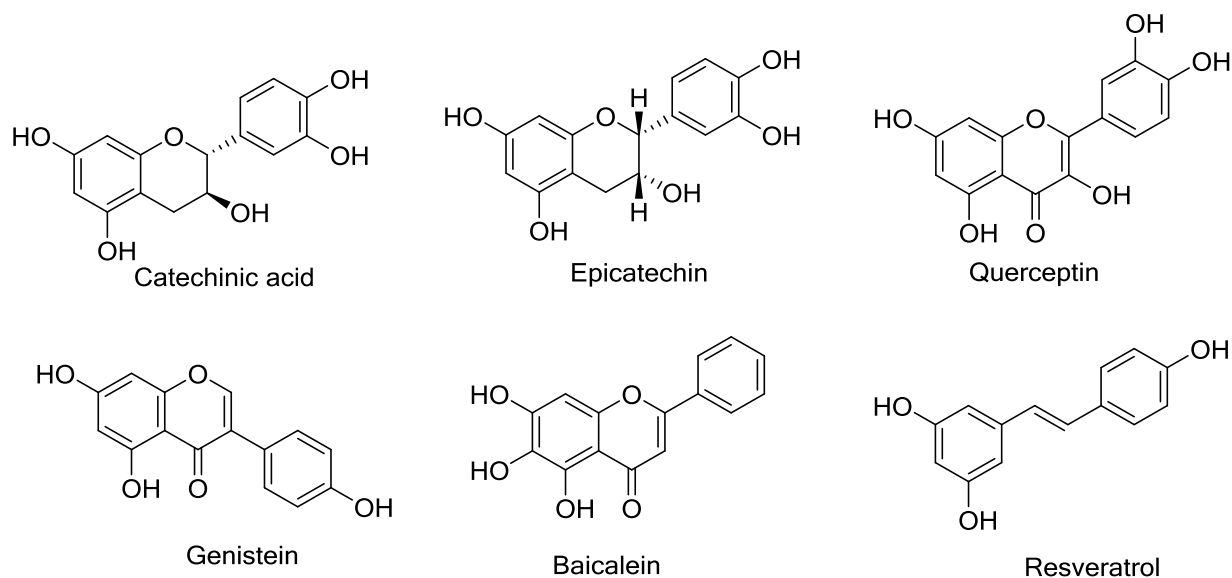


**Figure 1-5 Molecular structures of natural antioxidants**

Vitamins A, C, E, and beta-carotene, have been shown to exhibit radioprotective properties [130]. Dietary intake of Vitamin A and beta-carotene resulted in reduced mortality and morbidity in mice

---

exposed to total body irradiation or partial-body irradiation. Vitamin C, at doses of 200-800 mg/kg, protected against radiation-induced chromosomal damage in mice [131]. Vitamin E was demonstrated to provide radioprotection in animal models with increased survival after whole-body irradiation. Furthermore, it was shown to significantly protect small bowel crypt cell numbers, mucosal height, and goblet cell numbers from radiation effects [132].

Patil et al. reported that administration of querceptin before irradiation resulted in a significant decrease in DNA damage compared to the irradiation only group in mice. This study demonstrated that the potential of querceptin in alleviating radiation-induced mortality and cytogenetic damage [133]. Wang et al. demonstrated that querceptin may play a radioprotective role in the lung of mice through inhibiting NF-KB and MAPK pathways [134]. Horton et al. reported that querceptin is capable of mitigating radiation induced skin fibrosis, but without affecting the radio-response of fibroblasts or murine tumors [135]. Bansal et al. confirmed that the quercetin-3-O-rutinoside, a flavonoid glycoside, protects the gastrointestinal tract and haematopoietic system by the restoration of radiation-induced reduction in villi height, number of crypt cells and spleen index. The radioprotective effect of this compound was attributed to the increase of pro-survival (ERK) and decrease of pro-apoptotic (BAX) gene expressions [136].

Radioprotector mechanisms are ascribed to either reduction of cellular oxygen content or direct participation in competitive reaction with oxygen for the DNA radical using thiol groups [137].

### **1.8.3 Other radioprotectors**

Other categories of radioprotectors were also studied, including ACE inhibitors (such as captopril, enalapril, pencillamine), metalloelements (such as manganese chloride and cadmium salts), immunomodulators (such as  $\gamma$ -interferon, polysaccharides), corticosteroids (such as BDP/SGX201), plant extracts and isolated compounds (such as curcumin, orientin, vicimil), and DNA binding ligands (such as Hoechst 33342) [138].

## **1.9. Conclusions**

In recent years, MEK inhibitors have been discovered and developed very rapidly. Trametinib became the first approved MEK inhibitor drug, and cobimetinib soon followed suit. MEK inhibitors,

---

as single agents or in combination with other therapies, have shown to be efficacious in treating melanoma, lung cancer, and colorectal cancer.

Dual inhibition of MEK and RAF kinase as a therapeutic strategy in targeting the MAPK pathway offers advantage in terms of both increased efficacy and minimized toxicity. Therefore, nearly every MEK inhibitor in the clinical studies has combined MEK inhibitor with BRAF inhibitor. According to available clinical data, combination treatments with MEK and BRAF inhibitors lead to superior outcomes.

Moreover, evidence suggests that BRAFi/MEKi treatment may enhance the efficacy of immune checkpoint inhibition with anti-PD1 agents. Thus, the combination of a MEK inhibitor plus a BRAF inhibitor and immunotherapy could represent a promising form of cancer treatment in order to improve outcomes.

MEK inhibitor treatment is still considered one of the most promising areas in cancer research. However, there are still concerns regarding toxicity, which is one of the obstacles for the development of MEK inhibitors. Novel small molecular inhibitors with high potency and low toxicity are expected to become the new breakthrough in cancer treatment, which was therefore chosen as the focus of this PhD research

### **1.10. Hypotheses**

Structure analyses of existing MEK inhibitors revealed some limitations and weaknesses. In GDC-0973, the hydrogen-bonding force at the F atom in the benzene ring is too weak, which causes the unsatisfactory activity. The activity of GSK212 is high; however the solubility is poor probably due to the high hydrophobicity of aromatic ring, which requires use of dimethylsulfoxide (DMSO) to form solvate, and causes drug accumulation and high toxicity. In addition, Tarik Silk et al. reported that MEK inhibitors interfere with MEK signaling efficiently in T-cell as well as macrophages, and pulsed treatment with MEK inhibitors resulted in increased viability of classically differentiated macrophages compared to continuous treatment [19]. The estimated elimination half-life of GSK212 is 3.9 to 4.8 days, demonstrating drug accumulation with treatment time. Therefore, the use of GSK212 is not beneficial for combinational treatment with immunotherapy. Conversely, AZD6244 and MEK162, two similar compounds, possess satisfactory PK profile, but their activity needs to be enhanced.

---

Analyses of core structure characteristics of the main MEK inhibitors, the core structure class of the compound AZD6244 was considered to be most advantageous and it was therefore selected as the lead compound. Considering the binding mode and the unsatisfactory potency of AZD6244, it is proposed that a large substituent group on the 3-nitrogen may be responsible for reduced antitumor activity. In addition, enzymatic de-methylation of the 3-nitrogen methyl of AZD6244 occurs *in vivo* [139].

On the second part of this research, the only approved small molecular entity Amifostine for radiation protection has good efficacy, however pharmacokinetics are not ideal with a short half life as well as no oral bioavailability. The most widely studied radioprotectors, natural anti-oxidants, have a good safety but poor oral bioavailability. Radiation induces DNA damage directly through reactive oxygen species [140] and activating p53 [141-145]. P53-mediated apoptosis has been implicated in regulating intestinal injuries [146].

Driven by these issues and knowledge gaps, the hypotheses tested in this research part are:

- i. Replacing the N-methyl in the benzoheterocyclic ring of AZD6244 with an O atom, and replacing the –Cl and –Br substituent on the aniline with –F and –I, respectively, can obtain a new MEK inhibitor with enhanced efficacy compared with AZD6244.
- ii. Analogous to synergistic effects observed for established MEK inhibitors, combination of the newly designed MEK inhibitor with a BRAF inhibitor can synergistically inhibit tumor growth *in vitro* and *in vivo*.
- iii. Combination of a MEK inhibitor with the chemotherapy agent docetaxel, a microtubule stabilizing agent approved by the FDA for the conventional therapy of NSCLC, can synergistically inhibit tumor growth *in vitro* and *in vivo*.
- iv. Bifunctional compounds, obtained by combining the natural anti-oxidant agent quercetin with aminothiols with different linkers, can exhibit good radiation protection. This design may retain both the efficacy of aminothiols and the safety properties of natural anti-oxidation agents, respectively. Moreover, introducing methyl groups can adjust the lipophilicity profile

---

thereby increasing drug bioavailability. Furthermore, two functional fragments can modulate pharmacokinetic (PK) profiles of each other, becoming mutually prodrugs to each other.

- v. Radiation induces DNA damage directly through reactive oxygen species [32] and destroys the expression of proteins in cells [140], activating p53 [141-145]. Radiation activates p53 in the GI epithelium, and p53-mediated apoptosis has been implicated in regulating intestinal injuries [146-147]. It is well known that p53 activates genes that regulate cell cycle checkpoints, DNA damage and repair, and apoptosis. The new radioprotector is beneficial for the protection of radiation-induced intestinal injury by inhibiting the p53-dependent apoptosis signaling pathway since it is well known that p53 activates genes that regulate DNA damage and apoptosis and also neuroprotection against cytotoxicity-induced by H<sub>2</sub>O<sub>2</sub> and Aβ<sub>1-42</sub>.

### 1.11. Aims of this thesis

The aims of the project are:

- i. To design and synthesize a new MEK inhibitor with an enhanced activity compared with the known MEK inhibitor AZD6244 for the treatment of RAS/RAF mutant cancers, and a series of radioprotectors for radiotherapy during the cancer treatment.
- ii. To evaluate the inhibitory activity of the new MEK inhibitor against MEK1/2 kinase as well as kinase selectivity, and investigate the mechanism by which the new compound inhibits cancer cell proliferation.
- iii. To determine the efficacy of the new MEK inhibitor against RAS/RAF mutant cancers *in vitro*.
- iv. To evaluate the pharmacokinetics of the new MEK inhibitor and the RAS/RAF mutant tumor growth inhibition *in vivo*.
- v. To investigate the synergistic effect of the combination of new MEK inhibitor with BARF inhibitor or chemotherapy agent docetaxel both *in vitro* and *in vivo*.
- vi. To investigate the protective effect of a new radioprotector against radiation-induced intestinal

---

injury.

- vii. To investigate the neuroprotective effect of another new radioprotector against H<sub>2</sub>O<sub>2</sub> and Aβ<sub>1-42</sub>-induced cytotoxicity.

### 1.12. Significance

RAS or RAF mutations are present in a significant proportion of malignancies, associated with aggressive clinic behaviors and poor prognosis. This research firstly designed and synthesized a new benzoxole compound and proved it to be a highly potent and selective MEK inhibitor which exhibited enhanced activity and safety in RAS/RAF mutant cancers, overcoming the shortcoming of existing MEK inhibitors. This MEK inhibitor may provide an effective therapy approach clinically.

Some subtypes of BRAF or KRAS mutant cancers are often associated with drug resistance and disease progress for single target inhibition. Combinational drugs therapy often results in improved therapeutic outcomes or delayed drug resistance, leading to increased progress-free survival and overall survival. Moreover, recent studies demonstrated that combination therapies are often better tolerated compared to monotherapy in patients with BRAF or KRAS mutation. Here the new MEK inhibitor showed synergistic anti-cancer activity both *in vitro* and *in vivo* with the BRAF inhibitor vemurafenib or the chemotherapy agent docetaxel. The synergistic effect of the combinations suggests suitability for combinational therapy to enhance therapeutic effects or delay drug resistance.

Approximately 50% of cancer patients receive radiation therapy during cancer treatment, and 53% of them report bowel symptoms. The small intestine is one of the most sensitive organs for ionizing radiation, and acute radiation injury to the colon can even lead to therapy interruption. Search for effective and nontoxic radioprotectors to protect patients from ionizing radiation side effects is important for radiotherapy, space traveling, and even nuclear emergencies. This research designed and synthesized a series of bifunctional radioprotectors which can protect against radiation injury. One radioprotector exhibited protective effects against radiation-induced intestinal injury, and is a promising novel compound to be used as a radioprotector.

Oxidative stress plays a critical role in the common pathophysiology of neurodegenerative diseases which are prevalent and the leading cause of disability globally in the aging population. In accordance with the free radical theory, radioprotectors may have effect on neurodegenerative

---

diseases which are partially caused by ROSs. Here, another radioprotector was found to demonstrate neuroprotective activity and significantly enhance neurite outgrowth.

---

### 1.13. References

1. Bray, F.; Ferlay, J.; Soerjomataram, I.; Siegel, R. L.; Torre, L. A.; Jemal, A., Global cancer statistics 2018: GLOBOCAN estimates of incidence and mortality worldwide for 36 cancers in 185 countries. *CA Cancer J Clin* 2018, 68, (6), 394-424.
2. Organization, W. H., Cancer. 2018.
3. Karin, L. C. M., Mammalian MAP kinase signalling cascades. *Nature* 2001, 410, (March 1), 37-40.
4. Leonard, J. T.; Raess, P. W.; Dunlap, J.; Hayes-Lattin, B.; Tyner, J. W.; Traer, E., Functional and genetic screening of acute myeloid leukemia associated with mediastinal germ cell tumor identifies MEK inhibitor as an active clinical agent. *J. of Hematol. & Oncol.* 2016, 9, (1), 31.
5. Thompson, N.; Lyons, J., Recent progress in targeting the Raf/MEK/ERK pathway with inhibitors in cancer drug discovery. *Curr Opin Pharmacol* 2005, 5, (4), 350-6.
6. Mahapatra, D. K.; Asati, V.; Bharti, S. K., MEK inhibitors in oncology: a patent review (2015-Present). *Expert Opin Ther Pat* 2017, 27, (8), 887-906.
7. Templeton, I. E.; Musib, L., MEK inhibitors beyond monotherapy: current and future development. *Curr Opin Pharmacol* 2015, 23, 61-7.
8. Martin-Liberal, J.; Lagares-Tena, L.; Larkin, J., Prospects for MEK inhibitors for treating cancer. *Expert Opin Drug Saf* 2014, 13, (4), 483-95.
9. Zhao, Y.; Adjei, A. A., The clinical development of MEK inhibitors. *Nature Revi Clin Oncol* 2014, 11, (7), 385-400.
10. Inamdar, G. S.; Madhunapantula, S. V.; Robertson, G. P., Targeting the MAPK pathway in melanoma: why some approaches succeed and other fail. *Biochem Pharmacol* 2010, 80, (5), 624-37.
11. Grimaldi, A. M.; Simeone, E.; Festino, L.; Vanella, V.; Strudel, M.; Ascierto, P. A., MEK inhibitors in the treatment of metastatic melanoma and solid tumors. *Am J Clin Dermatol* 2017, 18, (6), 745-754.
12. Uehling, D. E.; Harris, P. A., Recent progress on MAP kinase pathway inhibitors. *Bioorg Med Chem Lett* 2015, 25, (19), 4047-56.

- 
13. Price, S., Putative allosteric MEK1 and MEK2 inhibitors. *Expert Opinion on Therapeutic Patents* 2008, 18, (6), 603-627.
  14. Richman, J.; Martin-Liberal, J.; Diem, S.; Larkin, J., BRAF and MEK inhibition for the treatment of advanced BRAF mutant melanoma. *Expert Opin Pharmacother* 2015, 16, (9), 1285-1297.
  15. Hertzman Johansson, C.; Egyhazi Brage, S., BRAF inhibitors in cancer therapy. *Pharmacol & Therapeut* 2014, 142, (2), 176-182.
  16. Hagemann, C.; Blank, J. L., The ups and downs of MEK kinase interactions. *Cellular Signalling* 2001, 13, (12), 863-875.
  17. Queirolo, P.; Picasso, V.; Spagnolo, F., Combined BRAF and MEK inhibition for the treatment of BRAF-mutated metastatic melanoma. *Cancer Treat Rev* 2015, 41, (6), 519-26.
  18. Neuzillet, C.; Tijeras-Raballand, A.; de Mestier, L.; Cros, J.; Faivre, S.; Raymond, E., MEK in cancer and cancer therapy. *Pharmacol Ther* 2014, 141, (2), 160-71.
  19. Wang, D.; Boerner, S. A.; Winkler, J. D.; LoRusso, P. M., Clinical experience of MEK inhibitors in cancer therapy. *Biochim Biophys Acta* 2007, 1773, (8), 1248-55.
  20. Saltiel, D. R. A. A. C. P. C. D. T. D. A. R., PD 098059 is a specific inhibitor of the activation of mitogen-activated protein kinase kinase in vitro and in vivo. *J BIO CHEM.* 1995, 270, (November 17), 27489–27494.
  21. Gilmartin, A. G.; Bleam, M. R.; Groy, A.; Moss, K. G.; Minthorn, E. A.; Kulkarni, S. G.; Rominger, C. M.; Erskine, S.; Fisher, K. E.; Yang, J.; Zappacosta, F.; Annan, R.; Sutton, D.; Laquerre, S. G., GSK1120212 (JTP-74057) is an inhibitor of MEK activity and activation with favorable pharmacokinetic properties for sustained in vivo pathway inhibition. *Clin Cancer Res* 2011, 17, (5), 989-1000.
  22. Rice, K. D.; Aay, N.; Anand, N. K.; Blazey, C. M.; Bowles, O. J.; Bussenius, J.; Costanzo, S.; Curtis, J. K.; Defina, S. C.; Dubenko, L.; Engst, S.; Joshi, A. A.; Kennedy, A. R.; Kim, A. I.; Koltun, E. S.; Loughheed, J. C.; Manalo, J. C.; Martini, J. F.; Nuss, J. M.; Peto, C. J.; Tsang, T. H.; Yu, P.; Johnston, S., Novel carboxamide-based allosteric MEK inhibitors: Discovery and optimization efforts toward XL518 (GDC-0973). *ACS Med Chem Lett* 2012, 3, (5), 416-21.

- 
23. FDA, [https://www.accessdata.fda.gov/drugsatfda\\_docs/label/2014/204114s001lbl.pdf](https://www.accessdata.fda.gov/drugsatfda_docs/label/2014/204114s001lbl.pdf). 2014.
  24. (FDA), U. S. F. D. A., Available online: [https://www.accessdata.fda.gov/drugsatfda\\_docs/nda/2015/206192Orig1s000PharmR.pdf](https://www.accessdata.fda.gov/drugsatfda_docs/nda/2015/206192Orig1s000PharmR.pdf). 2015.
  25. FDA Trametinib pharmacology review.
  26. Takahashi, R. H.; Ma, S.; Yue, Q.; Kim-Kang, H.; Yi, Y.; Ly, J.; Boggs, J. W.; Fettes, A.; McClory, A.; Deng, Y.; Hop, C. E.; Khojasteh, S. C.; Choo, E. F., Absorption, metabolism and excretion of cobimetinib, an oral MEK inhibitor, in rats and dogs. *Xenobiotica* 2017, 47, (1), 50-65.
  27. Infante, J. R.; Fecher, L. A.; Falchook, G. S.; Nallapareddy, S.; Gordon, M. S.; Becerra, C.; DeMarini, D. J.; Cox, D. S.; Xu, Y.; Morris, S. R.; Peddareddigari, V. G. R.; Le, N. T.; Hart, L.; Bendell, J. C.; Eckhardt, G.; Kurzrock, R.; Flaherty, K.; Burris, H. A.; Messersmith, W. A., Safety, pharmacokinetic, pharmacodynamic, and efficacy data for the oral MEK inhibitor trametinib: a phase 1 dose-escalation trial. *Lancet Oncol.* 2012, 13, (8), 773-781.
  28. Rosen, L. S.; LoRusso, P.; Ma, W. W.; Goldman, J. W.; Weise, A.; Colevas, A. D.; Adjei, A.; Yazji, S.; Shen, A.; Johnston, S.; Hsieh, H. J.; Chan, I. T.; Sikic, B. I., A first-in-human phase I study to evaluate the MEK1/2 inhibitor, cobimetinib, administered daily in patients with advanced solid tumors. *Invest New Drugs* 2016, 34, (5), 604-13.
  29. Dombi, E.; Baldwin, A.; Marcus, L. J.; Fisher, M. J.; Weiss, B.; Kim, A.; Whitcomb, P.; Martin, S.; Aschbacher-Smith, L. E.; Rizvi, T. A.; Wu, J.; Ershler, R.; Wolters, P.; Therrien, J.; Glod, J.; Belasco, J. B.; Schorry, E.; Brofferio, A.; Starosta, A. J.; Gillespie, A.; Doyle, A. L.; Ratner, N.; Widemann, B. C., Activity of selumetinib in neurofibromatosis type 1-related plexiform neurofibromas. *N Engl J Med* 2016, 375, (26), 2550-2560.
  30. Yamaguchi, T.; Kakefuda, R.; Tajima, N.; Sowa, Y.; Sakai, T., Antitumor activities of JTP-74057 (GSK1120212), a novel MEK1/2 inhibitor, on colorectal cancer cell lines in vitro and in vivo. *Int J Oncol* 2011, 39, (1), 23-31.
  31. Abe, H.; Kikuchi, S.; Hayakawa, K.; Iida, T.; Nagahashi, N.; Maeda, K.; Sakamoto, J.; Matsumoto, N.; Miura, T.; Matsumura, K.; Seki, N.; Inaba, T.; Kawasaki, H.; Yamaguchi, T.; Kakefuda, R.; Nanayama, T.; Kurachi, H.; Hori, Y.; Yoshida, T.; Kakegawa, J.; Watanabe, Y.;

- 
- Gilmartin, A. G.; Richter, M. C.; Moss, K. G.; Laquerre, S. G., Discovery of a highly potent and selective MEK inhibitor: GSK1120212 (JTP-74057 DMSO solvate). *ACS Med Chem Lett* 2011, 2, (4), 320-4.
32. Lugowska, I.; Kosela-Paterczyk, H.; Kozak, K.; Rutkowski, P., Trametinib: a MEK inhibitor for management of metastatic melanoma. *Onco Targets Ther* 2015, 8, 2251-9.
33. Menzies, A. M.; Long, G. V., Dabrafenib and trametinib, alone and in combination for BRAF-mutant metastatic melanoma. *Clin Cancer Res* 2014, 20, (8), 2035-43.
34. Gandara, D. R.; Leighl, N.; Delord, J. P.; Barlesi, F.; Bennouna, J.; Zalcman, G.; Infante, J. R.; Reckamp, K. L.; Kelly, K.; Shepherd, F. A.; Mazieres, J.; Janku, F.; Gardner, O. S.; Mookerjee, B.; Wu, Y.; Cox, D. S.; Schramek, D.; Peddareddigari, V.; Liu, Y.; D'Amelio, A. M., Jr.; Blumenschein, G., Jr., A phase 1/1b study evaluating trametinib plus docetaxel or pemetrexed in patients with advanced non-small cell lung cancer. *J Thorac Oncol* 2017, 12, (3), 556-566.
35. Long, G. V.; Stroyakovskiy, D.; Gogas, H.; Levchenko, E.; de Braud, F.; Larkin, J.; Garbe, C.; Jouary, T.; Hauschild, A.; Grob, J.-J.; Chiarion-Sileni, V.; Lebbe, C.; Mandalà, M.; Millward, M.; Arance, A.; Bondarenko, I.; Haanen, J. B. A. G.; Hansson, J.; Utikal, J.; Ferraresi, V.; Kovalenko, N.; Mohr, P.; Probachai, V.; Schadendorf, D.; Nathan, P.; Robert, C.; Ribas, A.; DeMarini, D. J.; Irani, J. G.; Swann, S.; Legos, J. J.; Jin, F.; Mookerjee, B.; Flaherty, K., Dabrafenib and trametinib versus dabrafenib and placebo for Val600 BRAF-mutant melanoma: a multicentre, double-blind, phase 3 randomised controlled trial. *The Lancet* 2015, 386, (9992), 444-451.
36. Hsueh, E. C.; Gorantla, K. C., Novel melanoma therapy. *Exp Hematol Oncol* 2015, 5, 23.
37. FDA grants regular approval to dabrafenib and trametinib combination for metastatic NSCLC with BRAF V600E mutation.
38. EMA  
[http://www.ema.europa.eu/docs/en\\_GB/document\\_library/Summary\\_of\\_opinion/human/002643/WC500222159.pdf](http://www.ema.europa.eu/docs/en_GB/document_library/Summary_of_opinion/human/002643/WC500222159.pdf).
39. Planchard, D.; Besse, B.; Groen, H. J. M.; Souquet, P.-J.; Quoix, E.; Baik, C. S.; Barlesi, F.; Kim, T. M.; Mazieres, J.; Novello, S.; Rigas, J. R.; Upalawanna, A.; D'Amelio, A. M.; Zhang, P.; Mookerjee, B.; Johnson, B. E., Dabrafenib plus trametinib in patients with previously

- 
- treated BRAFV600E-mutant metastatic non-small cell lung cancer: an open-label, multicentre phase 2 trial. *Lancet Oncol* 2016, 17, (7), 984-993.
40. Dholaria, B.; Hammond, W.; Shreders, A.; Lou, Y., Emerging therapeutic agents for lung cancer. *J Hematol Oncol* 2016, 9, (1), 138.
  41. Ma, W.; Gilligan, B. M.; Yuan, J.; Li, T., Current status and perspectives in translational biomarker research for PD-1/PD-L1 immune checkpoint blockade therapy. *J Hematol Oncol* 2016, 9, (1), 47.
  42. Tsai, K. K.; Daud, A. I., Nivolumab plus ipilimumab in the treatment of advanced melanoma. *J Hematol Oncol* 2015, 8, 123.
  43. Diggs, L. P.; Hsueh, E. C., Utility of PD-L1 immunohistochemistry assays for predicting PD-1/PD-L1 inhibitor response. *Biomark Res* 2017, 5, 12.
  44. Pelster, M. S.; Amaria, R. N., Combined targeted therapy and immunotherapy in melanoma: a review of the impact on the tumor microenvironment and outcomes of early clinical trials. *Ther Adv Med Oncol* 2019, 11, 1758835919830826.
  45. Subbiah, V.; Baik, C.; Kirkwood, J. M., Clinical development of BRAF plus MEK inhibitor combinations. *Trends Cancer* 2020.
  46. Simeone, E.; Grimaldi, A. M.; Festino, L.; Vanella, V.; Palla, M.; Ascierto, P. A., Combination treatment of patients with BRAF-mutant melanoma: A new standard of care. *BioDrugs* 2017, 31, (1), 51-61.
  47. Choo, E. F.; Ng, C. M.; Berry, L.; Belvin, M.; Lewin-Koh, N.; Merchant, M.; Salphati, L., PK-PD modeling of combination efficacy effect from administration of the MEK inhibitor GDC-0973 and PI3K inhibitor GDC-0941 in A2058 xenografts. *Cancer Chemotherapy and Pharmacol* 2013, 71, (1), 133-143.
  48. Ascierto, P. A.; McArthur, G. A.; Dréno, B.; Atkinson, V.; Liskay, G.; Di Giacomo, A. M.; Mandalà, M.; Demidov, L.; Stroyakovskiy, D.; Thomas, L.; de la Cruz-Merino, L.; Dutriaux, C.; Garbe, C.; Yan, Y.; Wongchenko, M.; Chang, I.; Hsu, J. J.; Koralek, D. O.; Rooney, I.; Ribas, A.; Larkin, J., Cobimetinib combined with vemurafenib in advanced BRAFV600-mutant melanoma (coBRIM): updated efficacy results from a randomised, double-blind, phase 3 trial. *Lancet Oncol* 2016, 17, (9), 1248-1260.
  49. Wilson H. Miller, T. M. K., Carrie B. Lee, Keith T. Flaherty, Sunil Reddy, Rahima Jamal,

- 
- Laura Q. Chow, Isabelle Anne Rooney, Bethany Pitcher, Edward Cha, Jeffrey R. Infante, Atezolizumab (A) + cobimetinib (C) in metastatic melanoma (mel): Updated safety and clinical activity. *J Clin Oncol* 2017, 35, (abstr 3057).
50. Ryan J. Sullivan, R. G., Karl D. Lewis, Omid Hamid, Jeffrey R. Infante, Manish R. Patel, F. Stephen Hodi, Jeffrey Wallin, Bethany Pitcher, Edward Cha, Louise Roberts, Marcus Ballinger, Patrick Hwu, Atezolizumab (A) + cobimetinib (C) + vemurafenib (V) in BRAFV600-mutant metastatic melanoma (mel): Updated safety and clinical activity. In *ASCO Annual Meeting*, 2017; p 3063.
51. Gutzmer, R.; Stroyakovskiy, D.; Gogas, H.; Robert, C.; Lewis, K.; Protsenko, S.; Pereira, R. P.; Eigentler, T.; Rutkowski, P.; Demidov, L.; Manikhas, G. M.; Yan, Y.; Huang, K.-C.; Uyei, A.; McNally, V.; McArthur, G. A.; Ascierto, P. A., Atezolizumab, vemurafenib, and cobimetinib as first-line treatment for unresectable advanced BRAFV600 mutation-positive melanoma (IMspire150): primary analysis of the randomised, double-blind, placebo-controlled, phase 3 trial. *The Lancet* 2020, 395, (10240), 1835-1844.
52. Bendell, J. C.; Kim, T. W.; Goh, B. C.; Wallin, J.; Oh, D.-Y.; Han, S.-W.; Lee, C. B.; Hellmann, M. D.; Desai, J.; Lewin, J. H.; Solomon, B. J.; Chow, L. Q. M.; Miller, W. H.; Gainor, J. F.; Flaherty, K.; Infante, J. R.; Das-Thakur, M.; Foster, P.; Cha, E.; Bang, Y.-J., Clinical activity and safety of cobimetinib (cobi) and atezolizumab in colorectal cancer (CRC). *J Clin Oncol* 2016, 34, (15\_suppl), 3502-3502.
53. Hatzivassiliou, G.; Haling, J. R.; Chen, H.; Song, K.; Price, S.; Heald, R.; Hewitt, J. F.; Zak, M.; Peck, A.; Orr, C.; Merchant, M.; Hoeflich, K. P.; Chan, J.; Luoh, S. M.; Anderson, D. J.; Ludlam, M. J.; Wiesmann, C.; Ultsch, M.; Friedman, L. S.; Malek, S.; Belvin, M., Mechanism of MEK inhibition determines efficacy in mutant KRAS- versus BRAF-driven cancers. *Nature* 2013, 501, (7466), 232-6.
54. Bendell, J. C.; Javle, M.; Bekaii-Saab, T. S.; Finn, R. S.; Wainberg, Z. A.; Laheru, D. A.; Weekes, C. D.; Tan, B. R.; Khan, G. N.; Zalupski, M. M.; Infante, J. R.; Jones, S.; Papadopoulos, K. P.; Tolcher, A. W.; Chavira, R. E.; Christy-Bittel, J. L.; Barrett, E.; Patnaik, A., A phase 1 dose-escalation and expansion study of binimetinib (MEK162), a potent and selective oral MEK1/2 inhibitor. *Br J Cancer* 2017, 116, (5), 575-583.
55. McCubrey, J. A.; Steelman, L. S.; Abrams, S. L.; Chappell, W. H.; Russo, S.; Ove, R.;

- 
- Milella, M.; Tafuri, A.; Lunghi, P.; Bonati, A.; Stivala, F.; Nicoletti, F.; Libra, M.; Martelli, A. M.; Montalto, G.; Cervello, M., Emerging MEK inhibitors. *Expert Opin Emerg Drugs* 2010, 15, (2), 203-23.
56. Ascierto, P. A.; Schadendorf, D.; Berking, C.; Agarwala, S. S.; van Herpen, C. M. L.; Queirolo, P.; Blank, C. U.; Hauschild, A.; Beck, J. T.; St-Pierre, A.; Niazi, F.; Wandel, S.; Peters, M.; Zube, A.; Dummer, R., MEK162 for patients with advanced melanoma harbouring NRAS or Val600 BRAF mutations: a non-randomised, open-label phase 2 study. *Lancet Oncol* 2013, 14, (3), 249-256.
57. Dummer, R.; Schadendorf, D.; Ascierto, P. A.; Arance, A.; Dutriaux, C.; Di Giacomo, A. M.; Rutkowski, P.; Del Vecchio, M.; Gutzmer, R.; Mandala, M.; Thomas, L.; Demidov, L.; Garbe, C.; Hogg, D.; Liskay, G.; Queirolo, P.; Wasserman, E.; Ford, J.; Weill, M.; Sirulnik, L. A.; Jehl, V.; Bozón, V.; Long, G. V.; Flaherty, K., Binimetinib versus dacarbazine in patients with advanced NRAS-mutant melanoma (NEMO): a multicentre, open-label, randomised, phase 3 trial. *Lancet Oncol* 2017, 18, (4), 435-445.
58. FDA,  
<https://www.fda.gov/drugs/resources-information-approved-drugs/fda-approves-selumetinib-neurofibromatosis-type-1-symptomatic-inoperable-plexiform-neurofibromas>.
59. Gross, A. M.; Wolters, P. L.; Dombi, E.; Baldwin, A.; Whitcomb, P.; Fisher, M. J.; Weiss, B.; Kim, A.; Bornhorst, M.; Shah, A. C.; Martin, S.; Roderick, M. C.; Pichard, D. C.; Carbonell, A.; Paul, S. M.; Therrien, J.; Kapustina, O.; Heisey, K.; Clapp, D. W.; Zhang, C.; Peer, C. J.; Figg, W. D.; Smith, M.; Glod, J.; Blakeley, J. O.; Steinberg, S. M.; Venzon, D. J.; Doyle, L. A.; Widemann, B. C., Selumetinib in children with inoperable plexiform neurofibromas. *N Engl J Med* 2020, 382, (15), 1430-1442.
60. El-Hoss, J.; Kolind, M.; Jackson, M. T.; Deo, N.; Mikulec, K.; McDonald, M. M.; Little, C. B.; Little, D. G.; Schindeler, A., Modulation of endochondral ossification by MEK inhibitors PD0325901 and AZD6244 (Selumetinib). *Bone* 2014, 59, 151-61.
61. Jain, N.; Curran, E.; Iyengar, N. M.; Diaz-Flores, E.; Kunnavakkam, R.; Popplewell, L.; Kirschbaum, M. H.; Karrison, T.; Erba, H. P.; Green, M.; Poire, X.; Koval, G.; Shannon, K.; Reddy, P. L.; Joseph, L.; Atallah, E. L.; Dy, P.; Thomas, S. P.; Smith, S. E.; Doyle, L. A.; Stadler, W. M.; Larson, R. A.; Stock, W.; Odenike, O., Phase II study of the oral MEK

- 
- inhibitor selumetinib in advanced acute myelogenous leukemia: a University of Chicago phase II consortium trial. *Clin Cancer Res* 2014, 20, (2), 490-8.
62. Ma, B. B.; Lui, V. W.; Cheung, C. S.; Lau, C. P.; Ho, K.; Hui, E. P.; Tsui, S. K.; Ng, M. H.; Cheng, S. H.; Ng, P. K.; Tsao, S. W.; Chan, A. T., Activity of the MEK inhibitor selumetinib (AZD6244; ARRY-142886) in nasopharyngeal cancer cell lines. *Invest New Drugs* 2013, 31, (1), 30-8.
63. Belouèche-Babari, M.; Jamin, Y.; Arunan, V.; Walker-Samuel, S.; Revill, M.; Smith, P. D.; Halliday, J.; Waterton, J. C.; Barjat, H.; Workman, P.; Leach, M. O.; Robinson, S. P., Acute tumour response to the MEK1/2 inhibitor selumetinib (AZD6244, ARRY-142886) evaluated by non-invasive diffusion-weighted MRI. *Br J Cancer* 2013, 109, (6), 1562-9.
64. Hung Huynh, V. C. N., Heng Nung Koong, Donald Poon, Su Pin Choo, Han Chong Toh, Choon Hua Thng, Pierce Chow, Hock Soo Ong, Alexander Chung, Boon Cher Goh, Paul D. Smith, Khee Chee Soo, AZD6244 enhances the anti-tumor activity of sorafenib in ectopic and orthotopic models of human hepatocellular carcinoma (HCC). *J of Hepatol* 2010, 52, (47), 79-87.
65. Kirkwood, J. M.; Bastholt, L.; Robert, C.; Sosman, J.; Larkin, J.; Hersey, P.; Middleton, M.; Cantarini, M.; Zazulina, V.; Kemsley, K.; Dummer, R., Phase II, open-label, randomized trial of the MEK1/2 inhibitor selumetinib as monotherapy versus temozolomide in patients with advanced melanoma. *Clin Cancer Res* 2012, 18, (2), 555-67.
66. Anuradha Krishnamurthy, A. D., Anne M. Noonan, Janice M. Mehnert, Albert C. Lockhart, Mark N. Stein, Hanna Kelly Sanoff, James J. Lee, Aaron Richard Hansen, Usha Malhotra, Sarah Rippke, Sarah Lindsey Davis, Wells A. Messersmith, S. Gail Eckhardt, Christopher Hanyoung Lieu, A phase IB study of the combination of selumetinib (AZD6244, ARRY-142886) and cyclosporin A (CsA) in patients with advanced solid tumors with an expansion cohort in metastatic colorectal cancer (mCRC). *J Clin Oncol* 35, 2017 suppl; abstr 2587.
67. Tai, W. M.; Yong, W. P.; Lim, C.; Low, L. S.; Tham, C. K.; Koh, T. S.; Ng, Q. S.; Wang, W. W.; Wang, L. Z.; Hartano, S.; Thng, C. H.; Huynh, H.; Lim, K. T.; Toh, H. C.; Goh, B. C.; Choo, S. P., A phase Ib study of selumetinib (AZD6244, ARRY-142886) in combination with sorafenib in advanced hepatocellular carcinoma (HCC). *Ann Oncol* 2016, 27, (12),

---

2210-2215.

68. Poltoratskiy, P. A. J. M. M. v. d. H. F. B. M. C. J. M. L. C. S. O. F. B. J. P. G. A., Selumetinib plus docetaxel compared with docetaxel alone and progression-free survival in patients with KRAS-mutant advanced non-small cell lung cancer. *JAMA* 2017, 317, 1844-1853.
69. Banerjee, A.; Jakacki, R. I.; Onar-Thomas, A.; Wu, S.; Nicolaidis, T.; Young Poussaint, T.; Fangusaro, J.; Phillips, J.; Perry, A.; Turner, D.; Prados, M.; Packer, R. J.; Qaddoumi, I.; Gururangan, S.; Pollack, I. F.; Goldman, S.; Doyle, L. A.; Stewart, C. F.; Boyett, J. M.; Kun, L. E.; Fouladi, M., A phase I trial of the MEK inhibitor selumetinib (AZD6244) in pediatric patients with recurrent or refractory low-grade glioma: a Pediatric Brain Tumor Consortium (PBTC) study. *Neuro Oncol* 2017.
70. Jason R. Fangusaro, A. O.-T., Tina Young-Poussaint, Shengjie Wu, Azra H Ligon, Neal Ian Lindeman, Anuradha Banerjee, Roger Packer, Lindsay B. Kilburn, Ian Pollack, Regina Jakacki, Ibrahim A. Qaddoumi, Paul Graham Fisher, Girish Dhall, Patricia Ann Baxter, Susan G. Kreissman, L. Austin Doyle, Malcolm A. Smith, Ira J. Dunkel, Maryam Fouladi, Pediatric Brain Tumor Consortium, A phase II prospective study of selumetinib in children with recurrent or refractory low-grade glioma (LGG): A pediatric brain tumor consortium (PBTC) study. *J Clin Oncol* 35, 2017 (suppl; abstr 10504).
71. Barrett, S. D.; Bridges, A. J.; Dudley, D. T.; Saltiel, A. R.; Fergus, J. H.; Flamme, C. M.; Delaney, A. M.; Kaufman, M.; LePage, S.; Leopold, W. R.; Przybranowski, S. A.; Sebolt-Leopold, J.; Van Becelaere, K.; Doherty, A. M.; Kennedy, R. M.; Marston, D.; Howard, W. A., Jr.; Smith, Y.; Warmus, J. S.; Teclé, H., The discovery of the benzhydroxamate MEK inhibitors CI-1040 and PD 0325901. *Bioorg Med Chem Lett* 2008, 18, (24), 6501-4.
72. Eli Wallace, J. L., James Blake, Allison Marlow, Julie Greschuk, Tammie Yeh, Michele Callejo, Vivienne Marsh, Gregory Poch, Jennifer Otten, Gary Hingorani, Shannon Winski, Deborah Anderson, Patrice Lee, James Winkler, Kevin Koch, Barry Davies, Darren Jones, Armelle Logie, Nicola Curtis, Christine Chresta, Paul Smith and David Robinson, AZD8330 (ARRY-424704): Preclinical evaluation of a potent, selective MEK 1/2 inhibitor currently in phase I trials. In *AACR*, 2009; Vol. 69.
73. Dong, Q.; Dougan, D. R.; Gong, X.; Halkowycz, P.; Jin, B.; Kanouni, T.; O'Connell, S. M.;

- 
- Scorah, N.; Shi, L.; Wallace, M. B.; Zhou, F., Discovery of TAK-733, a potent and selective MEK allosteric site inhibitor for the treatment of cancer. *Bioorg Med Chem Lett* 2011, 21, (5), 1315-9.
74. Iverson, C.; Larson, G.; Lai, C.; Yeh, L. T.; Dadson, C.; Weingarten, P.; Appleby, T.; Vo, T.; Maderna, A.; Vernier, J. M.; Hamatake, R.; Miner, J. N.; Quart, B., RDEA119/BAY 869766: a potent, selective, allosteric inhibitor of MEK1/2 for the treatment of cancer. *Cancer Res* 2009, 69, (17), 6839-47.
75. Delord, J. P.; Houédé, N.; Awada, A.; Lebbe, C.; Lesimple, T.; Schellens, J. H. M.; Rottey, S.; Kefford, R.; Rejeb, N.; Raymond, E., Pimasertib (MSC1936369B/AS703026), a selective oral MEK1/2 inhibitor, shows clinical activity in melanoma. *European Journal of Cancer* 2012, 48, 190.
76. Isshiki, Y.; Kohchi, Y.; Ikura, H.; Matsubara, Y.; Asoh, K.; Murata, T.; Kohchi, M.; Mizuguchi, E.; Tsujii, S.; Hattori, K.; Miura, T.; Yoshimura, Y.; Aida, S.; Miwa, M.; Saitoh, R.; Muraio, N.; Okabe, H.; Belunis, C.; Janson, C.; Lukacs, C.; Schück, V.; Shimma, N., Design and synthesis of novel allosteric MEK inhibitor CH4987655 as an orally available anticancer agent. *Bioorg Med Chem Lett* 2011, 21, (6), 1795-1801.
77. Jamieson, D.; Griffin, M. J.; Sludden, J.; Drew, Y.; Cresti, N.; Swales, K.; Merriman, M.; Allen, R.; Bevan, P.; Buerkle, M.; Mala, C.; Coyle, V.; Rodgers, L.; Dean, E.; Greystoke, A.; Banerji, U.; Wilson, R. H.; Evans, T. R.; Anthoney, A.; Ranson, M.; Boddy, A. V.; Plummer, R., A phase I pharmacokinetic and pharmacodynamic study of the oral mitogen-activated protein kinase kinase (MEK) inhibitor, WX-554, in patients with advanced solid tumours. *Eur J Cancer* 2016, 68, 1-10.
78. Tian, H. J., C.; Liu, C.; Kong, L.; Cheng, Y.; Huang, G.C. Benzoheterocyclic compounds and Use Thereof. 2013.
79. Wabnitz, P. A.; Mitchell, D.; Wabnitz, D. A. M., In vitro and in vivo metabolism of the anti-cancer agent CI-1040, a MEK inhibitor, in rat, monkey, and human. *Pharmaceut Res* 2004, 21, (9), 1670-1679.
80. Rinehart, J.; Adjei, A. A.; Lorusso, P. M.; Waterhouse, D.; Hecht, J. R.; Natale, R. B.; Hamid, O.; Varterasian, M.; Asbury, P.; Kaldjian, E. P.; Gulyas, S.; Mitchell, D. Y.; Herrera, R.; Sebolt-Leopold, J. S.; Meyer, M. B., Multicenter phase II study of the oral MEK inhibitor,

- 
- CI-1040, in patients with advanced non-small-cell lung, breast, colon, and pancreatic cancer. *J Clin Oncol* 2004, 22, (22), 4456-62.
81. Brown, A. P.; Carlson, T. C.; Loi, C. M.; Graziano, M. J., Pharmacodynamic and toxicokinetic evaluation of the novel MEK inhibitor, PD0325901, in the rat following oral and intravenous administration. *Cancer Chemother Pharmacol* 2007, 59, (5), 671-9.
82. Haura, E. B.; Ricart, A. D.; Larson, T. G.; Stella, P. J.; Bazhenova, L.; Miller, V. A.; Cohen, R. B.; Eisenberg, P. D.; Selaru, P.; Wilner, K. D.; Gadgeel, S. M., A phase II study of PD-0325901, an oral MEK inhibitor, in previously treated patients with advanced non-small cell lung cancer. *Clin Cancer Res* 2010, 16, (8), 2450-7.
83. Boasberg, P. D.; Redfern, C. H.; Daniels, G. A.; Bodkin, D.; Garrett, C. R.; Ricart, A. D., Pilot study of PD-0325901 in previously treated patients with advanced melanoma, breast cancer, and colon cancer. *Cancer Chemother Pharmacol* 2011, 68, (2), 547-52.
84. Marlow, A., L. ; Wallace, Eli; SEO, Jeongbeob; Lyssikatos, Joseph, P.; Yang, Hong, Woon; Blake, Jim; Storey, Richard, Anthony, Rebecca, Jane; Pittam, John, David Heterocyclic inhibitors of mek and methods of use thereof. 2007.
85. Haasbach, E.; Hartmayer, C.; Planz, O., Combination of MEK inhibitors and oseltamivir leads to synergistic antiviral effects after influenza A virus infection in vitro. *Antiviral Res* 2013, 98, (2), 319-24.
86. Cohen, R. B.; Aamdal, S.; Nyakas, M.; Cavallin, M.; Green, D.; Learoyd, M.; Smith, I.; Kurzrock, R., A phase I dose-finding, safety and tolerability study of AZD8330 in patients with advanced malignancies. *Eur J Cancer* 2013, 49, (7), 1521-9.
87. Adjei, A. A.; LoRusso, P.; Ribas, A.; Sosman, J. A.; Pavlick, A.; Dy, G. K.; Zhou, X.; Gangolli, E.; Kneissl, M.; Faucette, S.; Neuwirth, R.; Bozon, V., A phase I dose-escalation study of TAK-733, an investigational oral MEK inhibitor, in patients with advanced solid tumors. *Invest New Drugs* 2017, 35, (1), 47-58.
88. Choo, E.; Belvin, M.; Merchant, M.; Chan, E.; Hollingshead, P.; Orr, C.; Boggs, J.; Plise, E.; Robarge, K.; Zak, M., Preclinical pharmacokinetics and efficacy assessment of a potent and selective MEK inhibitor, GDC-0623. *Eur J Cancer* 2012, 48, 155.
89. Van Laethem, J. L.; Riess, H.; Jassem, J.; Haas, M.; Martens, U. M.; Weekes, C.; Peeters, M.; Ross, P.; Bridgewater, J.; Melichar, B.; Cascinu, S.; Saramak, P.; Michl, P.; Van

- 
- Brummelen, D.; Zaniboni, A.; Schmiegel, W.; Dueland, S.; Giurescu, M.; Garosi, V. L.; Roth, K.; Schulz, A.; Seidel, H.; Rajagopalan, P.; Teufel, M.; Childs, B. H., Phase I/II study of Refametinib (BAY 86-9766) in combination with Gemcitabine in advanced pancreatic cancer. *Target Oncol* 2017, 12, (1), 97-109.
90. Lim, H. Y.; Heo, J.; Choi, H. J.; Lin, C. Y.; Yoon, J. H.; Hsu, C.; Rau, K. M.; Poon, R. T.; Yeo, W.; Park, J. W.; Tay, M. H.; Hsieh, W. S.; Kappeler, C.; Rajagopalan, P.; Krissel, H.; Jeffers, M.; Yen, C. J.; Tak, W. Y., A phase II study of the efficacy and safety of the combination therapy of the MEK inhibitor refametinib (BAY 86-9766) plus sorafenib for Asian patients with unresectable hepatocellular carcinoma. *Clin Cancer Res* 2014, 20, (23), 5976-85.
91. Lim, H. Y.; Merle, P.; Weiss, K. H.; Yau, T.; Ross, P.; Mazzaferro, V.; Blanc, J. F.; Ma, Y. T.; Yen, C. J.; Kocsis, J.; Choo, S. P.; Sukeepaisarnjaroen, W.; Gerolami, R.; Dufour, J. F.; Gane, E. J.; Ryoo, B. Y.; Peck-Radosavljevic, M.; Dao, T.; Yeo, W.; Lamletthton, W.; Thongsawat, S.; Teufel, M.; Roth, K.; Reis, D.; Childs, B. H.; Krissel, H.; Llovet, J. M., Phase II studies with Refametinib or Refametinib plus Sorafenib in patients with RAS-mutated hepatocellular carcinoma. *Clin Cancer Res* 2018, 24, (19), 4650-4661.
92. Houédé, N.; Delord, J. P.; Awada, A.; Lebbe, C.; Lesimple, T.; Schellens, J. H. M.; Rottey, S.; Kefford, R.; von Richter, O.; Raymond, E., Pharmacokinetics and pharmacodynamics of a selective oral MEK1/2 inhibitor, Pimasertib (MSC1936369B/AS703026), in patients with advanced solid tumors. *Eur J Cancer* 2012, 48, 184.
93. Naing, A.; Mita, M.; Komarnitsky, P.; Milner, A.; von Richter, O.; Ogden, J.; Piha-Paul, S.; Fu, S.; Asatiani, E.; Kurzrock, R., Phase I dose-escalation trial of a selective oral MEK1/2 inhibitor, Pimasertib (MSC1936369B), combined with an mTOR inhibitor, temsirolimus, in patients with advanced solid tumors. *Eur J Cancer* 2012, 48, 187.
94. Awada, A.; Delord, J. P.; Houédé, N.; Lebbe, C.; Lesimple, T.; Schellens, J. H. M.; Rottey, S.; Kefford, R.; Rejeb, N.; Raymond, E., Safety and recommended phase II dose (RP2D) of the selective oral MEK1/2 inhibitor Pimasertib (MSC1936369B/AS703026): Results of a Phase I trial. *Eur J Cancer* 2012, 48, 185-186.
95. Arend, R. C.; Davis, A. M.; Chomiczewski, P.; O'Malley, D. M.; Provencher, D.; Vergote, I.; Ghamande, S.; Birrer, M. J., EMR 20006-012: A phase II randomized double-blind placebo controlled trial comparing the combination of pimasertib (MEK inhibitor) with SAR245409

- 
- (PI3K inhibitor) to pimasertib alone in patients with previously treated unresectable borderline or low grade ovarian cancer. *Gynecol Oncol* 2020, 156, (2), 301-307.
96. Lebbe, C.; Dutriaux, C.; Lesimple, T.; Kruit, W.; Kerger, J.; Thomas, L.; Guillot, B.; Braud, F.; Garbe, C.; Grob, J. J.; Loquai, C.; Ferraresi, V.; Robert, C.; Vasey, P.; Conry, R.; Isaacs, R.; Espinosa, E.; Schueler, A.; Massimini, G.; Dreno, B., Pimasertib versus Dacarbazine in patients with unresectable NRAS-mutated cutaneous melanoma: Phase II, randomized, controlled trial with crossover. *Cancers (Basel)* 2020, 12, (7).
97. Kraeber-Bodere, F.; Carlier, T.; Naegelen, V. M.; Shochat, E.; Lumbroso, J.; Trampal, C.; Nagarajah, J.; Chua, S.; Hugonnet, F.; Stokkel, M.; Gleeson, F.; Tessier, J., Differences in the biologic activity of 2 novel MEK inhibitors revealed by <sup>18</sup>F-FDG PET: analysis of imaging data from 2 phase I trials. *J Nucl Med* 2012, 53, (12), 1836-46.
98. Leijen, S.; Middleton, M. R.; Tresca, P.; Kraeber-Bodere, F.; Dieras, V.; Scheulen, M. E.; Gupta, A.; Lopez-Valverde, V.; Xu, Z. X.; Rueger, R.; Tessier, J. J.; Shochat, E.; Blotner, S.; Naegelen, V. M.; Schellens, J. H.; Eberhardt, W. E., Phase I dose-escalation study of the safety, pharmacokinetics, and pharmacodynamics of the MEK inhibitor RO4987655 (CH4987655) in patients with advanced solid tumors. *Clin Cancer Res* 2012, 18, (17), 4794-805.
99. Shinji Nakamichi, H. N., Noboru Yamamoto, Yasuhide Yamada, Yutaka Fujiwara, Yosuke Tamura, Hiroshi Wakui, Kazunori Honda, Hidenori Mizugaki, Satoru Kitazono, Yuko Tanabe, Hajime Asahina, Naoya Yamazaki, Shigenobu Suzuki, Mieko Matsuoka, Yoshitaka Ogita, Tomohide Tamura, Phase I and pharmacokinetics/pharmacodynamics study of the MEK inhibitor RO4987655 in Japanese patients with advanced solid tumors. *Invest New Drugs* 2015, 41, (33), 641–651.
100. Martinez-Garcia, M.; Banerji, U.; Albanell, J.; Bahleda, R.; Dolly, S.; Kraeber-Bodere, F.; Rojo, F.; Routier, E.; Guarin, E.; Xu, Z. X.; Rueger, R.; Tessier, J. J.; Shochat, E.; Blotner, S.; Naegelen, V. M.; Soria, J. C., First-in-human, phase I dose-escalation study of the safety, pharmacokinetics, and pharmacodynamics of RO5126766, a first-in-class dual MEK/RAF inhibitor in patients with solid tumors. *Clin Cancer Res* 2012, 18, (17), 4806-19.
101. Haagensen, E. J.; Thomas, H. D.; Schmalix, W. A.; Payne, A. C.; Kevorkian, L.; Allen, R. A.; Bevan, P.; Maxwell, R. J.; Newell, D. R., Enhanced anti-tumour activity of the combination

- 
- of the novel MEK inhibitor WX-554 and the novel PI3K inhibitor WX-037. *Cancer Chemother Pharmacol* 2016, 78, (6), 1269-1281.
102. Wang, X.; Si, L.; Mao, L.; Cui, C.; Chi, Z.; Sheng, X.; Bai, X.; Zhou, L.; LIAN, B.; Tang, B.; Yan, X.; Li, S.; Kong, Y.; Guo, J., A first-in-human phase I/II study of HL-085, a MEK Inhibitor, in Chinese patients with NRAS<sup>m</sup> advanced melanoma. *J Clin Oncol* 2020, 38, (15\_suppl), 10047-10047.
103. Kim, D. J.; Lee, M. H.; Reddy, K.; Li, Y.; Lim, D. Y.; Xie, H.; Lee, S. Y.; Yeom, Y. I.; Bode, A. M.; Dong, Z., ClnQ-03, a novel allosteric MEK inhibitor, suppresses cancer growth in vitro and in vivo. *Carcinogenesis* 2013, 34, (5), 1134-43.
104. Choo, E. F.; Belvin, M.; Chan, J.; Hoeflich, K.; Orr, C.; Robarge, K.; Yang, X.; Zak, M.; Boggs, J., Preclinical disposition and pharmacokinetics-pharmacodynamic modeling of biomarker response and tumour growth inhibition in xenograft mouse models of G-573, a MEK inhibitor. *Xenobiotica* 2010, 40, (11), 751-62.
105. Klein, P. J.; Schmidt, C. M.; Wiesenauer, C. A.; Choi, J. N.; Gage, E. A.; Yip-Schneider, M. T.; Wiebke, E. A.; Wang, Y.; Omer, C.; Sebolt-Leopold, J. S., The effects of a novel MEK inhibitor PD184161 on MEK-ERK signaling and growth in human liver cancer. *Neoplasia* 2006, 8, (1), 1-8.
106. Yung, H. W.; Wyttenbach, A.; Tolkovsky, A. M., Aggravation of necrotic death of glucose-deprived cells by the MEK1 inhibitors U0126 and PD184161 through depletion of ATP. *Biochem Pharmacol* 2004, 68, (2), 351-60.
107. Han, S.; Zhou, V.; Pan, S.; Liu, Y.; Hornsby, M.; McMullan, D.; Klock, H. E.; Haugen, J.; Lesley, S. A.; Gray, N.; Caldwell, J.; Gu, X. J., Identification of coumarin derivatives as a novel class of allosteric MEK1 inhibitors. *Bioorg Med Chem Lett* 2005, 15, (24), 5467-5473.
108. David T. Dudley, L. P., Stuart J. Decker, Alexander J. Bridges, and Alan R. Saltiel, A synthetic inhibitor of the mitogen-activated protein kinase cascade. *Proc. Natl. Acad. Sci. USA* 1995, 92, 7686–7689.
109. Di Paola, R.; Galuppo, M.; Mazzon, E.; Paterniti, I.; Bramanti, P.; Cuzzocrea, S., PD98059, a specific MAP kinase inhibitor, attenuates multiple organ dysfunction syndrome/failure (MODS) induced by zymosan in mice. *Pharmacol Res* 2010, 61, (2), 175-87.
110. Cerioni, L.; Palomba, L.; Cantoni, O., The Raf/MEK inhibitor PD98059 enhances ERK1/2

- 
- phosphorylation mediated by peroxynitrite via enforced mitochondrial formation of reactive oxygen species. *FEBS Lett* 2003, 547, (1-3), 92-96.
111. Daouti, S.; Higgins, B.; Kolinsky, K.; Packman, K.; Wang, H.; Rizzo, C.; Moliterni, J.; Huby, N.; Fotouhi, N.; Liu, M.; Goelzer, P.; Sandhu, H. K.; Li, J. K.; Railkar, A.; Heimbrook, D.; Niu, H., Preclinical in vivo evaluation of efficacy, pharmacokinetics, and pharmacodynamics of a novel MEK1/2 kinase inhibitor RO5068760 in multiple tumor models. *Mol Cancer Ther* 2010, 9, (1), 134-44.
  112. Lee, L.; Niu, H.; Goelzer, P.; Rueger, R.; Deutsch, J.; Busse-Reid, R.; DeSchepper, S.; Blotner, S.; Barrett, J.; Weissgerber, G.; Peck, R., The safety, tolerability, pharmacokinetics, and pharmacodynamics of single oral doses of RO5068760, an MEK inhibitor, in healthy volunteers: assessment of target suppression. *J Clin Pharmacol* 2010, 50, (12), 1397-405.
  113. Kwon, B.; Houpt, T. A., Mitogen-activated protein kinase in the amygdala plays a critical role in lithium chloride-induced taste aversion learning. *Neurobiol Learn Mem* 2012, 97, (1), 132-9.
  114. Dokladda, K.; Green, K. A.; Pan, D. A.; Hardie, D. G., PD98059 and U0126 activate AMP-activated protein kinase by increasing the cellular AMP:ATP ratio and not via inhibition of the MAP kinase pathway. *FEBS Lett* 2005, 579, (1), 236-40.
  115. Wang, W.; Zhou, J.; Zhao, L.; Chen, S., Combination of SL327 and Sunitinib malate leads to an additive anti-cancer effect in doxorubicin resistant thyroid carcinoma cells. *Biomed Pharmacother* 2017, 88, 985-990.
  116. Baskar, R.; Lee, K. A.; Yeo, R.; Yeoh, K. W., Cancer and radiation therapy: current advances and future directions. *Int J Med Sci* 2012, 9, (3), 193-9.
  117. Bhandari, P., A review of radioprotective plants. *Int J Green Pharm* 2013, 7, (2), 90.
  118. Monti, P.; Wysocki, J.; van der Meeren, A.; Griffiths, N. M., The contribution of radiation-induced injury to the gastrointestinal tract in the development of multi-organ dysfunction syndrome or failure. *The British J Radiol* 2005, Supplement\_27, (1), 89-94.
  119. Jackson, S. P.; Bartek, J., The DNA-damage response in human biology and disease. *Nature* 2009, 461, (7267), 1071-8.
  120. Citrin, D. E.; Mitchell, J. B., Mechanisms of normal tissue injury from irradiation. *Semin Radiat Oncol* 2017, 27, (4), 316-324.

- 
121. Moussa, L.; Usunier, B.; Demarquay, C.; Benderitter, M.; Tamarat, R.; Semont, A.; Mathieu, N., Bowel Radiation Injury: Complexity of the pathophysiology and promises of cell and tissue engineering. *Cell Transplant* 2016, 25, (10), 1723-1746.
  122. Lina Lu, W. L., Lihua Chen, Qiong Su, Yanbin Wang, Zhong Guo, Yongjuan Lu, BinLiu, Song Qin, Radiation-induced intestinal damage: latest molecular and clinical developments. *Future Oncol* 2019, 15, (35), 4105–4118.
  123. Brown, P. E., Mechanism of action of aminothioli radioprotectors. *Nature* 1967, 213, (5074), 363-364.
  124. Ueno, M.; Matsumoto, S.; Matsumoto, A.; Manda, S.; Nakanishi, I.; Matsumoto, K.-i.; Mitchell, J. B.; Krishna, M. C.; Anzai, K., Effect of amifostine, a radiation-protecting drug, on oxygen concentration in tissue measured by EPR oximetry and imaging. *J Clin Biochem and Nutrit* 2017, 60, (3), 151-155.
  125. Vassilis E. Kouloulias, J. R. K., Cytoprotective efficacy of amifostine against radiation-induced rectal toxicity: Objective and subjective grading scales for radiomucositis. *Molecules* 2008, 13, 892-903.
  126. Mun, G. I.; Kim, S.; Choi, E.; Kim, C. S.; Lee, Y. S., Pharmacology of natural radioprotectors. *Arch Pharm Res* 2018, 41, (11), 1033-1050.
  127. Rades, D.; Fehlauer, F.; Bajrovic, A.; Mahlmann, B.; Richter, E.; Alberti, W., Serious adverse effects of amifostine during radiotherapy in head and neck cancer patients. *Radiother Oncol* 2004, 70, (3), 261-4.
  128. Fahl WE, P. D., Copp RR. Amino thiol compounds and compositions for use in conjunction with cancer therapy. 2008.
  129. Soref, C. M.; Hacker, T. A.; Fahl, W. E., A new orally active, aminothiol radioprotector-free of nausea and hypotension side effects at its highest radioprotective doses. *Int J Radiat Oncol Biol Phys* 2012, 82, (5), e701-7.
  130. Weiss, J. F.; Landauer, M. R., Protection against ionizing radiation by antioxidant nutrients and phytochemicals. *Toxicology* 2003, 189, (1-2), 1-20.
  131. Lakshmi, S.; P.C. Kesavan, Protective effects of Vitamins C and E Against  $\gamma$ -ray-induced chromosomal damage in mouse. *Int J of Radiation Biol* 1993, 63, (6), 759-764
  132. Felemovicius, I.; Bonsack, M. E.; Baptista, M. L.; Delaney, J. P., Intestinal radioprotection

- 
- by vitamin E (alpha-tocopherol). *Ann Surg* 1995, 222, (4), 504-510.
133. Patil, S. L.; Rao, N. B.; Somashekarappa, H. M.; Rajashekhar, K. P., Antigenotoxic potential of rutin and quercetin in Swiss mice exposed to gamma radiation. *Biomed J* 2014, 37, (5), 305-13.
134. Wang, J.; Zhang, Y. Y.; Cheng, J.; Zhang, J. L.; Li, B. S., Preventive and therapeutic effects of quercetin on experimental radiation induced lung injury in mice. *Asian Pac J Cancer Prev* 2015, 16, (7), 2909-14.
135. Horton, J. A.; Li, F.; Chung, E. J.; Hudak, K.; White, A.; Krausz, K.; Gonzalez, F.; Citrin, D., Quercetin inhibits radiation-induced skin fibrosis. *Radiat Res* 2013, 180, (2), 205-15.
136. Bansal, P.; Paul, P.; Kunwar, A.; Jayakumar, S.; Nayak, P. G.; Priyadarsini, K. I.; Unnikrishnan, M. K., Radioprotection by quercetin-3-O-rutinoside, a flavonoid glycoside – A cellular and mechanistic approach. *J Funct Foods* 2012, 4, (4), 924-932.
137. Vasin, M. V., Comments on the mechanisms of action of radiation protective agents: basis components and their polyvalence. *SpringerPlus* 2014, 3, (1), 414.
138. Velpula, N.; Ugrappa, S.; Kodangal, S., A role of radioprotective agents in cancer therapeutics: a review. *Int J Basic & Clin Pharmacol* 2013, 2, (6), 677.
139. Dymond, A. W.; Howes, C.; Pattison, C.; So, K.; Mariani, G.; Savage, M.; Mair, S.; Ford, G.; Martin, P., Metabolism, excretion, and pharmacokinetics of selumetinib, an MEK1/2 inhibitor, in healthy adult male subjects. *Clin Ther* 2016, 38, (11), 2447-2458.
140. Han, X.; Mann, E.; Gilbert, S.; Guan, Y.; Steinbrecher, K. A.; Montrose, M. H.; Cohen, M. B., Loss of guanylyl cyclase C (GCC) signaling leads to dysfunctional intestinal barrier. *PLoS One* 2011, 6, (1), e16139.
141. David G. Kirsch; P. M. S.; Emmanuelle di Tomaso; Julie M. Sullivan; Wu-Shiun Hou; Talya Dayton; Laura B. Jeffords; Pooja Sodha; Kim L. Mercer; Rhianna Cohen; Osamu Takeuchi; Stanley J. Korsmeyer; Roderick T. Bronson; Carla F. Kim; Kevin M. Haigis; Rakesh K. Jain; Tyler Jacks, p53 controls radiation-induced gastrointestinal syndrome in mice independent of apoptosis. *Science* 2010, 327, 593-596.
142. Morita, A.; Takahashi, I.; Sasatani, M.; Aoki, S.; Wang, B.; Ariyasu, S.; Tanaka, K.; Yamaguchi, T.; Sawa, A.; Nishi, Y.; Teraoka, T.; Ujita, S.; Kawate, Y.; Yanagawa, C.; Tanimoto, K.; Enomoto, A.; Neno, M.; Kamiya, K.; Nagata, Y.; Hosoi, Y.; Inaba, T., A

- 
- chemical modulator of p53 transactivation that acts as a radioprotective agonist. *Mol Cancer Ther* 2018, 17, (2), 432-442.
143. Sullivan, J. M.; Jeffords, L. B.; Lee, C. L.; Rodrigues, R.; Ma, Y.; Kirsch, D. G., p21 protects "Super p53" mice from the radiation-induced gastrointestinal syndrome. *Radiat Res* 2012, 177, (3), 307-10.
144. Leibowitz, B. J.; Qiu, W.; Liu, H.; Cheng, T.; Zhang, L.; Yu, J., Uncoupling p53 functions in radiation-induced intestinal damage via PUMA and p21. *Mol Cancer Res* 2011, 9, (5), 616-25.
145. Paul H. Kussie; S. G.; Vincent Marechal; Brian Elenbaas; Jacque Moreau; Arnold J. Levine; Nikola P. Pavletich, Structure of the MDM2 oncoprotein bound to the p53 tumor suppressor transactivation domain. *Science* 1996, 274, 948-953.
146. Qiu, W.; Carson-Walter, E. B.; Liu, H.; Epperly, M.; Greenberger, J. S.; Zambetti, G. P.; Zhang, L.; Yu, J., PUMA regulates intestinal progenitor cell radiosensitivity and gastrointestinal syndrome. *Cell Stem Cell* 2008, 2, (6), 576-83.
147. Anita J. Merritt; C. S. P.; Christopher J. Kemp; John A. Hickman; Allan Balmain; David P. Lane; Peter A. Hall, The role of p53 in spontaneous and radiation-induced apoptosis in the gastrointestinal tract of normal and p53-deficient mice. *Cancer Res* 1994, 54, 614-617.
148. Sun, X.; Wang, Q.; Wang, Y.; Du, L.; Xu, C.; Liu, Q., Brusatol enhances the radiosensitivity of A549 cells by promoting ROS production and enhancing DNA damage. *Int J Mol Sci* 2016, 17, (7).

---

## 2. CHAPTER 2: DESIGN, SYNTHESIS, AND CHARACTERIZATION OF A BENZOXAZOLE COMPOUND AS A NOVEL POTENTIAL MEK INHIBITOR

This study was published in *International Journal of Cancer*, Year 2019, Vol. 145, Pages 586-596.

---

## 2.1. Abstract

The RAS/RAF/MEK/ERK pathway plays a key role in regulating cell proliferation and apoptosis. This pathway is deregulated in approximately one third malignant tumors. Mutations in RAS/RAF occur in a large portion of malignancies and are associated with aggressive clinical behaviors of tumors and poor prognosis. Existing MEK inhibitors show either unsatisfactory potency or poor PK profiles. For example, the potency of AZD6244 is unsatisfactory, likely causing the failure of a Randomized Clinical Trial for the KRAS-mutant NSCLC. Potencies of MEK162, GDC0973, and REDA119 are similarly low. GSK212 has a poor PK profile with drug accumulation. To improve the clinical application potential for the treatment of RAS/RAF mutant cancers, benzoxazole derivatives with improved potencies and good PK profiles need to be developed. Therefore, the aim of this research was to develop a novel, highly potent and selective MEK 1/2 inhibitor. Based on previously reported X-ray structure, AZD6244 was chosen as the lead compound. Efforts focused on producing derivatives of AZD6244 with enhanced activity whilst also overcoming existing PK shortcomings.

Based on the binding mode, the molecular structure of AZD6244 was modified by replacing the N-methyl in the benzoheterocyclic ring of AZD6244 with an O atom, and replacing the –Cl and –Br substituent on the aniline with –F and –I, respectively. A new benzoxazole derivative with a new core structure, designated as KZ-001, was obtained. After retrosynthesis analysis, a consecutive 10-step reaction synthesis route was designed. Consequently, KZ-001 was synthesized and purified herein with overall product yield rate of 11.0%. The structures of key intermediates and target compound KZ-001 were characterized by <sup>1</sup>HNMR, <sup>13</sup>CNMR, MS, HRMS, and HPLC. Based on structure overlays with AZD6244 and the co-crystal structure of MEK1, a similar binding mode with the same key binding site on MEK1 was postulated, suggesting that KZ-001 would also act as MEK inhibitor with potentially enhanced activity.

## 2.2. Introduction

### 2.2.1 Cancer and RAS/RAF/MEK/ERK signaling pathway

Cancer is expected to rank as the leading cause of death and major barrier to increasing life expectancy around the world. Incidence and lethality rates show an increasing global trend. The Global Cancer Statistics 2018 estimated 18.1 million new cancer diagnoses and 9.6 million cancer death. In China, cancer rate increased by an estimated 4.1 million new cases and 2.6 million malignancy-induced death [1]. This represents an increasing financial burden with 147.3 billion US dollars (USD) spent on cancer care in 2017 in the USA. The costs are expected to increase to around 173 billion USD by 2020, due to cancer prevalence and an increasing ageing population [2].

---

The RAS/RAF/MEK/ERK signaling pathway (also named mitogen-activated protein kinase pathway, MAPK) plays a critical role in the pathogenesis of human cancer, and is one of the most frequently dysregulated signaling cascades in human cancer [3, 4]. In this pathway, recruitment of RAS to the plasma membrane leads to phosphorylation of RAF and activation of MEK 1/2, which are dual specificity protein kinases that phosphorylate serine/threonine and tyrosine residues, respectively. The MEK kinases in turn phosphorylate and activate their only currently known substrates, ERK 1/2 (extracellular signal-regulated kinases). Consequently, this signaling pathway promotes cell proliferation, cell survival and metastasis [5]. Particularly, the RAS/RAF/MEK/ERK pathway is frequently dysregulated in malignant tumors with a large fraction of tumors harboring RAS or RAF mutations resulting in constitutive activation of the pathway [5]. That is, the aberrant activation of MAPK pathway commonly occurs through gain-of-function mutations in genes encoding RAS and RAF family members [4].

Approximately one-third of all human cancers have RAS gene activating mutations, including carcinomas of the lung (30%), colon (50%) and pancreas (90%), thyroid (50%), and melanoma (25%) [5, 6]. There are three types of human RAS genes [Neuroblastoma RAS viral (v-ras) oncogene homolog (NRAS)], Kirsten rat sarcoma viral oncogene homolog (KRAS), and Harvey rat sarcoma viral oncogene homolog (HRAS). NRAS mutations are found in 15-20% of melanoma. Moreover, NRAS-mutant melanomas are more aggressive and associated with poorer outcomes, compared to non-NRAS-mutant subtypes of melanoma [7]. KRAS is inactive in the GDP-bound state and activity is closely regulated by GTPase-activating proteins (GAP) and guanine nucleotide exchange-factors (GEFs) in normal cells. KRAS mutations are present in approximately 30% of all cancers, with an especially high prevalence in lung cancer, colon cancer, and pancreatic cancer [8].

The RAF family includes ARAF, BRAF and CRAF (The latter is encoded by *RAF-1*). Activated RAS binding to RAF leads to the formation of RAF homodimers (i.e. CRAF-CRAF) or heterodimers (i.e. BRAF-CRAF) resulting in activated RAF kinase activity [9]. Mutation of BRAF is present in 7-10% of all human cancers, while mutated forms of ARAF and CRAF are extremely rare [9]. Typically, activating RAS- and BRAF-mutations are mutually exclusive in cancers [10].

MEK1 and MEK2 are dual-specificity protein kinases that phosphorylate downstream ERK on specific tyrosine and threonine residues. MEK1, which is coded by gene *MAP2K1* located on chromosome 15q22.31, is the prototype member of MEK family proteins. MEK 2 is encoded by the gene *MAP2K2* on chromosome 19p13.3. MEK1 and MEK2 are highly homologous, both of them comprising a kinase domain, a MAPK docking region, and a negative-regulatory region [4].

---

The x-ray structures of MEK1 and MEK2 reveal that each of them has a unique inhibitor-binding pocket adjacent to the MgATP-binding site. MEK1 and MEK2 share 79% amino acid identity, and are equally competent to phosphorylate ERK substrate [11]. MEK1 is activated by the phosphorylation of S218 and S222 in its activation segment which is catalyzed by RAF kinases [12]. Potent MEK inhibitors induce several conformational changes in the unphosphorylated MEK1 and MEK2 enzymes that lock them into closed, catalytically inactive forms. Although MEK1/2 is not frequently mutated, high incidence of elevated phospho-ERK1/2 in cancer tissues reflects the multiple upstream events that can lead to the increased activity of MEK1/2 [13].

As MEK is a common effector downstream of both wild-type and mutant RAF inhibitors, MEK inhibitors have the potential to target all tumors associated with MAPK pathway signaling [14].

### **2.2.2 Current progress with molecular structures of MEK inhibitors**

In the past few years, great progress has been achieved with the development of a number of MEK inhibitors [15]. During the MEK inhibitor development history, CI-1040 was the first MEK inhibitor run at the clinical stage by Pfizer/Warner-Lambert [16]. This compound represented a novel series of benzhydroxamate esters derived from their precursor anthranilic acids, which are also MEK inhibitors. Efficacy was limited, however, due to poor solubility and rapid clearance, consequently leading to insufficient antitumor activity in two phase II studies completed in 2003 [17]. Optimization of the hydroxamate side chain of CI-1040 improved solubility and exposure for oral doses and contributed to the discovery of the PD-0325901 by Pfizer/Warner-Lambert. Due to the BBB (Blood Brain Barrier) penetration and neurological side effects observed in patients associated with the PD-0325901, some optimization efforts were conducted which consequently lead to the discovery of the GDC-0973 (cobimetinib, approved by FDA in 2015) [18], but the activity was not prominent. Simultaneously a new series of benzimidazole compound AZD6244 (selumetinib) was designed by Array BioPharma on the basis of the PD-0325901; by utilizing 4-N to replace the 4-F, H-receptor function was retained as well as BBB penetration was avoided, but the potency decreased. Another compound MEK162 (binimetinib, approved by FDA in 2018) has the same core structure as AZD6244 and the potency is similar to AZD6244. Recently, the AZD8330, whose core structure is 6-oxo-1,6-dihydropyridazine, a different class of MEK inhibitors, was developed. This compound, however, passes the BBB which leads to central nervous system (CNS) toxicity. After some efforts to enhance activity as well as preventing BBB penetration, GSK212 (trametinib, approved by FDA in 2013) was developed, but solubility was poor and the drug accumulated.

Structure analyses of MEK inhibitors yield valuable insights into their characteristics. For the compound GDC0973 (cobimetinib), the interaction force of F- in the benzene ring as the H-acceptor

---

is too weak, resulting in unsatisfactory potency. The compound GSK212 shows high potency, but poor solubility, and needs DMSO as a co-solvent, leading to drug accumulation and high toxicity. Moreover, Tarik Silk et al. reported that MEK inhibitors interfere with MEK signaling efficiently in T-cell as well as macrophages, and pulsatile treatment of MEK inhibitors resulted in increased viability of classically differentiated macrophages compared to continuous treatment [19]. Therefore, the core structure of GSK212 (estimated elimination half-life is 3.9 to 4.8 days with drug accumulation) is not beneficial for combinational treatment with immunotherapy. Conversely, AZD6244 and MEK162, two similar compounds, possess good PK profile without drug accumulation issues which may be beneficial for combination treatment with immunotherapy, but activity needs to improve.

AZD6244 is a highly selective MEK1 inhibitor with an  $IC_{50}$  (50% inhibition concentration) of 14 nM for purified MEK1 [13], as well as has been extensively studied both pre-clinically and clinically. AZD6244 is a benzimidazole derivative that inhibits tumor growth in various xenograft models, including HT-29, BxPC3, Calu-6, A375, Colo-205, and SW-620 [13, 20, 21]. However, one randomized clinical trial that evaluated combination treatment with the MEK inhibitor selumetinib (AZD6244) and chemotherapy (selumetinib and docetaxel) showed no additional benefit based on progression-free survival compared to docetaxel alone [22, 23]. One of the reasons might be associated with the low efficacy of the compound.

As a result, this research aimed to enhance the activity of the existing MEK inhibitors to develop activity-improved new MEK inhibitors.

After analyzing the core structure characteristics of common MEK inhibitors, based on the advantageous core structure class of the compound AZD6244, it was chosen as a lead compound. Binding mode investigations indicated that a large substituent group on the 3-nitrogen may be responsible for unsatisfactory potency of AZD6244. In addition, enzyme-mediated de-methylation of the 3-nitrogen methyl of AZD6244 occurs *in vivo* [24]. As a result, efforts were focused on circumventing the shortcomings of the molecular structure of AZD6244, aiming to enhance the activity of novel derivatives of existing MEK inhibitors. Synthesis efforts resulted in the design of a new MEK inhibitor derived through the modification of the structure of AZD6244. The synthesis route was designed, and the new compound was synthesized and characterized.

## **2.3. Material and methods**

### **2.3.1. Chemistry**

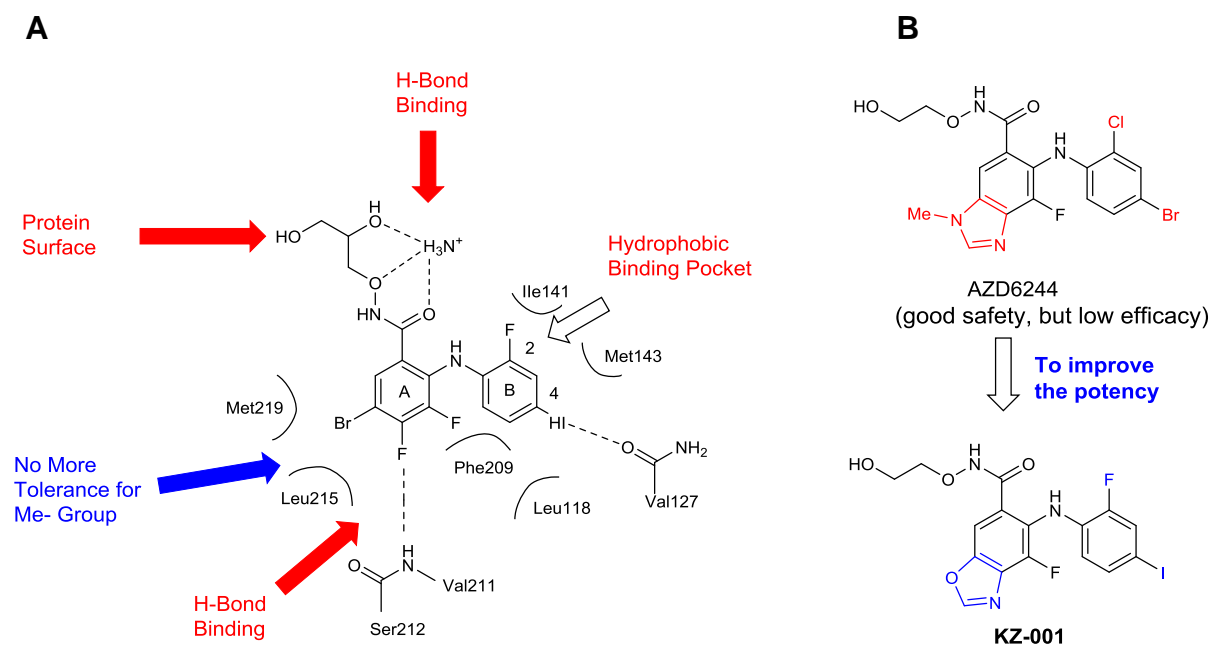
---

2,3,4-trifluorophenol and 2-fluoroaniline were purchased from Energy Chemical. The reactions were monitored by thin layer chromatography, which was performed on commercially available Sanpoint precoated plates (silicagel GF254, 0.25mm). Organic solvents were evaporated using rotary evaporator. NMR ( $^1\text{H}$  and  $^{13}\text{C}$ ) spectra were recorded on a Bruker AVANCE (400MHz, 101MHz) spectrophotometer using deuterated reagent as a solvent. HRM-MS (high resolution mass spectra) were recorded on an AB SCIEX TripleTOF® 4600 System (SCIEX, Canada). Analyses were performed on a Agilent 1260 Infinity HPLCs system equipped with a reverse phase C18, Inertsil column (5  $\mu\text{m}$ , 4.6\*250 mm column)

### 2.3.2. Design of KZ-001

Based on known MEK inhibitors, the representative generic structure is the substituted biarylamine with the A- and B-rings (Figure 2-1 .A). Previously reported X-ray structures indicated that there are several key interactions between the MEK inhibitor and the allosteric pocket [14, 16, 25-29]. 1). The lipophilic B-ring of the inhibitor forms numerous van der Waal interactions within a deep hydrophobic pocket and also forms a critical edge-to-face aromatic interaction with Phe209; 2). An important electrostatic interaction is formed between the backbone carbonyl oxygen of Val127 and the 4-iodine atom on the B-ring in the kinase hinge region; 3). A critical hydrogen bond interaction is formed between the 4-fluoro of the inhibitor A-ring and the backbone amide of Ser212 [27]; 4). A halo substituent at the 4 position of A-ring, in particular a fluorine atom, was optimal. The fluorine has a dipolar interaction with the Ser212 amide backbone hydrogen in the MEK1 structure [16].

Hence, based on the binding mode, AZD6244 was modified by replacing the N-methyl in the benzoheterocyclic ring with an O atom, and replacing the -Cl and -Br substituent on the aniline with -F and -I, respectively. This compound has a new core structure (Figure 2-1 B).



### 2.3.3. Synthesis route of KZ-001

Based on retrosynthesis analysis, the desired 4-fluoro-5-((2-fluoro-4-iodophenyl)amino)-N-(2-hydroxyethoxy)benzo[d]oxazole-6-carboxamide (KZ-001) was synthesized following the route outlined in Figure 2-2. Briefly, commercially available 2,3,4-trifluorophenol was initially converted into **2**. Metalation with lithium diisopropylamide (LDA) was performed, which was then added into dry ice followed by HCl quenching, yielding **3**. Treatment of **3** with 2-fluoroaniline, using lithium hexamethyldisilamide (LHMDS) as a base, resulted in SNAr displacement at a low temperature, which yielded compound **4**. Subsequent reaction with benzyl bromide provided **5**. Azide reaction with sodium azide gave **6** which was then subjected to hydrogenation catalyzed by Pd/C to give **7**. Cyclization of **7** gave benzoxazole **8**, and iodination by NIS (N-iodosuccinimide) provided **9**. Installation of the hydroxamate side-chain was achieved by condensation reaction with O-(2-(vinylloxy)ethyl) hydroxylamine followed by acid-mediated deprotection.

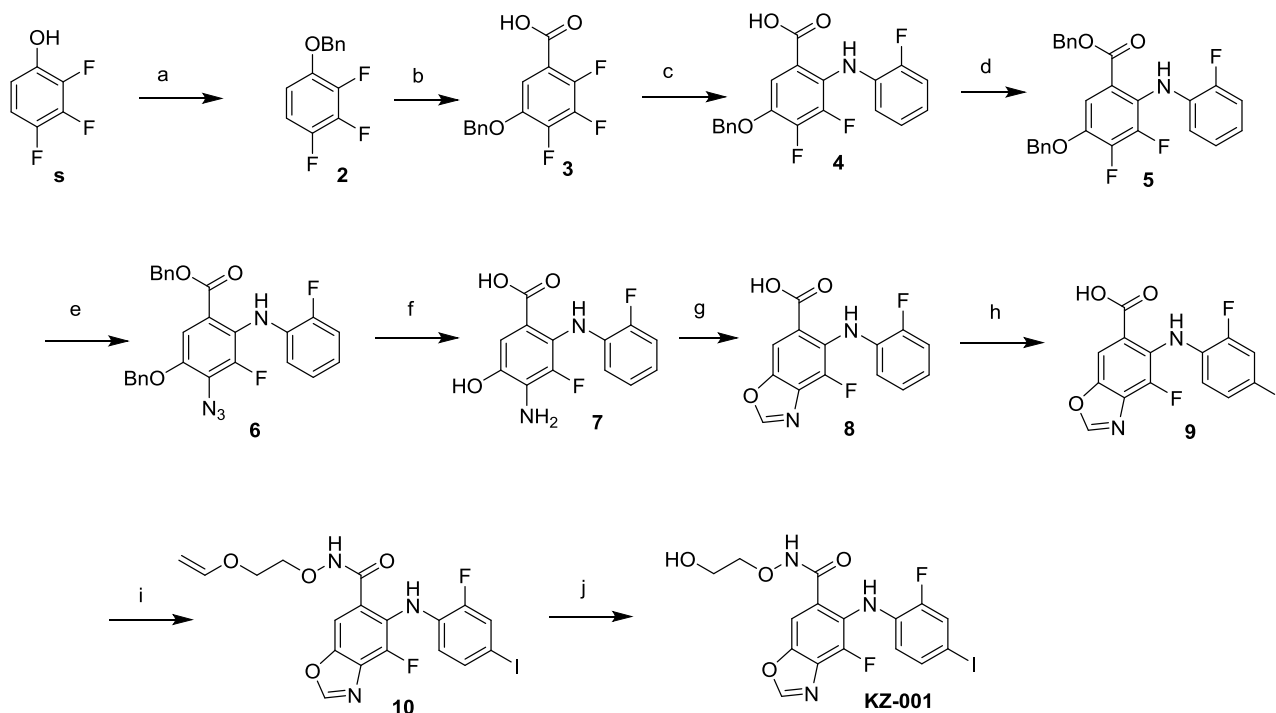
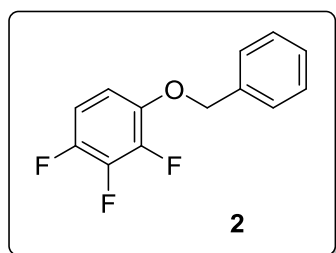


**Figure 2-2 Synthesis route of KZ-001**

**Reagents and condition:** (a). BnBr, Na<sub>2</sub>CO<sub>3</sub>, acetone, 50 °C, 24 h; (b). i) n-BuLi, DIPEA, Tetrahydrofuran, N<sub>2</sub>, -78 °C, 1h; ii) N<sub>2</sub>, -78 °C, 1 h; iii) dry ice, rt., overnight; iv) HCl, pH 1 — 2; (c) i) 2-fluoroaniline, LiHMDS, Tetrahydrofuran, -78 °C to rt., overnight, ii) 10% HCl, pH 2 — 3; (d) BnBr, KHCO<sub>3</sub>, N,N-dimethylformamide, rt., 5 h; (e) NaN<sub>3</sub>, N,N-dimethylformamide, 90 °C, 3 h, (f) 10% Pd/C, H<sub>2</sub>, Methanol, 3 h; (g) trimethyl orthoformate, p-TsOH, 1 h.

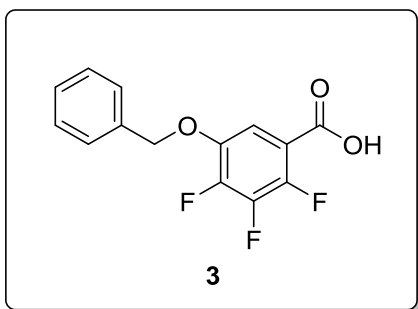
### 2.3.4. Preparation of KZ-001

#### Step 1: Synthesis of 1-(benzyloxy)-2,3,4-trifluorobenzene (2)



Sodium carbonate (19.50 g, 183.96 mmol) was dispersed into a solution of 2,3,4-trifluorophenol (13.64 g, 92.10 mmol) in acetone (300 mL). Benzyl bromide (17.31 g, 101.21 mmol) was added dropwise to the stirred suspension. The mixture was heated under reflux at 50°C for 24 h. Then the acetone was removed under reduced pressure and the resultant residue was dissolved in water (300 mL). The solution was extracted with ethyl acetate (100 mL x 2). The combined organic extracts were washed with 5% sodium hydroxide (100 mL) and brine (100 mL) sequentially and dried over Na<sub>2</sub>SO<sub>4</sub>. The solvent was removed in vacuo to yield a pale yellow solid. 19.89 g of pale yellow solid was obtained (yield: 90.7%). <sup>1</sup>H NMR (400 MHz, CDCl<sub>3</sub>): δ 7.43 – 7.30 (m, 5H), 6.87 – 6.77 (m, 1H), 6.72 – 6.63 (m, 1H), 5.10 (s, 2H).

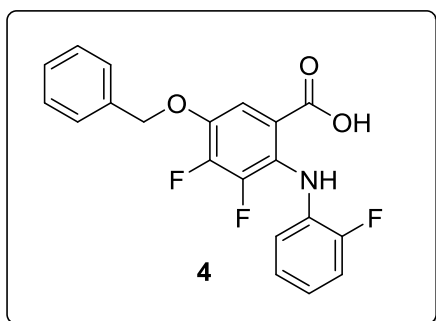
### Step 2: Synthesis of 5-(benzyloxy)-2,3,4-trifluorobenzoic acid (3)



n-BuLi (40.08 mL, 2.5 M in hexane, 100.20 mmol) was added dropwise to a solution of diisopropylamine (10.14 g, 100.20 mmol) in THF (100 mL) at -78 °C under nitrogen. The stirring was maintained at this temperature for 1 h. Then a solution of 1-(benzyloxy)-2,3,4-trifluorobenzene (19.89 g, 83.50 mmol) in THF (120 mL) was added. After stirring for 1 h at -78 °C, the

mixture was transferred to a bottle containing dry ice and stirred overnight at room temperature. The reaction was quenched with 10% aqueous HCl and pH was adjusted to 1 — 2. The mixture was extracted with ethyl acetate (100 mL x 3). The combined organic extracts were washed with water (100 mL) and brine (100 mL) sequentially, dried over Na<sub>2</sub>SO<sub>4</sub>, filtered and concentrated under reduced pressure to afford the desired product. 19.33 g of a white solid was obtained (yield: 82%). <sup>1</sup>H NMR (400 MHz, CDCl<sub>3</sub>): δ 7.42 (m, 6H), 5.14 (s, 2H).

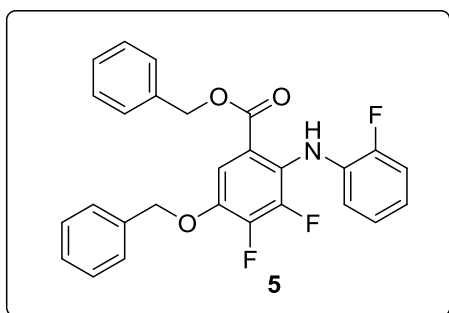
### Step 3: Synthesis of 5-benzyloxy-3,4-difluoro-2-((2-fluorophenyl)amino)benzoic acid (4)



LiHMDS (205.5 mL, 1 M in THF, 205.50 mmol) was added to a solution of 2-fluoroaniline (15.23 g, 137 mmol) and 5-benzyloxy-2,3,4-trifluorobenzoic acid (19.33 g, 68.50 mmol) in THF (120 mL) at -78 °C. The mixture was allowed to slowly warm to room temperature and stirred at this temperature overnight. The reaction was quenched with water (100 mL) and

acidified to pH 2—3 with 10% HCl (aq.). The aqueous layer was extracted with ethyl acetate (100 mL x 3). The combined organic extracts were washed with water (100 mL) and brine (100 mL) sequentially, dried over Na<sub>2</sub>SO<sub>4</sub>, filtered and concentrated in vacuo to afford the desired product (pale yellow solid, 19.17 g, 75% yield). <sup>1</sup>H NMR (400 MHz, DMSO- d<sub>6</sub>): δ 13.76 (s, 1H), 8.58 (s, 1H), 7.61 (dd, *J* = 8.8, 1.7 Hz, 1H), 7.44 (m, 5H), 7.20 (m, 1H), 7.05 (m, 1H), 6.90 (m, 2H), 5.26 (s, 2H). MS (ESI, pos ion) *m/z*: 374.1.

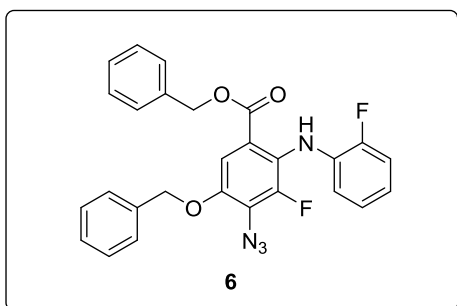
### Step 4: Synthesis of benzyl 5-benzyloxy-3,4-difluoro-2-((2-fluorophenyl) amino) benzoate (5)



Potassium bicarbonate (6.16 g, 61.62 mmol) followed by benzyl bromide (6.2 mL, 51.41 mmol) was added to a solution of 5-benzyloxy-3,4-difluoro-2-((2-fluorophenyl) amino) benzoic acid (19.17 g, 51.35 mmol) in DMF (150 mL). The mixture was

stirred for 5 h at room temperature and water was added. The solution was extracted with ethyl acetate (100 mL x 3). The combined organic extracts were washed with water (100 mL) and brine (100 mL) sequentially, dried over Na<sub>2</sub>SO<sub>4</sub>, filtered and concentrated in vacuo. After purification by column chromatography on silica gel (petroleum ether / ethyl acetate, 50:1, v/v), the corresponding product was obtained as a white solid (21.42 g, 90% yield). <sup>1</sup>H NMR (400 MHz, CDCl<sub>3</sub>): δ 8.51 (s, 1H), 7.51 (dd, *J* = 8.5, 2.1 Hz, 1H), 7.41 (m, 10H), 7.09 (m, 1H), 7.03 (m, 1H), 6.94 (m, 1H), 6.85 (m, 1H), 5.33 (s, 2H), 5.15 (s, 2H).

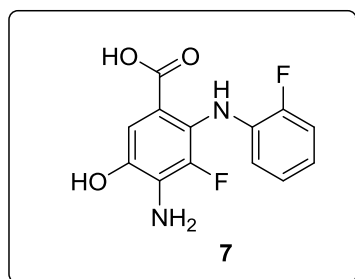
#### Step 5: Synthesis of benzyl 4-azido-5-benzyloxy-3-fluoro-2-((2-fluorophenyl) amino)benzoate (6)



NaN<sub>3</sub> (3.61 g, 55.46 mmol) was added to a solution of benzyl 5-benzyloxy-3,4-difluoro-2-((2-fluoro-phenyl)amino) benzoate (21.42 g, 46.22 mmol) in DMF (150 mL). The mixture was stirred at 90°C for 3 h. Then water (300 mL) was added. The solution was extracted with ethyl acetate (100 mL x 3). The combined organic extracts were washed with water (100 mL)

and brine (100 mL), dried over Na<sub>2</sub>SO<sub>4</sub> and concentrated in vacuo. The residue was purified by flash column chromatography on silica gel (petroleum ether/ethyl acetate, 50:1, v/v) and gave the desired product (pale yellow solid, 14.63 g, 65% yield). <sup>1</sup>H NMR (400 MHz, CDCl<sub>3</sub>): δ 8.45 (s, 1H), 7.49 (s, 1H), 7.39 (m, 10H), 7.07 (m, 1H), 7.04 (m, 1H), 6.90 (m, 1H), 6.83 (m, 1H), 5.31 (s, 2H), 5.13 (s, 2H).

#### Step 6: Synthesis of 4-amino-3-fluoro-2-((2-fluorophenyl)amino)-5-hydroxy benzoic acid (7)

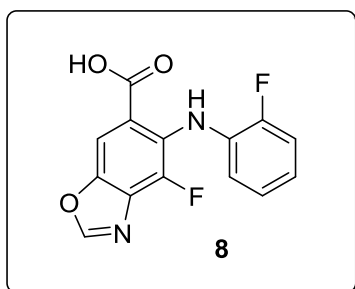


10% palladium on carbon (2.55 g) was added to a solution of benzyl 4-azido-5-benzyloxy-3-fluoro-2-((2-fluoro-phenyl)amino) benzoate (14.63 g, 30.07 mmol) in MeOH (200 mL) under nitrogen atmosphere. Then the nitrogen atmosphere was completely changed to a hydrogen atmosphere. The mixture was stirred for 3 h at ambient temperature. After the insoluble matter was filtered off, the solvent

was concentrated in vacuo to give the desired product, which was used directly in the next step without further purification. MS (ESI, pos ion) *m/z*: 281.1 (M+1).

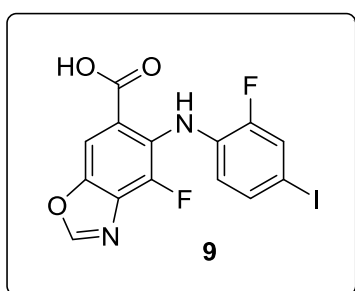
#### Step 7: Synthesis of 4-fluoro-5-((2-fluorophenyl)amino)benzo[d]oxazole-6-carboxylic acid (8)

*p*-TsOH (0.23 g, 1.35 mmol) was added to a solution of 4-amino-3-fluoro-2-((2-fluorophenyl)amino)-5-hydroxy benzoic acid (7.58 g, 27.05 mmol) in



trimethyl orthoformate (50 mL). The reaction mixture was stirred for 1 h and treated with water (200 mL). The resultant precipitate was filtered off and the filter cake was washed with water to afford the desired product (7.22 g, 82.7% yield for two steps).  $^1\text{H NMR}$  (400 MHz, DMSO- $d_6$ )  $\delta$  13.80 (s, 1H), 8.98 (s, 1H), 8.68 (s, 1H), 8.20 (s, 1H), 7.21 (dt,  $J = 21.0, 10.5$  Hz, 1H), 7.04 (t,  $J = 7.6$  Hz, 1H), 6.90 (dd,  $J = 12.8, 7.1$  Hz, 1H), 6.80 (dd,  $J = 13.6, 8.0$  Hz, 1H). MS (ESI, pos ion)  $m/z$ : 291.1 ( $M+1$ ).

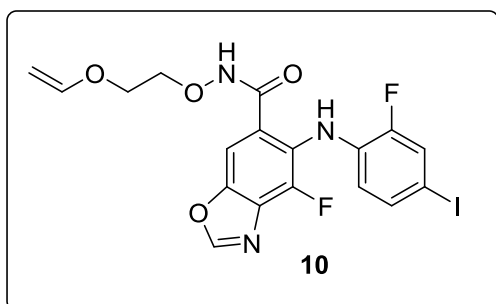
### Step 8: Synthesis of 4-fluoro-5-((2-fluoro-4-iodophenyl)amino)benzo[d]oxazole-6-carboxylic acid (9)



N-Iodosuccinimide (6.08 g, 26.37 mmol) was added to a solution of 4-fluoro-5-((2-fluorophenyl)amino)benzo[d]oxazole-6-carboxylic acid (7.22 g, 24.88 mmol) in DMF (50 mL), followed by trifluoroacetic acid (1.0 mL). After stirring for 5 h at ambient temperature, the reaction was quenched with saturated  $\text{NH}_4\text{Cl}$  (aq.). The solution was extracted with ethyl acetate (150 mL x 3). The combined organic extracts were

washed with water (100 mL) and brine (100 mL) successively, dried over  $\text{Na}_2\text{SO}_4$  and concentrated in vacuo. The crude product was purified by column chromatography on silica gel ( $\text{CH}_2\text{Cl}_2/\text{MeOH}$ , 50:1, v/v) and gave the desired product (brown solid, 6.34g, 61.2% yield).  $^1\text{H NMR}$  (400 MHz, DMSO- $d_6$ ):  $\delta$  8.97 (s, 1H), 8.58 (s, 1H), 8.18 (s, 1H), 7.58 (dd,  $J = 11.0, 1.7$  Hz, 1H), 7.34 (d,  $J = 8.5$  Hz, 1H), 6.55 (m, 1H).

### Step 9: Synthesis of 4-fluoro-5-((2-fluoro-4-iodophenyl)amino)-N-(2-(vinylloxy) ethoxy)benzo[d]oxazole-6-carboxamide (10)

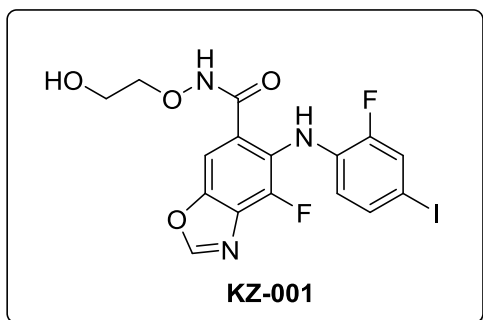


HOBt (254 mg, 1.63 mmol) and EDCI (314 mg, 1.63 mmol) was added to a solution of 4-fluoro-5-((2-fluoro-4-iodophenyl)amino)benzo[d]oxazole-6-carboxylic acid (500 mg, 1.2 mmol) in  $\text{CH}_2\text{Cl}_2$  (10 mL). The mixture was stirred for 1 h and O-(2-(vinylloxy)ethyl) hydroxylamine (172 mg, 1.62 mmol) was added. After stirring for 4 h at ambient temperature, the reaction was

treated with saturated  $\text{NH}_4\text{Cl}$  (aq.). The resultant mixture was extracted with  $\text{CH}_2\text{Cl}_2$  (30 mL x 3). The combined organic extracts were washed with water (30 mL) and brine (30 mL), dried over  $\text{Na}_2\text{SO}_4$ , filtered and concentrated in vacuo. The crude product was purified by column chromatography on silica gel ( $\text{CH}_2\text{Cl}_2/\text{MeOH}$ , 100:1, v/v) and gave the desired product (white solid, 450 mg, 74.8% yield).  $^1\text{H NMR}$  (400 MHz,  $\text{CD}_3\text{OD}$ ):  $\delta$  11.59 (s, 1H), 8.34 (s, 1H), 7.71 (s, 1H), 7.37

– 7.24 (m, 1H), 7.23 – 7.12 (m, 1H), 6.45 – 6.27 (m, 2H), 4.09 (ddd,  $J = 21.2, 14.1, 4.5$  Hz, 3H), 4.02 – 3.92 (m, 2H), 3.84 (s, 2H).

### Step 10: Synthesis of 4-fluoro-5-((2-fluoro-4-iodophenyl)amino)-N-(2-hydroxy ethoxy)benzo[d]oxazole-6-carboxamide (KZ-001)



1.0 N HCl (aq., 6.7 mL, 6.72 mmol) was added to a solution of compound 4-fluoro-5-((2-fluoro-4-iodophenyl)amino)-N-(2-(vinylloxy)ethoxy)benzo[d]oxazole-6-carboxamide (450 mg, 0.9 mmol) in CH<sub>2</sub>Cl<sub>2</sub> (10 mL). After stirring for 1 h, the reaction mixture was washed with saturated NaHCO<sub>3</sub> (aq.). The aqueous layer was washed with CH<sub>2</sub>Cl<sub>2</sub> (10 mL x 2). The combined organic layer was washed with water (10 mL)

and brine (10 mL), dried over Na<sub>2</sub>SO<sub>4</sub>, filtered and concentrated in vacuo. The crude product was purified by column chromatography on silica gel (CH<sub>2</sub>Cl<sub>2</sub>/MeOH, 50:1, v/v) and gave the desired product (white solid, 380 mg, 88.9% yield).

## 2.4. Results and discussion

### 2.4.1. KZ-001 as a new MEK inhibitor with a new core structure

Taking AZD6244 as a lead compound, its structure was modified based on the binding mode with MEK, resulting in discovery of compound KZ-001, a novel MEK inhibitor with a new core structure, which represents a new benzoxazole compound. KZ-001 contains an O- atom with smaller steric hindrance than the N-methyl group of AZD6244, but fits the hinge of Met219 and Leu215 better, resulting in enhanced kinase inhibition. The N- atom on 4-position of the A ring was kept as the H-bond receptor to maintain binding to the pocket. Moreover, the substitution of -Br in the B ring with -I on the lipophilic ring of KZ-001 should facilitate the formation of an important electrostatic interaction with the backbone carbonyl oxygen of Val127 base on reported SAR analysis.

### 2.4.2. Binding mode of KZ-001

In order to predict the affinity of the new compound KZ-001 for MEK1, based on the published X-ray structure of AZD6244 with MEK1 (PDB code: 4U7Z), a model of KZ-001 interacting with MEK1 was made and the predicted binding mode was compared to that of AZD6244 (Figure 2-3). The binding mode model shows that the two inhibitors bind in a similar orientation with MEK1. The key binding sites of KZ-001 were retained. Firstly, the N atom of KZ-001 on the oxazole ring forms

a hydrogen-bond interaction with backbone amide S212, which is the same as for AZD6244. Secondly, the iodine atom of KZ-001 on the lipophilic ring forms an electrostatic interaction with Val127, and forms a critical edge-to-face aromatic interaction with Phe209 not present in AZD6244, which could be beneficial for inhibitory activity. Like AZD6244, the side chain of KZ-001 provides a hydrogen bond acceptor for Lys97.

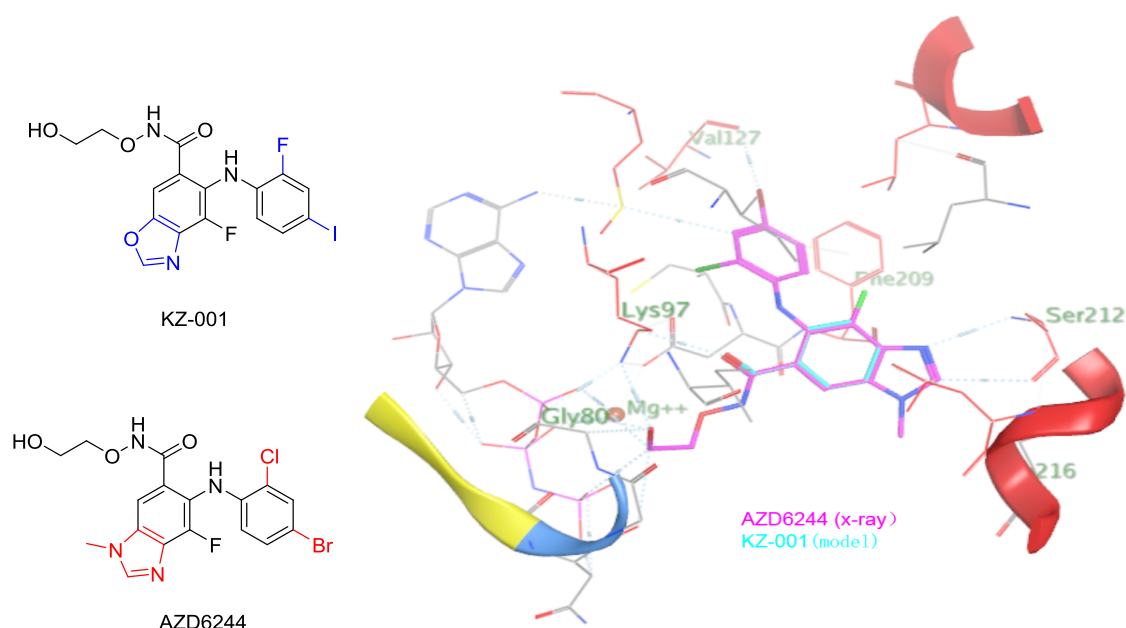


**Figure 2-3 KZ-001 structure overlay with AZD6244 with the co-crystal structure of MEK1 (PDB code: 4U7Z) as the model.** KZ-001 shows similar binding mode with MEK1, and binds to the important binding site of MEK1 kinase.

### 2.4.3. Characterization of KZ-001

The structure of the new compounds KZ-001 was firstly identified with  $^1\text{H}$  NMR spectra by the chemical shift.  $^1\text{H}$  NMR (400 MHz, DMSO):  $\delta$  11.76 (s, 1H), 8.96 (s, 1H), 8.01 (s, 1H), 7.88 (s, 1H), 7.53 (d,  $J = 9.7$  Hz, 1H), 7.28 (d,  $J = 8.6$  Hz, 1H), 6.37 (tt,  $J = 41.3, 20.6$  Hz, 1H), 4.71 (s, 1H), 3.89 – 3.72 (m, 2H), 3.57 (t,  $J = 11.4$  Hz, 2H). The  $^1\text{H}$  NMR spectrum is presented in the Figure 2-4.

Then the structure was further confirmed by  $^{13}\text{C}$  NMR spectra.  $^{13}\text{C}$  NMR (100 MHz, DMSO)  $\delta$  164.30 (s), 157.37 (s), 153.17 (s), 150.73 (s), 149.34 (s), 147.93 (d,  $J = 7.0$  Hz), 146.78 (s), 135.97 – 132.14 (m), 131.23 (d,  $J = 15.6$  Hz), 127.79 (s), 124.18 (dd,  $J = 64.7, 15.5$  Hz), 117.78 (s), 108.03 (s), 79.49 (d,  $J = 7.1$  Hz), 77.81 (s), 59.11 (s). The  $^{13}\text{C}$  NMR spectrum is presented in the Figure 2-5.

The mass spectrum and high resolution mass spectrum were used to determine the molecular weight. HRMS APCI (+)  $m/z$  ( $M^+ + H$ ), calculated: 476.19, observed: 475.9965 (Figure 2-6 and

Figure 2-7). The purity was determined by HPLC which showed 95.9% purity (Figure 2-8).

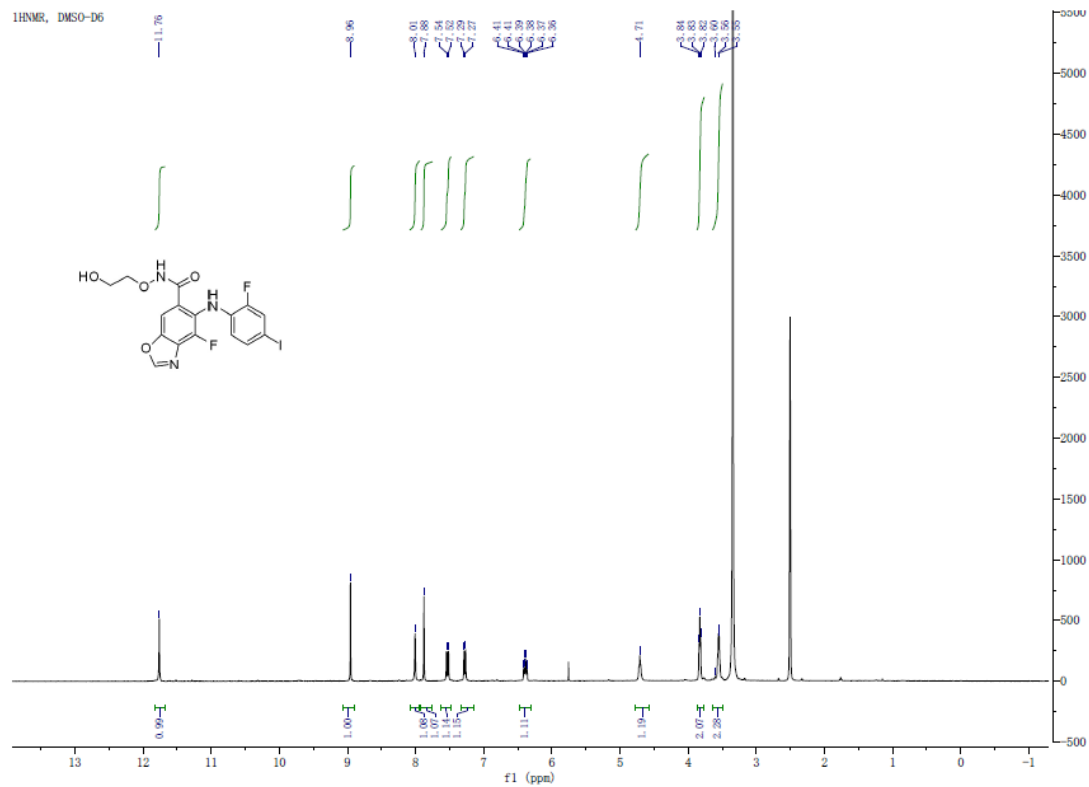


Figure 2-4 <sup>1</sup>H NMR spectrum of KZ-001

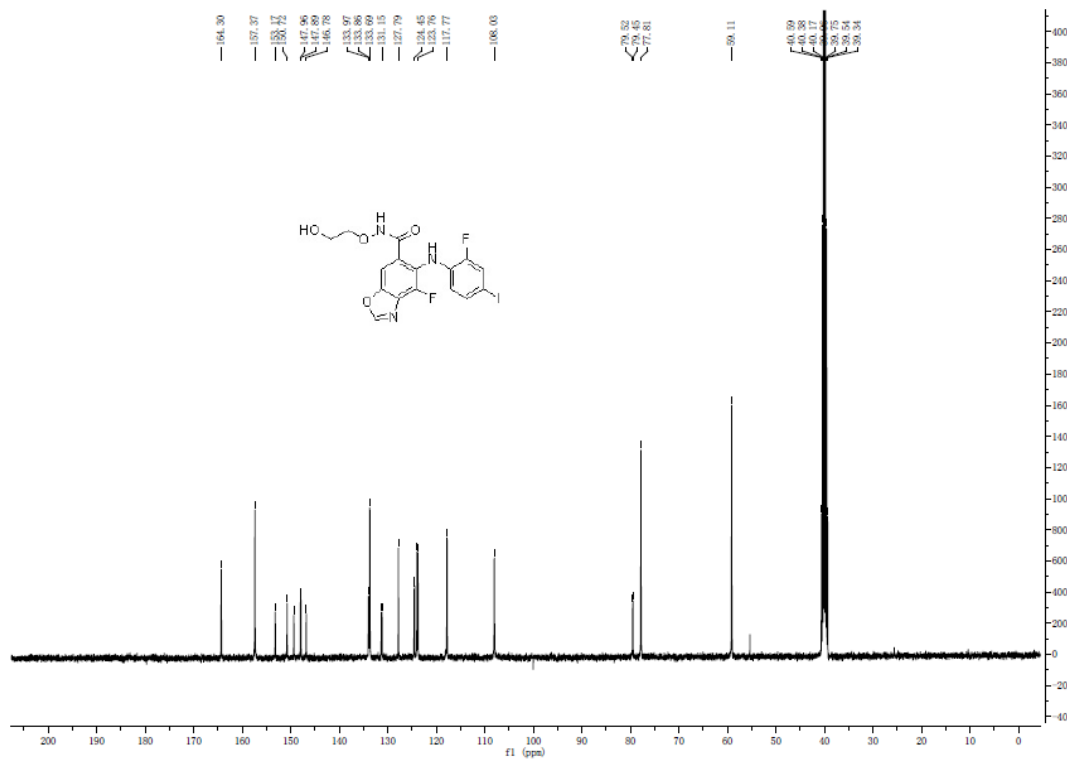


Figure 2-5 <sup>13</sup>C NMR spectra of KZ-001

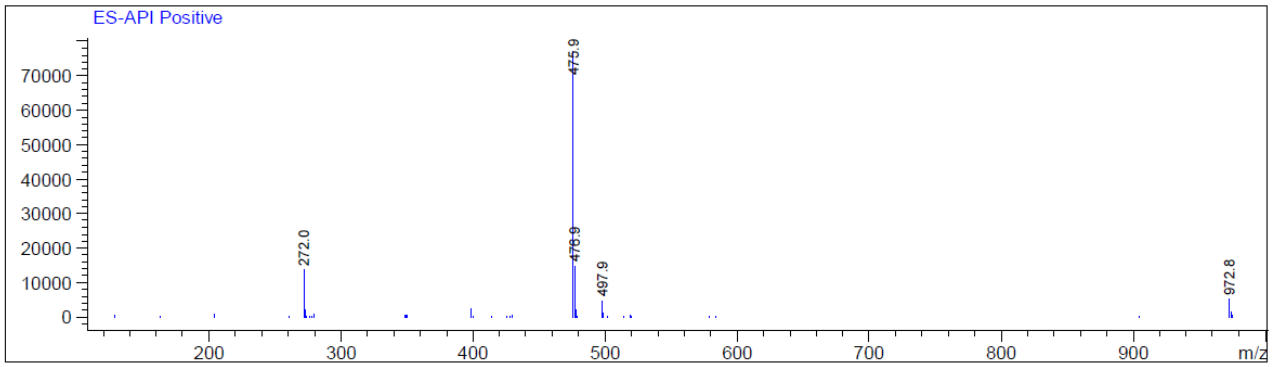


Figure 2-6 MS spectrum of KZ-001

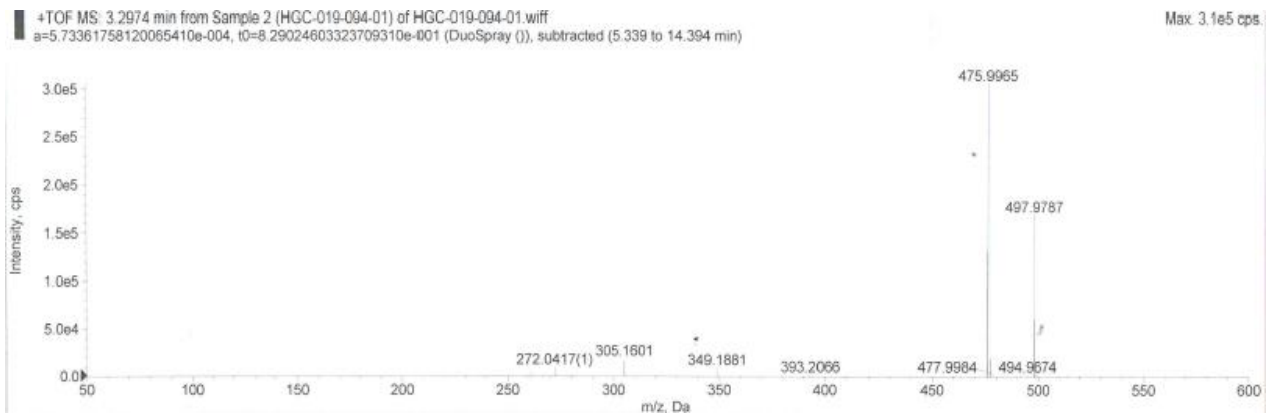
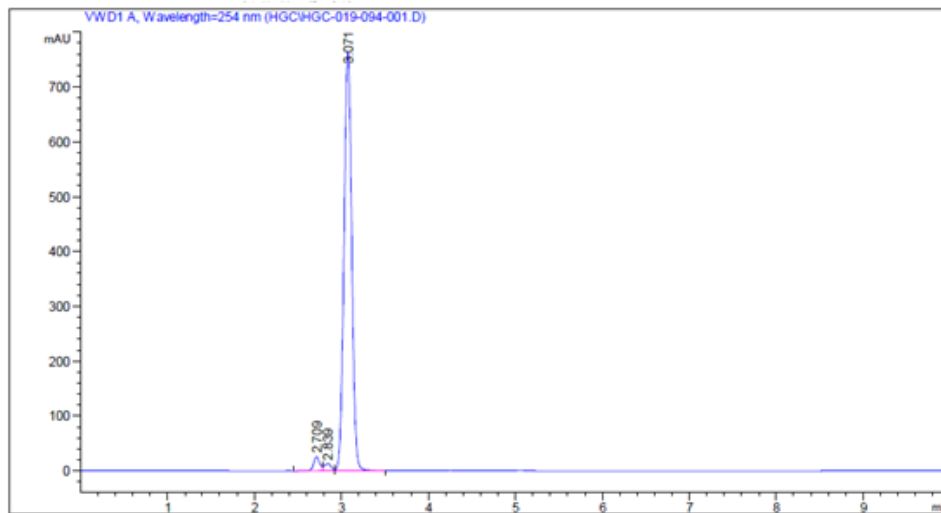


Figure 2-7 HRMS-TOF spectrum of KZ-001



Peak #	RT time (min)	Type	Width (min)	Area (mAU*s)	Height (mAU)	Area %
1	2.709	BV	0.0735	125.37388	25.90740	2.5451
2	2.839	VV	0.0836	76.59459	13.61424	1.5549
3	3.071	VB	0.0962	4724.15625	762.96399	95.9001

Figure 2-8 HPLC spectrum of KZ-001

---

## 2.5. Conclusions

In this study, a novel benzoxazole compound KZ-001 was designed as a MEK inhibitor based on the reported X-ray structure. AZD6244 was chosen as a lead compound because of the superiority of its core in existing MEK inhibitors, and here efforts focused on enhancing the activity by modifying AZD6244. KZ-001 was synthesized in an 11-step reaction achieving an overall yield of 11%. The molecular structure and the purity were characterized and identified by <sup>1</sup>H-NMR, <sup>13</sup>C-NMR, MS, HR-MS, and HPLC. Modelled fit with MEK1 and overlay with the binding of AZD6244 to MEK1 suggests that this compound represents a new MEK inhibitor with a new core structure. The results are of significance and provide the basis for the further biological study to validate *in vitro* kinase inhibition and potency in RAS/RAF mutant cells inhibition studies, and for required pharmacokinetics and potential drug combination synergistic effect studies.

---

## 2.6. References

1. Bray, F.; Ferlay, J.; Soerjomataram, I.; Siegel, R. L.; Torre, L. A.; Jemal, A., Global cancer statistics 2018: GLOBOCAN estimates of incidence and mortality worldwide for 36 cancers in 185 countries. *CA Cancer J Clin* 2018, 68, (6), 394-424.
2. Park, J.; Look, K. A., Health Care Expenditure Burden of Cancer Care in the United States. *Inquiry* 2019, 56, 46958019880696.
3. Antonella D. L., M. R. M., Amelia D. A, Maria P., Nicola N., The RAS/RAF/MEK/ERK and the PI3K/AKT signalling pathways: role in cancer pathogenesis and implications for therapeutic approaches. *Expert Opin. Ther. Targets* 2012, 16, (Suppl. 2), S17-S27.
4. Zhao, Y.; Adjei, A. A., The clinical development of MEK inhibitors. *Nat Rev Clin Oncol* 2014, 11, (7), 385-400.
5. Roberts, P. J.; Der, C. J., Targeting the Raf-MEK-ERK mitogen-activated protein kinase cascade for the treatment of cancer. *Oncogene* 2007, 26, (22), 3291-310.
6. Diaz-Flores, E.; Shannon, K., Targeting oncogenic Ras. *Genes Dev* 2007, 21, (16), 1989-92.
7. Munoz-Couselo, E.; Adelantado, E. Z.; Ortiz, C.; Garcia, J. S.; Perez-Garcia, J., NRAS-mutant melanoma: current challenges and future prospect. *Onco Targets Ther* 2017, 10, 3941-3947.
8. Li, S.; Liu, S.; Deng, J.; Akbay, E. A.; Hai, J.; Ambrogio, C.; Zhang, L.; Zhou, F.; Jenkins, R. W.; Adeegbe, D. O.; Gao, P.; Wang, X.; Paweletz, C. P.; Herter-Sprie, G. S.; Chen, T.; Gutierrez-Quiceno, L.; Zhang, Y.; Merlino, A. A.; Quinn, M. M.; Zeng, Y.; Yu, X.; Liu, Y.; Fan, L.; Aguirre, A. J.; Barbie, D. A.; Yi, X.; Wong, K. K., Assessing therapeutic efficacy of MEK inhibition in a KRAS(G12C)-driven mouse model of lung cancer. *Clin Cancer Res* 2018, 24, (19), 4854-4864.
9. Yaeger, R.; Corcoran, R. B., Targeting alterations in the RAF-MEK pathway. *Cancer Discov* 2019, 9, (3), 329-341.
10. Solit, D. B.; Garraway, L. A.; Pratilas, C. A.; Sawai, A.; Getz, G.; Basso, A.; Ye, Q.; Lobo, J. M.; She, Y.; Osman, I.; Golub, T. R.; Sebolt-Leopold, J.; Sellers, W. R.; Rosen, N., BRAF mutation predicts sensitivity to MEK inhibition. *Nature* 2006, 439, (7074), 358-62.

- 
11. Ohren, J. F.; Chen, H.; Pavlovsky, A.; Whitehead, C.; Zhang, E.; Kuffa, P.; Yan, C.; McConnell, P.; Spessard, C.; Banotai, C.; Mueller, W. T.; Delaney, A.; Omer, C.; Sebolt-Leopold, J.; Dudley, D. T.; Leung, I. K.; Flamme, C.; Warmus, J.; Kaufman, M.; Barrett, S.; Teclé, H.; Hasemann, C. A., Structures of human MAP kinase kinase 1 (MEK1) and MEK2 describe novel noncompetitive kinase inhibition. *Nat Struct Mol Biol* 2004, 11, (12), 1192-7.
  12. Li, L.; Zhao, G. D.; Shi, Z.; Qi, L. L.; Zhou, L. Y.; Fu, Z. X., The Ras/Raf/MEK/ERK signaling pathway and its role in the occurrence and development of HCC. *Oncol Lett* 2016, 12, (5), 3045-3050.
  13. Yeh, T. C.; Marsh, V.; Bernat, B. A.; Ballard, J.; Colwell, H.; Evans, R. J.; Parry, J.; Smith, D.; Brandhuber, B. J.; Gross, S.; Marlow, A.; Hurley, B.; Lyssikatos, J.; Lee, P. A.; Winkler, J. D.; Koch, K.; Wallace, E., Biological characterization of ARRY-142886 (AZD6244), a potent, highly selective mitogen-activated protein kinase kinase 1/2 inhibitor. *Clin Cancer Res* 2007, 13, (5), 1576-83.
  14. Hatzivassiliou, G.; Haling, J. R.; Chen, H.; Song, K.; Price, S.; Heald, R.; Hewitt, J. F.; Zak, M.; Peck, A.; Orr, C.; Merchant, M.; Hoeflich, K. P.; Chan, J.; Luoh, S. M.; Anderson, D. J.; Ludlam, M. J.; Wiesmann, C.; Ultsch, M.; Friedman, L. S.; Malek, S.; Belvin, M., Mechanism of MEK inhibition determines efficacy in mutant KRAS- versus BRAF-driven cancers. *Nature* 2013, 501, (7466), 232-6.
  15. Cheng, Y.; Tian, H., Current development status of MEK inhibitors. *Molecules* 2017, 22, (10).
  16. Barrett, S. D.; Bridges, A. J.; Dudley, D. T.; Saltiel, A. R.; Fergus, J. H.; Flamme, C. M.; Delaney, A. M.; Kaufman, M.; LePage, S.; Leopold, W. R.; Przybranowski, S. A.; Sebolt-Leopold, J.; Van Becelaere, K.; Doherty, A. M.; Kennedy, R. M.; Marston, D.; Howard, W. A., Jr.; Smith, Y.; Warmus, J. S.; Teclé, H., The discovery of the benzhydroxamate MEK inhibitors CI-1040 and PD 0325901. *Bioorg Med Chem Lett* 2008, 18, (24), 6501-4.
  17. Lee F. Allen, J. S.-L., and Mark B. Meyer, In vitro and in vivo metabolism of the anti-cancer agent CI-1040, a MEK inhibitor, in rat, monkey, and human. *Seminars in Oncol* 2003, 30,

---

105-116.

18. Rice, K. D.; Aay, N.; Anand, N. K.; Blazey, C. M.; Bowles, O. J.; Bussenius, J.; Costanzo, S.; Curtis, J. K.; Defina, S. C.; Dubenko, L.; Engst, S.; Joshi, A. A.; Kennedy, A. R.; Kim, A. I.; Koltun, E. S.; Loughheed, J. C.; Manalo, J. C.; Martini, J. F.; Nuss, J. M.; Peto, C. J.; Tsang, T. H.; Yu, P.; Johnston, S., Novel carboxamide-based allosteric MEK inhibitors: Discovery and optimization efforts toward XL518 (GDC-0973). *ACS Med Chem Lett* 2012, 3, (5), 416-21.
19. Silk, T.; Choi, H.; Deng, J.; Pourpe, S.; Wong, K.-K.; Merghoub, T.; Wolchok, J. D., Exploring effects of MEK inhibition in tumor microenvironment in non-small cell lung cancer (NSCLC) pre-clinical models. *J Clin Oncol* 2018, 36, (15\_suppl), 12060-12060.
20. Davies, B. R.; Logie, A.; McKay, J. S.; Martin, P.; Steele, S.; Jenkins, R.; Cockerill, M.; Cartlidge, S.; Smith, P. D., AZD6244 (ARRY-142886), a potent inhibitor of mitogen-activated protein kinase/extracellular signal-regulated kinase 1/2 kinases: mechanism of action in vivo, pharmacokinetic/pharmacodynamic relationship, and potential for combination in preclinical models. *Mol Cancer Ther* 2007, 6, (8), 2209-19.
21. Denton, C. L.; Gustafson, D. L., Pharmacokinetics and pharmacodynamics of AZD6244 (ARRY-142886) in tumor-bearing nude mice. *Cancer Chemother Pharmacol* 2011, 67, (2), 349-60.
22. Casaluce, F.; Sgambato, A.; Maione, P.; Sacco, P. C.; Santabarbara, G.; Gridelli, C., Selumetinib for the treatment of non-small cell lung cancer. *Expert Opin Investig Drugs* 2017, 26, (8), 973-984.
23. Janne, P. A.; van den Heuvel, M. M.; Barlesi, F.; Cobo, M.; Mazieres, J.; Crino, L.; Orlov, S.; Blackhall, F.; Wolf, J.; Garrido, P.; Poltoratskiy, A.; Mariani, G.; Ghiorghiu, D.; Kilgour, E.; Smith, P.; Kohlmann, A.; Carlile, D. J.; Lawrence, D.; Bowen, K.; Vansteenkiste, J., Selumetinib plus docetaxel compared with docetaxel alone and progression-free survival in patients with KRAS-mutant advanced non-small cell lung cancer: The SELECT-1 randomized clinical trial. *JAMA* 2017, 317, (18), 1844-1853.
24. Dymond, A. W.; Howes, C.; Pattison, C.; So, K.; Mariani, G.; Savage, M.; Mair, S.; Ford, G.; Martin, P., Metabolism, excretion, and pharmacokinetics of selumetinib, an MEK1/2

- 
- inhibitor, in healthy adult male subjects. *Clin Ther* 2016, 38, (11), 2447-2458.
25. Price, S., Putative allosteric MEK1 and MEK2 inhibitors. *Expert Opin Therap Patents* 2008, 18, 603-627.
26. Iverson, C.; Larson, G.; Lai, C.; Yeh, L. T.; Dadson, C.; Weingarten, P.; Appleby, T.; Vo, T.; Maderna, A.; Vernier, J. M.; Hamatake, R.; Miner, J. N.; Quart, B., RDEA119/BAY 869766: a potent, selective, allosteric inhibitor of MEK1/2 for the treatment of cancer. *Cancer Res* 2009, 69, (17), 6839-47.
27. Ohren, J. F.; Chen, H.; Pavlovsky, A.; Whitehead, C.; Zhang, E.; Kuffa, P.; Yan, C.; McConnell, P.; Spessard, C.; Banotai, C.; Mueller, W. T.; Delaney, A.; Omer, C.; Sebolt-Leopold, J.; Dudley, D. T.; Leung, I. K.; Flamme, C.; Warmus, J.; Kaufman, M.; Barrett, S.; Teclé, H.; Hasemann, C. A., Structures of human MAP kinase kinase 1 (MEK1) and MEK2 describe novel noncompetitive kinase inhibition. *Nat Struct Mol Biol* 2004, 11, (12), 1192-1197.
28. Han, S.; Zhou, V.; Pan, S.; Liu, Y.; Hornsby, M.; McMullan, D.; Klock, H. E.; Haugen, J.; Lesley, S. A.; Gray, N.; Caldwell, J.; Gu, X.-j., Identification of coumarin derivatives as a novel class of allosteric MEK1 inhibitors. *Bioorg Med Chem Lett* 2005, 15, (24), 5467-5473.
29. Robarge, K. D.; Lee, W.; Eigenbrot, C.; Ultsch, M.; Wiesmann, C.; Heald, R.; Price, S.; Hewitt, J.; Jackson, P.; Savy, P.; Burton, B.; Choo, E. F.; Pang, J.; Boggs, J.; Yang, A.; Yang, X.; Baumgardner, M., Structure based design of novel 6,5 heterobicyclic mitogen-activated protein kinase kinase (MEK) inhibitors leading to the discovery of imidazo[1,5- a ] pyrazine G-479. *Bioorg. Med Chem Lett* 2014, 24, (19), 4714-4723.

---

### **3. CHAPTER 3: MEK INHIBITOR KZ-001 FOR THE TREATMENT OF RAS/RAF MUTANT CANCERS**

This study was published in *International Journal of Cancer*, Year 2019, Vol. 145, Pages 586-596.

---

### 3.1. Abstract

RAS/RAF mutations occur in large portion of malignancies, and have been associated with aggressive clinic behaviors and poor prognosis. Using AZD6244 as a lead compound, a novel benzoxazole compound (KZ-001) was developed (chapter 2), which based on model outcomes could be a highly potent and selective MEK1/2 inhibitor for the treatment of RAS/RAF mutant cancers. The biological activity both *in vitro* and *in vivo* was investigated. Furthermore, the pharmacokinetic profile in mice was studied. The potential mechanism of action of KZ-001 was also explored.

In *in vitro* studies, KZ-001 and AZD6244 inhibited the MEK1 activity, with  $IC_{50}$ s of  $7.40 \pm 1.96$  nM and  $199.73 \pm 38.25$  nM, respectively, at an ATP concentration of 45  $\mu$ M in the Z'-LYTE assay. Concentrations for the inhibition of MEK2 were higher ( $IC_{50}$  at 64 nM and 742 nM, respectively) in radiometric protein kinase assays, indicating that KZ-001 is a MEK1/2 inhibitor. The inhibitory potential of KZ-001 were evaluated for 14 representative protein kinases (including MEK1/2) and no inhibition was observed at 10  $\mu$ M for the other 12 protein kinases examined, suggesting that KZ-001 is a highly selective MEK1/2 inhibitor.

Compared to the reference drug AZD6244 with an  $IC_{50}$   $74.5 \pm 3.0$  nM –  $184.3 \pm 5.0$  nM and over 3000 nM in BRAF and KRAS mutant cancer cell lines, KZ-001 was a much more potent inhibitor of proliferation with an  $IC_{50}$  of  $2.9 \pm 0.6$  nM –  $5.7 \pm 0.3$  nM and  $169.9 \pm 97.7$  nM in MTT and MTS assays, while proliferation of  $RAF^{WT}$  and  $RAS^{WT}$  cell lines A431 was not inhibited ( $IC_{50} > 3000$ nM). KZ-001 exhibited 26- to 32- and over 17-fold greater inhibition against BRAF- and KRAS-mutant tumor cells than that of AZD6244, respectively. Similar results were also obtained in *in vivo* xenograft models, where the body weight did not change significantly. Chronic dosing of mice with KZ-001 (6 mg/kg) significantly inhibited the growth of A375 tumors (TGI 91.0%;  $p < 0.001$ ), while AZD6244 at 10 mg/kg QD resulted in 45.8% inhibition ( $p < 0.01$ ). Calu-6 xenografts were also inhibited by 3 mg/kg KZ-001 (TGI 63.2%;  $p < 0.01$ ), while AZD6244 was also effective at <10 mg/kg (TGI 54.8%;  $p < 0.05$ ). Chronic dosing with 3 mg/kg and 6 mg/kg KZ-001 completely inhibited the growth of Colo-205 tumors (TGI 103.9% and 108.8%, respectively;  $p < 0.01$ ), while AZD6244 at 10 mg/kg resulted in a significant inhibition of 83.3% ( $p < 0.01$ ) compared to the vehicle control.

KZ-001 inhibited the MAPK pathway like other known MEK inhibitors. In the BRAF-mutant A375, Colo-205, and HT-29 cell lines, MEK phosphorylation levels did not change significantly at concentrations ranging from 1 nM to 625 nM, but the ERK phosphorylation was blocked completely by KZ-001 at concentrations ranging from 5 nM to 625 nM. Interestingly, in the Calu-6

---

(KRAS-mutant cell line), MEK phosphorylation increased at concentrations ranging from 1 nM to 625 nM, whereas ERK phosphorylation was still blocked by KZ-001. By using the FITC Annexin V apoptosis detection assay, KZ-001 induced 7.1% and 37.0% of early apoptosis in Calu-6 cell population at 10 nM and 10  $\mu$ M, respectively. Likewise, KZ-001 induced 24% and 33.4% of early apoptosis in Colo-205 cells at 10 nM and 10  $\mu$ M. In contrast, KZ-001 at neither 10 nM nor 10  $\mu$ M induced apoptosis in A375 and HT-29 cells. By using a DNA content quantitation assay, in A375 cells, KZ-001 induced a significant increase of cells in the G1 phase, with a concomitant decrease of cells in S - and G2 phase, causing a cell cycle delay in A375 cells at the G0/G1 phase at both 10 nM and 10 $\mu$ M.

Furthermore, pharmacokinetics (PK) analysis was performed for KZ-001 in mice over 24 h, and PK parameters were calculated. Results showed that KZ-001 exhibited good orally bioavailability (28%) and exposure ( $AUC_{0-\infty} = 337 \pm 169$  ng\*hr/mL).

KZ-001 exhibited good potency both *in vitro* and *in vivo*, indicating a great potential for therapeutic application for RAS/RAF-mutant cancers in clinical trials.

### 3.2. Introduction

The dysregulation of RAS/RAF/MEK/ERK signalling pathway commonly occurs in human cancers, and constitutively or highly upregulated signalling is a hallmark of tumorigenesis and progression [1]. In this pathway, after recruiting RAS to the plasma membrane, RAF phosphorylates and activates MEK 1/2, which are dual specificity protein kinases that phosphorylate serine/threonine and tyrosine residues. The MEK kinases in turn phosphorylate and activate their only currently known substrates, ERK 1/2 (extracellular signal-regulated kinases). Consequently, this signaling pathway promotes cell proliferation, cell survival and metastasis [2]. RAS and RAF are related protein kinases involved in the Ras/Raf/MEK/ERK signal transduction cascade. Mutations in RAS/RAF occur in a large portion of malignancies and have been associated with aggressive clinic behaviours and poor prognosis. As the direct substrate of MEK, elevated levels of phosphorylated ERK1/2 in primary cancer tissues and cancer lines have also been identified.

Inhibitors of MEK have demonstrated efficacy against RAS and RAF-mutant malignant tumours in preclinical models. Yamaguchi T. et al. reported that trametinib (JTP-74057, GSK1120212) strongly inhibited activities of MEK1/2 kinase. It caused growth inhibition in BRAF and KRAS-mutant

---

colorectal cancer cell lines, and tumor growth suppression in HT-29 and Colo-205 xenografts [3]. Gilmartin A. et al. reported that in enzymatic studies GSK1120212 prevented Ras-dependent MEK phosphorylation, resulting in prolonged inhibition of ERK1/2 phosphorylation. Greatest tumor inhibition was documented for tumors harbouring mutation of RAF or RAS [4]. A MDA-MB-231T efficacy study by Rice K. et al showed that cobimetinib (GDC-0973, XL518) inhibited tumour growth with 60% and 93% at dosages of 1 mg/kg and 3 mg/kg, and higher doses led to statistically significant tumor regression [1]. Similarly, Hoeflich K., et al. reported that GDC-0973 at the dose above 3 mg/kg led to strong tumor growth inhibition in A375 BRAF<sup>V600E</sup> mutant melanoma xenograft model [5]. Likewise, Lee P. et al. demonstrated that binimetinib (MEK162, ARRY-162) inhibited cell proliferation of mutant B-Raf and Ras cell lines, such as HT29, Malme-3M, SK-MEL-2, COLO 205, SK-MEL-28 and A375 (IC<sub>50s</sub> from 30-250 nM). Also, the efficacy of ARRY-162 was also demonstrated in xenograft models such as HT29, COLO 205, Calu-6 and tumour growth inhibition showed correlating with decreased phospho-ERK levels in tumor xenografts [6]. Yeh T., et al. reported that selumetinib (AZD6244, ARRY-142886) inhibited growth of several cell lines harbouring BRAF and RAS mutations, and demonstrated antitumor activity against HT-29 colorectal tumour xenograft [7].

Melanomas are the most aggressive cancer of skin and are highly resistant to conventional chemotherapy, immunotherapy, and targeted therapy. Though the incidence rate of melanoma is not high, the 5-year survival of metastatic melanoma is only 20% [8]. About 60% of melanoma cases have RAF mutations [9]. A375 is a human melanoma cell line harbouring the BRAF<sup>V600E</sup> mutation, and the endogenous expression of BRAF<sup>V600E</sup> results in constitutive activation of the MAPK kinase pathway and phosphorylation of Erk2 in the absence of ligands, which confers this cell line as an ideal model.

Colorectal cancers (CRCs) are accounting for 10.2% incidence rate with a 9.2% mortality rate. Up to 10% of metastatic CRCs are BRAF<sup>V600</sup> mutants, with a worse prognosis [10]. These tumours are unresponsive to chemotherapy, and treatment with EGFR-antibodies is rarely beneficial. The HT-29 cell line is a human colorectal adenocarcinoma cell line with BRAF<sup>V600E</sup> mutation [11]. Colo-205 is

---

also a human colon cancer cell line with BRAF<sup>V600E</sup> mutation. Therefore HT-29 and Colo-205 were used in this study as colorectal cancer models.

KRAS mutant lung cancers account for about 30% of lung adenocarcinomas in western countries and 10% in Asian countries [12]. Until now, there is no effective targeted therapy, and chemotherapies remain the standard for patient care with lung cancers with KRAS mutations [12]. Calu-6 is a human lung cancer cell line harbouring KRAS<sup>Q61K</sup>, whereas A431 cells are wild-type for RAS and RAF.

In this chapter enzymatic studies investigated MEK1/2 kinase inhibition as well as kinase selectivity. The potency of KZ-001 and pharmacokinetics was determined in RAS or RAF-mutant cells, including A375, Colo-205, HT-29, and Calu-6 cells. Thereafter, the efficacy of KZ-001 in A375, Colo-205, HT-29, and Calu-6 xenografts was evaluated. AZD 6244 was used as a reference compound to compare the potency and efficacy both *in vitro* and *in vivo*. Inhibition of phosphorylation of ERK, the direct and sole known substrate, by KZ-001 was determined. Finally, the potential mechanism of action was investigated.

### **3.3. Materials and methods**

#### **3.3.1. Cell lines and subculture**

A375, A431, HT-29, and Calu-6 cell lines were purchased from the typical culture preservation commission cell bank of the Chinese Academy of Sciences in China, and the Colo-205 cell line was from the Institute of Basic Medical Sciences, Chinese Academy of Medical Sciences in China. All cell lines were authenticated by short tandem repeat analysis. A375, HT-29, Calu-6, Colo-205, and A431 cell lines were maintained in DMEM (Dulbecco's minimal essential medium), McCoy's 5a, MEM (minimal essential medium), RPMI (Roswell Park Memorial Institute) 1640 medium, and DMEM, respectively. Media were supplemented with 10% heat-inactivated fetal bovine serum (FBS), 1 mM sodium pyruvate and 100 U/mL penicillin and 0.1 mg/mL streptomycin. Cells were maintained in a 37°C incubator containing 5% CO<sub>2</sub> and 95% air. The medium was changed every 2 to 3 days.

#### **3.3.2. Animals**

---

Female Balb/c nude mice (18-22 g weight) were purchased from Shanghai SLAC Laboratory Animal Co., Ltd and Beijing HFK Bioscience Co., Ltd. An acclimation period of approximately one week was allowed between animal arrival and tumor implantation to accustom the animals to the laboratory environment. The Specific-Pathogen-Free (SPF) animals were kept in cages under  $22 \pm 2$  °C, with 40-70% relative humidity. Food and water were supplied adequately on 12-hour light/dark cycle schedule. All animal operations were based on guidelines for care and use of laboratory animals, and were approved by the Institutional Animal Care and Use Committee of the Institute of Radiation Medicine (IRM) (1649), Chinese Academy of Medical Sciences (CAMS).

### **3.3.3. Cell-free kinase assay: Inhibition of MEK1 kinase**

The assay was performed following the instructions of the Z'-LYTE kinase assay kit (Life Technologies). Reactions were performed in a 384-well plate with an incubation mixture (10  $\mu$ L) composed of 1x kinase buffer (50 mM HEPES pH 7.5, 10 mM MgCl<sub>2</sub>, 1 mM EGTA, 0.01% BRIJ-35), 0.2 nM MEK1, 114.8 nM ERK2. KZ-001 and positive control compound AZD6244 were serially diluted to eight appointed concentrations (containing 1% DMSO; triplicate for each concentration) and added to the mixture solution. After 10 min pre-incubation at room temperature, reactions were initiated by adding 45  $\mu$ M ATP and 1.5  $\mu$ M Ser/Thr3 peptide (provided in the kit) and incubated at room temperature for 1 h. After that, the reaction was terminated with the Stop Reagent solution, and the fluorescent signal was determined using a Synergy 2 microplate reader (Biotek). Inhibitory activity of KZ-001 was evaluated by IC<sub>50</sub> value. IC<sub>50</sub> values were calculated according to the concentration-response curve of KZ-001, fitted using the software GraphPad Prism 5 with "log (inhibitor)-response (variable slope)" equation provided in the kit.

### **3.3.4. Cell-free kinase assay: Inhibition of MEK2 kinase**

Inhibition of MEK2 kinase by KZ-001 was investigated using the radiometric protein kinase assay in Eurofins Pharma, using an established protocol. KZ-001 was prepared to a concentration equal to 50x final concentration of KZ-001 in the reaction mix in 100% DMSO. The reaction was initiated by the addition of the Mg/ATP mix. After incubation for 40 min at room temperature, the reaction was stopped by the addition of phosphoric acid to a concentration of 0.5%. 10  $\mu$ L of the reaction was then spotted onto a P30 filtermat and washed four times for 4 min in 0.425% phosphoric acid and once in methanol prior to drying and scintillation counting. Inhibition activity of KZ-001 was evaluated by IC<sub>50</sub> value. IC<sub>50</sub> values were calculated according to the concentration-response curve of KZ-001, fitted using software GraphPad Prism 5 with "log (inhibitor)-response (variable slope)" equation.

---

### **3.3.5. Cell-free kinase assay: Kinase selectivity assay**

The protein kinase selective activity of KZ-001 was screened, against several representative serine/threonine and tyrosine kinases, including Abl, ALK, EGFR, FGFR3, MEK1, MEK2, Met, mTOR, PDGFR $\alpha$ , PKA, Ron, TrkA, TrkB, and TrkC. This screening study was performed by Eurofins Pharma Discovery Services UK Limited according to their established protocols. The compound was prepared to 500  $\mu$ M concentration in 100% DMSO. This working stock solution was added to the assay well as the first component in the reaction, followed by further components. The positive control wells contained all components of the reaction, except the tested compound KZ-001. DMSO (at a final concentration of 2%) was also included in the wells to control for solvent effects. The blank wells contained all components of the reaction, with a reference inhibitor replacing the tested compound. This abolishes kinase activity and establishes the base-line (0% kinase activity remaining).

### **3.3.6. Western blot analysis in A375, Colo-205, HT-29, Calu-6 cells**

RIPA buffer (R0020), protein phosphatase inhibitor (All-in-one, 100 $\times$ ) (P1260), BCA protein assay kit (PC0020) were purchased from Solarbio. NuPage 10% Bis-Tris Gel (NP0301BOX) was purchased from Invitrogen. PVDF membrane (Immobilon-P) was purchased from Millipore. eECL western blot kit (CW0049) was purchased from CWBIO. Anti-p-MEK1/2 antibody, anti-MEK1/2 antibody, anti-p-ERK1/2 antibody, and anti-ERK1/2 antibody were purchased from Cell Signaling Technology.

MEK, phospho-MEK, ERK and phospho-ERK levels were evaluated by Western blot analysis. Cell lines (A375, Colo-205, HT-29, Calu-6) were seeded into 6-well plates at a density of  $5 \times 10^5$  cells/well and treated the next day with KZ-001 at concentrations of 1, 5, 25, 125, and 625 nM, respectively. Cells were treated with medium containing 0.1% DMSO as controls. All cells were treated for 1h. After that, cell lysates were prepared with RIPA (radioimmunoprecipitation assay) buffer containing protein phosphatase inhibitor (All-in-one, 100 $\times$ ). The cell protein concentrations were determined using the BCA protein assay kit. Equal amounts of total protein of cell and tumor (see section 3.3.7) lysates were resolved on NuPage 10% Bis-Tris Gel, and then transferred to PVDF membrane. MEK1/2 and ERK1/2 protein (both phosphorylated and total) were probed with the respective antibodies (Cell Signaling Technology, anti-p-MEK1/2 antibody: 9121; anti-MEK1/2 antibody: 9122; anti-p-ERK1/2 antibody: 4370; anti-ERK1/2 antibody: 4695). Chemiluminescent signals were generated with the eECL Western blot kit (CW0049, CWBIO) and detected with a Bio-Rad ChemiDoc XRS + System.

### **3.3.7. Western blot analysis in tumor tissues**

---

When the volume of xenografts tumors reached approximately 300 mm<sup>3</sup>, mice were given a single dose of 3 mg/kg KZ-001 or vehicle via oral gavage. After 1 h, tumors were harvested and stored at -80°C after snap freezing in liquid nitrogen. Tumor tissue was cut into small pieces and digested in cold RIPA buffer containing protein phosphatase inhibitor. After incubation on ice for 20 to 30 min, the lysates were centrifuged at 18,626 g for 15 min. Tumor protein concentrations were determined with the BCA protein assay kit.

### **3.3.8. Cell proliferation assay for single agent treatment**

For A375, HT-29, Calu-6, and A431 cell lines, cell proliferation was analyzed using the 3-(4,5-dimethylthiazole-2-yl)-2,5-diphenyl-2H-tetrazolium bromide (MTT) assay. As for the Colo-205 cell line, cell proliferation was analyzed using the (3-(4,5-dimethylthiazol-2-yl)-5-(3-carboxymethoxyphenyl)-2-(4-sulfophenyl)-2H-tetrazolium) (MTS) assay. Cells were seeded into 96-well microtiter plates at a density of 500 to 3000 cells per well and plated for 24 h and appropriately diluted KZ-001 or AZD6244 was added to each test well in triplicate. Cell viability was assayed after the cells were treated for 72 h according to the procedure originally described by Mosmann [13]. Survival rate was calculated using the formula:

$$\text{Survival rate} = \frac{(\text{Mean absorbance of experimental wells} - \text{Mean absorbance of DMSO wells})}{(\text{Mean absorbance of control wells} - \text{Mean absorbance of DMSO wells})} \times 100\%$$

IC<sub>50s</sub> were calculated from semi-log regression plots (logarithm of the concentration versus survival rate) using GraphPad Prism 6 and a four parameter non-linear regression dose-response inhibition model.

### **3.3.9. Tumor cell apoptosis assay**

A375, HT-29, Colo-205 and Calu-6 cells used in this assay were inoculated in 6-well plates. Cells were processed according to the instruction of the apoptosis detection kit (Lot: 6155987, BD Biosciences) and analyzed by flow cytometry (BD Biosciences, Accuri C6). Briefly, cell culture media were changed after 18 h. KZ-001 at final concentrations of 0 nM, 10 nM, 10 μM was added respectively. The solvent control group was the cell culture media containing 0.5% DMSO. After treatment for 24 h, trypsin was added to detach the cells from the substrate for 2 min. After that, the cells were centrifuged at 400 g, and washed twice with cold PBS. The cells were resuspended and stained with FITC Annexin V and propidium iodide (PI). Then the cells were analyzed by flow cytometry. Cells that were FITC Annexin V positive and PI negative were considered to be in early apoptosis.

---

### 3.3.10. Cell cycle assay

Cells were processed following the instruction of the DNA content quantitation assay kit (Lot: CA1510, Solarbio) and analyzed by flow cytometry (BD Bioscience, Accuri C6). A375 cells were seeded at a density of  $1.5 \times 10^5$  cells/mL in 6-well plates, grown overnight and then treated with KZ-001 at concentrations of 10 nM and 10  $\mu$ M respectively for 24 h. The vehicle control group was treated with culture medium containing 0.5% DMSO. Then cells were trypsin-treated for detachment and washed with PBS, fixed in 70% ice-cold ethanol overnight at 4°C, followed by digestion with 100  $\mu$ L RNase A at 37°C for 30 min. Next, 400  $\mu$ L of PI was added to the cell mixture and incubated in the dark for 30 min at 4°C. The fluorescence intensity of each cell sample was measured using flow cytometry (BD Bioscience, Accuri C6) and analyzed with ModFit LT software.

### 3.3.11. Pharmacokinetic (PK) studies

SBE- $\beta$ -CD was purchased from Dalian Meilunbio; 96 deep-well plates were purchased from Bioscience. The objective of the study was to evaluate the pharmacokinetics of KZ-001 in the widely used Institute of Cancer Research (ICR) mice via intravenous (IV) and oral gavage (PO) administration. Six male ICR mice were randomized into IV and PO administration groups. Each group was treated with a single dose of KZ-001 (3 mg/kg, solubilized in 20% SBE- $\beta$ -CD and 10% DMSO aqueous solution, 10 mL/kg). After administration, 20  $\mu$ L of plasma were collected from the IV and the PO administration group at 0, 5, 15, and 30 min, and 1, 2, 4, 8, and 24 h; each sample was added to a well of a 96-deep well plate, and each well was mixed with 200  $\mu$ L acetonitrile (containing 200 ng/mL tolbutamide) by vortexing. The mixture was centrifuged at 3,200 g for 20 min. Then, 180  $\mu$ L supernatant was transferred to each well of 96-well plates, dried under a stream of N<sub>2</sub>, and mixed with 300  $\mu$ L 50% acetonitrile in 0.1% formic acid (FA) water by vortexing for 10 min. Finally, the samples were analyzed by LC/MS/MS. This experiment used a Poroshell 120 EC-C18 4.0  $\mu$ m 2.1 $\times$ 50 mm column, and a 0.5 mL/min flow rate. The initial solvent system was 98% water containing 0.1% formic acid (mobile phase A) and 2% acetonitrile containing 0.1% formic acid (mobile phase B) for 0.3 min, from 0.3 until 0.6 min, the mobile phase B was set up to 98% and this gradient kept up to 1.5 min. Finally, the gradient of mobile phase B was changed to 2% at 1.51 min and until 3.5 min (Table 3-1). WinNonlin7.0 (non-compartmental model) was used to calculate the pharmacokinetics parameters by using mean plasma concentration time data from individual animals.

**Table 3-1 LC/MS/MS mobile phase gradients**

Step	Total Time (min)	Flow rate (mL/min)	A%	B%
0	0	0.5	98	2
1	0.3	0.5	98	2
2	0.6	0.5	2	98
3	1.5	0.5	2	98
4	1.51	0.5	98	2
5	3.5	0.5	98	2

### 3.3.12. Tumor xenografts

Female Balb/c nude mice (18-22 g weight) were purchased from Shanghai SLAC Laboratory Animal Co., Ltd and Beijing HFK Bioscience Co., Ltd. An acclimation period of approximately one week was allowed between animal arrival and tumor implantation to accustom the animals to the laboratory environment. Tumor fragments were implanted subcutaneously on the right flank. When the average tumor volume reached approximately 130~180 mm<sup>3</sup>, the tumor-bearing mice were randomly assigned into the vehicle, positive control, and treatment groups (n = 6 animals per group).

### 3.3.13. *In vivo* efficacy of single drug treatment studies

The vehicle control groups were treated with 10 mL/kg of vehicle, PO, QD. The positive control groups were given AZD6244 (10 mg/kg, PO, QD). The treatment groups received KZ-001, PO, QD. Emulsions of KZ-001 and AZD6244 were prepared in vehicle (containing 20% SBE- $\beta$ -CD in distilled water) respectively on the basis of the appointed concentration for each dose group.

For A375 and Calu-6 xenografts, the doses were set at 1.5 mg/kg, 3 mg/kg, and 6 mg/kg. For Colo-205 xenograft, the concentrations were set at 3 mg/kg and 6 mg/kg. The group setting is shown in Table 3-2. Tumor volumes (measured by a caliper), animal body weight and tumor condition were recorded twice every week during the study period. Mice were sacrificed when tumors reached 2000 mm<sup>3</sup>, were moribund, or had a >20% decrease in weight. In the AZD6244 treatment groups (A375 xenograft), one mouse was sacrificed due to >20% decrease in body weight on day 5; the remaining five mice were studied until completion of the study.

**Table 3-2 Group setting of mice in single drug studies**

<b>Tumor xenograft model</b>	<b>Groups</b>	<b>Dose (mg/kg)</b>	<b>Treatment</b>	<b>Animals (N)</b>
A375	Vehicle	-	PO, QD × 10 days	6
	AZD6244, 10	10	PO, QD × 10 days	6
	KZ-001, 1.5	1.5	PO, QD × 10 days	6
	KZ-001, 3	3	PO, QD, × 10 days	6
	KZ-001, 6	6	PO, QD, × 10 days	6
Colo-205	Vehicle	-	PO, QD, × 15 days	6
	AZD6244, 10	10	PO, QD × 15 days	6
	KZ-001, 3	3	PO, QD × 15 days	6
	KZ-001, 6	6	PO, QD × 15 days	6
Calu-6	Vehicle	-	PO, QD × 22 days	6
	AZD6244, 10	10	PO, QD × 22 days	6
	KZ-001, 1.5	1.5	PO, QD × 22 days	6
	KZ-001, 3	3	PO, QD × 22 days	6
	KZ-001, 6	6	PO, QD × 22 days	6

Tumor volumes were calculated using the following ellipsoid formula:  $[D \times (d^2)] / 2$ , in which D and d represent the large and small diameter, respectively. TGI (tumor growth inhibition) was calculated for each group using the formula:  $TGI (\%) = [1 - (T - T_0) / (V - V_0)] \times 100$ ; T and T<sub>0</sub> are the average tumor volume of a treatment group at the last day of treatment and at the beginning of the treatment, respectively; V and V<sub>0</sub> are the average tumor volume of the vehicle control group on the same day (T) and at the beginning of treatment.

### 3.3.14. Statistical analyses

All biochemistry and cell experiments were performed in triplicate per treatment. A t-test was used to analyze differences between two groups in the efficacy study. Differences between groups were considered significant at  $p < 0.05$ .

## 3.4. Results and discussion

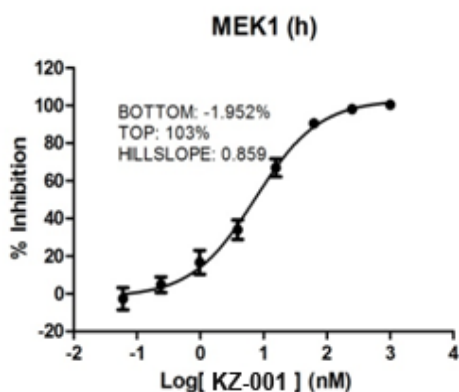
### 3.4.1. KZ-001 is a potent and highly selective MEK inhibitor.

KZ-001 was designed as a MEK inhibitor; therefore, the enzymatic activity of MEK1 and MEK2 was determined. Furthermore, the kinase selectivity of KZ-001 against a panel of kinases was evaluated.

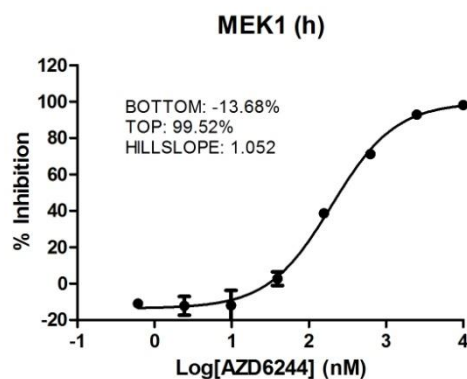
The enzymatic activity of MEK1 was determined, in the presence of increasing concentrations of KZ-001, by measuring the fluorescence transfer in the Z'-LYTE assay. To compare the target kinase inhibition activity between the new compound and the lead compound AZD6244, inhibition of enzyme activity of AZD6244 was determined in the same way as for KZ-001. It was not surprising that both KZ-001 and AZD6244 demonstrated concentration-dependent inhibition of MEK activity, with IC<sub>50</sub> value 7.40 ± 1.96 nM and 199.73 ± 38.25 nM with ATP concentration at 45 μM (Figure 3-1 A, B). KZ-001 exhibited 27-fold greater potency to the target kinase than AZD6244, providing strong evidence that the efficacy of compound was improved successfully.

Inhibition of MEK2 activity was also evaluated in the presence of increasing concentrations of KZ-001 (from 1 nM to 10 μM), by measuring the conversion of [ $\gamma$ -<sup>33</sup>P] ATP phosphate from [ $\gamma$ -<sup>33</sup>P] ATP to MAPK2(m) in a radiometric protein kinase assay. To compare the target kinase inhibition between the new compound and the lead compound AZD6244, the enzyme activity of AZD6244 was determined in the same way as for KZ-001. Both KZ-001 and AZD6244 demonstrated concentration-dependent inhibition of MEK enzyme activity, with IC<sub>50</sub> values of 64 nM and 742 nM, respectively (Figure 3-1 C, D).

A



B



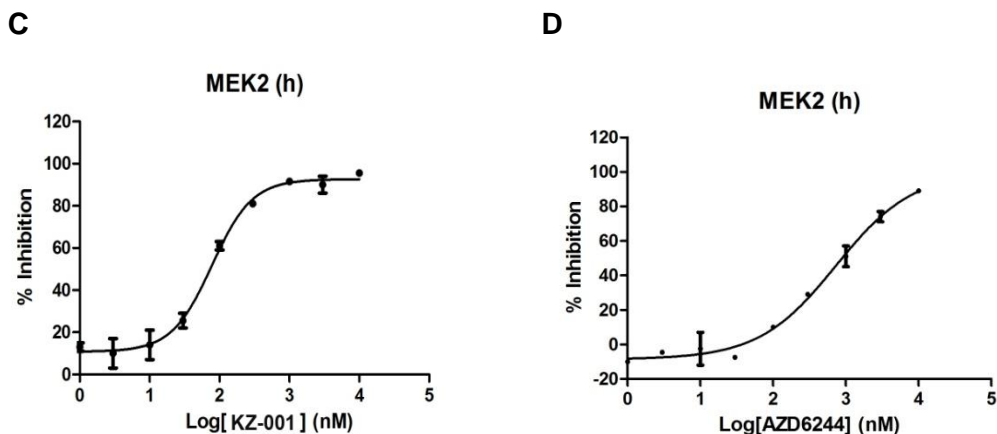


**Figure 3-1 Dose-dependent inhibition of MEK1 and MEK2 activity in the presence of KZ-001 and AZD6244 using the Z'-LYTE kinase assay kit with ATP concentration at 45  $\mu$ M and the radiometric assay with ATP concentration at 10  $\mu$ M, respectively.** A: The  $IC_{50}$  for KZ-001 against MEK1 is  $7.40 \pm 1.96$  nM. B: The  $IC_{50}$  for AZD6244 against MEK1 is  $199.73 \pm 38.25$  nM. C: The  $IC_{50}$  for KZ-001 against MEK2 is 64 nM. D: The  $IC_{50}$  for AZD6244 against MEK2 is 742 nM.

The selectivity of KZ-001 (10  $\mu$ M) against 14 serine/threonine and tyrosine kinases was evaluated by radiometric protein kinase assays. No inhibition was observed at 10  $\mu$ M against the other 12 protein kinases examined, except for MEK1/2, suggesting that KZ-001 is a highly selective MEK1/2 inhibitor (Table 3-3).

**Table 3-3 Inhibitory activity of KZ-001 (10  $\mu$ M) against a panel of protein kinases**

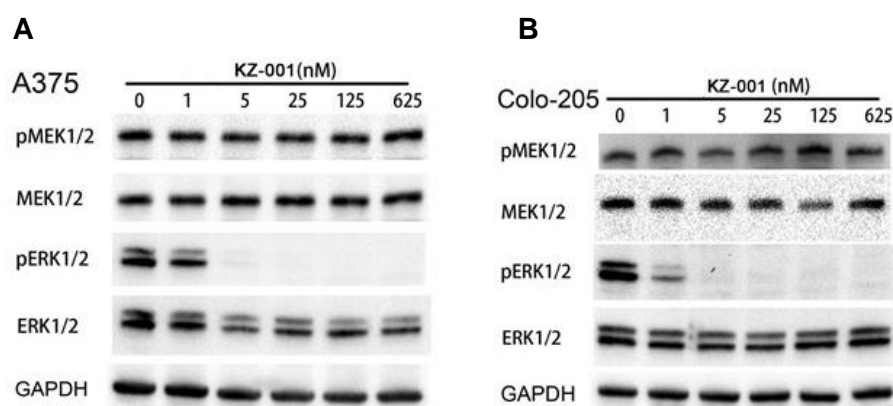
Kinase	KZ-001 Concentration	KZ-001 Activity (Percentage of control $\pm$ SD) (%)
Abl(h)	10 $\mu$ M	101 $\pm$ 2
ALK(h)	10 $\mu$ M	99 $\pm$ 2
EGFR(h)	10 $\mu$ M	102 $\pm$ 6
FGFR3(h)	10 $\mu$ M	95 $\pm$ 3
MEK1(h)	10 $\mu$ M	2 $\pm$ 0
MEK2(h)	10 $\mu$ M	5 $\pm$ 1
Met(h)	10 $\mu$ M	108 $\pm$ 4
mTOR(h)	10 $\mu$ M	118 $\pm$ 5
PDGFR $\alpha$ (h)	10 $\mu$ M	96 $\pm$ 2
PKA(h)	10 $\mu$ M	112 $\pm$ 7
Ron(h)	10 $\mu$ M	98 $\pm$ 8

Kinase	KZ-001 Concentration	KZ-001 Activity (Percentage of control $\pm$ SD) (%)
TrkA(h)	10 $\mu$ M	112 $\pm$ 11
TrkB(h)	10 $\mu$ M	101 $\pm$ 9
TrkC(h)	10 $\mu$ M	91 $\pm$ 6

**Abbreviations:** ALK: Anaplastic lymphoma kinase; EGFR: Epidermal growth factor receptor FGFR3: Fibroblast growth factor receptor 3; MEK1: Dual specificity mitogen-activated protein kinase kinase 1; MEK2: Dual specificity mitogen-activated protein kinase kinase 2; mTOR: Mechanistic target of rapamycin; PDGFR $\alpha$ : Platelet-derived growth factor receptor A; PKA: Protein kinase A; TrkA: Tropomyosin receptor kinase A; TrkB: Tropomyosin receptor kinase B; TrkC: Tropomyosin receptor kinase C

### 3.4.2. KZ-001 inhibits cellular ERK phosphorylation.

Inhibition of MEK1/2 by KZ-001 was further investigated in their cellular environment by measuring the phosphorylation status of ERK1/2 (phospho-ERK (p-ERK)), the direct substrates of MEK1/2, in A375, Calu-6, Colo-205, and HT-29 cell lines. In the BRAF<sup>V600E</sup>-mutant A375, Colo-205, and HT-29 cell lines, MEK phosphorylation levels did not change significantly at concentrations ranging from 1 nM to 625 nM (five-fold gradient dilution), but phosphorylation of ERK was completely inhibited by KZ-001 at concentrations ranging from 5 nM to 625 nM. Interestingly, in the Calu-6 cells (KRAS<sup>Q61K</sup>-mutant cell line), MEK phosphorylation increased at concentrations ranging from 1 nM to 625 nM, but phosphorylation of ERK was still inhibited by KZ-001. While MEK phosphorylation was induced in Calu-6 with KRAS<sup>Q61K</sup>, phosphorylation levels remained unchanged in A375, Colo-205, and HT-29 with BRAF<sup>V600E</sup>. ERK phosphorylation levels in all cell lines decreased in the presence of KZ-001, but extent varied in the different mutant cell lines (Figure 3-2).



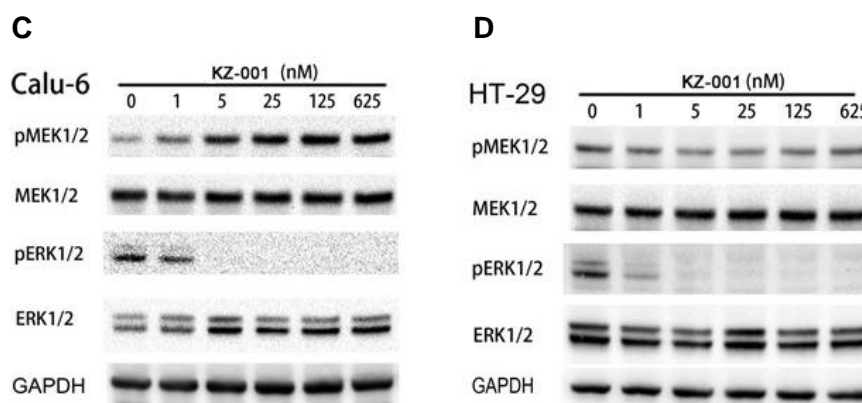


**Figure 3-2 Western blot analyses of dose-dependent effects of KZ-001 on phosphorylation of MEK1/2 and ERK1/2 and MEK1/2 and ERK1/2 expression levels in different cancer cell lines .** In all panels, cells were treated with the indicated concentration of KZ-001 for 1 h before lysis. A: Phospho-MEK1/2 (pMEK1/2) and -ERK1/2 (pERK1/2), and MEK1/2 and ERK1/2 levels in cell lysates of A375 cancer cell lines. B: Phospho-MEK1/2 (pMEK1/2) and -ERK1/2 (pERK1/2), and MEK1/2 and ERK1/2 levels in cell lysates of Colo-205 cancer cell lines. C: Phospho-MEK1/2 (pMEK1/2) and -ERK1/2 (pERK1/2), and MEK1/2 and ERK1/2 levels in the cell lysates of Calu-6 cancer cell lines. D: Phospho-MEK1/2 (pMEK1/2) and -ERK1/2 (pERK1/2), and MEK1/2 and ERK1/2 levels in cell lysates of HT-29 cancer cell lines. GAPDH was used as loading control.

As MEK directly phosphorylates ERK, ERK phosphorylation levels are widely accepted as the biomarker of inhibition of the RAS/RAF/MEK/ERK pathway. This study suggested that KZ-001 has a prominent ability to block this pathway, thereby inhibiting tumorigenesis. Yeh T. reported that the MEK inhibitor AZD6244 disrupts both molecular interactions required for catalysis and access to the ERK activation loop [7]. The present study observed a strong and significant inhibition of phosphorylation of ERK. It is therefore proposed that KZ-001 could interfere with catalysis interactions and access to the ERK activation loop, in the same way as AZD6244.

In this study, inhibition of MEK phosphorylation was not observed in all cells, indicating that KZ-001 did not inhibit the phosphorylation of MEK protein kinase directly.

### 3.4.3. KZ-001 shows high potency in single agent *in vitro* studies.

To investigate the antitumor efficacy of KZ-001 as a single agent, the anti-proliferation effect of KZ-001 was evaluated in three BRAF<sup>V600E</sup> cancer cell lines (A375, Colo-205, and HT-29), one KRAS<sup>Q61K</sup> cancer cell line (Calu-6), and one RAS and RAF wild type cell line (A431). The IC<sub>50</sub> values are shown in Table 3-4, and dose-response of four cell lines on survival rate after treatment with KZ-001 and AZD6244 are presented in Figure 3-3. Compared to the positive control drug AZD6244 with IC<sub>50</sub> values ranging from 74.5 ± 3.0 – 184.3 ± 5.0 nM and >3000 nM for BRAF<sup>V600E</sup> and KRAS<sup>Q61K</sup> mutant cancer cell line, respectively, KZ-001 inhibited cell proliferation much more

potently, with  $IC_{50}$  in the range of  $2.9 \pm 0.6$  –  $5.7 \pm 0.3$  nM and  $169.9 \pm 97.7$  nM for the BRAF<sup>V600E</sup> and KRAS<sup>Q61K</sup> cancer cell lines, respectively. In contrast, KZ-001 did not affect cell proliferation of the RAF<sup>WT</sup> and RAS<sup>WT</sup> cell line A431. In summary, KZ-001 showed improved anti-proliferation activity of 26- to 32- and over 17-fold compared to AZD6244 using the BRAF<sup>V600E</sup> and KRAS<sup>Q61K</sup> cancer cell lines, respectively.

After comparing *in vitro* efficacy in different cell lines, KZ-001 is likely more effective in RAF-mutant cancers than RAS-mutant cancer. The greater viability of RAS-mutated cells than RAF-mutated cells might be explained by the crosstalk of ras proteins, which triggers signaling pathways, such as PI3K, whereas MEK1/2 kinases are the sole widely recognized substrates of raf proteins [14]. The PI3K–AKT pathway which relies on RAS action might contribute to the insensitivity of RAS mutation cells [15].

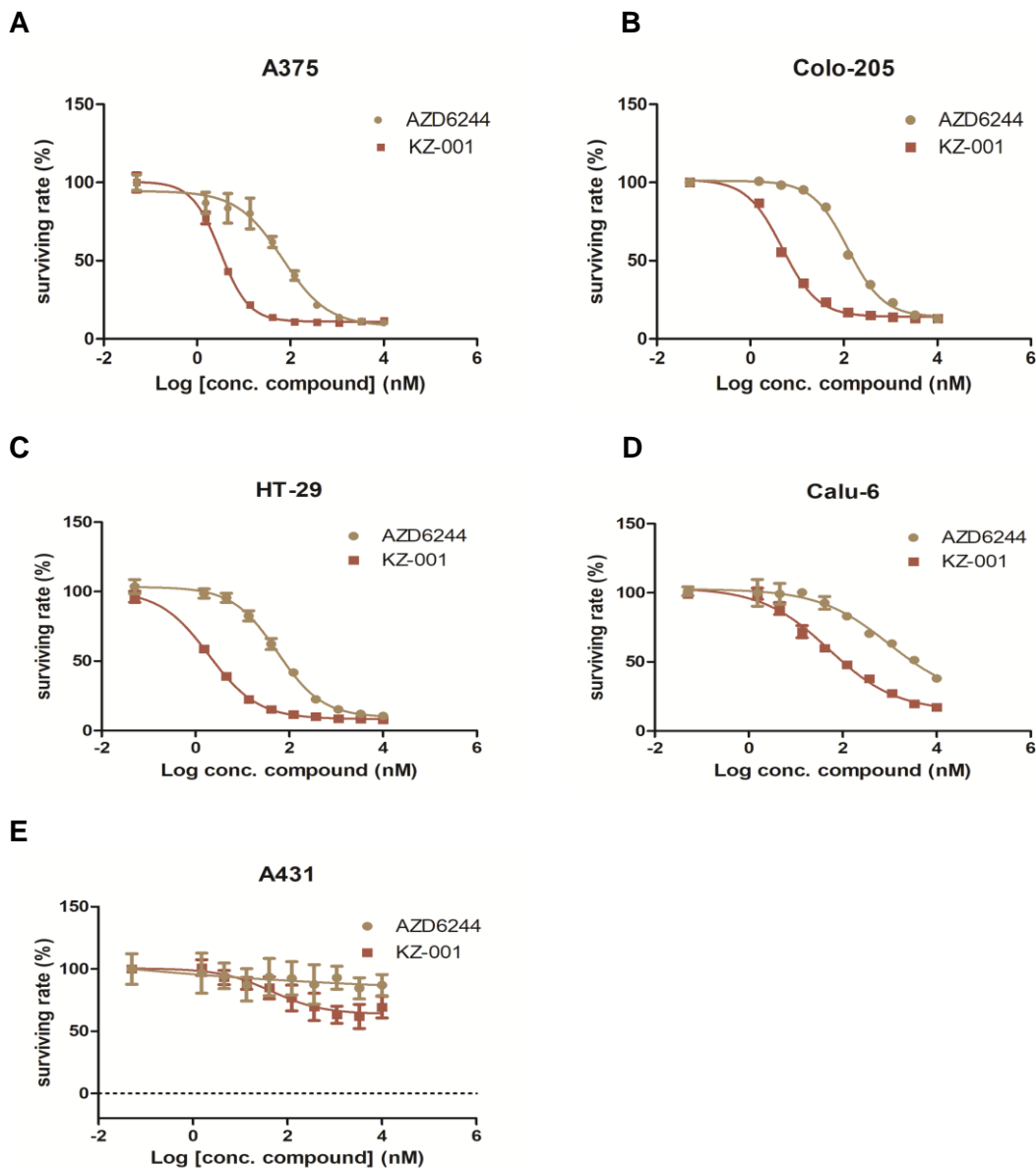


**Figure 3-3 Dose-response of A375, Colo-205, HT-29, Calu-6, and A431 cell lines on survival rate following treatment with KZ-001 and AZD6244.** Cells were seeded in 96-well microtiter plates at a density of 500 to 3,000 cells per well in a volume of 90  $\mu$ L. KZ-001 and AZD6244 were prepared at 10-fold the final assay concentration in media containing 5% DMSO. After the cells were plated for 24 h, 10  $\mu$ L of the appropriate diluted drug was added to each test well in triplicate. The cell viability was assayed 5 days after the cells were plated according to the procedure originally described by Mosmann[13]. For the A375, HT-29, Calu-6, and A431 cell lines, cell proliferation was analyzed using the 3-(4,5-dimethylthiazole-2-yl)-2,5-diphenyl-2H-tetrazolium bromide (MTT) assay. As for the Colo-205 cell line, cell proliferation was analyzed using the (3-(4,5-dimethylthiazol-2-yl)-5-(3-carboxymethoxyphenyl)-2-(4-sulfophenyl) -2H-tetrazolium) (MTS) assay.

**Table 3-4 IC<sub>50</sub> values of a panel of cancer cell lines exposed to KZ-001 and AZD6244**

Cell lines	RAS/RAF Mutation status	Cancer type	KZ-001 <sup>a</sup> IC <sub>50</sub> $\pm$ SD <sup>b</sup>	AZD6244 <sup>a</sup> IC <sub>50</sub> $\pm$ SD <sup>b</sup>
A375	BRAF <sup>V600E</sup>	Melanoma	4.3 $\pm$ 0.7 nM	74.5 $\pm$ 3.0 nM
Colo-205	BRAF <sup>V600E</sup>	Colon cancer	5.7 $\pm$ 0.3 nM	184.3 $\pm$ 5.0 nM
HT-29	BRAF <sup>V600E</sup>	Colorectal adenocarcinoma	2.9 $\pm$ 0.6 nM	75.9 $\pm$ 0.2 nM
Calu-6	KRAS <sup>Q61K</sup>	Lung cancer	169.9 $\pm$ 97.7 nM	>3000 nM
A431	WT	N/A	>3000 nM	>3000 nM

<sup>a</sup> Mean of 3 independent experiments.

<sup>b</sup> *In vitro* cell viability was determined by the MTT or MTS assay.

#### **3.4.4. KZ-001 induces apoptosis in Colo-205 and Calu-6 cells, but not A375 and HT-29 cells.**

Apoptosis, programmed cell death, exists in all types of cells, including tumor cells. Loss of plasma membrane integrity is one of the earliest features of apoptosis. In apoptotic cells, the membrane phospholipid phosphatidylserine (PS) is translocated from the inner to the outer leaflet of the plasma membrane, thereby exposing PS to the external cellular environment. Viable cells with intact membranes exclude PI, whereas the membranes of dead and damaged cells are permeable to PI, thereby distinguishing apoptotic from necrotic cells. Hence, the conjunction of staining with FITC Annexin V and PI could identify cells in early apoptosis.

It is unclear whether KZ-001 induces apoptosis to inhibit the growth of tested cell lines. Therefore, an FITC Annexin V apoptosis detection kit was used to test for apoptotic effects of KZ-001. This compound induced 7.1% early apoptosis and 2.2% late apoptosis/death of cell population at 10 nM;

and 37.0% early apoptosis and 2.7% late apoptosis/death of cell population at 10  $\mu\text{M}$  in Calu-6 cells (Figure 3-4). Likewise, for Colo-205 cells, KZ-001 induced 24% early apoptosis and 10.3% cell death at 10 nM, and this rate increased to 33.4% early apoptosis and 13.5% cell death when KZ-001 concentration was 10  $\mu\text{M}$ . In contrast, KZ-001 at neither 10 nM nor 10  $\mu\text{M}$  induced apoptosis in A375 and HT-29 cells. These results indicate that apoptosis might not be the key mechanism of KZ-001 for growth inhibition in A375 and HT-29 cells, but might contribute to the proliferation inhibition in Calu-6 and Colo-205 cells.

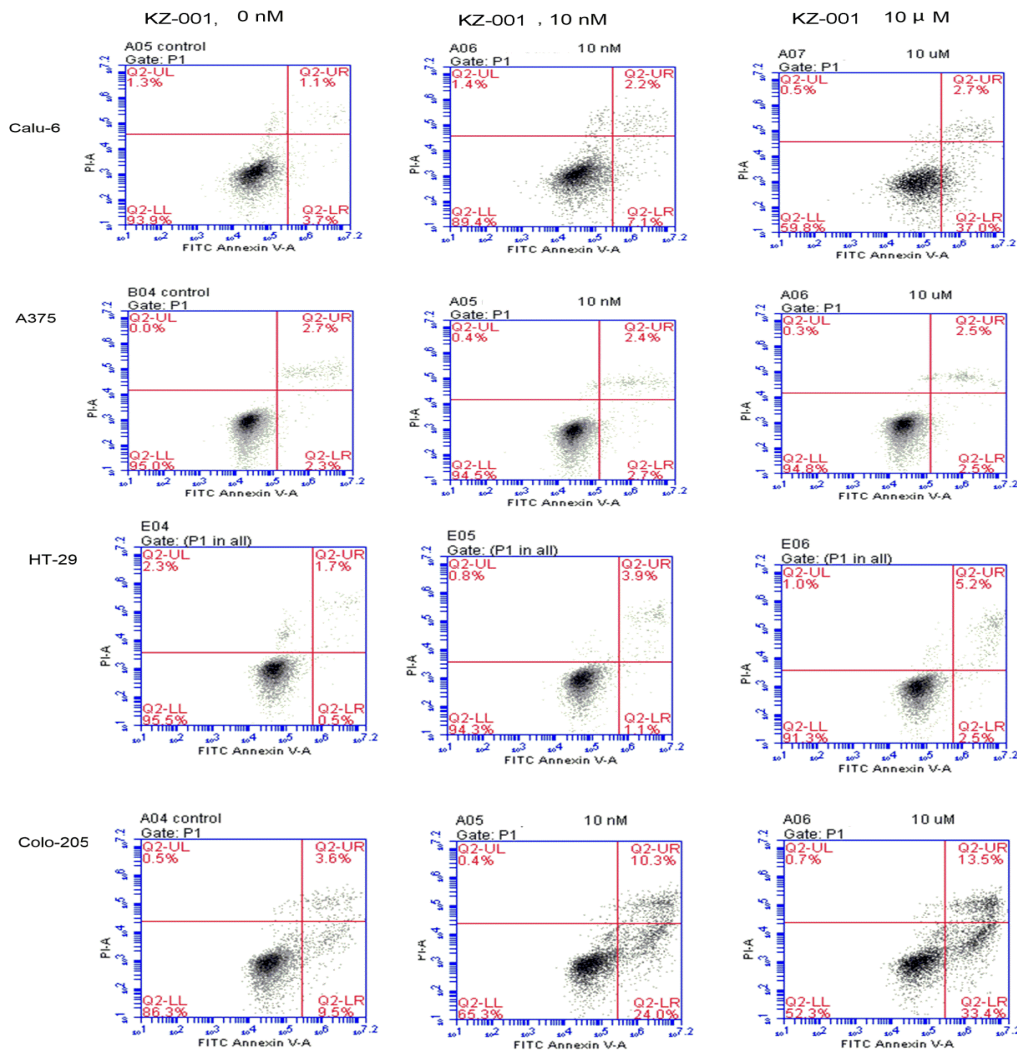


**Figure 3-4 KZ-001 induced apoptosis in Calu-6, A375, HT-29, and Colo-205 cells.** Calu-6, A375, HT-29 cells were left untreated or treated with 10 nM or 10  $\mu\text{M}$  KZ-001 for 24 h. Colo-205 cells were left untreated or treated for 14 h. Cells were incubated with FITC Annexin V in a buffer containing propidium iodide (PI) and analyzed by flow cytometry.

For the cell apoptosis assay, different cell lines exhibited various levels of apoptosis in response to the treatment with KZ-001. This could be explained by the possibility that MEK inhibitors may induce apoptosis through various mechanisms, depending on cell types [14]. It is likely that A375

and HT-29 cells respond to KZ-001 by inhibition of cell proliferation through cell cycle arrest or other mechanisms, rather than apoptosis.

### 3.4.5. KZ-001 induces cell cycle arrest in A375 cells.

Since the RAS pathway regulates the cell cycle, the effect of KZ-001 on cell cycle progression was examined in A375 cells. The results showed that KZ-001 at concentrations of 10 nM and 10  $\mu$ M caused cell cycle delay at the G0/G1 phase in A375 cells. Compared to vehicle controls, 10 nM and 10  $\mu$ M KZ-001 induced a significant increase of cells in the G1 phase (61.690  $\pm$  0.633% *versus* 94.473 $\pm$ 3.158% and 95.477  $\pm$  1.895%), with concomitant decrease of cells in S phase (24.093  $\pm$  3.311% *versus* 2.827  $\pm$  3.995% and 1.460  $\pm$  1.307%) and G2 phase (14.223  $\pm$  2.681% *versus* 2.670  $\pm$  0.956% and 3.063  $\pm$  0.733%) (Figure 3-5). In the vehicle group and treatment group, double peaks near the G1 and G2 phase were observed, which might be a result of aneuploidy. Hence, cell cycle distribution was quantified using ModFit LT 4.1.7 (Verity Software House).

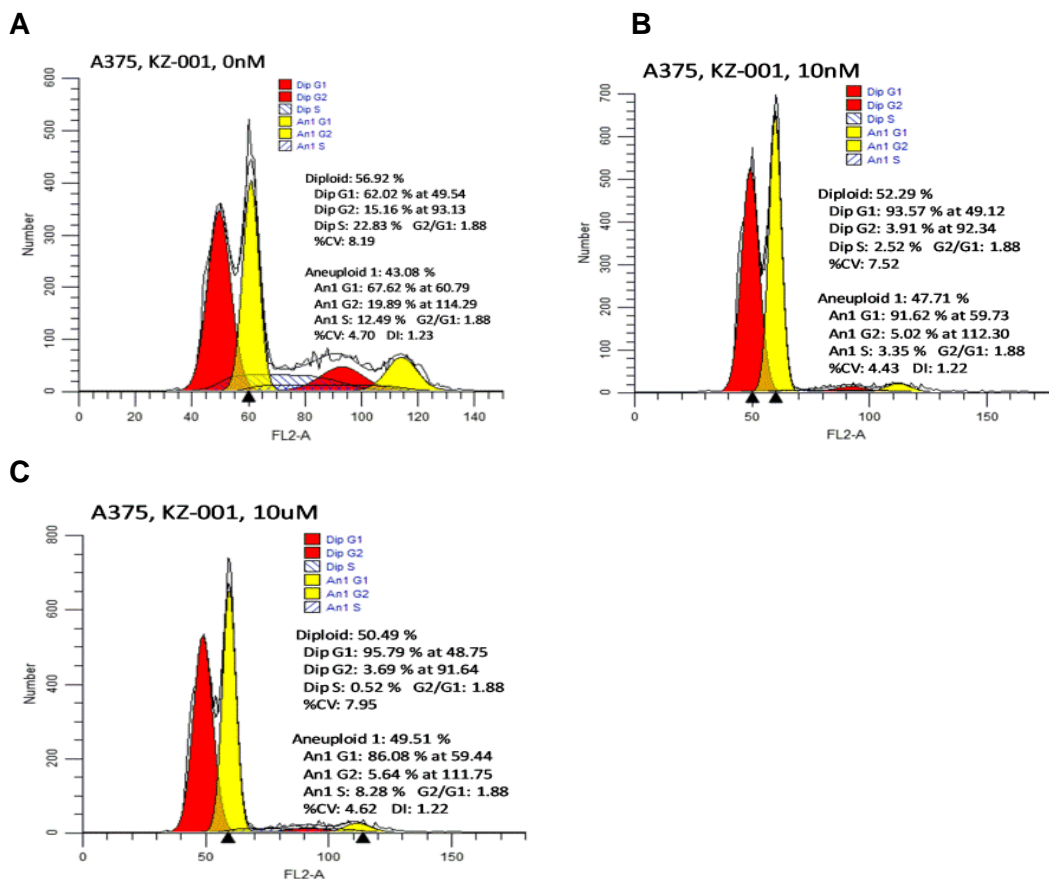


**Figure 3-5 KZ-001 induced cell cycle arrests in A375 cells.** Cells were treated for 24 h with 10 nM or 10  $\mu$ M KZ-001, or vehicle. Cells were fixed with 70% ethanol, digested with RNase, incubated with propidium iodide and analyzed by flow cytometry.

Ma B. et al. reported that AZD6244 induced G0/G1 cell cycle arrest in HONE-1-EBV and HK1-LMP1 (B95.8) cells [16]. Haass N. et al. reported that in two-dimensional cell culture, AZD6244 reduced the growth of melanoma cells through the induction of G1-phase cell cycle arrest [17].

#### 3.4.6. Pharmacokinetic evaluation of KZ-001 in ICR mice via I.V. and P.O. administration

Pharmacokinetic studies are an essential component of the drug discovery and development process. The pharmacokinetics of KZ-001 in ICR mice after single dose was assessed over a 24-h period. The concentration-time curve of KZ-001 after dosing by P.O. and I.V. are shown in Figure 3-6. KZ-001 was rapidly absorbed within 25 min to reach peak concentration ( $T_{max} = 0.25$  h). Its exposure was excellent following oral administrations with the maximum plasma concentration ( $C_{max}$ ) of 672 ng/mL and with the area under the concentration-time curve ( $AUC_{0-t}$ ) of 327 ng·h/mL (Table 3-5). Terminal half life ( $T_{1/2}$ ) of KZ-001 was satisfactory through both routes of administration: 1.96 h for Intravenous injection (IV) and 2.51 h for oral gavage (PO) administration. The oral bioavailability of KZ-001 was 28%. The PK profile of KZ-001 indicates its adequate druggability for conventional oral therapy.

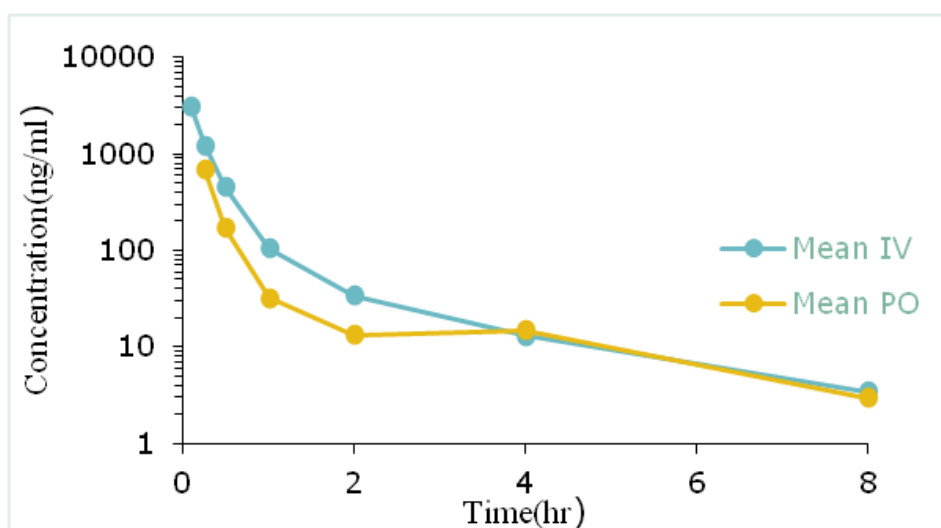


**Figure 3-6 Concentration-Time curves of KZ-001 after single dosing by IV and PO.** Mice (n=3) were administered KZ-001 by IV or PO, and the blood was collected at the time point of 0.5, 15 and 30 min, and 1, 2, 4, 8, and 24 h. At 24 h, the drug concentration of KZ-001 in the plasma was below the limit of quantification.

**Table 3-5 Plasma concentration and PK parameters of KZ-001**

IV	Mean		S.D.	CV (%)
$t_{1/2}$ (h)	1.96	±	0.64	32.9%
AUC <sub>0-t</sub> (ng·h /mL)	1192	±	186	15.6%
AUC <sub>0-∞</sub> (ng·h /mL)	1202	±	188	15.6%
Vd (L/Kg)	7.16	±	2.65	37.1%
CL (mL/min/kg)	42.2	±	6.21	14.7%

PO	Mean		S.D.	CV (%)
$t_{1/2}$ (h)	2.51	±	0.76	30.4%
T <sub>max</sub> (h)	0.25	±	0.00	0.0%
C <sub>max</sub> (ng/g)	672	±	392	58.3%
AUC <sub>0-t</sub> (ng·h /mL)	326	±	172	52.7%
AUC <sub>0-∞</sub> (ng·h /mL)	337	±	169	50.2%
Bioavailability	28%			

### 3.4.7. The antitumor efficacy of KZ-001 in single agent administration using xenograft models

After the *in vitro* enzymatic and cell-based assays, the antitumor activity of KZ-001 was further investigated in A375, Colo-205, Calu-6 tumor xenograft models. Also, AZD6244 was used as a reference compound for the *in vivo* efficacy comparison.

#### 3.4.7.1 The *in vivo* antitumor efficacy of KZ-001 alone in mice with A375 xenografts

When dosing was commenced at a mean tumor size of 200 mm<sup>3</sup>, chronic dosing of mice with KZ-001 (6 mg/kg) significantly inhibited the growth of A375 tumors (TGI 91.0%;  $p < 0.001$ ) (Figure 3-7). A dose response was observed in this model. Tumor growth was moderately inhibited at 3 mg/kg QD (TGI 39.2%;  $p < 0.05$ ), and the effect of 1.5 mg/kg QD was not considered significant (TGI 9.4%;  $p > 0.05$ ). In contrast, AZD6244 at 10 mg/kg QD resulted in 45.8% inhibition ( $p < 0.01$ ) using the A375 tumor xenograft model. Compared to AZD6244, KZ-001 inhibited tumor growth at remarkable lower doses (KZ-001 *versus* AZD6244: TGI 91.0% at 6 mg/kg,  $p < 0.001$  *versus* TGI 45.8% at 10 mg/kg,  $p < 0.01$ ). During the whole study, the body weight did not change significantly except in the vehicle group, which means that the mice tolerated applied dosages of KZ-001 well.

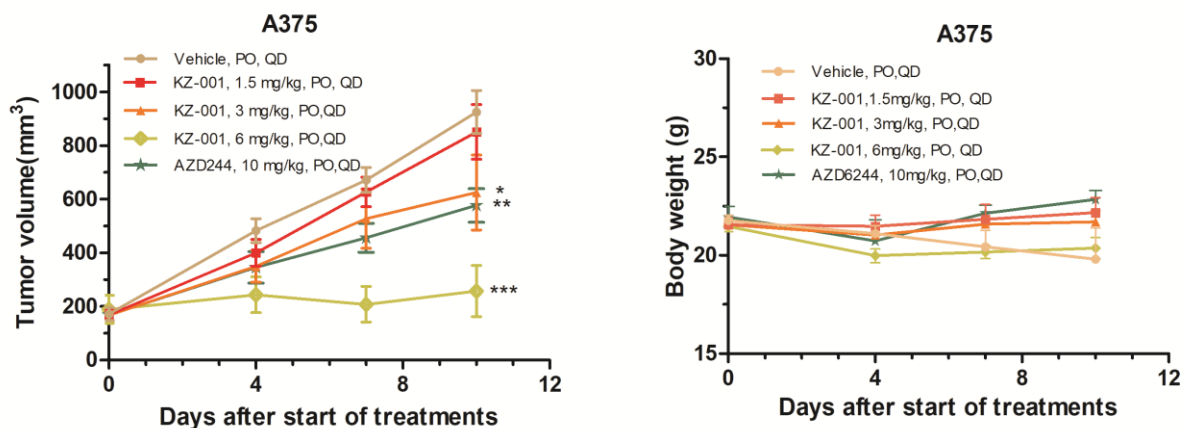


**Figure 3-7 Tumor growths and body weight change of A375 xenografts *in vivo* in single drug treatments.** Mice with A375 xenografts model were treated with vehicle, KZ-001 (1.5, 3 and 6 mg/kg, QD) or AZD6244 (10 mg/kg, QD). The body weights were recorded in each dosing and vehicle group when the tumor sizes were measured.

### 3.4.7.2 The *in vivo* antitumor efficacy of KZ-001 in single drug treatments in mice with Colo-205 xenografts

Chronic dosing with 3 mg/kg and 6 mg/kg KZ-001 completely inhibited the growth of Colo-205 tumors (TGI 103.9% and 108.8%, respectively;  $p < 0.01$ ) (Figure 3-8). Mice even obtained tumor regression. Likewise, AZD6244 at 10 mg/kg using the Colo-205 tumor xenograft model resulted in a significant inhibition of 83.3% ( $p < 0.01$ ) compared to the vehicle control. Mouse body weight did not change except in the vehicle group in the Colo-205 xenografts.

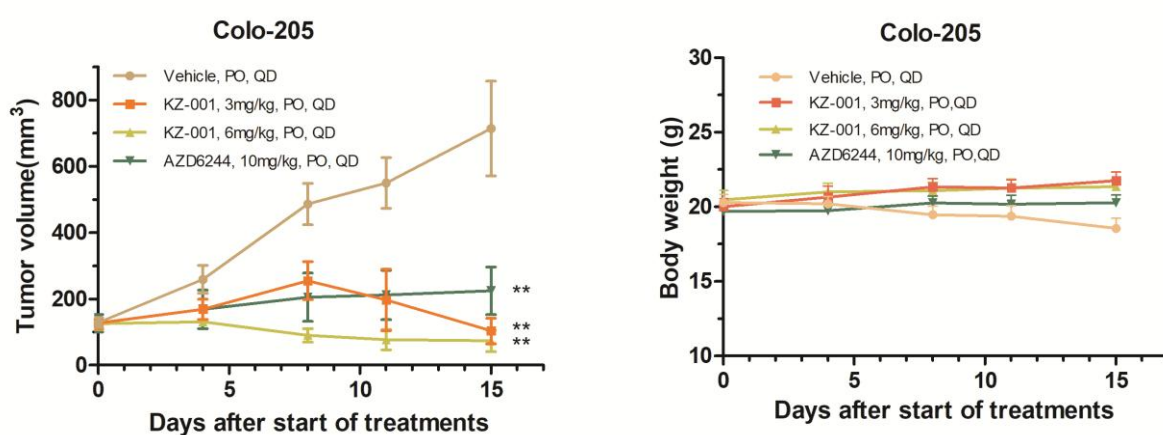


**Figure 3-8 Tumor growths and body weight change of Colo-205 xenografts *in vivo* in single drug treatment.** Mice with Colo-205 xenografts were treated with vehicle, KZ-001 (3 and 6 mg/kg, QD) or AZD6244 (10 mg/kg). The body weights were recorded in each dosing and vehicle group when the tumor sizes were measured.

### 3.4.7.3 The *in vivo* antitumor efficacy of KZ-001 in single drug treatments in mice with Calu-6 xenografts

Calu-6 xenografts were also inhibited by 3 mg/kg KZ-001 (TGI 63.2%;  $p < 0.01$ ). Dosing mice at 6 mg/kg KZ-001 also led to significant tumor growth inhibition ( $p < 0.01$ ). However, dosing mice with 1.5 mg/kg did not result in any distinct difference compared to the vehicle control. An inhibitory effect of AZD6244 was also observed when mice with Calu-6 xenografts were treated with 10 mg/kg (TGI 54.8%;  $p < 0.05$ ) (Figure 3-9). Mouse body weight did not change except in the vehicle group in the Calu-6 xenografts.

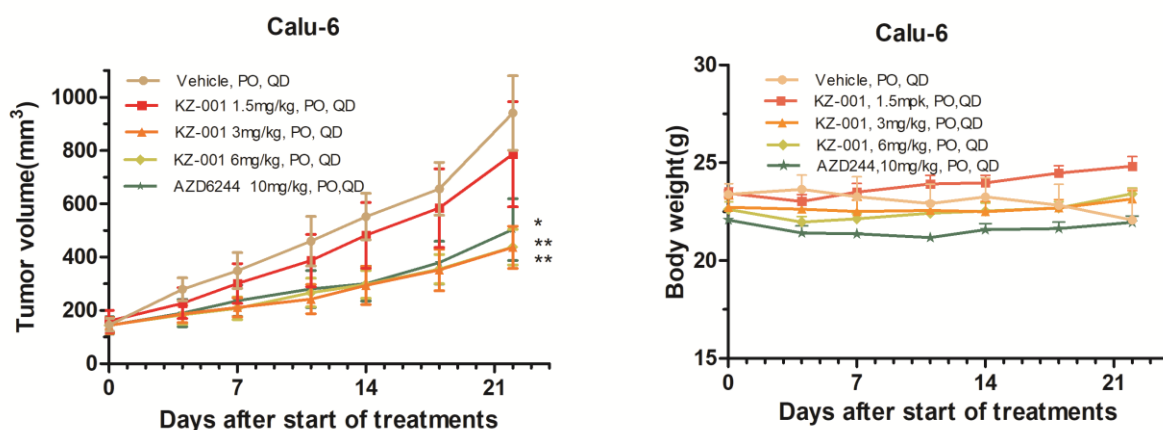


**Figure 3-9 Tumor growths and body weight change of Calu-6 xenografts *in vivo* in single drug treatment.** Mice with Calu-6 xenografts were treated with vehicle, KZ-001 (1.5, 3 and 6 mg/kg, QD) or AZD6244 (10 mg/kg, QD). The body weights were recorded in each dosing and vehicle group when the tumor sizes were measured.

Comparing the activity of KZ-001 in different xenograft models, it is concluded that RAF-mutant cancers are more sensitive to KZ-001 compared to RAS-mutant cancer, which is consistent with the *in vitro* study in cells. The possible reasons were discussed in *in vitro* studies section in this thesis.

In summary, these *in vivo* tumor growth inhibition studies indicate that KZ-001 has stronger antitumor activity than AZD6244.

### 3.4.8. The *in vivo* pharmacodynamic effects of KZ-001 in mice with A375, Calu-6, Colo-205 xenografts

The primary biomarker, phospho-ERK level, was evaluated by Western blotting of *ex vivo* tissues of A375, Calu-6, and Colo-205 xenografts (Figure 3-10). Compared to the vehicle-treated groups, KZ-001 significantly decreased the p-ERK levels, whereas the total ERK levels remained

consistent. Because KZ-001 only reduces the level of p-ERK, but not the expression of ERK, we speculate that KZ-001 inhibits the growth of tumor cells by preventing ERK phosphorylation, similar to other MEK inhibitors. These results indicate that KZ-001 exerts an antitumor effect *in vivo* through the mechanisms of action that was demonstrated in the *in vitro* studies.

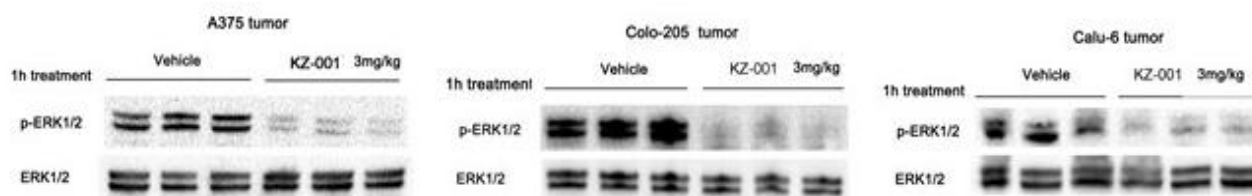


**Figure 3-10 Western blot analyses of effects of KZ-001 on phosphorylation of ERK1/2 and ERK1/2 expression levels for tissue lysates obtained from A375, Calu-6 and Colo-205 xenografts.** In all xenografts, mice were treated with 3 mg/kg of KZ-001 or vehicle for 1 h before analysis.

### 3.5. Conclusion

In conclusion, this study demonstrated that KZ-001 is a highly selective MEK1/2 inhibitor. This new compound shows significant antitumor activity against BRAF-mutant (A375 and Colo-205) and KRAS-mutant (Calu-6) cancer cells both *in vitro* and *in vivo* through inhibition of ERK phosphorylation. Compared to AZD6244, KZ-001 is more potent *in vitro* and *in vivo*. Mechanistically, KZ-001 behaved as a classic MEK inhibitor and inhibited the MAPK pathway. KZ-001 also induced apoptosis and cell cycle arrest to some extent. Furthermore, KZ-001 possesses a favorable PK profile with satisfactory drug exposure in plasma and bioavailability. Therefore, KZ-001 is an excellent new MEK1/2 inhibitor with great potential for cancer treatment. Our results suggest that KZ-001 has potential therapeutic implications for tumors with BRAF and KRAS mutations.

---

### 3.6 References

1. Rice, K. D.; Aay, N.; Anand, N. K.; Blazey, C. M.; Bowles, O. J.; Bussenius, J.; Costanzo, S.; Curtis, J. K.; Defina, S. C.; Dubenko, L.; Engst, S.; Joshi, A. A.; Kennedy, A. R.; Kim, A. I.; Koltun, E. S.; Loughheed, J. C.; Manalo, J. C.; Martini, J. F.; Nuss, J. M.; Peto, C. J.; Tsang, T. H.; Yu, P.; Johnston, S., Novel carboxamide-based allosteric MEK inhibitors: Discovery and optimization efforts toward XL518 (GDC-0973). *ACS Med Chem Lett* 2012, 3, (5), 416-21.
2. Roberts, P. J.; Der, C. J., Targeting the Raf-MEK-ERK mitogen-activated protein kinase cascade for the treatment of cancer. *Oncogene* 2007, 26, (22), 3291-310.
3. Yamaguchi, T.; Kakefuda, R.; Tajima, N.; Sowa, Y.; Sakai, T., Antitumor activities of JTP-74057 (GSK1120212), a novel MEK1/2 inhibitor, on colorectal cancer cell lines in vitro and in vivo. *Int J Oncol* 2011, 39, (1), 23-31.
4. Gilmartin, A. G.; Bleam, M. R.; Groy, A.; Moss, K. G.; Minthorn, E. A.; Kulkarni, S. G.; Rominger, C. M.; Erskine, S.; Fisher, K. E.; Yang, J.; Zappacosta, F.; Annan, R.; Sutton, D.; Laquerre, S. G., GSK1120212 (JTP-74057) is an inhibitor of MEK activity and activation with favorable pharmacokinetic properties for sustained in vivo pathway inhibition. *Clin Cancer Res* 2011, 17, (5), 989-1000.
5. Hoeflich, K. P.; Merchant, M.; Orr, C.; Chan, J.; Den Otter, D.; Berry, L.; Kasman, I.; Koeppen, H.; Rice, K.; Yang, N. Y.; Engst, S.; Johnston, S.; Friedman, L. S.; Belvin, M., Intermittent administration of MEK inhibitor GDC-0973 plus PI3K inhibitor GDC-0941 triggers robust apoptosis and tumor growth inhibition. *Cancer Res* 2012, 72, (1), 210-9.
6. Lee PA, W. E., Marlow A, Yeh T, Marsh V, Anderson D, Woessner R,; Hurley B, L. J., Poch G, Gross S, Rana S, Winski S, Koch K, Preclinical development of ARRY-162, a potent and selective MEK 1/2 inhibitor [abstract]. *Cancer Res* 2010, 70, 2515.
7. Yeh, T. C.; Marsh, V.; Bernat, B. A.; Ballard, J.; Colwell, H.; Evans, R. J.; Parry, J.; Smith, D.; Brandhuber, B. J.; Gross, S.; Marlow, A.; Hurley, B.; Lyssikatos, J.; Lee, P. A.; Winkler, J. D.; Koch, K.; Wallace, E., Biological characterization of ARRY-142886 (AZD6244), a potent, highly selective mitogen-activated protein kinase kinase 1/2 inhibitor. *Clin Cancer Res* 2007, 13, (5), 1576-83.
8. Patel, H.; Yacoub, N.; Mishra, R.; White, A.; Long, Y.; Alanazi, S.; Garrett, J. T., Current

- 
- advances in the treatment of BRAF-mutant melanoma. *Cancers (Basel)* 2020, 12, (2).
9. Sullivan, R. J.; Flaherty, K. T., BRAF in melanoma: Pathogenesis, diagnosis, inhibition, and resistance. *J Skin Cancer* 2011, 2011, 423239.
  10. Miele, E.; Abballe, L.; Spinelli, G. P.; Besharat, Z. M.; Catanzaro, G.; Chiacchiarini, M.; Vacca, A.; Po, A.; Capalbo, C.; Ferretti, E., BRAF mutant colorectal cancer: ErbB2 expression levels as predictive factor for the response to combined BRAF/ErbB inhibitors. *BMC Cancer* 2020, 20, (1), 129.
  11. Ahmed, D.; Eide, P. W.; Eilertsen, I. A.; Danielsen, S. A.; Eknaes, M.; Hektoen, M.; Lind, G. E.; Lothe, R. A., Epigenetic and genetic features of 24 colon cancer cell lines. *Oncogenesis* 2013, 2, e71.
  12. Yang, H.; Liang, S. Q.; Schmid, R. A.; Peng, R. W., New Horizons in KRAS-Mutant Lung Cancer: Dawn After Darkness. *Front Oncol* 2019, 9, 953.
  13. M., T., Rapid colorimetric assay for cellular growth and survival: Application to proliferation and cytotoxicity assays. *J Immunol Methods* 1983, 65, (1-2), 55-63.
  14. Davies, B. R.; Logie, A.; McKay, J. S.; Martin, P.; Steele, S.; Jenkins, R.; Cockerill, M.; Cartledge, S.; Smith, P. D., AZD6244 (ARRY-142886), a potent inhibitor of mitogen-activated protein kinase/extracellular signal-regulated kinase 1/2 kinases: mechanism of action in vivo, pharmacokinetic/pharmacodynamic relationship, and potential for combination in preclinical models. *Mol Cancer Ther* 2007, 6, (8), 2209-19.
  15. Zhao, Y.; Adjei, A. A., The clinical development of MEK inhibitors. *Nature Reviews Clin Oncol* 2014, 11, (7), 385-400.
  16. Ma, B. B.; Lui, V. W.; Cheung, C. S.; Lau, C. P.; Ho, K.; Hui, E. P.; Tsui, S. K.; Ng, M. H.; Cheng, S. H.; Ng, P. K.; Tsao, S. W.; Chan, A. T., Activity of the MEK inhibitor selumetinib (AZD6244; ARRY-142886) in nasopharyngeal cancer cell lines. *Invest New Drugs* 2013, 31, (1), 30-8.
  17. Haass, N. K.; Sproesser, K.; Nguyen, T. K.; Contractor, R.; Medina, C. A.; Nathanson, K. L.; Herlyn, M.; Smalley, K. S., The mitogen-activated protein/extracellular signal-regulated kinase kinase inhibitor AZD6244 (ARRY-142886) induces growth arrest in melanoma cells and tumor regression when combined with docetaxel. *Clin Cancer Res* 2008, 14, (1), 230-9.

---

## **4. CHAPTER 4: SYNERGISTIC EFFECTS OF KZ-001 COMBINED WITH COMMERCIAL ANTI-CANCER DRUGS**

This study was published in *International Journal of Cancer*, Year 2019, Vol. 145, Pages 586-596.

---

#### 4.1. Abstract

Some subtypes of BRAF or KRAS mutant cancers are often associated with drug-resistance and disease progression in single drug treatments. MEK inhibitors were initially used for BRAF-mutant melanoma, however, acquired drug-resistance was observed and some patients relapsed due to an abundance of escape mechanisms present. Increasing evidence showed that multi-targeted combination therapy delays the onset of acquired resistance, leading to increased progress-free survival and overall survival. Moreover, recent studies demonstrated that combination therapy is better tolerated compared to monotherapy in patients harboring BRAF or KRAS mutation. The study investigated the effect of KZ-001 in combination with other agents both *in vitro* and *in vivo* xenograft models.

The combination of KZ-001 with the BRAF inhibitor vemurafenib was evaluated in A375, Colo-205 and HT-29 cells, and analyzed by fraction affected-combination index (CI) curves. The results indicated that there was a wide range of synergistic effects between these two compounds. The combination between KZ-001 and docetaxel was tested in A375, Colo-205, HT-29, and Calu-6 tumor cell lines *in vitro*. This combination imparted a synergistic effect on all cell lines tested except for A375. Moreover, the CI values in Calu-6 and Colo-205 decreased to  $< 0.2$ , indicating a strong synergistic effect.

The combination of KZ-001 and vemurafenib was investigated in A375 (typical BRAF mutant melanoma cells) xenografts, and tumor growth inhibition was analysed in both single and combination treatment groups. Although the anticancer effect of single drug was minimal, with 20.4% inhibition for vemurafenib at 25 mg/kg BID, and 9.4% inhibition for KZ-001 at 1.5 mg/kg QD, the combination treatment showed significant inhibition of A375 xenograft with TGI at 87.4% ( $p < 0.0001$ ) with Q value of 3.14, indicating high-level synergism.

A vemurafenib and KZ-001 combination study in Colo-205 (typical BRAF mutant colon cancer cells) xenografts was conducted. As monotherapy, vemurafenib (100 mg/kg, QD) did not cause remarkable inhibition of tumor growth (TGI 47.5%). The combination treatment regimen (vemurafenib at 100 mg/kg QD and KZ-001 at 3 mg/kg QD) resulted in 111.7% tumor growth inhibition ( $p < 0.01$ ), and the Q value was 1.10, indicating a synergistic effect of this drug combination.

---

Calu-6, a typical KRAS-mutant NSCLC expressing cell line, is an ideal candidate for the combination study of KZ-001 and docetaxel. In single agent treatments, tumor growth inhibition of KZ-001 at a dose of 1.5 mg/kg QD and docetaxel at a dose of 5 mg/kg QW was 21.2% and 14.7%, respectively, while their combination resulted in 59.1% ( $p < 0.05$ ) tumor growth inhibition with a Q value of 1.80, showing synergistic effect.

In summary, KZ-001, a structurally new type of benzoxazole compound was developed as a MEK inhibitor that may be potentially used clinically for the treatment of RAS/RAF mutant cancers to overcome drug resistance.

## 4.2. Introduction

BRAF mutations are detected in about 50% of patients with melanoma, approximately 10% of patients with colorectal cancer (CRC), about 2-8% of patients with non-small cell lung cancer [1]. Resistance to BRAF inhibitors develops within a short period in melanoma patients with BRAF<sup>V600E</sup> mutations. Only approximately 5% of patients with BRAF<sup>V600E</sup> CRC respond to BRAF inhibitor monotherapy [2]. Vemurafenib is a BRAF inhibitor approved by FDA for treatment of patients with unresectable or metastatic melanoma with BRAF<sup>V600E</sup> mutation. Resistance to vemurafenib and disease progress usually develops within 6–8 months. Preclinical studies demonstrated that resistance to BRAF inhibitor is associated with recovery of MAPK pathway signalling. Thus, it may be critical to completely block the MAPK pathway. The combination of BRAF with downstream inhibition of MEK 1/2 was postulated to maximize MAPK pathway inhibition and prevent/delay the onset of resistance [1], thereby improving clinical outcomes in patients with melanoma. Furthermore, the phase III clinical study demonstrated that the addition of cobimetinib (a MEK inhibitor) to vemurafenib achieved a significant improvement in progression-free survival among patients with BRAF<sup>V600E</sup>-mutated metastatic melanoma, at the cost of some increase in toxicity [3]. Moreover, recent studies demonstrated that combination therapy is better tolerated compared to monotherapy in patients harboring BRAF or KRAS mutation.

Activating mutations in KRAS are present in nearly 90% of pancreatic cancers, in about 50% of all colorectal cancers, and in approximately 25% of non-small cell lung cancer. Genotype-directed targeted therapy is the standard of care for patients with advanced non-small cell lung cancer

---

(NSCLC) [4]. However, there are currently no targeted therapies for KRAS mutant non-small cell lung cancer [5]. These patients exhibit a worse prognosis and may gain less benefit from chemotherapy than the other NSCLC patients [6]. The development therapies directly targeting KRAS has, however, proven to be challenging. Hence, to inhibit KRAS effector proteins downstream, including MEK, has been a promising therapeutic strategy. MEK inhibitors were initially used for BRAF mutant melanoma, however, acquired drug-resistance can occur and some patients relapse due to an abundance of escape mechanisms present [7]. Moreover, MEK inhibitors in combination with chemotherapy have been proven to be effective in preclinical studies [8]. Docetaxel is a conventional therapeutical agent, and is believed to have two-fold mechanism of anti-cancer activity: inhibiting microtubular depolymerization; countering the effects of bcl-2 and bcl-xL gene expression [9]. The most widely accepted mechanism of action, associates with the binding of docetaxel to  $\beta$ -tubulin, thus promoting polymerization.

Combination therapy is a well established clinical approach for cancer treatment and can also contribute to address emerging resistance. Multi-targeted therapy can reside in the same or different pathways and tissues, and this can produce more than additive effects triggered by actions converging at a specific pathway site [10]. A combination is pharmacodynamically synergistic, additive or antagonistic if the effect is greater than, equal to, or lower than the summed effects of the partner drugs. Clinically, a great potential for combinations of MEK inhibitors and conventional chemotherapeutics has been established. However, in order to increase the chance of success in trials, dosing schedules of dual therapies must be explored pre-clinically.

In recent years, the combination of MEK inhibitors with other therapies has shown to be effective in cancer treatment. Therefore, this study investigated combination treatments of KZ-001 with two commonly used and well-studied anticancer drugs, vemurafenib and docetaxel (a microtubule stabilizing agent) both *in vitro* and *in vivo*.

### **4.3. Materials and methods**

#### **4.3.1. Cell lines and subculture**

A375, HT-29, Calu-6 and A431 cell lines were purchased from the Typical Culture Preservation Commission Cell Bank of the Chinese Academy of Sciences in China and Colo-205 cell line was

---

from Institute of Basic Medical Sciences, Chinese Academy of Medical Sciences in China. All cell lines were authenticated by short tandem repeat analysis. A375, HT-29, Calu-6, Colo-205, and A431 cell lines were maintained in DMEM (Dulbecco's minimal essential medium), McCoy's 5a, MEM (minimal essential medium), and RPMI 1640 medium, respectively. All the media were supplemented with 10% heat-inactivated FBS (BI), 1 mM sodium pyruvate and 100 U/mL penicillin and 0.1 mg/mL streptomycin.

#### **4.3.2. *In vitro* combination drug treatment study**

For A375, HT-29, Calu-6, and A431 cell lines, cell proliferation was analyzed using the 3-(4,5-dimethylthiazole-2-yl)-2,5-diphenyl-2H-tetrazolium bromide (MTT) assay, while for the Colo-205 cell line the (3-(4,5-dimethylthiazol-2-yl)-5-(3-carboxymethoxyphenyl)-2-(4-sulfophenyl)-2H-tetrazolium) (MTS) assay was used. Cells were seeded into 96-well microtiter plates at a density of 500 to 3,000 cells per well and appropriately diluted drug was added to each test well in triplicate after a cell adhesion period of 24 h. Cell viability was assayed 72 h after the cells were plated according to the procedure originally described by Mosmann [11]. Survival rate was calculated using the formula:

$$\text{Survival rate} = \frac{(\text{Mean absorbance of experimental wells} - \text{Mean absorbance of DMSO wells})}{(\text{Mean absorbance of control wells} - \text{Mean absorbance of DMSO wells})} \times 100\%$$

IC<sub>50</sub> was determined using a dose-response inhibition model with non-linear, four parameter regressions of semi-logarithm plots of the drug concentration versus survival rate using GraphPad Prism 6. The combination index (CI) value between KZ-001 and other compounds was determined using CalcuSyn Version 2.1 software (Biosoft, Cambridge, UK). CI <1, =1 or >1 showed synergy, additive or antagonistic effects, respectively.

#### **4.3.3. *In vivo* efficacy studies of combination drug treatments**

Vemurafenib was also dispersed completely in 2% Klucel LF (Hydroxypropylcellulose) (Aqualon) and adjusted to pH 4 with diluted hydrochloric acid. Docetaxel was solubilized in normal saline with 5% Tween80 and 5% ethanol.

The vehicle control groups were treated with 10 mL/kg vehicle, PO, and QD for all xenograft models. KZ-001 single drug treatment groups were treated with KZ-001 (1.5 mg/kg for A375 and Calu-6 xenografts; 3 mg/kg for Colo-205 xenograft), PO, QD. The ancillary drug treatment groups were treated with vemurafenib (25 mg/kg, BID, PO) for A375 xenograft, or docetaxel [5 mg/kg, once weekly (QW), IV] for Calu-6 xenograft, vemurafenib (100 mg/kg, QD, PO) for Colo-205 xenograft. In

the docetaxel and vemurafenib treatment groups (25 mg/kg, BID, PO), one mouse from each group was sacrificed due to a >20% decrease in body weight on days 11 and 5, respectively; the remaining five mice were studied until the completion of the study. The combination drug treatment groups received the concentrations stated above. When given in combination, the drugs were given separately. All animal experiments were approved by the Animal Care and Ethics Committee at the Institute of Radiation Medicine, Chinese Academy of Medical Sciences (2016ZX310199).

**Table 4-1 Group setting of mice in drug combination studies**

Tumor xenograft model	Groups	Dose (mg/kg)	Treatment	Animals (N)
A375	Vehicle	-	PO, QD × 10 days	6
	KZ-001, 1.5	1.5	PO, QD × 10 days	6
	Vemurafenib, 25	25	PO, QD × 10 days	6
	KZ-001+Vemurafenib	(1.5, 25)	PO+ QD, × 10 days	6
Colo-205	Vehicle	-	PO, QD, × 15 days	6
	KZ-001, 3	3	PO, QD × 15 days	6
	Vemurafenib, 100	100	PO, QD × 15 days	6
	KZ-001+Vemurafenib	(3, 100)	PO, QD × 15 days	6
Calu-6	Vehicle	-	PO, QD × 22 days	6
	KZ-001, 1.5	1.5	PO, QD × 22 days	6
	Docetaxel	5	IV, QW × 22 days	6
	KZ-001+ Docetaxel	(1.5, 5)	PO+IV × 22 days	6

Q values were used to validate whether two compounds acted synergistically or not [12]. Q values were calculated using the formula:  $Q = TGI_{AB} / [TGI_A + (1 - TGI_A) \times TGI_B]$ ,  $TGI_A$  or  $TGI_B$  represents growth inhibition due to either of the two compounds, and  $TGI_{AB}$  is the growth inhibition due to the combination of the two compounds.  $Q > 1$ ,  $= 1$ , or  $< 1$  show synergy, additive or antagonistic effects, respectively.

#### 4.3.4. Statistical analyses

All biochemistry and cell experiments were performed in three replicates per treatment. A t-test was used to analyse differences between two groups in the efficacy study. Differences between groups were considered significant for  $p < 0.05$ .

---

## 4.4. Results and discussion

### 4.4.1. The combination of KZ-001 and vemurafenib shows synergistic effects in BRAF mutant cell lines *in vitro*.

In recent years, the combination of MEK inhibitors with other therapies has shown to be effective in cancer treatment. Therefore, the combined effects of KZ-001 with two commonly used and well-studied anticancer drugs, vemurafenib (a BRAF<sup>V600E</sup> inhibitor) and docetaxel (a microtubule stabilizing agent) was investigated, respectively. According to the model of drug combination based on median-effect equation, calculusyn software was used to analyze the results of combination treatment experiments [13].

The fraction affected-combination index (CI) curve of KZ-001 and vemurafenib on BRAF mutant cell lines (A375, Colo-205 and HT-29) indicated a wide range of synergistic effects between these two compounds (Figure 4-1, points below CI=1 line). This finding implies that the inhibition of BRAF enhances the effect of KZ-001 on cell growth.

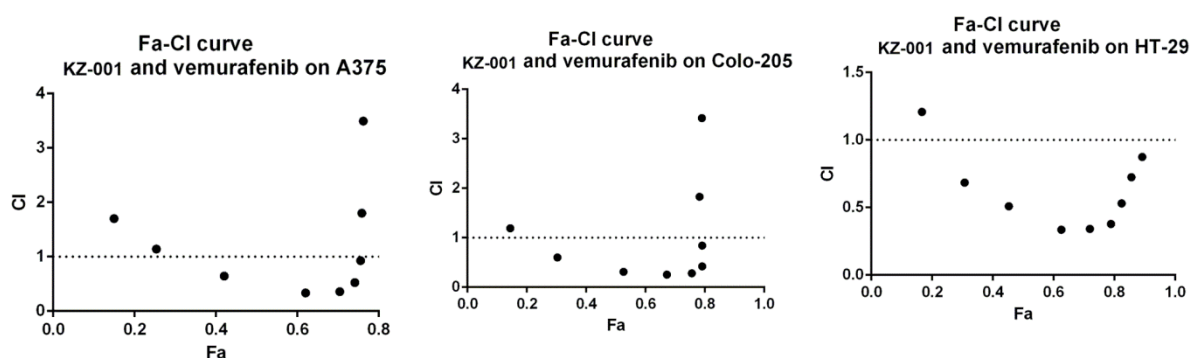


**Figure 4-1** Fa-CI curves of BRAF mutant cell lines treated with KZ-001 combined with vemurafenib. CI = 1 line represents additive effect; dots below or above CI = 1 line represent synergistic or antagonistic effect, respectively.

### 4.4.2. The combination of KZ-001 and docetaxel shows synergistic effects against BRAF and KRAS mutant cell lines *in vitro*.

Docetaxel is a commonly used microtubule-stabilizing cytotoxic drug that has great potential for combination with MEK inhibitors in clinical application. A previous study demonstrated an accumulation of cells in the G2-M phase of the cell cycle after treatment with docetaxel, resulting in increased abundance of MEK but compromised activity. Therefore the combination of MEK inhibitor and docetaxel may reciprocally enhance their efficacy [8]. Moreover, the combination treatment greatly reduced sphere size with loss of cell viability using a three-dimensional spheroid model,

suggesting that the combination of MEK inhibitors with the chemotherapy agent docetaxel could be more efficient for cancer treatment [14].

The combination between KZ-001 and docetaxel was tested on tumor cell lines to determine whether it has a synergistic activity *in vitro*. This combination imparted a synergistic effect on all cell lines tested except for A375 (Figure 4-2). Moreover, the CI value in Calu-6 and Colo-205 decreased to < 0.2, indicative of a strong synergistic effect.

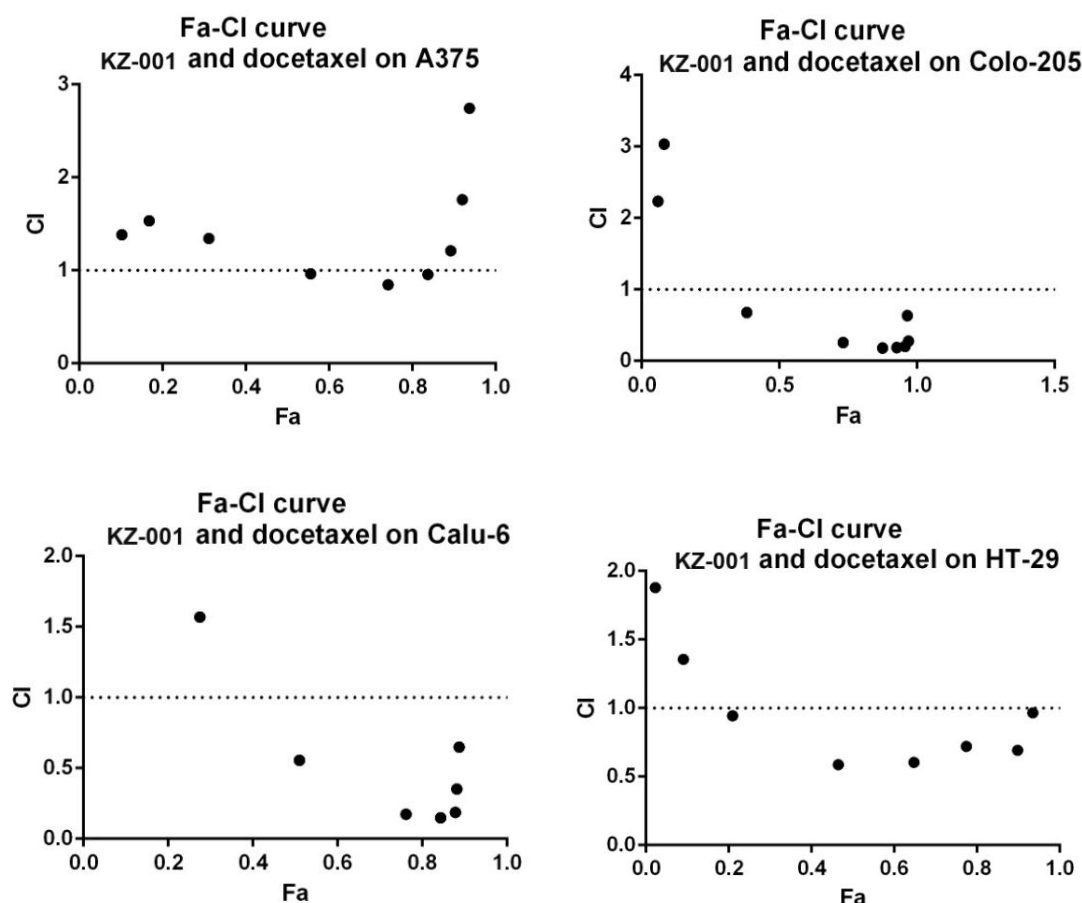


**Figure 4-2 Fa-CI curves of BRAF and KRAS mutant cell lines treated with KZ-001 combined with the cytotoxic drug docetaxel.** CI = 1 line represents additive effect; Dots below CI = 1 line represent synergistic effect; Dots above CI = 1 line represent antagonistic effect.

#### 4.4.3. The effect of the combination of KZ-001 with vemurafenib on the treatment of A375 tumor xenografts *in vivo*

As a selective BRAF<sup>V600E</sup> inhibitor, vemurafenib displays potent antitumor activity against melanoma [15]. The above *in vitro* tests indicated that vemurafenib at concentrations ranging from 100 nM to 800 nM has a potent synergistic effect on A375 cells when combined with KZ-001. Therefore, the

potential of vemurafenib to reinforce the efficacy of KZ-001 was evaluated. Although the anticancer effect of the single drug treatments was minimal, with 20.4% inhibition for vemurafenib at 25 mg/kg BID, and 9.4% inhibition for KZ-001 at 1.5 mg/kg QD, the combination treatment showed significant inhibition of A375 xenografts with TGI at 87.4% ( $p < 0.0001$ ) (Figure 4-3). Moreover, Jin Zheng-Juen's formulation [12] yielded a Q value of 3.14, indicative of high-level synergism.

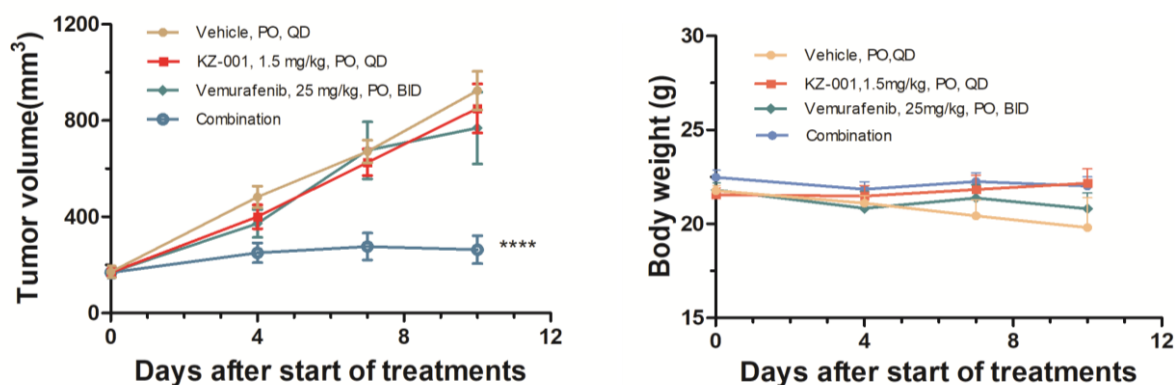


**Figure 4-3 Synergistic effect of KZ-001 combined with vemurafenib on BRAF-mutant A375 tumor xenografts.** A375 was treated with KZ-001 (1.5 mg/kg, QD), vemurafenib (25 mg/kg, BID), or KZ-001 (1.5 mg/kg, QD) plus vemurafenib (25 mg/kg, BID). N=6 per treatment group. Data are expressed as the mean tumor volume and mean body weight  $\pm$  SEM, respectively. \*:  $p < 0.05$ ; \*\*:  $p < 0.01$ ; \*\*\*:  $p < 0.001$ ; \*\*\*\*:  $p < 0.0001$  by t-test compared with vehicle control group.

#### 4.4.4. Effects of combination treatments with KZ-001 and vemurafenib on Colo-205 tumor xenografts *in vivo*

Colo-205 is a colon cancer cell line bearing the BRAF<sup>V600E</sup> mutation. A vemurafenib and KZ-001 combination study was performed on Colo-205 xenografts in parallel. In monotherapy, vemurafenib (100 mg/kg, QD) did not cause remarkable inhibition of tumor growth (TGI 47.5%). The combination treatment regimen (vemurafenib at 100 mg/kg QD and KZ-001 at 3 mg/kg QD) resulted in 111.7% tumor growth inhibition ( $p < 0.01$ ), and the Q value was 1.10, indicative of synergistic effects (Figure 4-4).

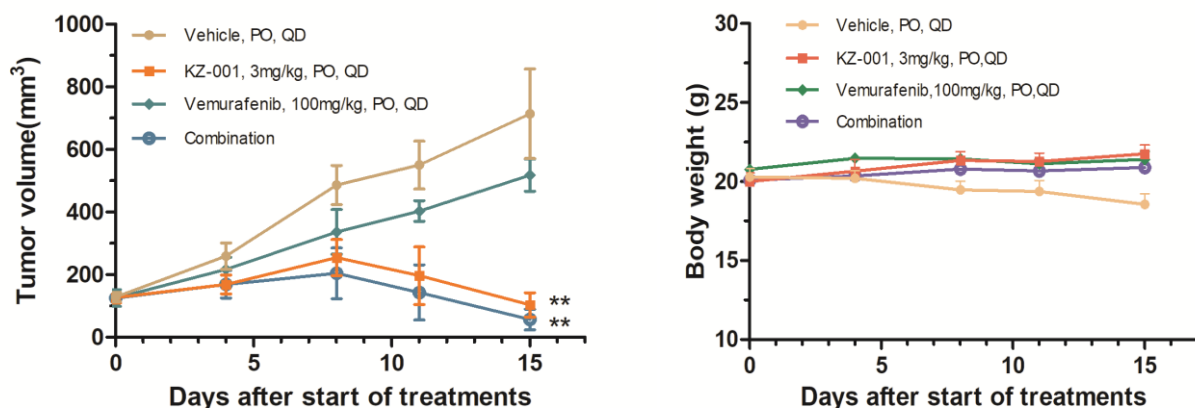


**Figure 4-4 Synergistic effects of KZ-001 combined with vemurafenib on BRAF mutant Colo-205 xenografts.** Colo-205 was treated with KZ-001 (3 mg/kg, QD), vemurafenib (100 mg/kg, QD), or KZ-001 (3 mg/kg, QD) plus vemurafenib (100 mg/kg, QD). N=6 per treatment group. Data are expressed as the mean tumor volume and mean body weight  $\pm$  SEM, respectively. \*:  $p < 0.05$ ; \*\*:  $p < 0.01$ ; \*\*\*:  $p < 0.001$ ; \*\*\*\*:  $p < 0.0001$  by t-test compared with vehicle control group.

#### 4.4.5. Effects of combination treatments with KZ-001 and docetaxel on Calu-6 tumor xenografts *in vivo*

Docetaxel is a standard-of-care chemotherapy for cancer patients, particularly for NSCLC [16]. It is often investigated with the combination of kinase inhibitors in preclinical studies of NSCLC. Calu-6, a typical KRAS-mutant NSCLC expressing cell line is an ideal candidate for the combination study of KZ-001 and docetaxel. As a single agent, the tumor growth inhibition of KZ-001 at a dose of 1.5 mg/kg QD and docetaxel at a dose of 5 mg/kg QW was 21.2% and 14.7%, respectively. The combination treatment inhibited tumor growth by 59.1% ( $p < 0.05$ ) with a Q value of 1.80, showing obvious synergistic effects (Figure 4-5).

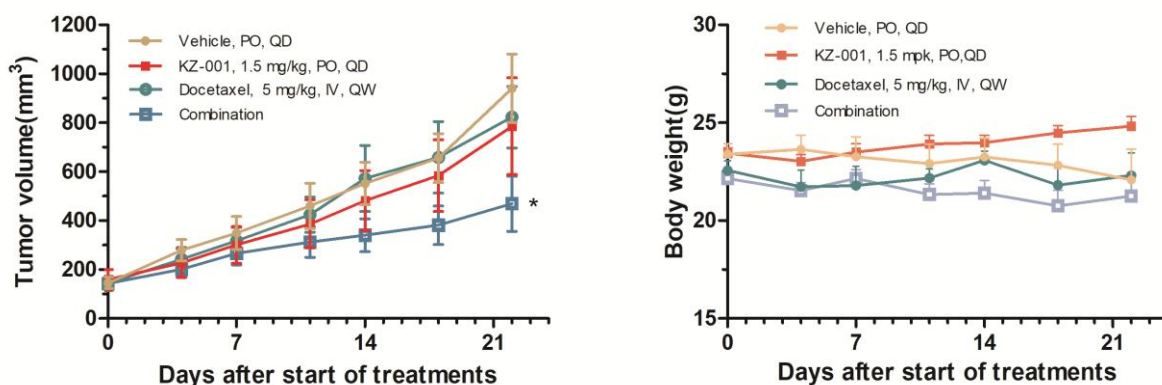


**Figure 4-5 Synergistic effects of KZ-001 combined with docetaxel on KRAS-mutant tumor Calu-6 xenografts.** Calu-6 was treated with KZ-001 (1.5 mg/kg, QD), docetaxel (5 mg/kg, QW), or KZ-001 (1.5

---

mg/kg, QD) plus docetaxel (5 mg/kg, QW). N=6 per treatment group. Data are expressed as the mean tumor volume and mean body weight  $\pm$  SEM, respectively. \*:  $p < 0.05$ ; \*\*:  $p < 0.01$ ; \*\*\*:  $p < 0.001$ ; \*\*\*\*:  $p < 0.0001$  by *t*-test compared with vehicle control group.

#### **4.5. Conclusion**

The combination treatments of KZ-001 investigated both *in vitro* cell proliferation studies and *in vivo* xenograft models demonstrated that combination of KZ-001 with the BRAF inhibitor vemurafenib or the chemotherapy agent docetaxel were synergistic. KZ-001, a structurally new type of benzoxazole compound was developed as a MEK inhibitor that may be combined with other drugs for potentially use in clinics for the treatment of RAS/RAF mutant cancer to overcome drug-resistant.

---

## 4.6 References

1. Subbiah, V.; Baik, C.; Kirkwood, J. M., Clinical development of BRAF plus MEK inhibitor combinations. *Trends Cancer* 2020.
2. Kopetz, S.; Desai, J.; Chan, E.; Hecht, J. R.; O'Dwyer, P. J.; Maru, D.; Morris, V.; Janku, F.; Dasari, A.; Chung, W.; Issa, J. P.; Gibbs, P.; James, B.; Powis, G.; Nolop, K. B.; Bhattacharya, S.; Saltz, L., Phase II pilot study of vemurafenib in patients with metastatic BRAF-mutated Colorectal Cancer. *J Clin Oncol* 2015, 33, (34), 4032-8.
3. Larkin, J.; Ascierto, P. A.; Dreno, B.; Atkinson, V.; Liskay, G.; Maio, M.; Mandala, M.; Demidov, L.; Stroyakovskiy, D.; Thomas, L.; de la Cruz-Merino, L.; Dutriaux, C.; Garbe, C.; Sovak, M. A.; Chang, I.; Choong, N.; Hack, S. P.; McArthur, G. A.; Ribas, A., Combined vemurafenib and cobimetinib in BRAF-mutated melanoma. *N Engl J Med* 2014, 371, (20), 1867-76.
4. Kris, M. G.; Johnson, B. E.; Berry, L. D.; Kwiatkowski, D. J.; Iafrate, A. J.; Wistuba, II; Varella-Garcia, M.; Franklin, W. A.; Aronson, S. L.; Su, P. F.; Shyr, Y.; Camidge, D. R.; Sequist, L. V.; Glisson, B. S.; Khuri, F. R.; Garon, E. B.; Pao, W.; Rudin, C.; Schiller, J.; Haura, E. B.; Socinski, M.; Shirai, K.; Chen, H.; Giaccone, G.; Ladanyi, M.; Kugler, K.; Minna, J. D.; Bunn, P. A., Using multiplexed assays of oncogenic drivers in lung cancers to select targeted drugs. *JAMA* 2014, 311, (19), 1998-2006.
5. Janne, P. A.; van den Heuvel, M. M.; Barlesi, F.; Cobo, M.; Mazieres, J.; Crino, L.; Orlov, S.; Blackhall, F.; Wolf, J.; Garrido, P.; Poltoratskiy, A.; Mariani, G.; Ghiorghiu, D.; Kilgour, E.; Smith, P.; Kohlmann, A.; Carlile, D. J.; Lawrence, D.; Bowen, K.; Vansteenkiste, J., Selumetinib plus docetaxel compared with docetaxel alone and progression-free survival in patients with KRAS-mutant Advanced Non-Small Cell Lung Cancer: The SELECT-1 randomized clinical trial. *JAMA* 2017, 317, (18), 1844-1853.
6. Barlesi, F.; Mazieres, J.; Merlio, J.-P.; Debieuvre, D.; Mosser, J.; Lena, H.; Ouafik, L. H.; Besse, B.; Rouquette, I.; Westeel, V.; Escande, F.; Monnet, I.; Lemoine, A.; Veillon, R.; Blons, H.; Audigier-Valette, C.; Bringuier, P.-P.; Lamy, R.; Beau-Faller, M.; Pujol, J.-L.; Sabourin, J.-C.; Penault-Llorca, F.; Denis, M. G.; Lantuejoul, S.; Morin, F.; Tran, Q.; Missy, P.; Langlais, A.; Milleron, B.; Cadranet, J.; Soria, J.-C.; Zalcman, G., Routine molecular profiling of

- 
- patients with advanced non-small-cell lung cancer: results of a 1-year nationwide programme of the French Cooperative Thoracic Intergroup (IFCT). *The Lancet* 2016, 387, (10026), 1415-1426.
7. Heppt, M. V.; Tietze, J. K.; Graf, S. A.; Berking, C., Combination therapy of melanoma using kinase inhibitors. *Curr Opin Oncol* 2015, 27, (2), 134-40.
  8. Davies, B. R.; Logie, A.; McKay, J. S.; Martin, P.; Steele, S.; Jenkins, R.; Cockerill, M.; Cartlidge, S.; Smith, P. D., AZD6244 (ARRY-142886), a potent inhibitor of mitogen-activated protein kinase/extracellular signal-regulated kinase 1/2 kinases: mechanism of action in vivo, pharmacokinetic/pharmacodynamic relationship, and potential for combination in preclinical models. *Mol Cancer Ther* 2007, 6, (8), 2209-19.
  9. Pienta, K. J., Preclinical mechanisms of action of docetaxel and docetaxel combinations in prostate cancer. *Seminars in Oncol* 2001, 28, (4M), 3-7.
  10. Jia, J.; Zhu, F.; Ma, X.; Cao, Z.; Cao, Z. W.; Li, Y.; Li, Y. X.; Chen, Y. Z., Mechanisms of drug combinations: interaction and network perspectives. *Nat Rev Drug Discov* 2009, 8, (2), 111-28.
  11. M., T., Rapid colorimetric assay for cellular growth and survival: Application to proliferation and cytotoxicity assays. *J Immunol Methods* 1983, 65, (1-2), 55-63.
  12. Z., J., Addition in drug combination. *Acta Pharmacol Sinica* 1980, 1, (2), 70-76.
  13. Chou, T. C., Theoretical basis, experimental design, and computerized simulation of synergism and antagonism in drug combination studies. *Pharmacol Rev* 2006, 58, (3), 621-81.
  14. Haass, N. K.; Sproesser, K.; Nguyen, T. K.; Contractor, R.; Medina, C. A.; Nathanson, K. L.; Herlyn, M.; Smalley, K. S., The mitogen-activated protein/extracellular signal-regulated kinase kinase inhibitor AZD6244 (ARRY-142886) induces growth arrest in melanoma cells and tumor regression when combined with docetaxel. *Clin Cancer Res* 2008, 14, (1), 230-9.
  15. Yang, H.; Higgins, B.; Kolinsky, K.; Packman, K.; Go, Z.; Iyer, R.; Kolis, S.; Zhao, S.; Lee, R.; Grippo, J. F.; Schostack, K.; Simcox, M. E.; Heimbrook, D.; Bollag, G.; Su, F., RG7204 (PLX4032), a selective BRAFV600E inhibitor, displays potent antitumor activity in preclinical melanoma models. *Cancer Res* 2010, 70, (13), 5518-27.

- 
16. B., D. F. G., Second-line chemotherapy for recurrent non-small cell lung cancer: do new agents make a difference? *Lung Cancer* 2000, 29, 91-104.

---

## 5. CHAPTER 5: DESIGN, SYTHESIS, AND CHARATERIZATION OF NEOVEL RADIOPROTECTORS

This study was published in *Journal of Cellular and Medicine*, Year 2019, Vol. 23, Pages 2238-2247.

---

## 5.1 Abstract

Approximately 50% of cancer patients receive radiation therapy during cancer treatment. Radiotherapy can cause injuries to normal tissues, a leading side effect. Radiation injury is mainly induced by reactive oxygen species (ROS) produced through the radiolysis of water in tissues. The ROS react with critical cellular macromolecules resulting in cell dysfunction and death, depletion of stem cells, and organ system dysfunction. Hence, it is of significance to eliminate free radical species from the cell environment for improved protection from radiation injury.

After a comprehensive review on radioprotectors, the natural anti-oxidation agent quercetin was chosen as a lead compound, and the aminothiols were combined with linker. Simultaneously, the thiol group was modified in order to modulate PK properties. Based on this concept, three new compounds (XH-101, XH-102, XH-103) were designed which were expected to cleave the designed compounds into polyphenol and aminothiols *in vivo* to exert their ROS scavenging function and mitigate radiation injury. These compounds were synthesized subsequently through a series of synthesis routes, and characterized by <sup>1</sup>HNMR, <sup>13</sup>CNMR, HRMS.

A 30-day survival rates study on mice exposed to 7.2 Gy total body irradiation was conducted. All mice in the vehicle group died 13 days after irradiation, while 60%, 80%, 100% animals were still alive in XH-101-, XH-102-, XH-103- treated groups at a dose of 200 mg/kg. On day 30, survival rates of the treatment groups were 40%, 0%, and 20%, respectively. A preliminary structure-activity relationship identified that the new molecular structure with five substituents in quercetin offered better protection from radiotherapy tissue injury than compounds with four substituents. In addition, the structure with methylation of the thiol group was better than without methylation. Hence, the best compound named XH-105 was designed, synthesized and characterized. XH-105 was chosen for the further study on the protective effects against intestinal injury.

---

## 5.2 Introduction

Though targeted therapy is promising for the cancer treatment, aggressive tumor behaviour is often associated with resistance to commonly used anti-cancer drugs. Approximately 50% of cancer patients receive radiation therapy during cancer treatment [1]. In radiotherapy, the radiation damages both tumor and normal tissues, thereby causing radiation injury to organs and tissues [2]. Radiation-induced reactive oxygen species (ROS) react with critical cellular macromolecules resulting in cell dysfunction and death, depletion of stem cells, and organ system dysfunction [3]. About 53% patients receiving radiotherapy reported bowel symptoms, and the small intestine is one of the most sensitive organs for ionizing radiation [4]. The main symptoms of radiation-induced intestinal damage include anorexia, vomiting, diarrhea, dehydration, systemic infection, and in extreme cases, septic shock and death [5]. Radiation-induced intestinal damage seriously affects the treatment of patients with abdominal or pelvic tumors, reducing the quality of life of patients. Acute radiation injury to the colon can be severe, and can lead to therapy interruption in 5-15% of patients [4]. Although dose escalation offers better local control of cancer in radiotherapy, it is accompanied by acute toxicity and normal tissue damage [6]. In order to allow clinicians to increase radiotherapy doses to achieve better tumor control rates, pharmacological approaches to selectively protect normal tissues must be developed [2]. However, there is no specific clinical treatment for radiation enteritis. Therefore, the development of efficient radiological intestinal damage protectors is an important area of study in radiation therapy. Side effects of chemotherapy are mainly caused by the induction of DNA damage and production of ROS which is responsible for toxicity. Some studies for reducing the side effects have been promising. Amifostine has been approved by the FDA for reducing nephrotoxicity and ototoxicity in women with ovarian cancer treated with cisplatin [7].

Amifostine is the only small molecular radiation-protective agent approved by the FDA. Amifostine is a phosphorothioate cytoprotective agent known chemically as 2-[(3-6 aminopropyl)amino]ethanethiol dihydrogen phosphate (ester). Amifostine is a cytoprotective drug used in cancer patients receiving radiotherapy and some forms of chemotherapy [8]. Amifostine is a pro-drug that converts into the -SH form (WR-1065,  $\text{H}_2\text{N}(\text{CH}_2)_3\text{NH}(\text{CH}_2)_2\text{SH}$ ) through dephosphorylation by alkaline phosphatase [8]. The protection mechanism includes free-radical scavenging, chemical repair by hydrogen atom donation, and modulation of the complex transcriptional regulation of genes involved in apoptosis, cell cycle and DNA repair [9]. It causes splenic vasodilation and blocks autonomic ganglia, but hypotension is the dose-limiting side effect of Amifostine. Amifostine is given by intravenous infusion before

---

radiation and chemotherapy starts. This drug will cause hypotension, nausea, and vomiting. Pharmacokinetics studies show that Amifostine is rapidly cleared from the plasma with an elimination half-life of only approximately 8 minutes [10].

In recent studies, natural antioxidant agents and aminothiols have been intensively investigated for application in radiation protection [11-13]. Flavonoids are a group of natural antioxidant agents that can suppress the formation of free radicals. However, poor stability and bioavailability are disadvantages [14]. Aminothiol compounds possess good efficacy profiles, but are characterized by a short half-life and high toxicity [15].

Several aminothiol compounds are known radioprotectors, such as Amifostine, cystine, PrC-210, PrC-211, PrC-252 [16]. The possible mechanism of action of aminothiol radioprotectors is the binding to and stabilization of those parts of the DNA helix which are not covered by histones, which is thought to be responsible for reducing treatment-induced primary and secondary damage [17]. The aminothiol radioprotector design concepts are: (1) a flexible alkyl chain backbone, which carries a positive charge due to one or more amine groups, to achieve ionic interaction and concentration around negatively charged DNA in cells; (2) a free or capped thiol group to scavenge free oxygen radicals formed by ionizing radiation [18].

Natural anti-oxidation agents exist widely in herbs and fruits and mainly include flavonoids and polyenes, offering potential use as radioprotectors [6, 13, 19, 20]. Both agents have the advantages of low toxicity and moderate efficacy, but display poor stability and bioavailability [14]. Aminothiols emerge as the most promising compounds, especially after amifostine was discovered and approved by the FDA. Although amifostine is currently used clinically, its drug toxicity, limited time of protection, and unfavorable routes of administration [15] limit the utility of the drug in nonclinical settings. The most probable protective mechanisms of aminothiols are the donation of a H atom, scavenging of hydroxyl radical or other ROS, chemical repair of DNA radicals and oxygen depletion [21, 22].

In this study, the natural plant-derived anti-oxidation agent quercetin, which belongs to flavonoids family, was used as a lead compound and the molecular structure was modified. Simultaneously, aminothiol analogues were combined with natural anti-oxidation agents by different linkers to retain the efficacy of the aminothiol group and incorporate the safety properties of natural anti-oxidation agents, respectively. Furthermore, the two functional fragments modulated the pharmacokinetic profile for each other, and they were mutually a prodrug to each other. The new compound was expected to cleave the combined compound

---

into polyphenol and aminothiols *in vivo* to mitigate radiation injury by their ROS scavenger capabilities. Based on this concept, the compound XH-105 was synthesized.

## **5.3 Materials and methods**

### **5.3.1 Chemistry**

2-(3,4-dihydroxyphenyl)-3,5,7-trihydroxy-4H-chromen-4-one was purchased from SHUYA Chemical Science and Technology (Shanghai, China). Bis(trichloromethyl) carbonate, thiazolidine, and 2,2-dimethylthiazolidine were purchased from Energy Chemical (Shanghai, China).

### **5.3.2 Animals and ethics approval and consent to participate**

Male C57BL/6 mice (8-10 weeks) were purchased from Beijing HFK Bioscience Co., Ltd. (Beijing, China). Animals were bred in the certified animal facility at the Institute of Radiation Medicine (IRM) of the Chinese Academy of Medical Sciences (CAMS).

All experimental procedures were carried out in accordance with the NIH Guidelines for the Care and Use of Laboratory Animals and were approved by the Institutional Animal Care and Use Committee of the Institute of Radiation Medicine (IRM), Chinese Academy of Medical Sciences (CAMS) (Permit Number 2017053). The animals were cared for in accordance with the guidelines of the National Animal Welfare Law of China.

### **5.3.3 Novel compounds design for radioprotection**

In this study, the plant-derived natural anti-oxidation agent quercetin, a flavonoid compound, was selected and investigated, as the lead compound. Efforts focused on modifying the molecular structure through introduction of an aminothiols into the structure of the molecule, attached by different linkers. This design may retain both the efficacy of aminothiols and the safety properties of quercetin, respectively. Moreover, methyl groups were employed to adjust the lipophilicity profile in order to increase the bioavailability. Furthermore, two functional fragments can modulate the pharmacokinetic (PK) profiles for each other, which were mutually prodrugs to each other (Figure 5-1). The new compounds were expected to cleave into polyphenol and aminothiols *in vivo* to mitigate radiation injury by their ROS scavenger capabilities. Based on this concept, four new compounds with the same core structure were designed (Figure 5-2). These compounds were synthesized subsequently through a series of synthesis routes.

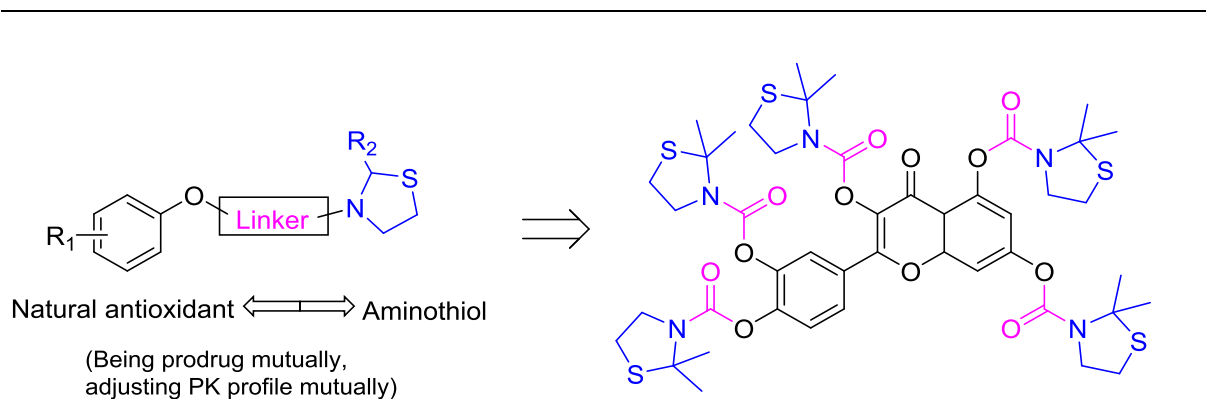


Figure 5-1 Design concepts of new compounds

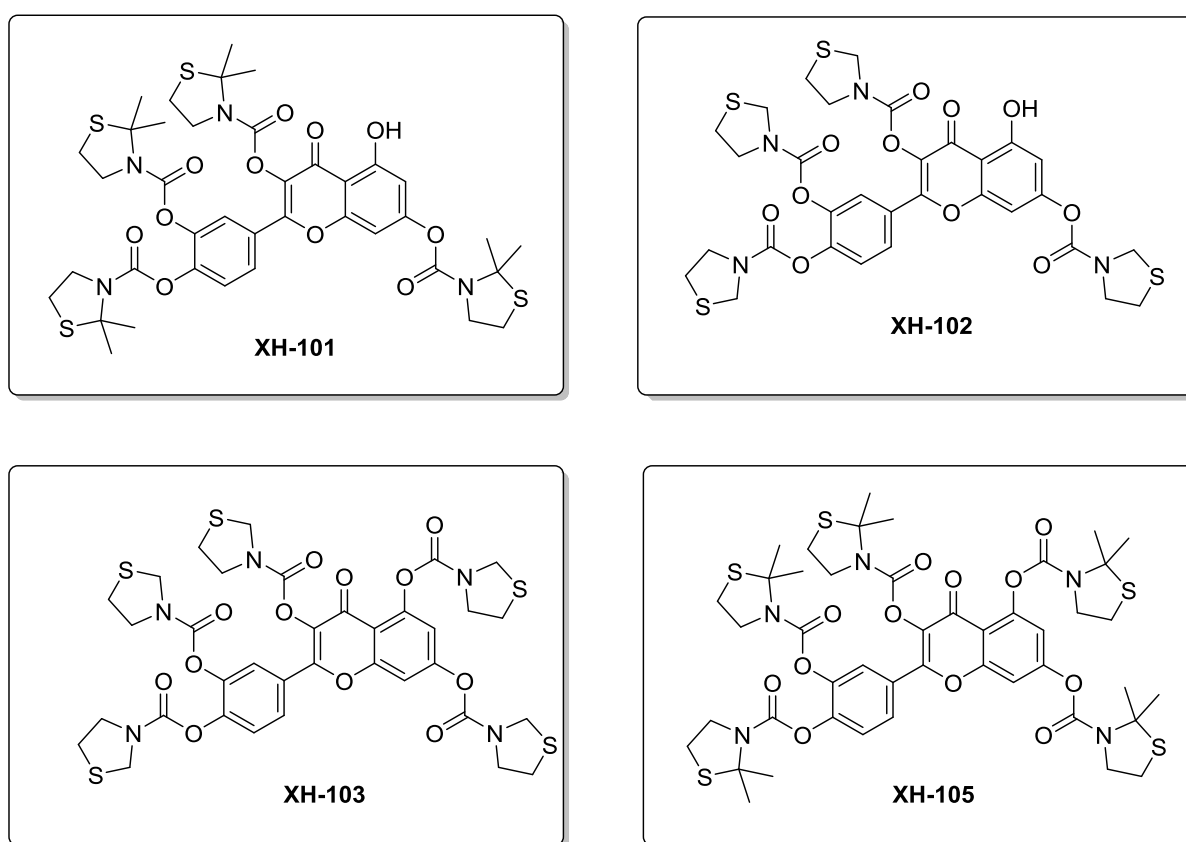
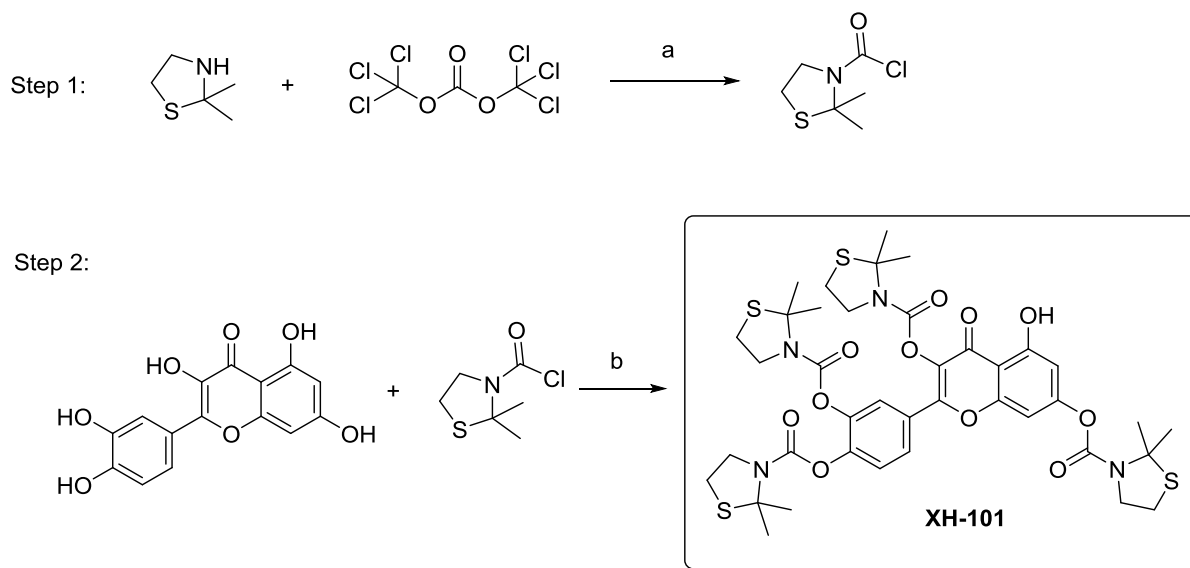


Figure 5-2 Molecular structures of four new compounds

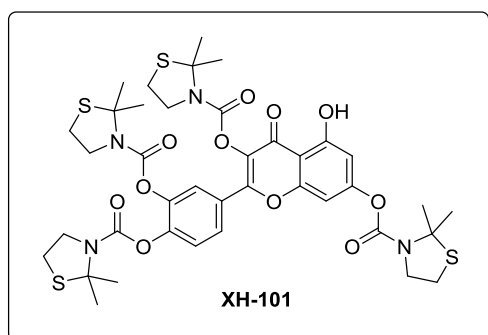
### 5.3.4 Synthesis of XH-101

The synthesis route of XH-101 was designed according to retrosynthesis analysis, and the compound was synthesized through a two-step reaction (Figure 5-3). Firstly, the 2,2-dimethylthiazolidine was reacted with bis(trichloromethyl) carbonate with triethylamine ( $\text{Et}_3\text{N}$ ) as base to prepare thiazolidine-3-carbonyl chloride. Then, the thiazolidine-3-carbonyl

chloride was coupled with quercetin in the presence of triethylamine and 4-dimethylaminopyridine to afford the target product XH-101.



**Figure 5-3 Synthesis route of XH-101.** Reagents and condition: (a). triethylamine (Et<sub>3</sub>N), Tetrafuran, 0 °C, 1 h; room temperature(r.t.), 10 h; (b). Et<sub>3</sub>N, 2-Diethylaminopyridine, Dimethylformamide (DMF), Nitrogen (N<sub>2</sub>), 0 °C, 1 h; rt., 10 h.



### Step 1: Synthesis of 2,2-dimethylthiazolidine-3-carbonyl chloride

To a solution of bis(trichloromethyl) carbonate (9.1 g, 27.32 mmol) in anhydrous tetrahydrofuran (60 mL), 2,2-dimethylthiazolidine (8 g, 89.74 mmol) was added in parts and triethylamine (12 mL) was added dropwise; the mixture was stirred under nitrogen in an

ice water bath for 1 h and then at room temperature (rt) for 10 h. The reaction mixture was filtered, and the residue was washed three times with dichloromethane (20 mL). The filtrate phase was combined and evaporated in vacuo. The resultant residue was used directly for the next step. This compound was also the immediate for the synthesis of compound XH-105.

### Step 2: Synthesis of 4-(3,7-bis((2,2-dimethylthiazolidine-3-carbonyl)oxy)-5-hydroxy-4-oxo-4H-chromen-2-yl)-1,2-phenylene bis(2,2-dimethylthiazolidine-3-carboxylate)

Triethylamine (6 mL), 4-dimethylaminopyridine (157 mg, 1.29 mmol), and 2,2-dimethylthiazolidine-3-carbonyl chloride (2 g, 11.11 mmol) were added to a solution of

2-(3,4-dihydroxyphenyl)-3,5,7-trihydroxy-4H-chromen-4-one (0.7 g, 2.32 mmol) in DMF (30 mL), and the mixture was stirred at 0°C for 1 h and at room temperature for 10 h. The reaction mixture was poured into a mixture solvent (300 mL, v/v/v, MeOH: H<sub>2</sub>O: DMSO = 8:1.5:0.5), and then water was added dropwise until the product precipitated. The residue was then filtered and washed three times with water (15 mL). The filter cake was then dried in vacuo and produced the title compound as a yellow solid (3.35 g, 65%). LC-MS was carried out on a Waters 3100 Mass Detector with an Agilent ZORBAX column (C18, 2.1×50mm, 3.5µm). <sup>1</sup>H NMR spectra were obtained using a Bruker spectrometer at 400MHz. LC-MS: R<sub>T</sub> = 7.06 min, [M+H]<sup>+</sup> = 1018.32, Calculated: 1018.25. <sup>1</sup>H NMR (400 MHz, DMSO-d<sub>6</sub>) δ 7.85 (d, J = 15.7 Hz, 2H), 7.64 (s, 1H), 7.56 (d, J = 8.4 Hz, 1H), 7.18 (s, 1H), 4.02 (d, J = 26.2 Hz, 10H), 3.15 (d, J = 30.1 Hz, 10H), 1.77 (d, J = 17.1 Hz, 30H).

### 5.3.5 Synthesis of XH-102

The synthesis route of XH-102 was designed according to retrosynthesis analysis, and the compound was synthesized through a 2-step reaction (Figure 5-4). Firstly, the thiazolidine was reacted with bis(trichloromethyl) carbonate with triethylamine as base to prepare thiazolidine-3-carbonyl chloride. Then, thiazolidine-3-carbonyl chloride was coupled with quercetin in the presence of triethylamine and 4-dimethylaminopyridine to afford the target product XH-102.

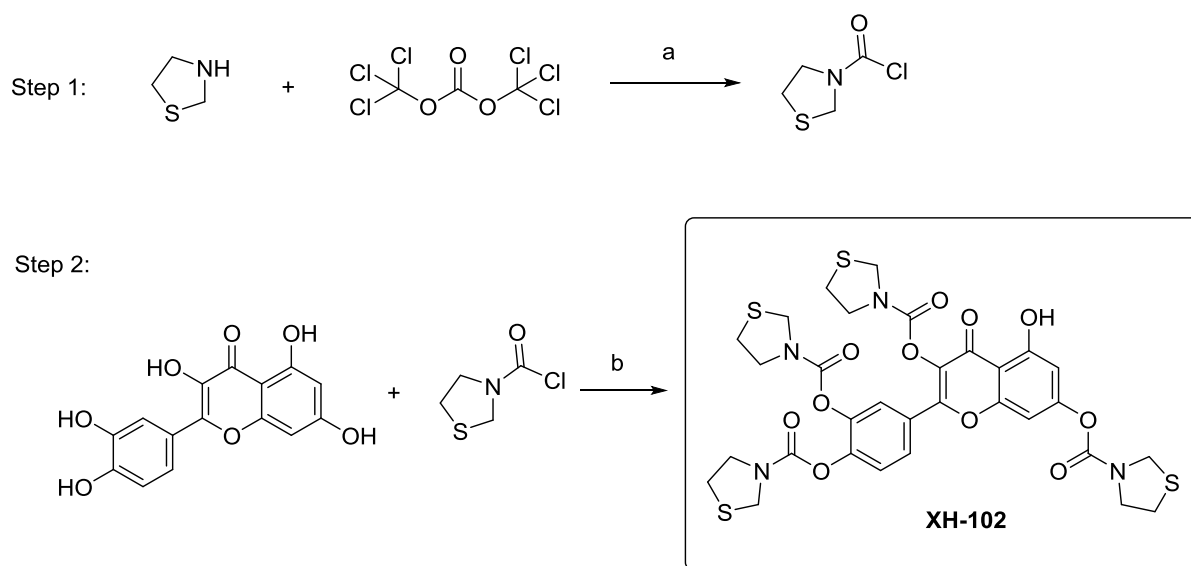
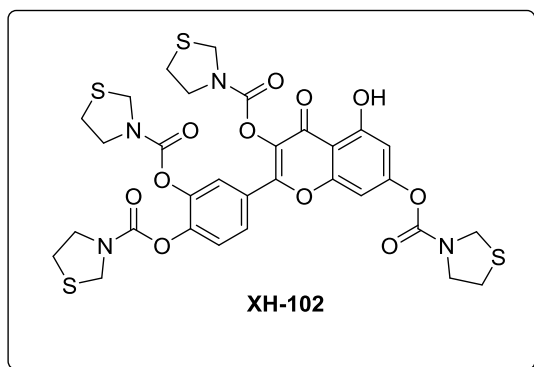


**Figure 5-4 Synthesis route of XH-102. Reagents and condition:** (a). Et<sub>3</sub>N, THF, 0 °C, 1 h; rt., 10h; (b). Et<sub>3</sub>N, 2-Diethylaminopyridine, DMF, N<sub>2</sub>, 0 °C, 1h; rt., 10h.



### Step1: Synthesis of thiazolidine-3-carbonyl chloride

To a solution of bis(trichloromethyl) carbonate (9.6 g, 107.64 mmol) in anhydrous tetrahydrofuran (60 mL) was added thiazolidine (8

g, 89.88 mmol) in parts and triethylamine (16 mL) dropwise, the mixture was stirred under a nitrogen atmosphere in an ice water bath for 1 h and then at room temperature for 10 h. The reaction mixture was filtered and the residue was washed with dichloromethane (20 mL) for three times. The filtrate phase was combined and evaporated in vacuo. The resultant residue was used directly for the next step.

### Step2: Synthesis of 2-(3,4-bis((thiazolidine-3-carbonyl)oxy)phenyl)-5-hydroxy-4-oxo-4H-chromene-3,7-diyl bis(thiazolidine-3-carboxylate)

To a solution of 2-(3,4-dihydroxyphenyl)-3,5,7-trihydroxy-4H-chromen-4-one (0.8 g, 2.65 mmol) in DMF (20 mL) was added triethylamine (4 mL), 4-dimethylaminopyridine (100 mg, 0.0008 mmol), and thiazolidine-3-carbonyl chloride, the mixture was stirred at 0 °C for 1 h and at room temperature for 10 h. The reaction mixture was poured into MeOH/H<sub>2</sub>O/ DMSO 8/1.5/0.5 v/v/v (250 mL) and then water was added dropwise until the product precipitated. The residue was then filtered and washed with water (15 mL) three times. The filter cake was then dried under vacuo to give the title compound as a yellow solid.

### 5.3.6 Synthesis of XH-103

XH-103 was synthesized through a 2-step reaction. The first step obtained thiazolidine-3-carbonyl chloride by using the same approach as for XH-102. Then, thiazolidine-3-carbonyl chloride was coupled with quercetin in the presence of triethylamine and 4-dimethylaminopyridine to afford the product XH-103 (Figure 5-5).

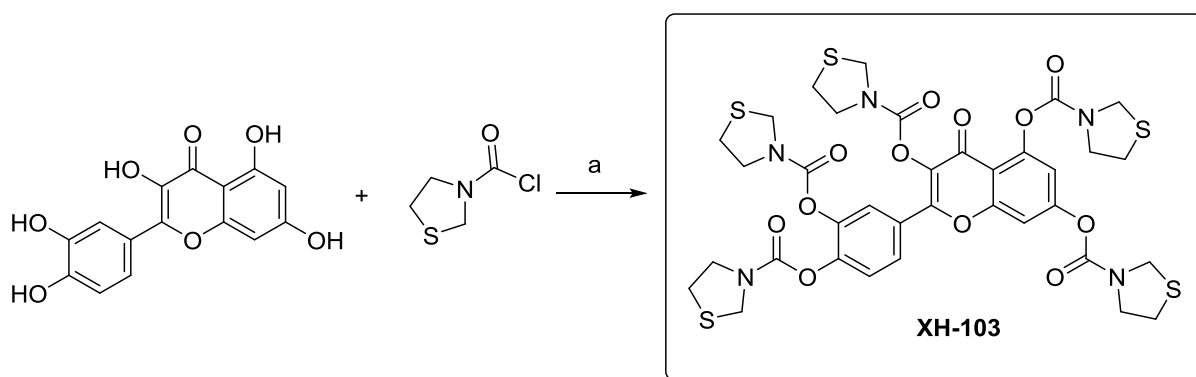
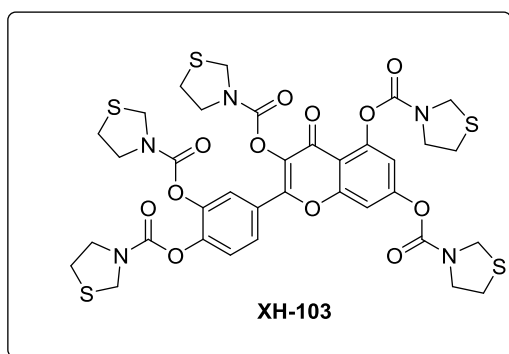


**Figure 5-5 Synthesis route of XH-103. Reagents and condition:** (a). Et<sub>3</sub>N, 2-Diethylaminopyridine, DMF, N<sub>2</sub>, 0 °C, 1h; rt., 10h.



**Step 1: Synthesis of thiazolidine-3-carbonyl chloride**

This step was the same as for the synthesis of XH-102.

**Step 2: Synthesis of 2-(3,4-bis((thiazolidine-3-carbonyl)oxy)phenyl)-4-oxo-4H-chromene-3,5,7-triyl tris(thiazolidine-3-carboxylate)**

**-4-oxo-4H-chromene-3,5,7-triyl tris(thiazolidine-3-carboxylate)**

To a solution of 2-(3,4-dihydroxyphenyl)-3,5,7-trihydroxy-4H-chromen-4-one (1.6 g, 5.3 mmol) in DMF (30 mL) was added triethylamine (7 mL), 4-dimethylaminopyridine (192 mg, 1.57 mol), and thiazolidine-3-carbonyl chloride, the mixture was stirred at 0 °C for 1 h and at room temperature for 10 h. The reaction mixture was poured into MeOH/H<sub>2</sub>O/DMSO 8/1.5/0.5 v/v/v (500 mL) and then water was added dropwise until the product precipitated. The residue was then filtered and washed with water (20 mL) three times. The filter cake was then dried in vacuo to give the title compound as a yellow solid (3.35 g, 72%). LC-MS: R<sub>T</sub> = 4.5 min. [M+H]<sup>+</sup> = 879.20, calculated 878.99, <sup>1</sup>H NMR (400 MHz, DMSO) δ ppm 7.95 – 7.85 (m, 2H), 7.68 (s, 1H), 7.58 (d, J = 8.3 Hz, 1H), 7.25 (s, 1H), 4.58 (dd, J = 52.9, 22.8 Hz, 10H), 3.97 – 3.65 (m, 10H), 3.14 (d, J = 20.2 Hz, 10H).

### 5.3.7 Synthesis of XH-105

The synthesis route of XH-105 was designed according to retrosynthesis analysis, and the compound was synthesized through a 2-step reaction. The first step was the same as the first step in 5.3.4 (Figure 5-6).

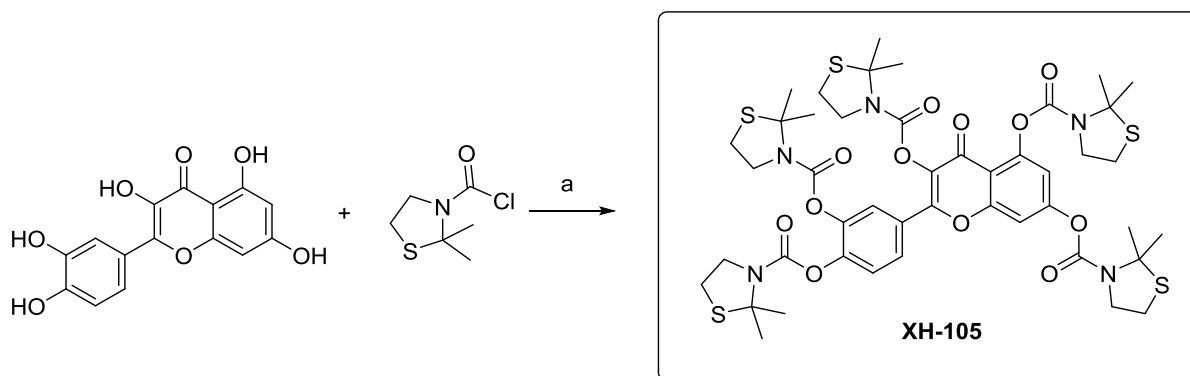
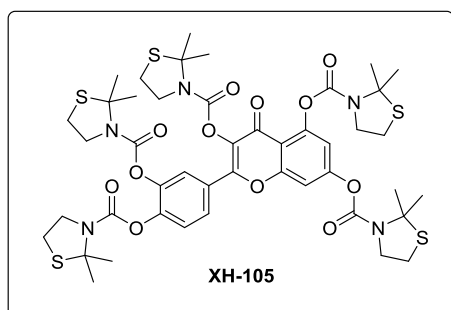


**Figure 5-6 Synthesis route of XH-105. Reagents and condition:** (a). Et<sub>3</sub>N, 2-Diethylaminopyridine, DMF, N<sub>2</sub>, 0 °C, 1h; rt., 10h.



**Step 1:** 2,2-dimethylthiazolidine-3-carbonyl chloride was obtained from the process of the synthesis of XH-101.

**Step 2:** Triethylamine (6 mL), 4-dimethylaminopyridine (157 mg, 1.29 mmol), and 2,2-dimethylthiazolidine-3-carbonyl chloride were added to a solution of

2-(3,4-dihydroxyphenyl)-3,5,7-trihydroxy-4H-chromen-4-one (1.3 g, 4.30 mmol) in DMF (30 mL), and the mixture was stirred at 0°C for 1 h and at room temperature for 10 h. The reaction mixture was poured into a mixture solvent (500 mL, v/v/v, MeOH/H<sub>2</sub>O/DMSO = 8/1.5/0.5), and then water was added dropwise until the product precipitated. The residue was then filtered and washed three times with water (20 mL). The filter cake was then dried in vacuo and produced the title compound as a yellow solid (3.35 g, 65%). LC-MS was carried out on a Waters 3100 Mass Detector with an Agilent ZORBAX column (C18, 2.1×50mm, 3.5µm). 1H NMR spectra were obtained using a Bruker spectrometer at 400MHz. LC-MS: RT = 7.06 min, [M+H]<sup>+</sup> =1018.32, Calculated: 1018.25. 1H NMR (400 MHz, DMSO-d<sub>6</sub>) δ 7.85 (d, J = 15.7

---

Hz, 2H), 7.64 (s, 1H), 7.56 (d, J = 8.4 Hz, 1H), 7.18 (s, 1H), 4.02 (d, J = 26.2 Hz, 10H), 3.15 (d, J = 30.1 Hz, 10H), 1.77 (d, J = 17.1 Hz, 30H).

### 5.3.8 30-day survival rate experiments

The compounds were dissolved in DMSO, and then diluted with edible oil to the corresponding concentration containing a final concentration of 10% DMSO. The suspension was vortexed to homogeneity before dosing.

Mice were exposed to ionizing radiation by using a <sup>137</sup>Cs source following an Exposure Instrument Gammacell-40 (Atomic Energy of Canada Lim, Chalk River, ON, Canada) at a dose rate of 1.0 Gy/min. The mice were exposed to 7.2 Gy total body irradiation in the survival experiments (n=5).

The animals were randomized into 3 different groups: vehicle + sham irradiation; vehicle + total body irradiation (TBI); dosing + TBI. The doses were set up according to Table 5-1. The mice in dosing groups were dosed 24 h and 0.5 h before applying one TBI.

**Table 5-1 Group setting of mice**

Experiments	Groups	Dose (mg/kg)	Treatment	Animals (N)
	Vehicle	-	PO, dosing at 30 min before sham IR	5
	IR+ vehicle	-	PO, dosing at 30 min before IR	5
30-day survival rate (7.2 Gy, TBI)	IR+XH-101, 200	200	PO, dosing at 30 min before IR	5
	IR+XH-102, 200	200	PO, dosing at 30 min before IR	5
	IR+XH-103, 200	200	PO, dosing at 30 min before IR	5

---

## 5.4 Results and discussion

### 5.4.1 New compounds design, synthesis, and characterization

Based on the concept of bi-functional structures, four new compounds, designated as XH-101, XH-102, XH-103, XH-105, were designed and synthesized. The synthesis routes and

methods are described in the experimental method section. Briefly, 2,2-dimethylthiazolidine or thiazolidine was reacted with bis(trichloromethyl) carbonate to obtain 2,2-dimethylthiazolidine-3-carbonyl chloride or thiazolidine-3-carbonyl chloride under the base triethylamine. Then the resultant compounds were coupled with quercetin, in the presence of triethylamine and 4-dimethylaminopyridine. The target compounds XH-101, XH-102, XH-103, XH-105 were obtained with overall yields of 21%, 24%, 33%, 65%, respectively. The target compounds were characterized by NMR, ESI-MS or HRMS.

#### 5.4.2 Characterization of XH-101

A white solid with overall yield 21% was obtained.  $^1\text{H}$  NMR(400 MHz,  $\text{CDCl}_3$ )  $\delta$  12.12 (s, 1H), 7.73 (d,  $J = 7.3\text{Hz}$ , 2H), 7.41 (d,  $J = 8.3\text{ Hz}$ , 1H), 6.95 (s, 1H), 6.60 (d,  $J = 1.8\text{ Hz}$ , 1H), 4.27 - 3.95 (m, 8H), 3.05 (s, 8H), 1.85 (d,  $J = 8.0\text{Hz}$ , 24H) (Figure 5-7); HRMS:  $\text{C}_{39}\text{H}_{46}\text{N}_4\text{O}_{11}\text{S}_4$ , Calculated 874.20, found 897.1954,  $[\text{M} + \text{Na}]^+$  (Figure 5-8).  $^{13}\text{C}$  NMR (101 MHz,  $\text{CDCl}_3$ )  $\delta$  176.97, 161.51, 156.65, 155.91, 149.26, 145.39, 142.85, 132.27, 127.41, 126.28, 123.93, 108.43, 104.99, 100.81, 77.36, 77.04, 76.72, 71.18, 54.40, 53.42, 52.86, 30.05, 29.64, 28.53, 27.75 (Figure 5-9).

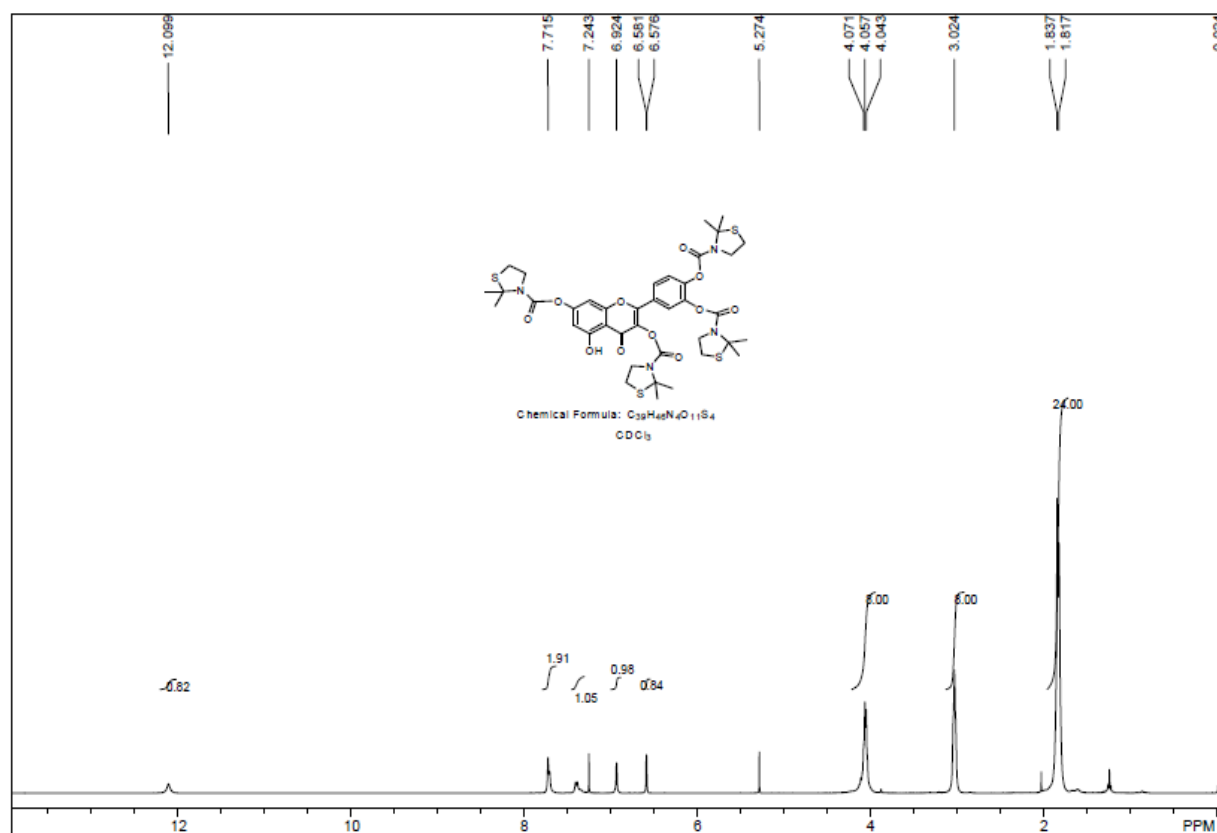
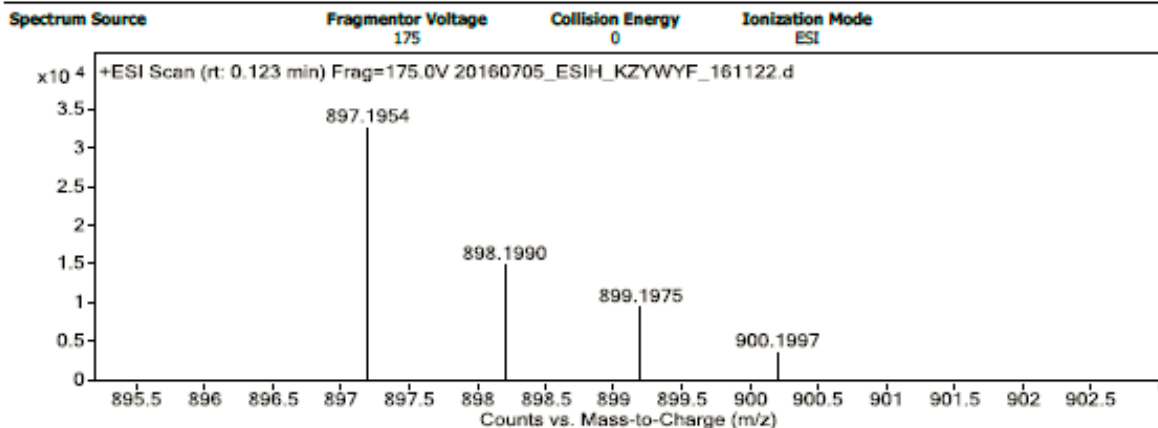


**Figure 5-7**  $^1\text{H}$ NMR spectrum of XH-101. The molecular structure of XH-101 was characterized by  $^1\text{H}$ NMR (400MHz,  $\text{CDCl}_3$ ).

User Spectra



Formula Calculator Results

m/z	Calc m/z	Diff (mDa)	Diff (ppm)	Ion Formula	Ion
897.1954	897.1938	-1.54	-1.72	C39 H46 N4 Na O11 S4	(M+Na)+

-- End Of Report --

Figure 5-8 MS spectrum of XH-101. Target peak of XH-101:  $[M+Na]^+$  897.1954.

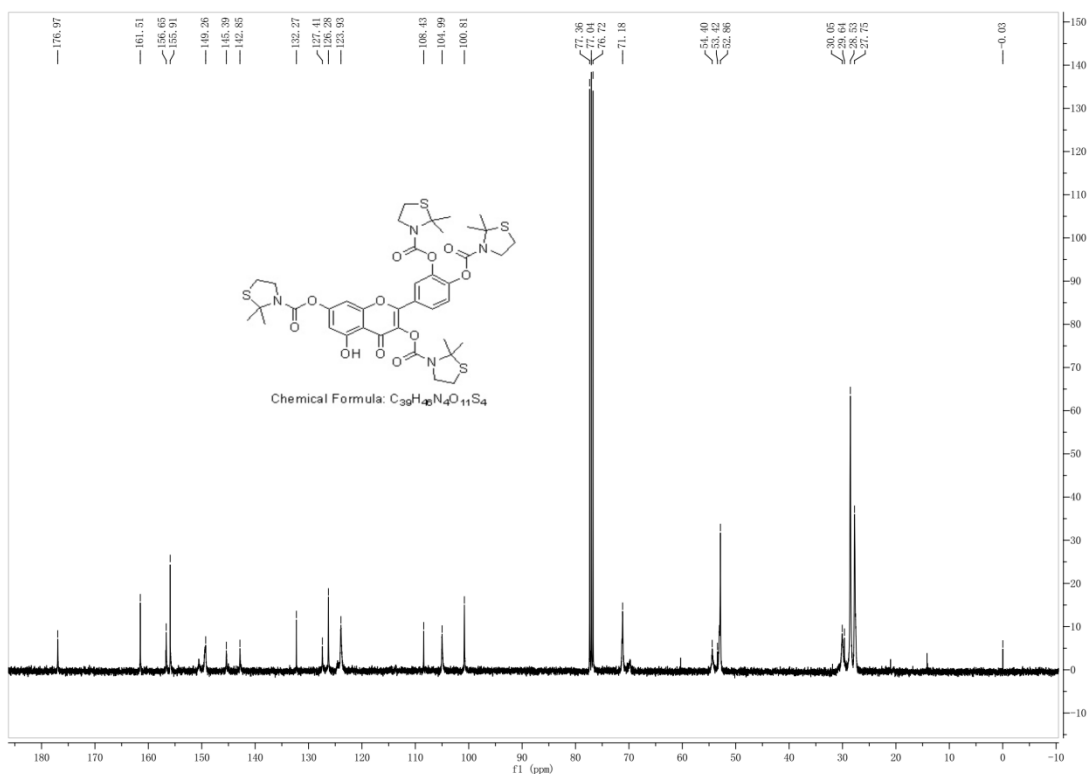
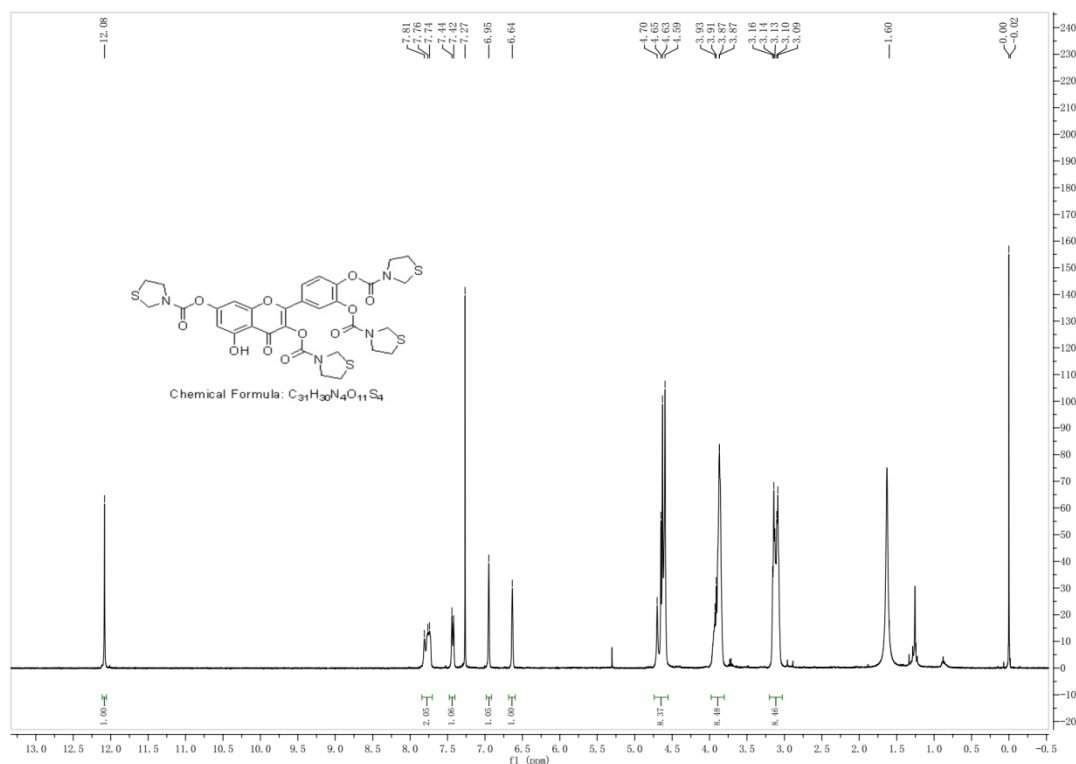


Figure 5-9  $^{13}\text{C}$  NMR spectrum of XH-101. The molecular structure of XH-101 was characterized by  $^{13}\text{C}$  NMR (101 MHz,  $\text{CDCl}_3$ ).

### 5.4.3 Characterization of XH-102

A white solid with an overall yield of 24% was obtained.  $^1\text{H}$  NMR(400 MHz,  $\text{CDCl}_3$ ) $\delta$ 12.08 (s, 1H), 7.84–7.71 (m, 2H), 7.43 (d, J = 9.3 Hz, 1H), 6.95 (s, 1H), 6.64 (s, 1H), 4.64 (dd, J = 25.3, 16.9 Hz, 8H), 3.89 (dd, J = 20.3, 3.5 Hz, 8H), 3.20–3.03 (m, 8H) (Figure 5-10);  $^{13}\text{C}$  NMR (101

MHz,  $\text{CDCl}_3$ ) $\delta$  176.87, 161.54, 156.69, 155.90, 150.96, 150.61, 145.12, 142.73, 132.32, 127.32, 126.42, 123.85, 123.80, 123.79, 123.76, 108.58, 105.16, 105.11, 100.89, 77.31, 76.99, 76.68, 58.43, 49.61, 49.41, 49.20, 48.45, 48.31, 31.24, 31.09, 30.08, 29.95, 18.39 (Figure 5-12); HRMS:  $\text{C}_{31}\text{H}_{30}\text{N}_4\text{O}_{11}\text{S}_4$ , Calculated 762.0794, found 785.0693,  $[\text{M} + \text{Na}]^+$  (Figure 5-11).



**Figure 5-10**  $^1\text{H}$  NMR spectrum of XH-102. The molecular structure of XH-102 was characterized by  $^1\text{H}$ NMR (400MHz,  $\text{CDCl}_3$ ).

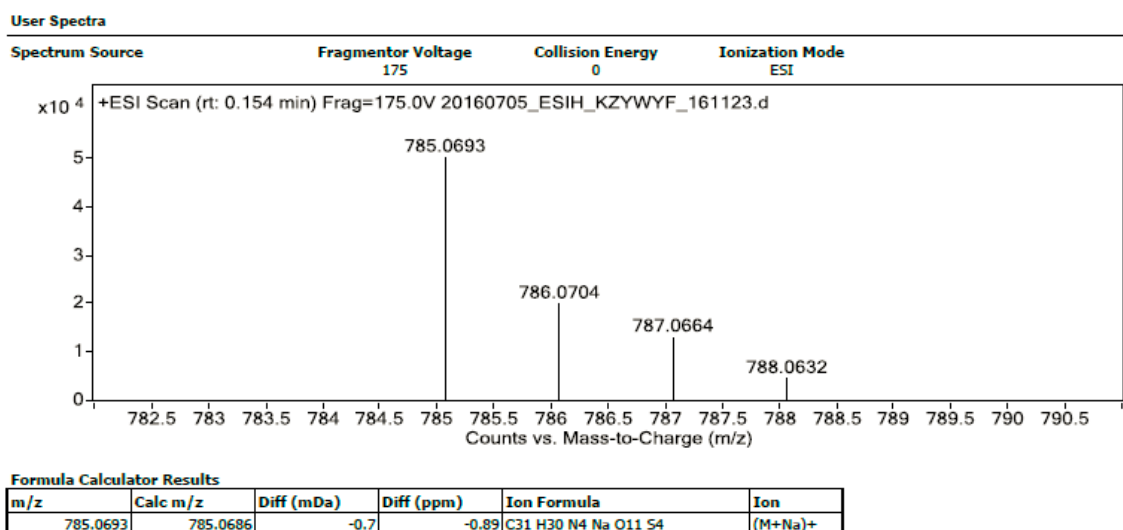


**Figure 5-11** MS spectrum of XH-102. Target peak of XH-102:  $[\text{M} + \text{Na}]^+$  785.0693.

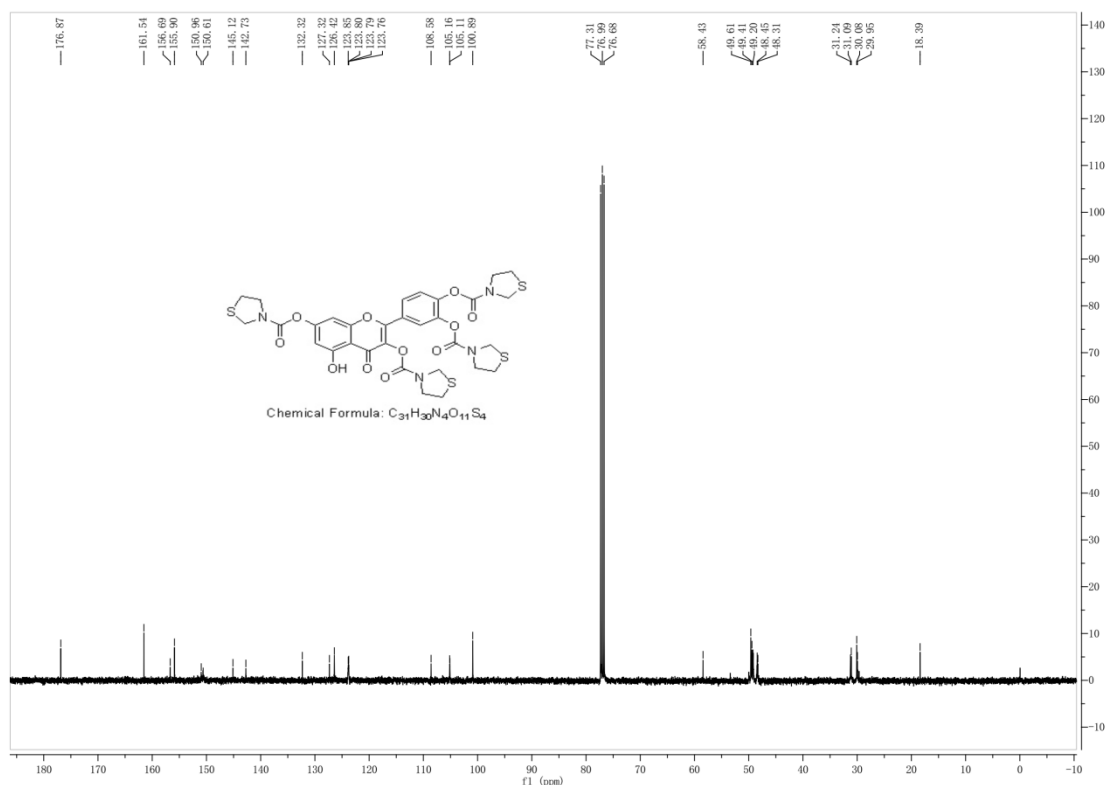


**Figure 5-12** <sup>13</sup>C NMR spectrum of XH-102 (101 MHz, CDCl<sub>3</sub>). The molecular structure of XH-103 was characterized by <sup>13</sup>CNMR (101MHz, CDCl<sub>3</sub>).

#### 5.4.4 Characterization of XH-103

A white solid with an overall yield of 33% was obtained. <sup>1</sup>HNMR(400 MHz, DMSO-d<sub>6</sub>)δ 7.96 – 7.82 (m, 2H), 7.69 (s, 1H), 7.58 (d, J = 8.5Hz, 1H), 7.25 (d, J = 1.7Hz, 1H), 4.56 (dd, J = 55.9, 24.0 Hz, 10H), 3.95 – 3.61 (m, 10H), 3.25 – 3.02 (m, 10H) (Figure 5-13); <sup>13</sup>C NMR (101 MHz, CDCl<sub>3</sub>)δ 170.70, 156.70, 154.41, 153.82, 151.99, 151.64, 151.12, 151.05, 151.00, 150.66, 150.55, 150.43, 150.33, 144.85, 142.67, 134.19, 127.59, 126.33, 123.65, 114.93, 113.88, 108.35, 49.90, 49.77, 49.65, 49.60, 49.40, 49.24, 49.16, 48.44, 48.30, 31.24, 31.09, 30.08, 30.01, 29.94 (Figure 5-15); HRMS: C<sub>35</sub>H<sub>35</sub>N<sub>5</sub>O<sub>12</sub>S<sub>5</sub>, Calculated 877.09, found 900.0769, [M +Na]<sup>+</sup> (Figure 5-14).

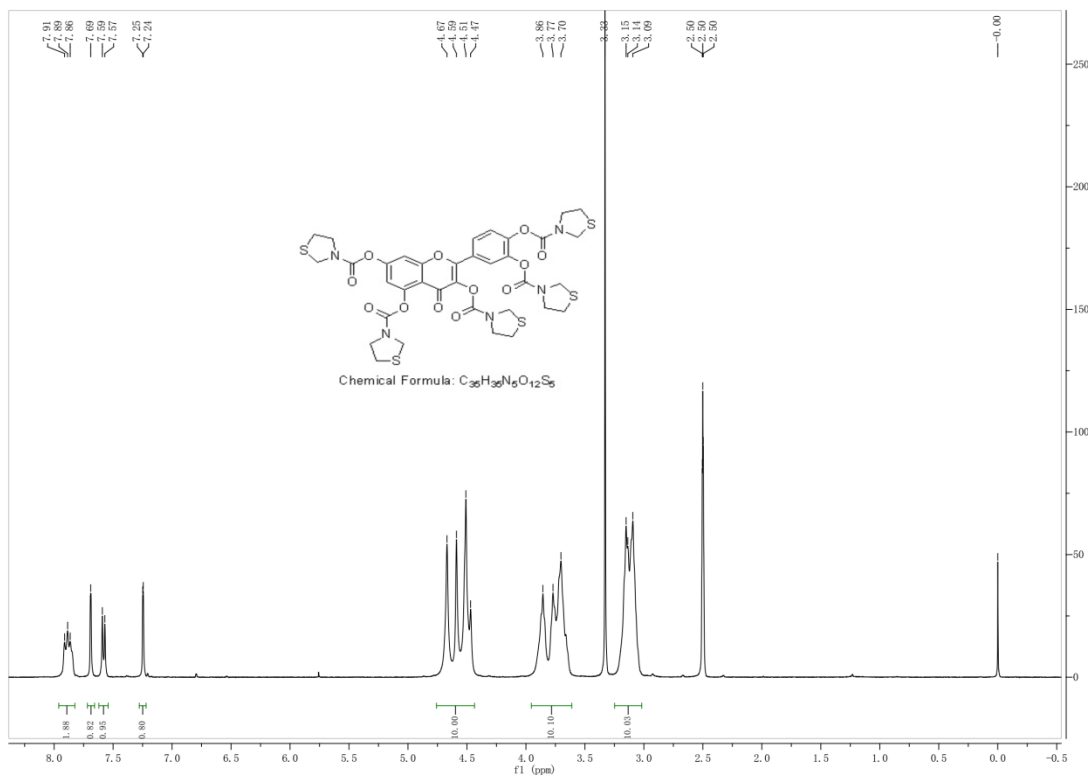
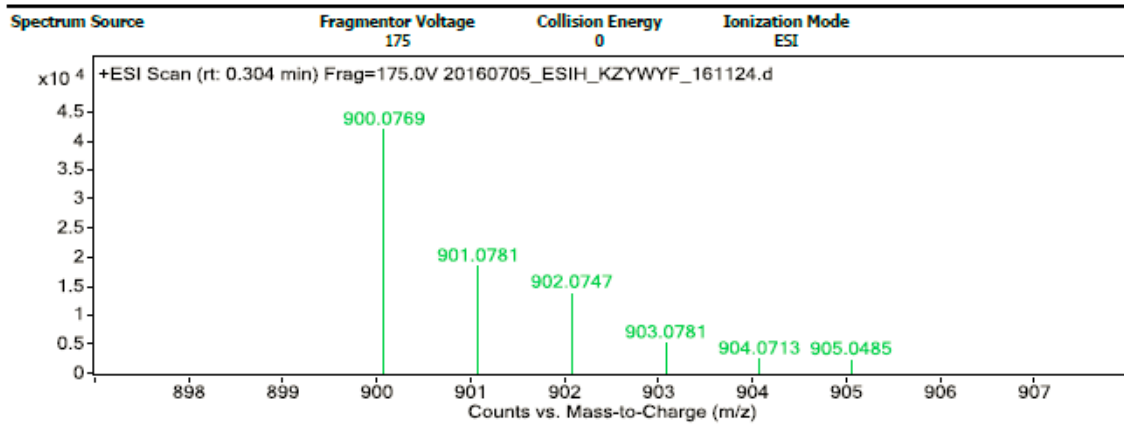


**Figure 5-13** <sup>1</sup>H NMR spectrum of XH-103. The molecular structure of XH-103 was characterized by <sup>1</sup>H NMR (400MHz, d-DMSO).

**User Spectra**



**Formula Calculator Results**

m/z	Calc m/z	Diff (mDa)	Diff (ppm)	Ion Formula	Ion
900.0769	900.0778	0.94	1.05	C <sub>35</sub> H <sub>35</sub> N <sub>5</sub> NaO <sub>12</sub> S <sub>5</sub>	(M+Na) <sup>+</sup>

--- End Of Report ---

**Figure 5-14** MS spectrum of XH-103. Target peak of XH-103: [M+Na]<sup>+</sup> 900.0769.

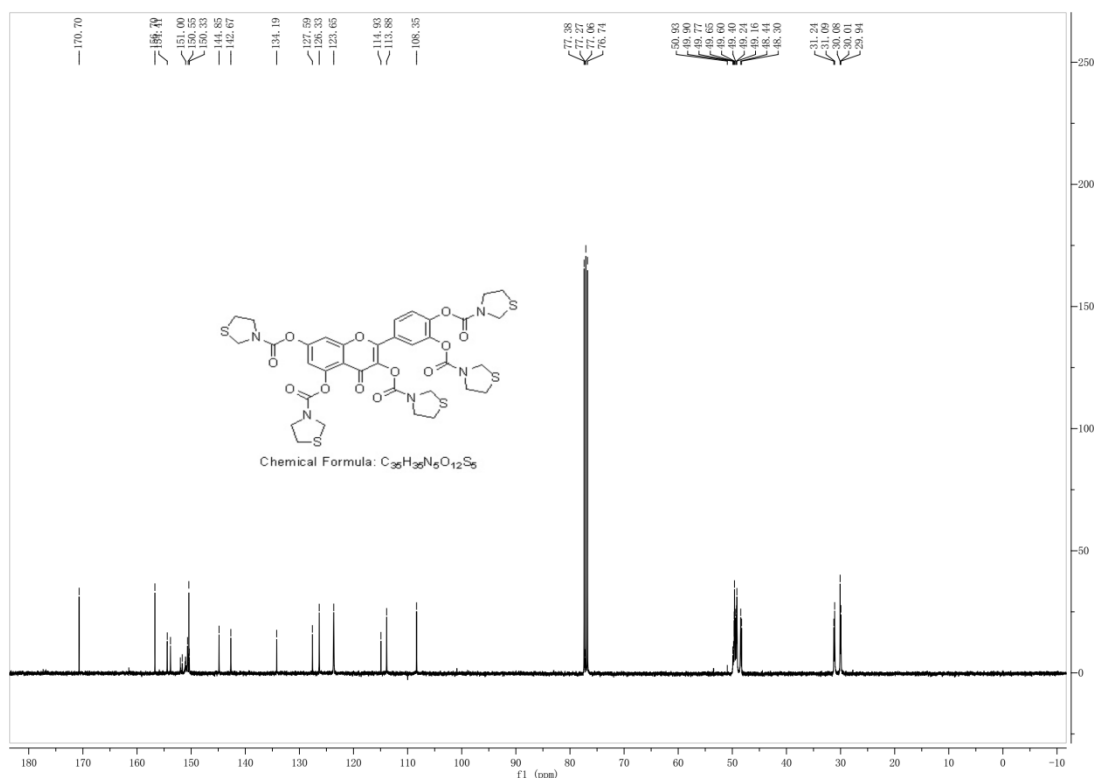


**Figure 5-15**  $^{13}\text{C}$  NMR (101 MHz,  $\text{CDCl}_3$ ) spectrum of XH-103. The molecular structure of XH-103 was characterized by  $^{13}\text{C}$ NMR (101 MHz,  $\text{CDCl}_3$ ).

#### 5.4.5 Characterization of XH-105

A white solid with an overall yield of 65% was obtained.  $^1\text{H}$  NMR (400 MHz,  $\text{DMSO-d}_6$ )  $\delta$  7.85 (d,  $J = 15.7$  Hz, 2H), 7.64 (s, 1H), 7.56 (d,  $J = 8.4$  Hz, 1H), 7.18 (s, 1H), 4.02 (d,  $J = 26.2$  Hz, 10H), 3.15 (d,  $J = 30.1$  Hz, 10H), 1.77 (d,  $J = 17.1$  Hz, 30H) (Figure 5-16). LC-MS: Waters 3100 detector, Agilent ZORBAX column (C18, 2.1x50mm, 3.5 $\mu\text{m}$ ). LC-MS:  $R_T = 7.06$  min,  $[\text{M}+\text{H}]^+ = 1018.32$ , Calculated: 1018.25 (Figure 5-17).

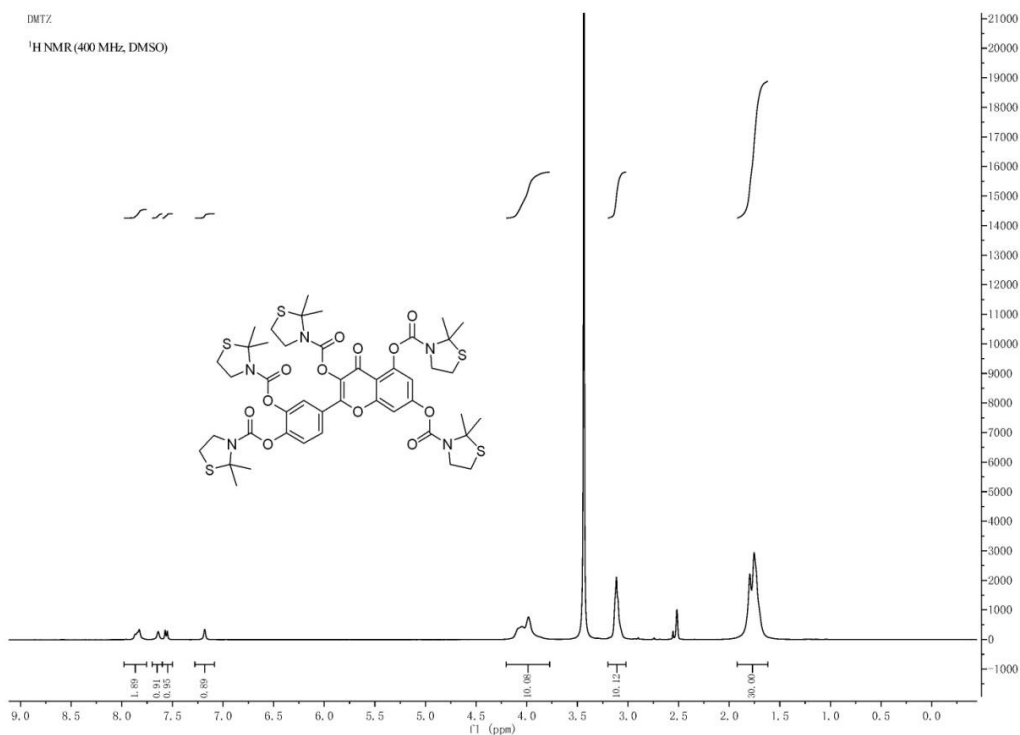


**Figure 5-16 <sup>1</sup>H NMR Spectra of XH-105.** The molecular structure of XH-105 was characterized by <sup>1</sup>H NMR (400MHz, d-DMSO).

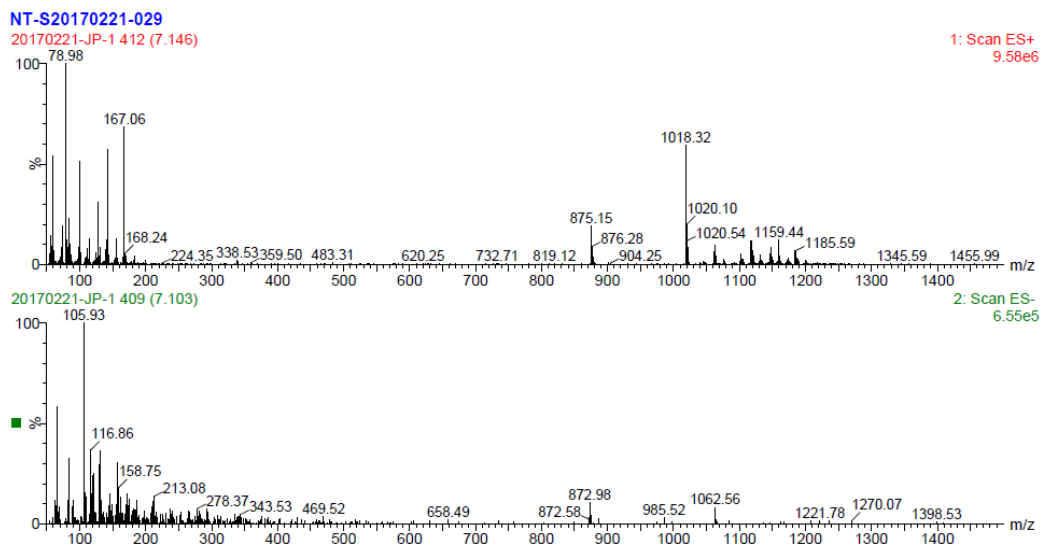


**Figure 5-17 LC-MS Spectra of XH-105.** XH-105 was identified by LC-MS spectra. Target peak [M+H]<sup>+</sup>=1018.32.

#### 5.4.6 30-day survival rate

In order to investigate the structure-activity relationship, mice survival after exposure to 7.2Gy irradiation was determined. In the sham irradiation groups, all mice survived the 30-day period. In the vehicle group, all mice died on day 13 after 7.2 Gy total body irradiation. In the XH-101-, XH-102-, XH-103- treated groups at a dosage of 200 mg/kg, 60%, 80%, 100% animals survived initially, respectively. On day 30, the survival rates in XH-101, XH-102, XH-103 were 40%, 0%, and 20%, respectively (Figure 5-18). After analysing the structure-activity relationship, it is concluded that new molecular structures with five substituents in the quercetin was better than four substituents. Also, compounds with methyls in the substituents showed an improved rat survival rate. Hence, another new compound named XH-105 was designed and synthesized based on this structure-activity relationship. XH-105 was chosen for the further study on the protective effects against intestinal injury (Chaper 6).

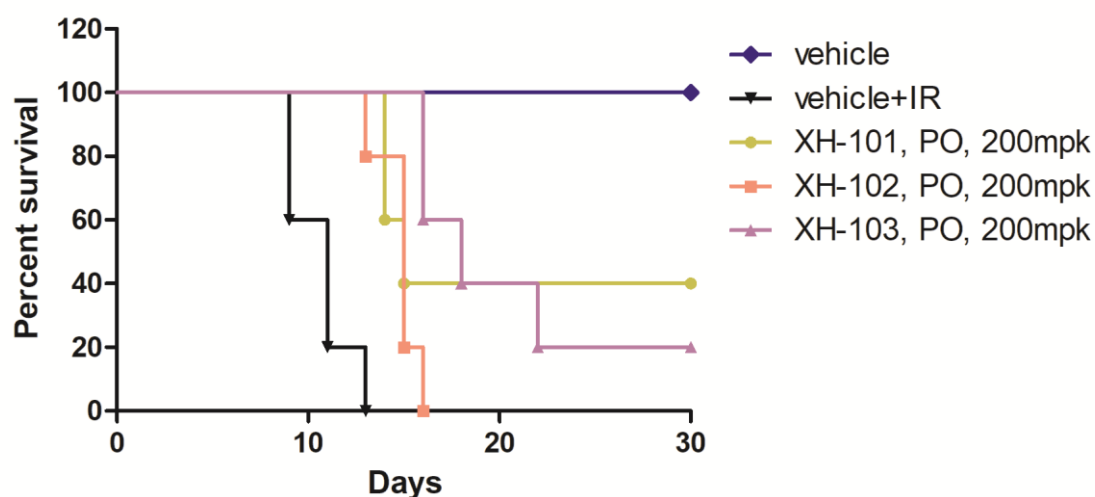


**Figure 5-18 30-day survival rate studies under 7.2 Gy TBI.** Kaplan–Meier survival analysis of mice exposed to 7.2Gy TBI. (a) XH-101 treated mice have 40% survival beyond 30 days post 7.2Gy TBI; XH-102 treated mice have 0% survival beyond 30 days; XH-103 treated mice have 20% survival beyond 30 days; compared with IR mice with 100% mortality within 13 days of radiation exposure ( $p < 0.05$ ,  $n = 5$  per group). The data were expressed as the percent of surviving mice.

## 5.5 Conclusion

Three new compounds (XH-101, XH-102, XH-103) were designed based on the produg concept. These compounds were synthesized by a series of synthesis routes, and characterized by  $^1\text{H NMR}$ ,  $^{13}\text{C NMR}$ , HRMS. A 30-day survival rates study on mice showed that mice exposed to 7.2 Gy total body irradiation died after 13 days, while 60%, 80%, 100%

---

animals were still alive in XH-101-, XH-102-, XH-103- treated groups at a dose of 200 mg/kg. At the end of the study, survival rates of the treatment groups were 40%, 0%, and 20%, respectively. A preliminary structure-activity relationship identified the new molecular structure named XH-105, and this compound was designed, synthesized and characterized. Finally, it was chosen for the further study on the protective effects against intestinal injury.

---

## 5.6 References

1. Baskar, R.; Lee, K. A.; Yeo, R.; Yeoh, K. W., Cancer and radiation therapy: current advances and future directions. *Int J Med Sci* 2012, 9, (3), 193-9.
2. Morita, A.; Takahashi, I.; Sasatani, M.; Aoki, S.; Wang, B.; Ariyasu, S.; Tanaka, K.; Yamaguchi, T.; Sawa, A.; Nishi, Y.; Teraoka, T.; Ujita, S.; Kawate, Y.; Yanagawa, C.; Tanimoto, K.; Enomoto, A.; Neno, M.; Kamiya, K.; Nagata, Y.; Hosoi, Y.; Inaba, T., A chemical modulator of p53 transactivation that acts as a radioprotective agonist. *Mol Cancer Ther* 2018, 17, (2), 432-442.
3. Pan, J.; He, H.; Su, Y.; Zheng, G.; Wu, J.; Liu, S.; Rao, P., In vivo radioprotective Aactivity of cell-permeable bifunctional antioxidant enzyme GST-TAT-SOD against whole-body ionizing irradiation in mice. *Oxid Med Cell Longev* 2017, 2017, 2689051.
4. Shadad, A. K.; Sullivan, F. J.; Martin, J. D.; Egan, L. J., Gastrointestinal radiation injury: symptoms, risk factors and mechanisms. *World J Gastroenterol* 2013, 19, (2), 185-98.
5. Monti, P.; Wysocki, J.; van der Meeren, A.; Griffiths, N. M., The contribution of radiation-induced injury to the gastrointestinal tract in the development of multi-organ dysfunction syndrome or failure. *Brit J Radiol* 2005, Supplement\_27, (1), 89-94.
6. Bhandari, P., A review of radioprotective plants. *Int J Green Pharmacy* 2013, 7, (2), 90.
7. Santabarbara, G.; Maione, P.; Rossi, A.; Gridelli, C., Pharmacotherapeutic options for treating adverse effects of Cisplatin chemotherapy. *Expert Opin Pharmacother* 2016, 17, (4), 561-70.
8. Simon, E. S.; Reyna, D.; Lister, R. J.; Harteg, C.; Lipka, E., Evaluation of a method for measuring the radioprotective metabolite WR-1065 in plasma using chemical derivatization combined with UHPLC-MS/MS. *J Chromatogr B Analyt Technol Biomed Life Sci* 2018, 1080, 82-89.
9. Praetorius, N. P.; Mandal, T. K., Alternate delivery route for amifostine as a radio-/chemo-protecting agent. *J Pharm Pharmacol* 2008, 60, (7), 809-15.
10. FDA, [https://www.accessdata.fda.gov/drugsatfda\\_docs/label/2017/020221s033lbl.pdf](https://www.accessdata.fda.gov/drugsatfda_docs/label/2017/020221s033lbl.pdf).
11. Daniel D. Peebles, C. M. S., Richard R. Copp, Allen L. Thunberg, and William E.; Fahl, ROS-scavenger and radioprotective efficacy of the new PrC-210 aminothiols. *Radiat*

- 
- Res 2012, 178, (1), 57-68.
12. Liu, W.; Chen, Q.; Wu, S.; Xia, X.; Wu, A.; Cui, F.; Gu, Y. P.; Zhang, X.; Cao, J., Radioprotector WR-2721 and mitigating peptidoglycan synergistically promote mouse survival through the amelioration of intestinal and bone marrow damage. *J Radiat Res* 2015, 56, (2), 278-86.
  13. Bansal, P.; Paul, P.; Kunwar, A.; Jayakumar, S.; Nayak, P. G.; Priyadarsini, K. I.; Unnikrishnan, M. K., Radioprotection by quercetin-3-O-rutinoside, a flavonoid glycoside – A cellular and mechanistic approach. *J Funct Foods* 2012, 4, (4), 924-932.
  14. Bilia, A. R.; Isacchi, B.; Righeschi, C.; Guccione, C.; Bergonzi, M. C., Flavonoids Loaded in Nanocarriers: An opportunity to increase oral bioavailability and bioefficacy. *Food Nutrit Sci* 2014, 05, (13), 1212-1327.
  15. David M. Brizel, T. H. W., Michael Henke, Vratislav Strnad, Volkmar Rudat, Alain Monnier, Francois Eschwege, J. Z., Lesley Russell, Wolfgang Oster, Rolf Sauer, Phase III randomized trial of amifostine as a radioprotector in head and neck cancer. *J Clin Oncol* 2000, 18, (19), 3339-3345.
  16. Copp, R. R.; Peebles, D. D.; Soref, C. M.; Fahl, W. E., Radioprotective efficacy and toxicity of a new family of aminothiols. *Int J Radiat Biol* 2013, 89, (7), 485-92.
  17. Brown, P. E., Mechanism of action of aminothiol radioprotectors. *Nature* 1967, 213, (5074), 363-364.
  18. Copp, R. R.; Peebles, D. D.; Fahl, W. E., Synthesis and growth regulatory activity of a prototype member of a new family of aminothiol radioprotectors. *Bioorg Med Chem Lett* 2011, 21, (24), 7426-30.
  19. Aizawa, Y.; Sunada, S.; Hirakawa, H.; Fujimori, A.; Kato, T. A.; Uesaka, M., Design and evaluation of a novel flavonoid-based radioprotective agent utilizing monoglucosyl rutin. *J Radiat Res* 2018, 59, (3), 272-281.
  20. Kayoko Shimoi, S. M., Bingrong Shen, Michiyo Furugori, Naohide Kinae, Radioprotective effects of antioxidative plant flavonoids in mice. *Mutation Research* 1996, 350, 153-161.
  21. BROWN, P. E., Mechanism of Action of Aminothiol Radioprotectors. *Nature* 1967, 28.

- 
22. H. Brocha, A. H., D. Vasilescua, Quantum molecular simulation of the radioprotection by the aminothiols WR-1065, active metabolite of amifostine (WR-2721). Part 2. Modeling of the hydrogen abstraction by C4' of DNA deoxyribose radical. *J Mol Struct* 2001, 538, 117-132.

---

## **6. CHAPTER 6: THE PROTECTIVE EFFECTS OF XH-105 AGAINST RADIATION-INDUCED INTESTINAL INJURY**

This study was published in *Journal of Cellular and Medicine*, Year 2019, Vol. 23, Pages 2238-2247.

---

## 6.1 Abstract

The small intestine is one of the most sensitive organs during the radiotherapy. Intestinal injury induced by ionizing irradiation may cause severe symptoms, including radiation enteritis. There is no specific treatment for radiation enteritis.

Radiation-induced intestinal injury is one of the major side effects in patients receiving radiation therapy. In this study, we described the beneficial effects of XH-105 that was designed for the protection against radiation-induced intestinal injury. C57BL/6J mice were treated by gavage with XH-105 one hour before total body irradiation (TBI), and the survival rate was monitored. Histological changes were examined, and survival of Lgr5<sup>+</sup> intestinal stem cells, Ki67<sup>+</sup> cells, villi<sup>+</sup> enterocytes and lysozymes was determined by immunohistochemistry. DNA damage and cellular apoptosis in intestinal tissue were also evaluated.

Compared to vehicle-treated mice after TBI, XH-105 treatment significantly enhanced the survival rate. The 7.5 Gy TBI led to a 100% mortality in the vehicle-treated group within 20 days compared with the 100 mg/kg XH-105-treated group that had a 30% survival rate beyond 30 days. When the mice were exposed to 9.0 Gy TBI, XH-105 at all doses of 50, 100 and 200 mg/kg improved mice survival rate compared to the vehicle-treated group, and, in particular, the 100 mg/kg dose dramatically improved median survival. There was 80% mortality in vehicle-treated mice at 6 days after 11.0 Gy TBI, while 60% of mice survived in the 100 mg/kg XH-105-treated group. XH-105 attenuated structural damage of the small intestine. XH-105-treated mice showed more survival crypts ( $p < 0.01$ ) and an increased villous height ( $p < 0.01$ ), as well as a significant increase in expression of villi<sup>+</sup> enterocytes compared with vehicle-treated mice. Furthermore, XH-105 decreased apoptotic rates, reduced DNA damage, maintained cell regeneration and promoted crypt proliferation and differentiation. XH-105 also reduced the expression of Bax and p53 in the small intestine. These data suggest that XH-105 is beneficial for the protection of radiation-induced intestinal injury by inhibiting the p53-dependent apoptosis signaling pathway.

**Keywords:** Total body irradiation, Small intestine, Apoptosis, DNA damage, p53

## 6.2 Introduction

The small intestine is one of the most sensitive organs for ionizing radiation. The main symptoms of radiation-induced intestinal damage include anorexia, vomiting, diarrhea,

---

dehydration, systemic infection, and in extreme cases, septic shock and death [1]. Radiation-induced intestinal damage seriously affects the treatment of patients with abdominal or pelvic tumors, reducing their quality of life. Radiotherapy induces ROS accumulation in the form of OH, single oxygen and peroxy radicals in normal tissues. Subsequently, ROS reacts with DNA, inducing double strand breaks (DSB), and proteins resulting aberrant function of physiology through a cascade of events. Therefore, it is of significance to develop effective radioprotectors to prevent and mitigate radiation-induced intestinal injuries.

The small intestine is a crucial component for nutrient absorption required for proper body function. Intestinal crypt cells are sensitive to radiation, leading to mucosal injury [2]. The mucosa layer of the small intestine is covered with continuous villi that increase the surface area and capability of absorption. The crypts are invaginations of the epithelium around the villi. Intestinal stem cells (ISCs) reside at the base of crypts, with continuous dividing and differentiating ability. Paneth cells, located at the base of the proliferative compartment, provide an important anti-bacterial defense function for the small intestine.

Total body irradiation affects multiple organ systems. Gastrointestinal syndrome leads to death in humans and rodents within 10-12 days after exposure to 8-20 Gy of  $\gamma$ -rays, due to fluid and electrolyte imbalance and bacterial translocation [3]. ISCs die rapidly after exposure to high doses of radiation by apoptosis which appears to be mediated by up-regulation of p53 [3]. Ionizing radiation-induced double strand breaks in DNA, triggers the activation of the p53 signaling pathway. This could lead to the cell cycle arrest or apoptosis. Moreover, the cellular levels of enzymes increase upon radiation treatment, affecting specific cellular surface receptors at distant sites [4].

The identification of reliable markers is beneficial for determining stem cell population. Leucine-rich-repeat-containing G-protein-coupled-5 (LGR5) was demonstrated in crypts of small intestines, but not in the villi [5]. Loss of LGR5 may affect the regeneration of crypts. The formation of  $\gamma$ H2AX is an early cellular response to the induction of DNA double-strand breaks.  $\gamma$ H2AX is the most sensitive and highly specific molecular marker for monitoring DNA damage initiation and resolution [6].

In this study, the plant-derived natural anti-oxidation flavonoid quercetin was examined as a lead compound and its molecular structure was modified by combining it with the aminothiols analogue and different linkers to retain the efficacy of aminothiols and the safety properties of quercetin, respectively. Furthermore, the two functional fragments, polyphenol and aminothiols,

---

modulate the pharmacokinetic profile of each other, being mutually prodrugs to each other. The new compound was expected to cleave into polyphenol and aminothiols *in vivo* to mitigate radiation injury by their ROS scavenger capabilities. Based on this concept, XH-105 was designed and synthesized.

To define the effects of XH-105 on intestinal radiation injury, a mouse model with exposure to 9.0 Gy total body irradiation (TBI) was used. XH-105 improved survival rates of mice and intestinal epithelium cells (IECs), and mitigated the crypt-villous structure injuries of the small intestine and apoptosis of IECs.

## **6.3 Materials and methods**

### **6.3.1 Animals**

Male C57BL/6 mice (8-10 weeks) were purchased from Beijing HFK Bioscience Co., Ltd. (Beijing, China). Animals were bred in the certified animal facility at the Institute of Radiation Medicine (IRM) of the Chinese Academy of Medical Sciences (CAMS).

### **6.3.2 Ethics approval and consent to participate**

All experimental procedures were carried out in accordance with the NIH Guidelines for the Care and Use of Laboratory Animals and were approved by the Institutional Animal Care and Use Committee of the Institute of Radiation Medicine (IRM), Chinese Academy of Medical Sciences (CAMS) (Permit Number 2017053). The animals were cared for in accordance with the guidelines of the National Animal Welfare Law of China.

### **6.3.3 Irradiation and treatment**

Mice were randomly assigned to different groups (Table 6-1). Animals in irradiation groups were exposed to ionizing radiation by using a  $^{137}\text{Cs}$  source following an Exposure Instrument Gammacell-40 (Atomic Energy of Canada Ltd, Chalk River, ON, Canada) at a dose rate of 1.0 Gy/min. The mice were exposed to 7.5 Gy, 9.0 Gy and 11.0 Gy TBI in the survival experiments (n=10). The animals in the control group received a sham irradiation. In the remaining experiments, animals were divided randomly into three groups (n=5): (a) control; (b) IR + vehicle; (c) IR + XH-105 and received 9.0 Gy TBI. XH-105 was dissolved in 4% DMSO, 96% of PEG 400 was added after heating to a final concentration of 10 mg/mL. Individual mice in the IR+XH-105 group received a dose of 100 mg/kg XH-105 administered by gavage 1 h before irradiation. Mice in the Control and IR groups were treated with vehicle similarly to the procedure described for the XH-105 treatment.

**Table 6-1 Group setting of mice**

Experiments	Groups	Dose (mg/kg)	Treatment	Animals (N)
30-day survival rate (7.5 Gy, TBI)	IR+vehicle	-	PO, dosing at 1 h before IR	10
	IR+XH-105, 100	100	PO, dosing at 1 h before IR	10
30-day survival rate (9.0 Gy, TBI)	IR+ vehicle	-	PO, dosing at 1 h before IR	10
	IR+XH-105, 50	50	PO, dosing at 1 h before IR	10
	IR+XH-105, 100	100	PO, dosing at 1 h before IR	10
30-day survival rate (11 Gy, TBI)	IR+XH-105, 200	200	PO, dosing at 1 h before IR	10
	IR+vehicle	-	PO, dosing at 1 h before IR	10
	IR+XH-105, 100	100	PO, dosing at 1 h before IR	10
Other (9.0 Gy, TBI)	Control	-	PO, dosing at 1 h before IR	5
	IR+vehicle	-	PO, dosing at 1 h before IR	5
	IR+XH-105, 100	100	PO, dosing at 1 h before IR	5

#### 6.3.4 Histological analysis

Three days after IR, mice were sacrificed, and the small intestines were collected, stained with hematoxylin-eosin (H&E) and analyzed by microscopy. For morphological analysis, six circular transverse sections were analyzed per mouse in a blind manner from coded digital H&E-stained photographs to measure villi length and crypt number by using ImageJ 1.37 software.

For the H&E staining, the tissue was deparaffinized with xylene for 15 min twice, then re-hydrated with absolute ethyl alcohol for 5 min twice. After that, they were washed for 5 min with 95% and 80% ethanol, and tap water, respectively. After briefly washing with distilled water, slices were stained with hematoxylin for 6 min, and then washed with tap water. Slices were differentiated in ethanol containing 1% hydrochloric acid for 10 s and washed with tap water, followed by bluing in ammonia water solution for 20 s and washing with tap water for 5 min, before dipping into distilled water. Then slices were stained with eosin for 25 s, washed with tap water for 5 min, and dipped into 75, 95%, and absolute alcohol, respectively. Slices were then placed in absolute ethyl alcohol for 5 min and in xylene for 15 min twice to clear excess dye. Finally, slices were covered and observed by light microscopy.

---

### **6.3.5 Immunohistochemistry analysis**

The 4- $\mu$ m-thick sections of paraffin-embedded small intestine were dewaxed and rehydrated with citrate buffer. Then, sections were boiled in 10 mM/L citrate buffer solution (pH 9.0) for antigen retrieval according to standard procedures. After antigen retrieval, sections were incubated with serum for 1 h at room temperature to block nonspecific antigen-binding sites; then, sections were incubated with anti-Lgr5 antibody (1:50 dilution, Abcam, Cambridge, MA, USA), anti-Ki67 antibody (1:300 dilution, Novus, Littleton, CO, USA), anti-lysozyme (1:800 dilution, Abcam, Cambridge, MA, USA) or anti-villi (1:800 dilution, Abcam, Cambridge, MA, USA) overnight at 4°C. Sections were then incubated in secondary antibody for 30 min at 37°C. Positive cells were detected using a DAB kit (Sigma Aldrich, Missouri, USA). The images were captured, and positive staining was quantified objectively by the IPP software as described previously in a blinded fashion.

### **6.3.6 TUNEL assay**

The 3- $\mu$ m-thick sections were treated according to the manufacturer's protocols (Roche, Mannheim, Germany). The tissue section was incubated for 15-30 min at 21-37 °C with proteinase K working solution. Then the slides were washed with PBS and dried. After that, 50  $\mu$ L of TUNEL reaction mixture (mixed with Label Solution and Enzyme solution at a ratio of 9:1) was added, and the samples were covered with a lid and incubated for 60 min at 37 °C in a humidified atmosphere in the dark. At this step, negative control and positive control were set up. For the negative control, tissues were incubated with 50  $\mu$ L/well of Label Solution instead of TUNEL reaction mixture. For the positive control, tissues were incubated with micrococcal nuclease, grade I for 10 min at 15-25 °C to introduce DNA strand breaks. Next, the slides were washed 3 times with PBS and dried and 50  $\mu$ L of Converter-POD was added, followed by incubation in a humidified chamber for 30 min at 37 °C and 3 times washing with PBS. 50-100  $\mu$ L of DAB substrate was added, incubated for 10 min at 15-25 °C, and rinsed 3 times with PBS. Sections were covered with a glass coverslip and analyzed by light microscopy.

### **6.3.7 Isolation of intestinal crypt cells**

Intestinal crypts were isolated as described [7, 8]. Briefly, after flushing with ice-cold PBS, small intestines were chopped into small pieces and then placed into cold crypt-chelating buffer for 30 min. After rinsing twice with ice-cold PBS, the fragments were resuspended in

---

cold dissociation buffer. The solution was filtered through a 70 µm strainer to remove the villus fraction and to collect the crypt fraction. The crypt fraction was centrifuged to isolate single cells.

### **6.3.8 Western Blot analysis**

Protein was extracted from small intestinal crypt cells with ice-cold lysis buffer (Solarbio Science and Technology, Beijing, China). The protein concentration was quantified using the BCA Protein Assay Kit (Beyotime, Shanghai, China), and equal amounts of protein were resolved by a SDS-polyacrylamide gel electrophoresis and then transferred to polyvinylidene difluoride membranes (Millipore, MA, USA). After blocking of unspecific binding sites with 5% nonfat milk, blocked membranes were incubated using antibodies against anti-Bax (1:1000 dilution, Ruiyingbio, Suzhou, China) or  $\beta$ -tubulin (1:2500 dilution, Proteintech, Wuhan, China) overnight at 4°C. Then, membranes were incubated with a suitable horseradish peroxidase-conjugated secondary antibody for 1-2 h at room temperature. Finally, the blots were detected with ECL chemiluminescence kit (Cat# P0018AS, Beyotime, Shanghai, China).

### **6.3.9 Immunofluorescence analysis**

Paraffin-embedded sections of the small intestine were subjected to antigen retrieval as described above and then washed thoroughly with PBS. The sections were blocked with 5% goat serum for 30 min at room temperature and incubated with anti-caspase-8 (1:100 dilution, CST, MA, USA), anti-caspase-9 (1:1000 dilution, CST, MA, USA), anti- $\gamma$ H2AX (1:1000 dilution, BD biosciences, NJ, USA) or anti-p53 (1:1000 dilution, Ruiyingbio, Suzhou, China) overnight at 4°C. After washing with PBS, sections were incubated in the secondary antibody for 40 min at 37°C while avoiding light. Sections were finally sealed with DAPI-containing sealing agent. The images were captured by laser scanning confocal microscopy.

### **6.3.10 Statistical analysis**

Mice survival curves were analyzed using the Kaplan-Meier method on GraphPad Prism 6.0 software for Mac. The data were expressed as the mean  $\pm$  standard deviation (SD). Analysis of variance (ANOVA) tests were used to analyze differences among groups. Data were normally distributed (Shapiro-Wilks test;  $p > 0.05$ ) and variances were homogeneous (Levene test,  $p > 0.05$ ) (IBM SPSS statistic 26, IBM, Chicago, USA). Difference between two groups was analyzed by Least Significant Difference (LSD) test and Student-Newman-Keuls test was used to compare variations in multiple groups.  $p < 0.05$  was considered statistically significant.

## 6.4 Results

### 6.4.1 XH-105 improves the survival rate of mice after TBI

To assess the protective effect of XH-105 on TBI-induced lethality in mice, survival rates of mice were observed first after 7.5 Gy TBI (Figure 6.1a). 7.5 Gy TBI induced 100% mortality in the vehicle-treatment group within 20 days compared to the 100 mg/kg XH-105-treatment group that had 30% survival beyond 30 days. Mice treated with XH-105 of 50, 100, or 200 mg/kg, followed by 9.0 Gy TBI 1 h later, showed improved survival rates compared to the vehicle-treatment group, particularly, the 100 mg/kg dose dramatically improved median survival (Figure 6.1b). There was 80% mortality in vehicle-treated mice at 6 days after 11.0 Gy TBI (Figure 6.1c), while 60% of mice survived in the 100 mg/kg XH-105-treated group, suggesting that XH-105 may have a protective effect on radiation-induced intestinal injuries in mice. These results indicated that XH-105 effectively mitigates the TBI-induced lethality in mice.

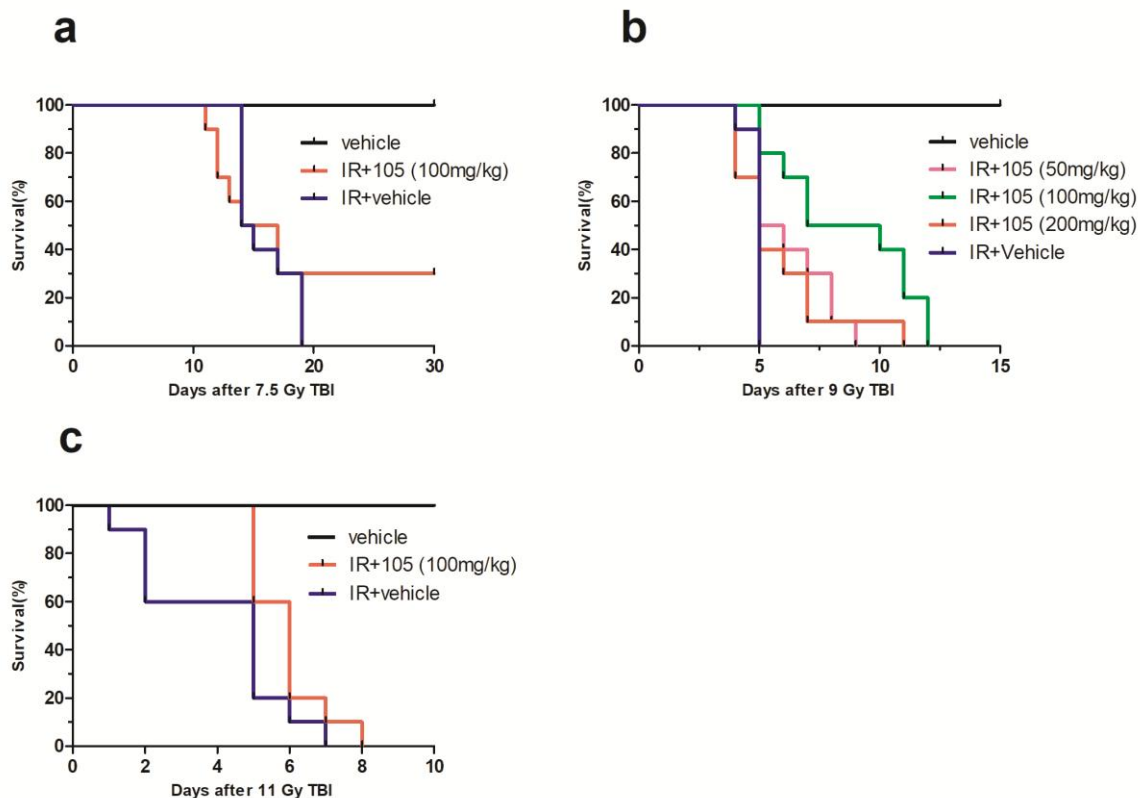


**Figure 6-1 XH-105 improves survival of mice after 9.0 Gy TBI.** Kaplan–Meier survival analysis of mice exposed to 7.5Gy, 9.0Gy or 11.0Gy TBI. (a) XH-105 treated mice showed 30% survival beyond 30 days post 7.5Gy TBI, compared to IR mice with 100% mortality within 20 days of radiation exposure ( $P<0.05$ ,  $n=10$  per group). (b) Three doses of XH-105-treated mice showed reduced mortality following lethal doses of TBI (9.0Gy) within 13 days, compare with IR group 100% mortality within 5 days ( $p<0.05$ ,

n=10 per group). (c) The Kaplan–Meier survival curve of vehicle and XH-105 treated mice ( $p<0.05$ , n=10 per group) after 11.0Gy TBI. Data were expressed as the percent of surviving mice.

Many studies reported reduced TBI-induced injuries in the brain, esophagus, and hematopoietic system of irradiated animals, receiving Chinese herbal medicines or extracts and other drugs [9-13], but studies of protective drugs in IR-induced intestinal injuries still require improvements [14-16]. In the present study, the new compound XH-105 demonstrated protective effects against radiation-induced intestinal injuries.

#### 6.4.2 XH-105 reduces the damages of intestinal morphology after TBI

To determine the effect of XH-105 on radiation-induced intestinal injuries, morphological changes of the small intestine in mice were evaluated. At 3.5 d after 9.0 Gy TBI, irradiated mice treated with vehicle caused damage to villi of small intestine and showed significantly shorter villous length ( $p<0.005$ ) and fewer crypts ( $p<0.005$ ) than the control group (Figure 6-2 a, Figure 6-2 b). In comparison to vehicle-treated mice, XH-105-treated mice showed more survival crypts ( $p<0.01$ ) and an increased villous height ( $p<0.01$ ). The expression of villi+ enterocytes was also affected by radiation (Figure 6-2 c, Figure 6-2 d), and mice treated with XH-105 exhibited a significant increase in expression compared with vehicle-treated mice. These results indicated that XH-105 treatment can prevent post-radiation damage of the intestinal villus-crypt structures in mice.

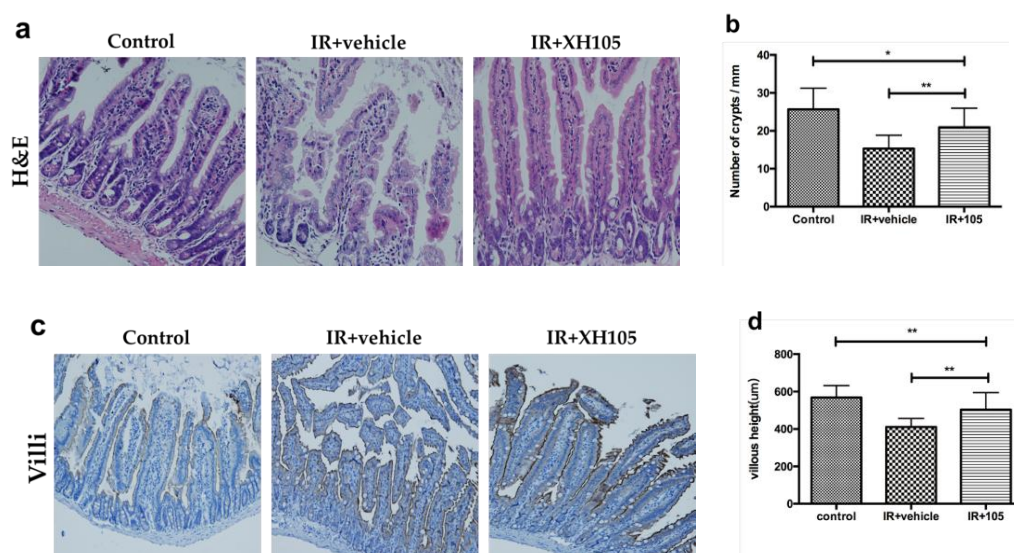


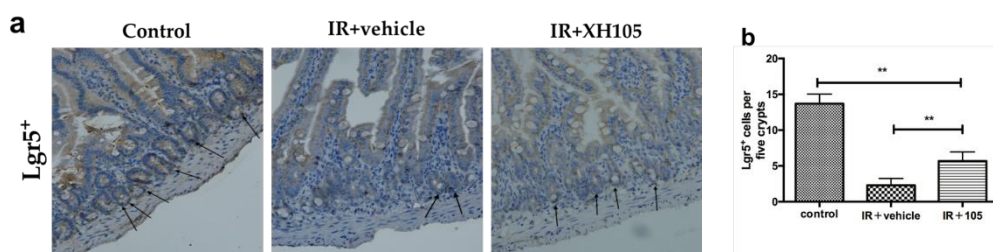
**Figure 6-2 XH-105 protects the intestinal morphology of mice after 9.0Gy TBI.** (a) Representative images showing the structure in cross-sections of the small intestine with H&E stained. (b) Histogram showing the number of crypts. (c) Immunohistochemistry images showing the expression of Villi. (d) Histogram demonstrating villus length in intestinal section from the control group, vehicle-treated group

and XH-105-treated group. The results are represented as mean  $\pm$  SEM, n=5 mice per group. \*\* $p$ <0.01, \* $p$ <0.05. Scale bar: 100  $\mu$ m and 50  $\mu$ m

After receiving radiation, various degrees of villi blunting and fusion may occur; villous epithelial cell attenuation and hypertrophy and severe loss of crypts lead to the destruction of epithelial cell homeostasis and epithelial integrity [17]. Intestinal epithelial cells cannot easily maintain intestinal absorption and defence functions [18]. Results shown here demonstrated that the intestinal crypt-villus structure in XH-105-treated mice was well preserved after 9.0 Gy TBI.

#### 6.4.3 XH-105 enhances Lgr5<sup>+</sup> ISC survival and maintains the regeneration of intestinal cells after TBI

To evaluate the effect of XH-105 on the proliferation and differentiation ability of crypt cells, Lgr5 and Ki67 were identified by immunohistochemistry staining. Lgr5<sup>+</sup> intestinal stem cells are indispensable for intestinal regeneration following radiation [19]. At 3.5 days after 9.0 Gy TBI, the number of Lgr5<sup>+</sup> ISCs was significantly increased in the XH-105-treated mice compared to the vehicle-treated group (Figure 6-3 a, Figure 6-3 b). Similarly, the number of Ki67<sup>+</sup> positive cells in XH-105-treated mice was also markedly greater than those in vehicle-treated mice after TBI (Figure 6-3 c, Figure 6-3 d). Paneth cells located at the bottom of intestinal crypts produce lysozymes. Changes in Paneth cells 3.5 days after 9.0 Gy TBI were therefore also investigated (Figure 6-3 f). Results showed that the number of lysozyme<sup>+</sup> positive cells (Figure 6-3 e) of XH-105-treated group were greater than that of the vehicle-treated group. In summary, these data clearly indicated that XH-105 enhances the regenerative response of radiation-induced intestinal injuries by promoting the differentiation and proliferation of ISCs in the small intestine.



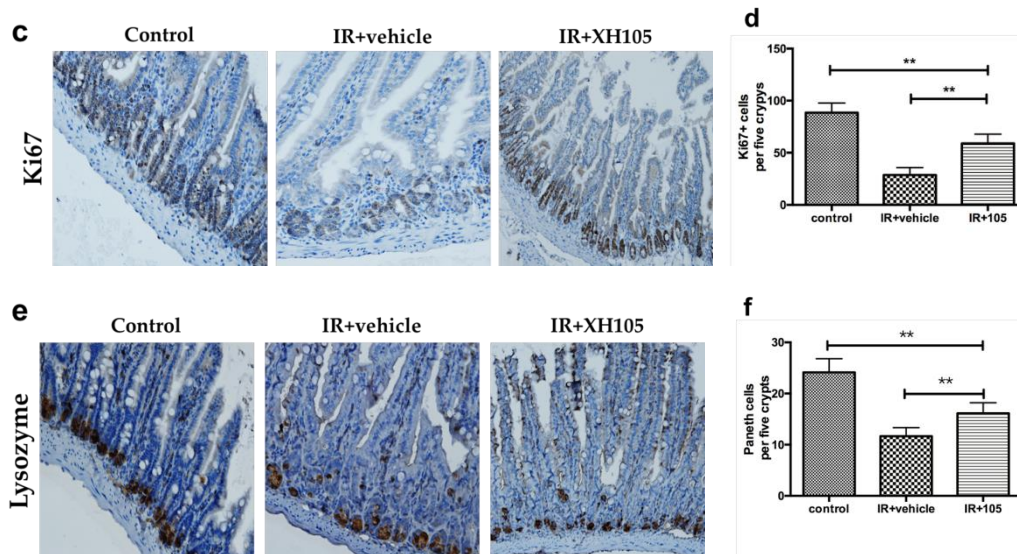


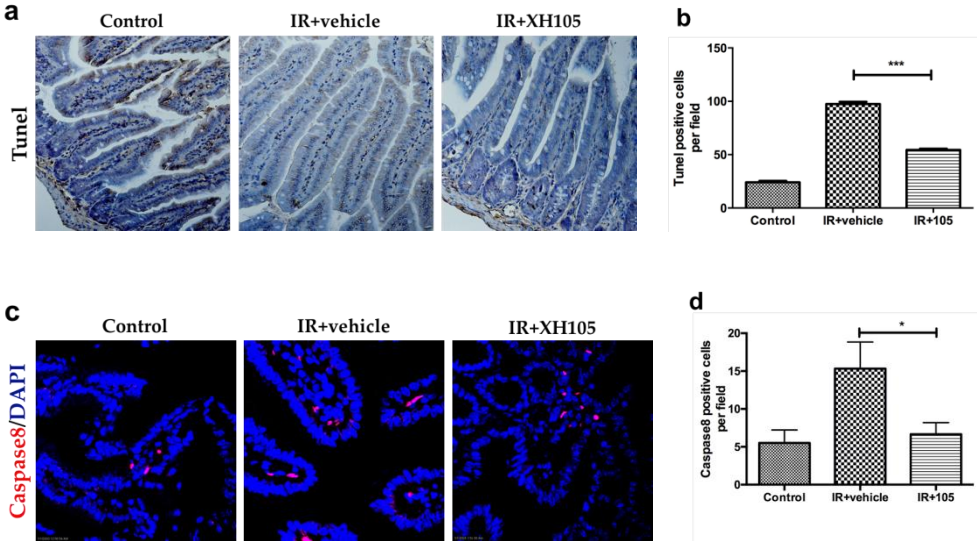
**Figure 6-3 XH-105 enhances proliferation and differentiation ability of the Lgr5<sup>+</sup> small intestine after 9.0 Gy TBI.** The small intestinal sections were analyzed by IHC. (a) Photomicrograph of Lgr5 immunostaining section of control, IR+vehicle and IR+105 groups. (b) Histogram showing Lgr5-positive cells were quantified in five crypts per section. (c) Immunomicrographs showing Ki67 expression of intestinal crypts. (d) Histogram demonstrating Ki67-positive cells were counted in five crypts per section. (e) Representative immunohistochemistry micrographs for lysozyme-stained sections of the small intestine. (f) Histogram showing the number of paneth cells per five crypts. The results are represented as mean  $\pm$  SEM, n=5 mice per group. \*\* $p < 0.01$ . Scale bar: 50  $\mu$ m.

The intestinal epithelium is one of the most rapidly self-renewing organs in mammals and is continuously renewed by intestinal epithelial stem cells (IESCs) located in the crypts [20, 21]. IESC renewal is identified by expression of Lgr5 [22, 23]. Under physiological conditions, epithelial homeostasis is maintained by proliferative cells in crypts, and the small intestinal crypt cells are particularly sensitive to IR due to their high rate of proliferation [24]. The stem cell niche located at the bottom of intestinal crypts contains Paneth cells, which can produce lysozymes. Previous studies have shown that the number of Paneth cells decrease with the loss of Lgr5<sup>+</sup> stem cells [25, 26]. Here, the number of Lgr5<sup>+</sup> intestinal stem cells increased in the XH-105-treated group after 9.0 Gy TBI and Lgr5<sup>+</sup> intestinal stem cells differentiated into Paneth cells and villus cells. Thus, XH-105 may play a protective role against IR-induced intestinal injuries by improving the proliferation and differentiation of Lgr5<sup>+</sup> intestinal stem cells. The increased expression of Ki67, a proliferation marker in the small intestine, in the XH-105-treated mice indicated the recovery of the intestinal cells after IR-induced injuries.

These results indicated that XH-105 may have a protective effect on irradiation-induced intestinal injury.

### 6.4.4 XH-105 decreases apoptosis of the small intestine after TBI

To investigate the effect of XH-105 on apoptosis of the small intestines after IR, apoptosis in the small intestine was investigated using the TUNEL assay. The results indicated that XH-105 had a protective role in preventing radiation-induced intestinal damage by suppressing apoptosis (Figure 6-4 a, Figure 6-4 b). To further validate these results, the rate of apoptosis was analyzed using caspase-8 and caspase-9 immunofluorescence staining of small intestinal sections from mice after 9.0 Gy TBI. The immunofluorescence micrographs showed expression of apoptosis-related proteins (Figure 6-4 c, Figure 6-4 e). Mice exposed to radiation showed an increase the number of apoptotic nuclei in the small intestinal crypts. At 3.5 days after 9.0 Gy TBI, XH-105-treated mice showed significantly lower numbers of apoptotic cells compared to vehicle-treated mice. These data suggested that XH-105 treatment could decrease the number of apoptotic cells and protect mice from irradiation-induced intestinal injuries.



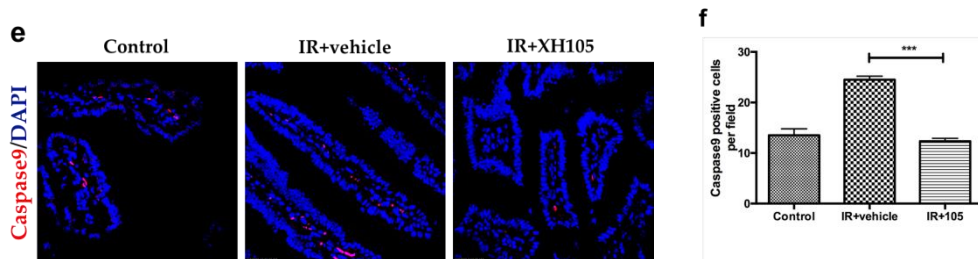


**Figure 6-4 XH-105 decreases apoptosis of the small intestine after 9.0 Gy TBI.** (a) Apoptosis was assayed by TUNEL staining. (b) The number of TUNEL positive cells was quantified per field. Paraffin-embedded sections of the small intestine were analyzed by immunofluorescence. (c) Representative DAPI and caspase 8-fluorescence of the small intestine (Red, caspase 8; Blue, DAPI). (d) Caspase 8-positive cells in a single field of view were quantified. (e) Photomicrograph of caspase 9-staining of the small intestine (Red, caspase 9; Blue, DAPI). (f) Bar graph showing quantitative analysis of caspase 9-positive cells per field of view. The results are represented as mean  $\pm$  SEM,  $n=5$  mice per group. \* $p<0.05$ , \*\*\* $p<0.005$ . Scale bar: 50  $\mu\text{m}$  and 10  $\mu\text{m}$ .

Many studies have shown that IR-induced tissue damage increases the amount of apoptotic cells [27-29]. Caspases are expressed by a family of genes important for maintaining homeostasis by regulating apoptosis and inflammation [30]. Caspases involved in apoptosis have been subclassified by their mechanism of action into initiator caspases (caspase-8 and -9) and executioner caspases (caspase-3, -6 and -7). This study showed that XH-105 decreased the number of apoptotic cells in the small intestine by inhibiting the expression of caspase 8 and caspase 9.

#### 6.4.5 XH-105 attenuates DNA damage of the small intestine after TBI

To determine whether XH-105 treatment could reduce TBI-induced DNA damage, histone H2AX phosphorylation was analyzed. There was an increase in  $\gamma$ H2AX in intestinal sections from the IR group compared with the control group (Figure 6-5). XH-105-treatment decreased H2AX phosphorylation in intestinal sections compared to vehicle-treated mice after 9.0 Gy of irradiation. The results indicated that XH-105 could reduce IR-induced DNA damage to the small intestine.

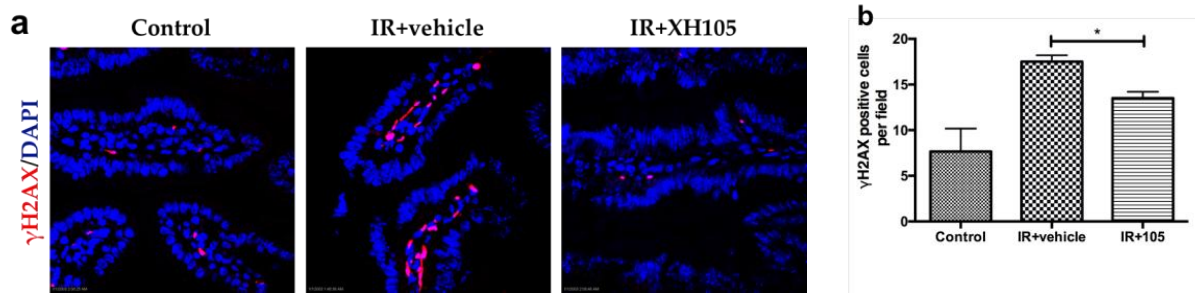
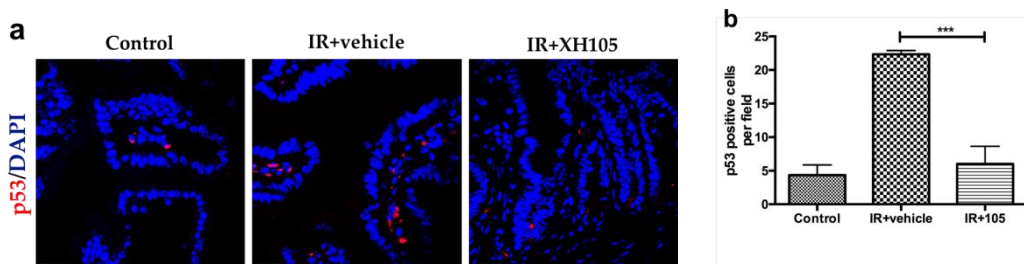


**Figure 6-5 XH-105 attenuates DNA damage of mice after 9.0 Gy TBI.** The small intestine of control mice, vehicle-treated mice and XH-105-treated mice were obtained at 3.5 d after 9.0 Gy TBI. (a) Representative immunofluorescence images for the expression of  $\gamma$ H2AX of the small intestine (Red,  $\gamma$ H2AX; Blue, DAPI). (b) Quantitative analysis histogram of  $\gamma$ H2AX-positive cells per field of view. The results are represented as mean  $\pm$  SEM, n=5 mice per group. \* $p$ <0.05. Scale bar: 10  $\mu$ m.

Phosphorylated H2AX is a variant form of histone H2A, which has been widely used as a marker for DNA double strand breaks [31]. In this study, the expression of  $\gamma$ H2AX decreased in XH-105-treated mice after TBI compared with the vehicle-treated mice.

#### 6.4.6 XH-105 protects the small intestine against radiation-induced injury at least in part via the p53 signaling pathway

To investigate the mechanisms by which XH-105 may protect against radiation-induced intestinal injuries, the expression of p53 was determined by immunofluorescence (Figure 6-6 a). Intestinal crypt cells were isolated and the expression of *Bax* was evaluated by Western blot at 3.5 days after 9.0 Gy TBI (Figure 6-6 c). IR increased the expression of p53 in the small intestine compared to the control group. In contrast, mice treated with XH-105 downregulated the expression of p53 (Figure 6-6 b). Similarly, XH-105-treatment decreased the expression of *Bax*. Taken together, these findings suggested that XH-105 protects the small intestine from IR at least in part by downregulation of the p53 signaling pathway.



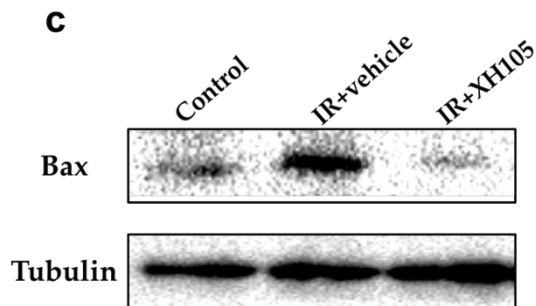


**Figure 6-6 XH-105 decreases the expression of p53 and Bax of the small intestine after 9.0 Gy TBI.** Small intestinal sections of control, IR+vehicle and IR+105 mice at 3.5 d after 9.0 Gy TBI. (a) Representative immunofluorescence images for the expression of p53 of the small intestine (Red, p53; Blue, DAPI). (b) Quantitative analysis of p53-positive cells per field of view. (c) Western blot for Bax and tubulin of intestinal crypts from non-IR mice, vehicle-treated mice and XH-105-treated mice at 3.5 d after 9.0 Gy TBI. The results are represented as mean  $\pm$  SEM, n=5 mice per group. \*\*\* $p$ <0.005. Scale bar: 10  $\mu$ m.

Radiation induces DNA damage directly through reactive oxygen species [32] and destroys the expression of proteins in cells [33], activating p53 [28, 29, 32, 34-36]. Radiation activates p53 in the GI epithelium, and p53-mediated apoptosis has been implicated in regulating intestinal injuries [17, 37]. It is well known that p53 activates genes that regulate cell cycle checkpoints, DNA damage and repair, and apoptosis [38]. In addition, p53 can promote apoptosis through interactions with Bcl-2 family proteins, such as Bax, in the cytoplasm [37, 39]. Studies reported that *Bax*<sup>-/-</sup> and *Bak1*<sup>-/-</sup> mice had reduced apoptosis of epithelial cells after exposure to irradiation [40, 41]. Treatment with XH-105 decreased the expression levels of Bax and p53. These data suggested that XH-105 mitigated DNA damage induced by IR and radiation-induced intestinal injuries via the p53-dependent apoptosis signaling pathway. A previous study showed that inhibiting p53-dependent apoptosis enabled GI epithelial cells to survive and is therefore an effective strategy for preventing radiation-induced damage in gastrointestinal epithelium [29].

## 6.5 Conclusion

XH-105 protected against radiation-induced intestinal injury, which may attenuate radiation-induced intestinal damage via the p53 signaling pathway. XH-105 is a promising novel compound for use as a radio-protector, but effects on the mechanism of radiation enteritis and as a therapeutic need to be further investigated.

## 6.6 Acknowledgement

---

This study was supported by the National Natural Science Foundation of China (No. 81573094), CAMS Innovation Fund for Medical Sciences (CIFMS, 2017-I2M-3-019) from the Chinese Academy of Medical Sciences & Peking Union Medical College, and Fundamental Research Fund for CAMS & PUMC (2016ZX310199).

---

## 6.7 References

1. Monti, P.; Wysocki, J.; van der Meeren, A.; Griffiths, N. M., The contribution of radiation-induced injury to the gastrointestinal tract in the development of multi-organ dysfunction syndrome or failure. *Brit J Radiol* 2005, Supplement\_27, (1), 89-94.
2. Shadad, A. K.; Sullivan, F. J.; Martin, J. D.; Egan, L. J., Gastrointestinal radiation injury: symptoms, risk factors and mechanisms. *World J Gastroenterol* 2013, 19, (2), 185-98.
3. Rosen, E. M.; Day, R.; Singh, V. K., New approaches to radiation protection. *Front Oncol* 2014, 4, 381.
4. Bhandari, P., A review of radioprotective plants. *International J Green Pharmacy* 2013, 7, (2), 90.
5. Umar, S., Intestinal stem cells. *Curr Gastroenterol Rep* 2010, 12, (5), 340-8.
6. Mah, L. J.; El-Osta, A.; Karagiannis, T. C., gammaH2AX: a sensitive molecular marker of DNA damage and repair. *Leukemia* 2010, 24, (4), 679-86.
7. Mahe, M. M.; Aihara, E.; Schumacher, M. A.; Zavros, Y.; Montrose, M. H.; Helmrath, M. A.; Sato, T.; Shroyer, N. F., Establishment of gastrointestinal epithelial organoids. *Curr Protoc Mouse Biol* 2013, 3, (4), 217-40.
8. Yang, W.; Sun, Z.; Yang, B.; Wang, Q., Nrf2-Knockout protects from intestinal injuries in C57BL/6J mice following abdominal irradiation with gamma Rays. *Int J Mol Sci* 2017, 18, (8).
9. Kindekov, I.; Mileva, M.; Krastev, D.; Vassilieva, V.; Raynova, Y.; Doumanova, L.; Aljakov, M.; Idakieva, K., Radioprotective effect of *Rapana thomasiana* hemocyanin in gamma induced acute radiation syndrome. *Biotechnol Biotechnol Equip* 2014, 28, (3), 533-539.
10. Suryavanshi, S.; Sharma, D.; Checker, R.; Thoh, M.; Gota, V.; Sandur, S. K.; Sainis, K. B., Amelioration of radiation-induced hematopoietic syndrome by an antioxidant chlorophyllin through increased stem cell activity and modulation of hematopoiesis. *Free Radic Biol Med* 2015, 85, 56-70.
11. Lu, L.; Wang, Y. Y.; Zhang, J. L.; Li, D. G.; Meng, A. M., p38 MAPK inhibitor insufficiently attenuates HSC senescence administered long-term after 6 Gy total body

- 
- irradiation in mice. *Int J Mol Sci* 2016, 17, (6).
12. Li, D.; Tian, Z.; Tang, W.; Zhang, J.; Lu, L.; Sun, Z.; Zhou, Z.; Fan, F., The protective effects of 5-methoxytryptamine-alpha-lipoic acid on ionizing radiation-induced hematopoietic injury. *Int J Mol Sci* 2016, 17, (6).
  13. Li, J.; Xu, J.; Xu, W.; Qi, Y.; Lu, Y.; Qiu, L.; Hu, Z.; Chu, Z.; Chai, Y.; Zhang, J., Protective effects of Hong Shan capsule against lethal total-body irradiation-induced damage in Wistar rats. *Int J Mol Sci* 2015, 16, (8), 18938-55.
  14. Eng-Yen Huang, F.-S. W., Yu-Min Chen, Yi-Fan Chen, Chung-Chi Wang, I-Hui Lin, Yu-Jie Huang, Kuender D. Yang, Amifostine alleviates radiation-induced lethal small bowel damage via promotion of 14-3-3 $\sigma$ -mediated nuclear p53 accumulation. *Oncotarget* 2014, 5, (20), 9756-9769.
  15. Huang, E. Y.; Wang, F. S.; Lin, I. H.; Yang, K. D., Aminoguanidine alleviates radiation-induced small-bowel damage through its antioxidant effect. *Int J Radiat Oncol Biol Phys* 2009, 74, (1), 237-44.
  16. Luka Milas, N. H., Betty O. Reid, and Howard D. Thames, Jr., Protective effects of s-2-(3-Aminopropylamino)ethylphosphorothioic acid against radiation damage of normal tissues and a fibrosarcoma in mice. *Cancer Res* 1982, 42, 1888-1897.
  17. Anita J. Merritt, C. S. P., Christopher J. Kemp, John A. Hickman, Allan Balmain, David P. Lane, and Peter A. Hall, The Role of p53 in spontaneous and radiation-induced apoptosis in the gastrointestinal tract of normal and p53-deficient mice. *Cancer Res* 1994, 54, 614-617.
  18. Gorski, A.; Jonczyk-Matysiak, E.; Lusiak-Szelachowska, M.; Miedzybrodzki, R.; Weber-Dabrowska, B.; Borysowski, J., Bacteriophages targeting intestinal epithelial cells: a potential novel form of immunotherapy. *Cell Mol Life Sci* 2018, 75, (4), 589-595.
  19. Metcalfe, C.; Kljavin, N. M.; Ybarra, R.; de Sauvage, F. J., Lgr5+ stem cells are indispensable for radiation-induced intestinal regeneration. *Cell Stem Cell* 2014, 14, (2), 149-59.
  20. Hugenholtz, F.; de Vos, W. M., Mouse models for human intestinal microbiota

- 
- research: a critical evaluation. *Cell Mol Life Sci* 2018, 75, (1), 149-160.
21. Suzuki, T., Regulation of intestinal epithelial permeability by tight junctions. *Cell Mol Life Sci* 2013, 70, (4), 631-59.
  22. Barker, N.; van Es, J. H.; Kuipers, J.; Kujala, P.; van den Born, M.; Cozijnsen, M.; Haegbarth, A.; Korving, J.; Begthel, H.; Peters, P. J.; Clevers, H., Identification of stem cells in small intestine and colon by marker gene Lgr5. *Nature* 2007, 449, (7165), 1003-7.
  23. Stzpourginski, I.; Nigro, G.; Jacob, J. M.; Dulauroy, S.; Sansonetti, P. J.; Eberl, G.; Peduto, L., CD34+ mesenchymal cells are a major component of the intestinal stem cells niche at homeostasis and after injury. *Proc Natl Acad Sci U S A* 2017, 114, (4), E506-E513.
  24. Grant, C. P. a. H., The relationship between ionizing radiation-induced apoptosis and stem cells in the small and large intestine. *Brit J Cancer* 1998, 78, (8), 993-1003.
  25. Sato, T.; Clevers, H., Growing self-organizing mini-guts from a single intestinal stem cell: mechanism and applications. *Science* 2013, 340, (6137), 1190-4.
  26. Sato, T.; Vries, R. G.; Snippert, H. J.; van de Wetering, M.; Barker, N.; Stange, D. E.; van Es, J. H.; Abo, A.; Kujala, P.; Peters, P. J.; Clevers, H., Single Lgr5 stem cells build crypt-villus structures in vitro without a mesenchymal niche. *Nature* 2009, 459, (7244), 262-5.
  27. Zhang, H.; Yan, H.; Zhou, X.; Wang, H.; Yang, Y.; Zhang, J.; Wang, H., The protective effects of Resveratrol against radiation-induced intestinal injury. *BMC Complement Altern Med* 2017, 17, (1), 410.
  28. David G. Kirsch, P. M. S., Emmanuelle di Tomaso, Julie M. Sullivan, Wu-Shiun Hou, Talya Dayton, Laura B. Jeffords, Pooja Sodha, Kim L. Mercer, Rhianna Cohen, Osamu Takeuchi, Stanley J. Korsmeyer, Roderick T. Bronson, Carla F. Kim, Kevin M. Haigis, Rakesh K. Jain, Tyler Jacks, p53 controls radiation-induced gastrointestinal syndrome in mice independent of apoptosis. *Science* 2010, 327, 593-596.
  29. Morita, A.; Takahashi, I.; Sasatani, M.; Aoki, S.; Wang, B.; Ariyasu, S.; Tanaka, K.; Yamaguchi, T.; Sawa, A.; Nishi, Y.; Teraoka, T.; Ujita, S.; Kawate, Y.; Yanagawa, C.;

- 
- Tanimoto, K.; Enomoto, A.; Neno, M.; Kamiya, K.; Nagata, Y.; Hosoi, Y.; Inaba, T., A chemical modulator of p53 transactivation that acts as a radioprotective agonist. *Mol Cancer Ther* 2018, 17, (2), 432-442.
30. McIlwain, D. R.; Berger, T.; Mak, T. W., Caspase functions in cell death and disease. *Cold Spring Harb Perspect Biol* 2013, 5, (4), a008656.
31. Shiloh, Y., ATM and related protein kinases: safeguarding genome integrity. *Nat Rev Cancer* 2003, 3, (3), 155-68.
32. Han, X.; Mann, E.; Gilbert, S.; Guan, Y.; Steinbrecher, K. A.; Montrose, M. H.; Cohen, M. B., Loss of guanylyl cyclase C (GCC) signaling leads to dysfunctional intestinal barrier. *PLoS One* 2011, 6, (1), e16139.
33. Sun, X.; Wang, Q.; Wang, Y.; Du, L.; Xu, C.; Liu, Q., Brusatol enhances the radiosensitivity of A549 cells by promoting ROS production and enhancing DNA damage. *Int J Mol Sci* 2016, 17, (7).
34. Sullivan, J. M.; Jeffords, L. B.; Lee, C. L.; Rodrigues, R.; Ma, Y.; Kirsch, D. G., p21 protects "Super p53" mice from the radiation-induced gastrointestinal syndrome. *Radiat Res* 2012, 177, (3), 307-10.
35. Leibowitz, B. J.; Qiu, W.; Liu, H.; Cheng, T.; Zhang, L.; Yu, J., Uncoupling p53 functions in radiation-induced intestinal damage via PUMA and p21. *Mol Cancer Res* 2011, 9, (5), 616-25.
36. Paul H. Kussie, S. G., Vincent Marechal, Brian Elenbaas, Jacques Moreau, Arnold J. Levine, Nikola P. Pavletich, Structure of the MDM2 oncoprotein bound to the p53 tumor suppressor transactivation domain. *Science* 1996, 274, 948-953.
37. Qiu, W.; Carson-Walter, E. B.; Liu, H.; Epperly, M.; Greenberger, J. S.; Zambetti, G. P.; Zhang, L.; Yu, J., PUMA regulates intestinal progenitor cell radiosensitivity and gastrointestinal syndrome. *Cell Stem Cell* 2008, 2, (6), 576-83.
38. Foster, S. S.; De, S.; Johnson, L. K.; Petrini, J. H.; Stracker, T. H., Cell cycle- and DNA repair pathway-specific effects of apoptosis on tumor suppression. *Proc Natl Acad Sci U S A* 2012, 109, (25), 9953-8.
39. John R. Jeffers, E. P., Youngsoo Lee, Chunying Yang, JinLing Wang, Jennifer

- 
- Brennan, Kirsteen H. MacLean, Jiawen Han, Thomas Chittenden, James N. Ihle, Peter J. McKinnon, John L. Cleveland, and Gerard P. Zambetti, Puma is an essential mediator of p53-dependent and -independent apoptotic pathways. *Cancer cell* 2003, 4, 321-328.
40. Garcia-Barros, M.; Paris, F.; Cordon-Cardo, C.; Lyden, D.; Rafii, S.; Haimovitz-Friedman, A.; Fuks, Z.; Kolesnick, R., Tumor response to radiotherapy regulated by endothelial cell apoptosis. *Science* 2003, 300, (5622), 1155-9.
41. Anita J Merritt, T. D. A., Christopher S Potten and John A Hickman, Apoptosis in small intestinal epithelia from p53-null mice: evidence for a delayed, p53-independent G2/M-associated cell death after  $\gamma$ -irradiation. *Oncogene* 1997, 14, 2759-2766.

---

**7. CHAPTER 7: PROTECTIVE EFFECT OF HL-008 AGAINST  
H<sub>2</sub>O<sub>2</sub> AND BETA-AMYLOID-INDUCED NEUROTOXICITY**

---

## 7.1 Abstract

Neurodegenerative diseases, including Alzheimer's and Parkinson's disease, are becoming more prevalent globally, correlating with the ageing population of many countries. Dementia is responsible for the greatest social and economic burden of neurodegenerative diseases, with Alzheimer's representing approximately 60-70% of dementia cases. Currently, there is no effective treatment for ageing-related neurodegenerative diseases. Hence, the development of new treatments for neurodegenerative diseases is urgently required.

Oxidative stress plays an important role in the common pathophysiology of neurodegenerative diseases. It has been reported that antioxidants that suppress lipid peroxidation can protect neurons against amyloid- $\beta$ -induced apoptosis. Previously, we synthesized a novel compound, designated as HL-008, which has been demonstrated to have anti-oxidant effect in *in vivo* studies. Therefore, this compound is predicted to have neuroprotective effects.

In this research, the neuroprotective effect of this novel synthesized compound was investigated *in vitro* using MTT assays for determining the cytotoxicity to neuronal cells and the protective effect against  $H_2O_2$ -induced cytotoxicity. The results demonstrated that HL-008 showed no toxicity to PC-12 cells at the tested concentrations and protected PC-12 cells against  $H_2O_2$ -induced cytotoxicity. Moreover, the protective effect against amyloid beta 1-42 ( $A\beta_{1-42}$ )-induced loss of cell viability was investigated by MTT assays. The results showed that pretreatment with HL-008 could increase cell viability upon exposure to  $A\beta_{1-42}$ . Furthermore, neurite outgrowth of PC-12 cells incubated with HL-008 was determined. The neurite outgrowth rate of the control group was only 2.3%, while it was 16.4% in the nerve growth factor (NGF)-induced positive control group. HL-008, at all concentrations investigated, enhanced neurite outgrowth in a dose-dependent manner. Compared to the control group, the neurite outgrowth rate was significantly increased from 9.57% at the lowest concentration of 50  $\mu$ M to 17.31% ( $p < 0.001$ ) at the highest concentration of 200  $\mu$ M. In conclusion, HL-008 is a promising compound for neuroprotection, such as neurodegenerative disease. This study provided the basis of further investigations on the mechanism of neuroprotection.

---

## 7.2 Introduction

Neurodegenerative diseases, such as Alzheimer's disease (AD) and Parkinson's disease (PD), have been prevalent and are among the leading causes of disability worldwide due to the global aging population problem [1]. Neurodegenerative diseases occur when neurons in the brain or peripheral nervous system lose function with age and ultimately die. In 2016, an estimated 5.4 million people were living with AD in the United States. It is predicted that 1.2 million Americans will be living with PD by 2030 [2]. Dementia is responsible for the greatest social and economic burden of neurodegenerative diseases, with AD representing approximately 60-70% of dementia cases. The most common neuropathologies are accumulation of amyloid-beta, aggregation of hyperphosphorylated tau, and neuroinflammation [3].

One of the major neuropathological hallmarks of AD is the accumulation of extracellular neurotoxic amyloid-beta peptide such as  $A\beta_{1-42}$  in the brain [4]. Considerable evidence points to soluble amyloid- $\beta$  oligomers as a strong neurotoxin, inducing neuronal damage and apoptosis, especially early on AD pathogenesis. Apoptosis induced by intracellular  $A\beta$  peptide and its aggregates contributed to the pathogenesis or progression of AD [5]. Pretreating  $A\beta$ -induced neurotoxicity is a potential therapeutic approach to ameliorate the progression and development of AD [6]. Accumulative evidence indicated that misfolded amyloid-beta induced oxidative stress, occurring within the lipid bilayer.  $A\beta$  inserts as oligomers into the bilayer and serves as a source of ROS. Oxidative stress occurs at early stages, prior to the appearance of amyloid plaques and neurofibrillary tangles. Excessive reactive oxidative species (ROS) production could trigger lipid peroxidation, leading to neuronal apoptosis in neurodegenerative disorders, causing neuronal death [7]. In addition to misfolded amyloid-beta, oligomeric  $\alpha$ -synuclein, tau and huntingtin also induce the production of ROS.

Though efforts to develop evidence-based treatment strategies for neurodegenerative disease are ongoing, neither highly effective treatments nor potent protective approaches have yet been identified [3, 8]. Current therapeutic strategies of merely targeted a small

---

subset of the population and focused on reducing symptoms only, unable to alter disease progression [9]. Hence, the development of therapeutic approaches for neurodegenerative disease is urgent. Antioxidant and ROS scavengers are promising candidates for managing neurodegenerative disease. Previously, we developed a new aminothiols compound, designated as HL-008, demonstrating prominent protective effects of ROS-mediated brain damage. For this study, the aims were to investigate the neuroprotective effect of HL-008 *in vitro*.

Rat pheochromocytoma cells (PC-12 cell) are a useful *in vitro* model of neuroprotection and neuronal differentiation. Nerve growth factor (NGF) is the classic inducer of neuronal differentiation, and is associated with neuronal growth and maintenance. Exposure to NGF results in PC12 cells to differentiate into sympathetic neuron-like cells that exhibit increased neurite outgrowth [10].

### **7.3 Materials and methods**

#### **7.3.1 Chemicals and medium**

3-(4,5-dimethylthiazol-2-yl)-2,5-diphenyltetrazolium bromide (MTT) (Sigma Lot# M5665-5G), 30% hydrogen peroxide (H<sub>2</sub>O<sub>2</sub>) (Sigma-Aldrich, catalogue# 216763-100mL, Lot# MKCD0825), and Roswell Park Memorial Institute medium 1640 (RPMI 1640) were purchased from Sigma-Aldrich (USA). Foetal bovine serum (FBS) was purchased from Scientifix Pty Ltd (France). Trypsin-EDTA (100x), PBS (100x) (Lot# SLBW5570), Penicillin-Streptomycin (10000U-10mg/mL) was purchased from Sigma-Aldrich. Mouse NGF 2.5S (99%) (Catalogue# N-240, Lot# N240NF1710) was purchased from Alomne Labs (Israel). Non-fibrillar A $\beta$ <sub>1-42</sub> (Cat# 1067-2, Lot# 081613427) was purchased from rPeptide (USA).

HL-008 solutions used were prepared in 1x PBS to obtain clear solutions at different concentrations. 20% sodium dodecyl sulfate (SDS) in 0.02 M HCl was prepared by adding 40 g of SDS to 200 mL of 0.02 M HCl. Non-fibrillar A $\beta$ <sub>1-42</sub> was first dissolved in DMSO to yield a protein concentration of 3.8 mM, and was then diluted with sterile PBS to obtain a final concentration of 100  $\mu$ M. A $\beta$ <sub>1-42</sub> was then aliquoted and frozen at -80 °C until use [11].

---

### 7.3.2 Cell culture and treatment

Rat pheochromocytoma PC-12 cells, displaying a semi-differentiated phenotype with neuronal projections, were used as model neuronal cells and maintained in RPMI1640 medium supplemented with 10% FBS, 1% MEM Non-essential Amino Acids (100x), and Penicillin (100 U/mL), Streptomycin (100 µg/mL) at 37°C in a humidified 95% air/5% CO<sub>2</sub> incubator, and cell culture media was changed every other day. Human embryonic kidney 293 (HEK293) cells were also used for the evaluation of cytotoxicity of HL-008. HEK293 cells were maintained in DMEM cell culture medium supplemented with 10% FBS, Penicillin (100 U/mL), and Streptomycin (100 µg/mL). The cells were plated into 96-well plates at an appropriate density and allowed to adhere for 24 h at 37°C in complete cell culture medium.

### 7.3.3 Cell viability assay

Cell viability was determined by measuring formazan produced by the reduction of MTT by cellular oxidoreductase enzymes in live cells. Cells were seeded at  $1 \times 10^4$  cells per well in 96-well plates and incubated for 24 h to allow adherence. PBS was used to dissolve HL-008 and then diluted to the final stock concentrations prior to addition to the cells. PC-12 or HEK293 cells were treated with serially diluted HL-008 solutions and then incubated for 48 h at 37 °C. After that, the cell culture media were replaced by 100 µL of 0.5mg/mL MTT and incubated for 4 h. Finally, 80 µL of 20% SDS in 0.02 M HCl was added, and the plate was incubated for 18 h [12]. The absorbance of the plate was measured at 570nm using a Microplate reader (GloMax Explorer, Promega Instrument, Madison, USA).

### 7.3.4 MTT assay for determining protection of PC-12 cells against H<sub>2</sub>O<sub>2</sub> cytotoxicity

PC-12 cells were seeded at  $1 \times 10^4$  cells per well and incubate 24 h to allow adherence. PBS was used to dissolve and dilute HL-008 to their final concentrations. Cells were incubated with HL-008 for 15 min prior to the addition of H<sub>2</sub>O<sub>2</sub> at different concentrations (100 µM, 150 µM and 200 µM), followed by incubation at 37°C for 24 h. Thereafter, the medium was replaced with 0.5 mg/mL of MTT, and incubated at 37°C for 4 h. Finally, 80 µL of 20% SDS in 0.02 M HCl was added, and the plate was incubated for 18 h. The absorbance of the plate was measured at 570 nm on a microplate reader.

---

### **7.3.5 MTT assay for determining protection of PC-12 cells against A $\beta$ <sub>1-42</sub> cytotoxicity**

PC-12 cells were seeded at a cell density of  $1 \times 10^4$  cells per well and incubated overnight to allow adherence. PBS was used to dissolve and dilute HL-008 to final concentrations ranging from 1  $\mu$ M to 100  $\mu$ M. Cells were pretreated with HL-008 for 15 min prior to the addition of A $\beta$ <sub>1-42</sub> at a final concentration of 1  $\mu$ M, followed by incubation at 37°C for 48 h. Thereafter, media were replaced with 0.5 mg/mL of MTT, and incubated at 37°C for 4 h. Finally, 80  $\mu$ L of 20% SDS in 0.02 M HCl was added, and the plate was incubated for 18 h [12]. The absorbance of the plate was measured at 570 nm on a microplate reader.

### **7.3.6 Neurite outgrowth assay**

PC-12 cells, seeded in 6-well plates at a density of  $8 \times 10^4$  cells/well, were incubated overnight at 37 °C. Thereafter, cells were treated with HL-008 at final concentrations ranging from 50  $\mu$ M to 200  $\mu$ M for 24 h. PBS and 50 ng/mL of NGF were used as negative and positive controls, respectively. Subsequently, cells were visualized using an inverted microscope (Nikon ECLIPSE Ts2R) and images were taken from at least six random fields and analysed using ImageJ software. Neurite outgrowth was counted as positive when the measured length of the neurite was equal or longer than the size of cells, and the amount of neurite outgrowth was calculated from at least 300 cells per treatment. Neurite outgrowth % was calculated as number of cells positive for neurite (regardless of number of neuritis per cell) / total number of cells.

### **7.3.7 Statistical analysis**

All results were based on at least three independent experiments (n=3). All data are expressed as mean  $\pm$  SD. Statistical comparisons were performed by one way analysis of variance (ANOVA), followed by Turkey's multiple comparison. Data were normally distributed (Shapiro-Wilks test;  $p > 0.05$ ) and variances were homogeneous (Levene test,  $p > 0.05$ ) (IBM SPSS statistic 26, IBM, Chicago, USA). A  $p$ -value of  $< 0.05$  was considered statistically significant.

## 7.4 Results and discussion

### 7.4.1 HL-008 shows no cytotoxicity to PC-12 and HEK293 cells

In order to evaluate potential neurotoxicity of HL-008, MTT assays with semi-differentiated PC-12 cells were carried out. HEK293 cells, human embryonic kidney cells, were used as normal cell controls in MTT assays. MTT is widely used for the quantification of cell viability, since viable cell with active metabolism converts MTT into a purple colored formazan product with an absorbance maximum near 570 nm, a reaction that does not occur in dead cells.

HL-008 at a range of concentrations of up to 400  $\mu\text{M}$  did not show any statistically significant cytotoxicity to either PC-12 or HEK293 cells over 48 h, with cell viability typically being >90%, compared to the PBS control group ( $p < 0.05$ ) (Figure 7-1 A and Figure 7-1 B). These results showed that HL-008 at concentrations up to 400  $\mu\text{M}$  is not toxic to PC-12 or HEK293 cells.

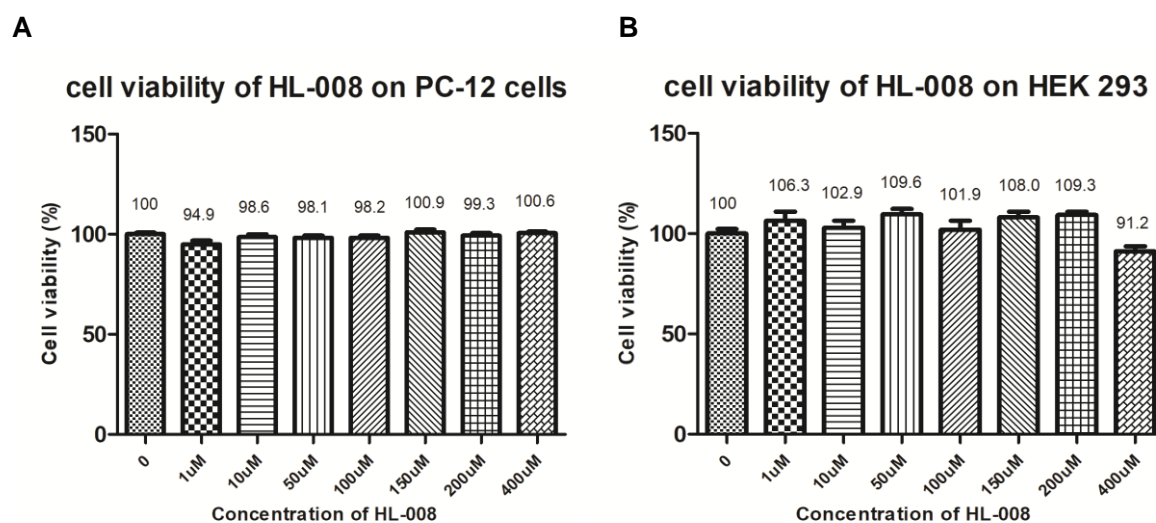


**Figure 7-1 Relative cell viability (%) of PC-12 cells and HEK293 cells determined by MTT assay following 48 h treatment with increasing concentrations of HL-008.** A. The viability of PC-12 cells after HL-008 treatment. B. The viability of HEK293 cells after HL-008 treatment.

### 7.4.2 Neuroprotection of HL-008 against $\text{H}_2\text{O}_2$ -induced cytotoxicity

Oxidative stress plays a critical role in pathogenesis of neurodegenerative disease. Metal-ions bound to the amyloid- $\beta$  ( $\text{A}\beta$ ) lead to production of Reactive Oxygen Species (ROS), such as hydroxyl radicals which are the most reactive ROS, resulting in the oxidative damage of surrounding molecules [13]. Ischemia/Reperfusion has been shown to induce generation of

---

large amounts of H<sub>2</sub>O<sub>2</sub>, one of the most common ROS, causing oxidative stress and cellular damage [14].

The neuroprotective activity of HL-008 against H<sub>2</sub>O<sub>2</sub> was evaluated using PC-12 cells. 100 μM, 150 μM, 200 μM H<sub>2</sub>O<sub>2</sub> reduced cell viability of PC-12 cells to about 47%, 38%, and 35% respectively, consistent with previously reported results [15]. Pretreatment of cells with HL-008 dramatically increased cell viability in a concentration-dependent manner (up to 100%) for all tested concentrations of H<sub>2</sub>O<sub>2</sub> (Figure 7-2). Hydrogen peroxide at 100 μM decreased the cell viability to 46.6% when cells were treated for 24 h, while pretreating cells with HL-008 at concentrations from 100 μM to 400 μM dramatically reduced H<sub>2</sub>O<sub>2</sub> cell cytotoxicity ( $p < 0.01$  or  $p < 0.001$ ) (Figure 7-2 A). Likewise, H<sub>2</sub>O<sub>2</sub> at 150 μM decreased the cell viability of PC-12 to approximately 38%, while pretreating cells with HL-008 at the concentrations from 1 μM to 400 μM increased cell viability from 39.4% to 104.6% in a concentration-dependent manner, significantly at concentrations from 150 μM to 400 μM HL-008 ( $p < 0.001$ ) (Figure 7-2 B). Similarly, H<sub>2</sub>O<sub>2</sub> at 200 μM decreased the cell viability to about 36%, while pretreating cells with HL-008 at concentrations from 200 μM to 400 μM increased cell viability to 68% and 99.5%, respectively, exhibiting significant neuroprotective effects ( $p < 0.001$ ) (Figure 7-2 C).

It is widely accepted that ROS is one of the indicators of oxidative stress associated with neurological diseases and neurodegenerative diseases. The above results indicated that HL-008 could be beneficial to combat ROS-related neuronal damage, likely attributable to ROS scavenger properties of HL-008.

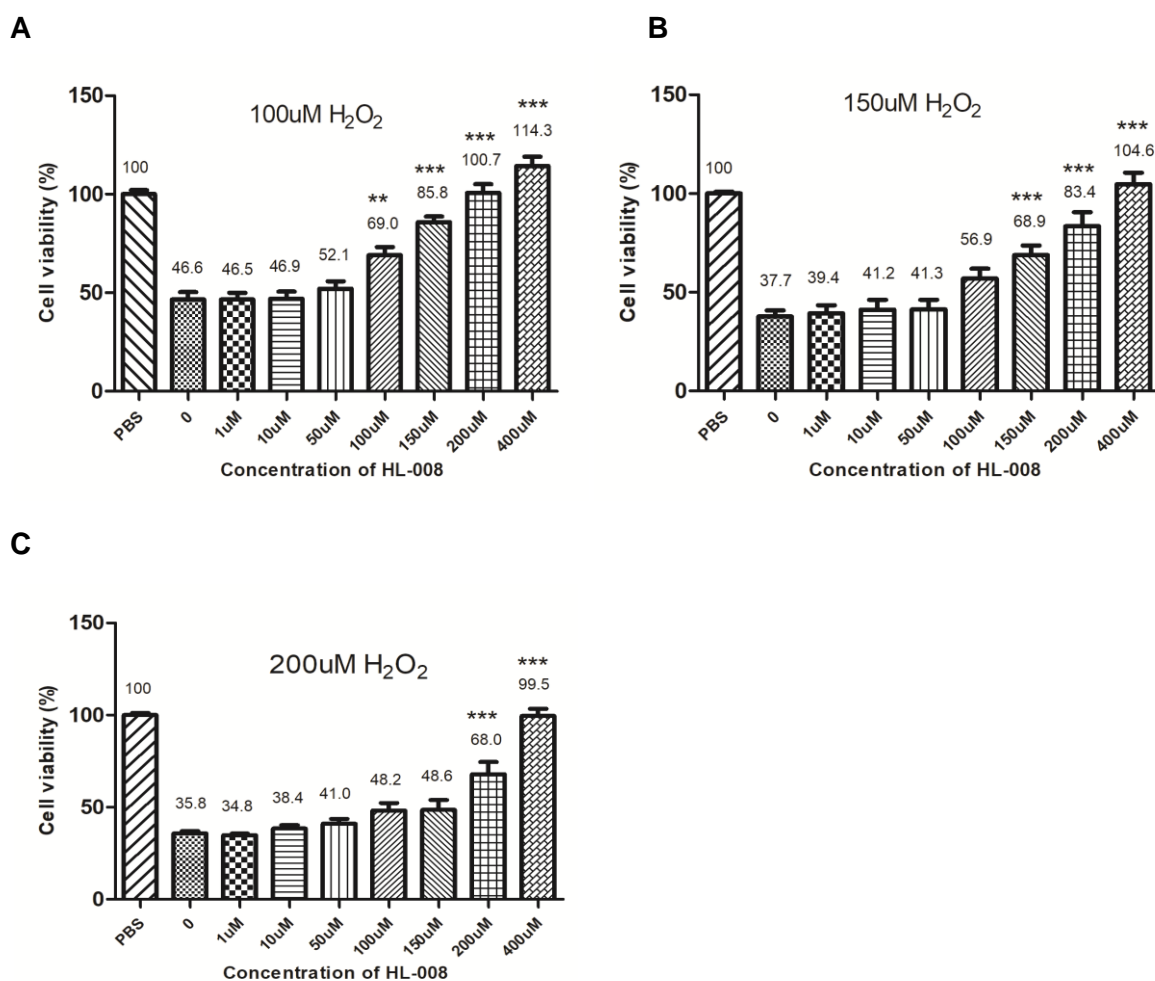


**Figure 7-2 Protective effects of HL-008 against H<sub>2</sub>O<sub>2</sub>-induced cytotoxicity in PC-12 cells.** A. Protective effects of HL-008 against 100 μM of H<sub>2</sub>O<sub>2</sub>. B. Protective effects of HL-008 against 150 μM of H<sub>2</sub>O<sub>2</sub>. C. Protective effects of HL-008 against 200 μM of H<sub>2</sub>O<sub>2</sub>.

### 7.4.3 Neuroprotection of HL-008 against Aβ<sub>1-42</sub>-induced cytotoxicity

One of the most important neuropathology of neurodegenerative disease is the aggregation of β-amyloid which can directly induce neuronal cell death. In this study, the protective effect of HL-008 against Aβ<sub>1-42</sub>-induced loss of PC-12 cell viability was investigated. Treatment with non-fibrillar Aβ<sub>1-42</sub> at a concentration of 1 μM [15] was chosen for cytotoxicity studies in PC-12 cells, as ~40% cell death was observed. Treating cells with HL-008 at all concentrations resulted in reduced cytotoxicity. Compared to untreated controls, HL-008 at the concentrations equal to or higher than 10 μM significantly reduced cytotoxicity induced by Aβ<sub>1-42</sub> to about 20% ( $p < 0.05$ ) (Figure 7-3). This study demonstrated that HL-008 could confer protective effects from Aβ<sub>1-42</sub> damage to PC-12 cells. However, the protective effect of HL-008

against H<sub>2</sub>O<sub>2</sub>-induced cytotoxicity was stronger than that against A $\beta$ <sub>1-42</sub>-treated PC-12 cells. One possible explanation to this difference is that A $\beta$ <sub>1-42</sub> induces cytotoxicity partially by ROS generation, and partially by other pathways, such as apoptotic or inflammatory pathway. A $\beta$  was demonstrated previously to induce neuronal apoptosis and cause the activation of inflammatory responses [16-18].

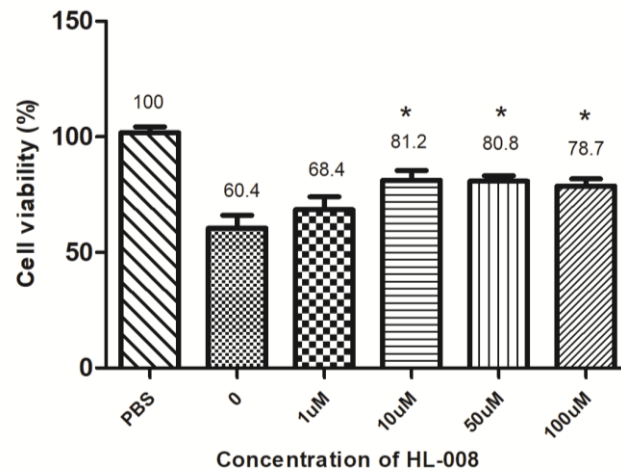


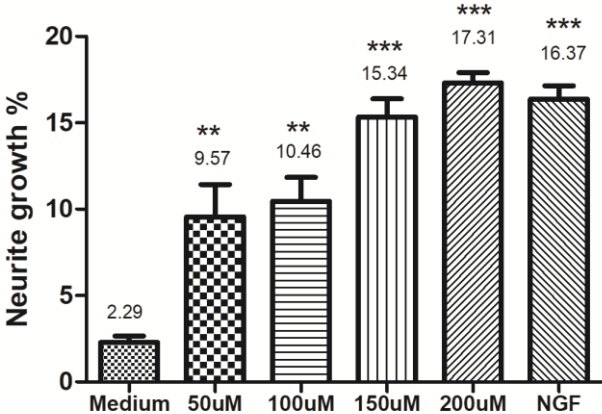
**Figure 7-3 Neuroprotection activity of HL-008 against A $\beta$ <sub>1-42</sub> (1  $\mu$ M) induced cytotoxicity measured by MTT assay following 48 h treatment.** Each value is the mean  $\pm$  SEM of three independent experiments (\* $p$ <0.05 versus control 1  $\mu$ M A $\beta$ <sub>1-42</sub>).

#### 7.4.4 HL-008 enhances neurite outgrowth

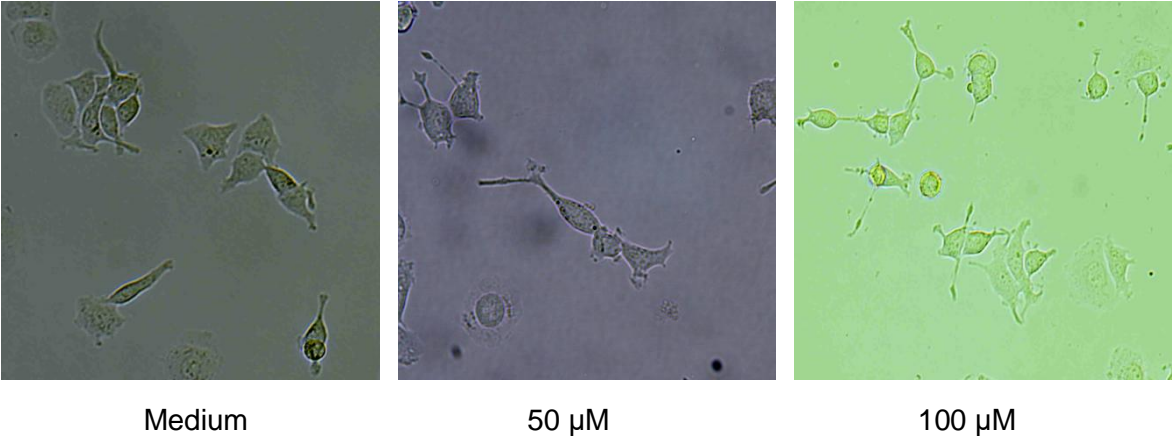
Neurite outgrowth plays a vital role in maintaining neuronal communication through the formation of specific synaptic contacts with spatial accuracy [19]. Hence, enhancing neurite growth is a potential strategy in treating neurodegenerative disease, as well as recovering from brain repair after stroke. This study investigated whether HL-008 can enhance neurite growth in PC-12 cells. Results showed that only about 2.3% of neurite outgrowth occurred in the culture medium control group, whereas in the NGF-treated positive control group rates of 16.4% were observed. HL-008, at all concentration investigated, enhanced neurite outgrowth in a dose-dependent manner (Figure 7-4). Compared to the culture medium control group, neurite outgrowth rates were significantly increased from 9.57% at the lowest concentration of 50  $\mu$ M to 17.31% ( $p$ <0.001) at the highest concentration of 200  $\mu$ M. Neuritogenic activity is important for the maintenance and regeneration of the neuronal communications network [20].

Neurite outgrowth occurs during nerve regeneration. Although the peripheral nervous system is capable of regeneration, the central nervous system has a limited capacity to regenerate after injury [21]. This study showed that HL-008 could potentially contribute to nerve regeneration, important for restoration of function after neuron injury. However, further work is needed to validate this effect and to understand its action mechanism.

**A.**



**B**



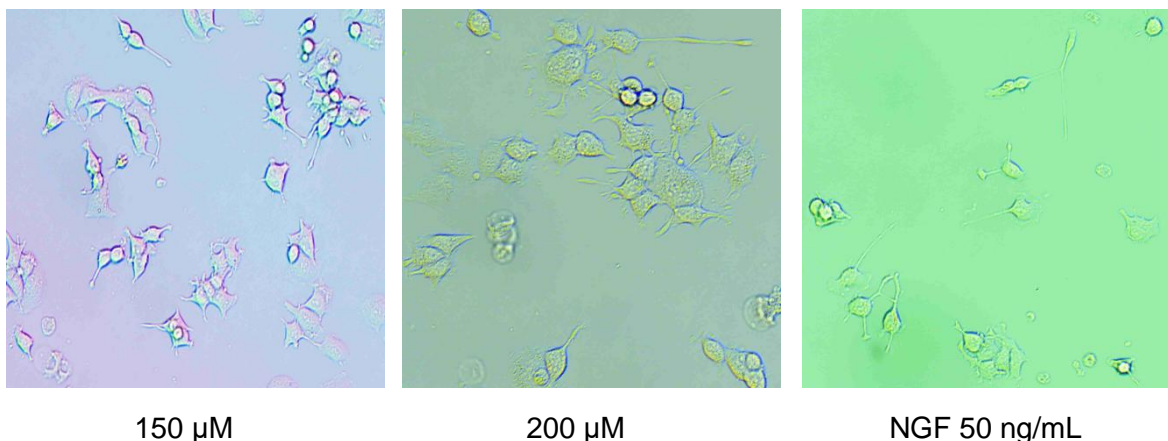


**Figure 7-4 Effect of different concentrations of HL-008 on neurite outgrowth in PC-12 cell.** A. Neurite outgrowth rate of HL-008 at different concentration, negative control, 50 ng/mL of NGF in PC-12 cells. B. Representative light micrographs of PC-12 cells. At least 300 cells were counted for every treatment. Each value is the mean  $\pm$  SEM of 4 independent experiments (\*\* $p < 0.01$  and \*\*\* $p < 0.001$  versus control media).

## 7.5 Conclusion

ROS, induced by  $A\beta$ , plays an important role in neurodegenerative diseases. This study demonstrated protective effects of HL-008 after  $H_2O_2$  or  $A\beta_{1-42}$ -induced damage to PC-12 cells and positive effects on neurite regeneration. MTT assays showed that there was no cytotoxicity of HL-008 to PC-12 cells and non-neurone cells (HEK293) up to 400  $\mu$ M. This aminothiols compound decreased cytotoxicity induced by  $H_2O_2$  in PC-12 cells in a concentration-dependent manner, reaching complete inhibition of the cell cytotoxicity induced by  $H_2O_2$  and exhibited significantly neuroprotective effects. Moreover, HL-008 significantly protected PC-12 cells against  $A\beta_{1-42}$ -induced cytotoxicity. Furthermore, HL-008 could enhance the neurite outgrowth of PC-12 cells.

These findings indicated that the aminothiols compound HL-008 is a promising compound for neuroprotection, such as neurodegenerative disease. This study provided the basis of further investigation on the mechanism of neuroprotection.

---

## 7.6 References

1. Castillo, X.; Castro-Obregon, S.; Gutierrez-Becker, B.; Gutierrez-Ospina, G.; Karalis, N.; Khalil, A. A.; Lopez-Noguerola, J. S.; Rodriguez, L. L.; Martinez-Martinez, E.; Perez-Cruz, C.; Perez-Velazquez, J.; Pina, A. L.; Rubio, K.; Garcia, H. P. S.; Syeda, T.; Vanoye-Carlo, A.; Villringer, A.; Winek, K.; Zille, M., Re-thinking the Etiological Framework of Neurodegeneration. *Front Neurosci* 2019, 13, 728.
2. Sciences, National Institute of Environmental Health Sciences. <https://www.niehs.nih.gov/research/supported/health/neurodegenerative/index.cfm>.
3. Hou, Y.; Dan, X.; Babbar, M.; Wei, Y.; Hasselbalch, S. G.; Croteau, D. L.; Bohr, V. A., Ageing as a risk factor for neurodegenerative disease. *Nat Rev Neurol* 2019, 15, (10), 565-581.
4. Kwakowsky, A.; Potapov, K.; Kim, S.; Peppercorn, K.; Tate, W. P.; Abraham, I. M., Treatment of beta amyloid 1-42 (A $\beta$ (1-42))-induced basal forebrain cholinergic damage by a non-classical estrogen signaling activator in vivo. *Sci Rep* 2016, 6, 21101.
5. Pereira C., Ferreiro E., Cardoso S. M., Oliveira C. R., Cell degeneration induced by Amyloid- $\beta$  peptides. *J Mol Neurosci* 2003, 23, 97-104.
6. Tong, Y.; Bai, L.; Gong, R.; Chuan, J.; Duan, X.; Zhu, Y., Shikonin protects PC12 cells against beta-amyloid peptide-induced cell injury through antioxidant and antiapoptotic activities. *Sci Rep* 2018, 8, (1), 26.
7. Butterfield, D. A.; Swomley, A. M.; Sultana, R., Amyloid beta-peptide (1-42)-induced oxidative stress in Alzheimer disease: importance in disease pathogenesis and progression. *Antioxid Redox Signal* 2013, 19, (8), 823-35.
8. Luo, F.; Sandhu, A. F.; Rungratanawanich, W.; Williams, G. E.; Akbar, M.; Zhou, S.; Song, B. J.; Wang, X., Melatonin and autophagy in aging-related neurodegenerative diseases. *Int J Mol Sci* 2020, 21, (19).
9. Hussain, R.; Zubair, H.; Pursell, S.; Shahab, M., Neurodegenerative diseases: Regenerative mechanisms and novel therapeutic approaches. *Brain Sci* 2018, 8, (9).
10. Terada, K.; Matsushima, Y.; Matsunaga, K.; Takata, J.; Karube, Y.; Ishige, A.; Chiba, K.,

- 
- The Kampo medicine Yokukansan (YKS) enhances nerve growth factor (NGF)-induced neurite outgrowth in PC12 cells. *Bosn J Basic Med Sci* 2018, 18, (3), 224-233.
11. Alghazwi, M.; Smid, S.; Zhang, W., In vitro protective activity of South Australian marine sponge and macroalgae extracts against amyloid beta (Abeta1-42) induced neurotoxicity in PC-12 cells. *Neurotoxicol Teratol* 2018, 68, 72-83.
  12. Young, F. M.; Phungtamdet, W.; Sanderson, B. J., Modification of MTT assay conditions to examine the cytotoxic effects of amitraz on the human lymphoblastoid cell line, WIL2NS. *Toxicol In Vitro* 2005, 19, (8), 1051-9.
  13. Cheignon, C.; Tomas, M.; Bonnefont-Rousselot, D.; Faller, P.; Hureau, C.; Collin, F., Oxidative stress and the amyloid beta peptide in Alzheimer's disease. *Redox Biol* 2018, 14, 450-464.
  14. Lee, D.; Park, S.; Bae, S.; Jeong, D.; Park, M.; Kang, C.; Yoo, W.; Samad, M. A.; Ke, Q.; Khang, G.; Kang, P. M., Hydrogen peroxide-activatable antioxidant prodrug as a targeted therapeutic agent for ischemia-reperfusion injury. *Sci Rep* 2015, 5, 16592.
  15. Alghazwi, M.; Smid, S.; Karpinić, S.; Zhang, W., Comparative study on neuroprotective activities of fucoidans from *Fucus vesiculosus* and *Undaria pinnatifida*. *Int J Biol Macromol* 2019, 122, 255-264.
  16. Morishima, Y.; Gotoh, Y.; Zieg, J.; Barrett, T.; et al.,  $\beta$ -Amyloid induces neuronal apoptosis via a mechanism that involves the c-Jun N-terminal kinase pathway and the induction of Fas ligand. *J Neurosci* 2001, 21(19), 7551-7560.
  17. Ransohoff, R. M.; How neuroinflammation contributes to neurodegeneration. *Science* 2016, 353 (6301), 777-783.
  18. Ghavami, S.; Shojaei, S.; Yeganeh, B.; et al., Autophagy and apoptosis dysfunction in neurodegenerative disorders, *Prog Neurobiol* 2014, 112, 24–49.
  19. Oyama, K.; Zeeb, V.; Kawamura, Y.; Arai, T.; Gotoh, M.; Itoh, H.; Itabashi, T.; Suzuki, M.; Ishiwata, S., Triggering of high-speed neurite outgrowth using an optical microheater. *Sci Rep* 2015, 5, 16611.
  20. Thoenen, H., Neurotrophins and neuronal plasticity. *Science* 1995, 270, (5236),

---

593-598.

21. Huebner, E. A.; Strittmatter, S. M., Axon regeneration in the peripheral and central nervous systems. *Results Probl Cell Differ* 2009, 48, 339-51.

---

## **8. CHAPTER 8: CONCLUSION AND FUTURE DIRECTIONS**

---

## 8.1 Conclusion and major findings

The RAS/RAF/MEK/ERK signalling pathway plays a key role in regulating cell proliferation and apoptosis. This pathway is deregulated in approximately one third of malignant tumors. Mutations in RAS/RAF occur in a large portion of malignancies and are associated with aggressive clinical behaviours and poor prognosis.

This research comprehensively reviewed the current development status of MEK inhibitors. Four FDA-approved MEK inhibitors were reviewed based on aspects of their molecular structures, enzyme activity, potency, *in vivo* efficacy, PK profiles, toxicity, clinical PK, as well as adverse reactions. Clinical studies on adverse effects were also reviewed, which concluded a promising future of MEK inhibitors in clinical anti-cancer research. Eleven MEK inhibitors have now entered phase I/II clinical studies.

The approved indications of approved MEK inhibitors are mainly about the treatment of BRAF mutant melanoma combined with BRAF inhibitors, such as: (1) trametinib combined with dabrafenib for the treatment of melanoma patients with BRAF<sup>V600E</sup> or <sup>V600K</sup> mutations; (2) combimetinib combined with vemurafenib for the treatment of unresectable or metastatic melanoma with a BRAF<sup>V600E</sup> or <sup>V600K</sup> mutations; (3) binimetinib and encorafenib in combination for unresectable or metastatic melanoma with BRAF<sup>V600E</sup> or <sup>V600K</sup> mutations. Different MEK inhibitors, possessing specific physico-chemical properties and bioactivity characteristics, may provide different options for patients seeking treatment for cancer.

After analyzing the molecular structures of existing MEK inhibitors, their efficacy and pharmacokinetic properties, AZD6244 was chosen as a lead compound due to its superior PK profiles. Based on the reported x-ray crystal structure of MEK kinase binding with MEK inhibitors, we proposed that a large substituent group on 3-nitrogen of AZD6244 resulted in a decrease in antitumor activity, which is associated with the unsatisfactory potency of AZD6244. Also the N-methyl in the benzoheterocyclic ring of AZD6244 was replaced with an O atom, and the –Cl and –Br substituent on the aniline were replaced with –F and –I, respectively. Consequently, a new compound, KZ-001, was designed which has a new core

---

structure, and is a benzoxazole derivative. The new compound KZ-001 was synthesized by consecutive 11-step reactions, purified and characterized.

Kinase inhibition against MEK1/2 was determined, and results showed nanomole scale of  $IC_{50}$ , with superior potency compared to AZD6244. KZ-001 was demonstrated to be a highly selective MEK1/2 inhibitor. KZ-001 potently inhibited cancer cell proliferation, with an  $IC_{50}$  of  $2.9 \pm 0.6$  nM –  $5.7 \pm 0.3$  nM against BRAF-mutant cancer cells and  $169.9 \pm 97.7$  nM against KRAS-mutant cancer cells. KZ-001 activity was 26- to 32- and over 17-fold higher compared to AZD6244 using the BRAF- and KRAS-mutant cancer cell lines, respectively. Similar results were obtained using *in vivo* xenograft model. KZ-001 inhibited the MAPK pathway like other known MEK inhibitors. ERK phosphorylation was completely inhibited by KZ-001 at concentration ranging from 5 nM to 625 nM. By using the FITC Annexin V apoptosis detection assay, KZ-001, at concentrations of both 10 nM and 10  $\mu$ M, induced cell apoptosis in Calu-6 and Colo-205, and induced a significant increase of the G1 phase, and caused cell cycle delay of A375 cells at G0/G1 phase.

The combination of KZ-001 and vemurafenib showed synergistic effects against BRAF mutant cell lines *in vitro*. The combination of KZ-001 and docetaxel showed synergistic effects against BRAF and KRAS mutant cell lines *in vitro*.

*In vivo*, the combination of KZ-001 and vemurafenib exhibited synergistic effects on the treatment of A375 and Colo-205 tumor xenografts. In addition, combination treatment of KZ-001 with docetaxel resulted in synergistic effects on Calu-6 tumor xenografts *in vivo*. Among these, combination of KZ-001 with vemurafenib in treatment of A375 tumor xenografts showed the best synergistic synergy effects, with a Q value of 3.14.

Though much progress has been achieved in targeted therapy, approximately 50% of cancer patients receive radiation therapy during cancer treatment. Radiotherapy causes injury to normal tissues, and intestinal injury is the leading side effects since the small intestine is one of the most sensitive organs. Pharmacologically, radiation injury is mainly induced by reactive oxygen species (ROS) produced through the radiolysis of water in tissues. For that reason, a

---

series of radioprotectors to eliminate ROS were designed and synthesized. The natural anti-oxidation agent quercetin was chosen as a lead compound, and combined with aminothiols via different-length linkers. The thiol group was modified simultaneously in order to modulate PK properties. Based on this concept, five new compounds (XH-101, XH-102, XH-103, XH-105, HL-008) were designed which were expected to exert ROS scavenging function and mitigate radiation injury. These compounds were synthesized subsequently through a series of synthesis routes, and characterized by  $^1\text{H}$ NMR,  $^{13}\text{C}$ NMR and HRMS.

The beneficial effects of XH-105 for the protection against radiation-induced intestinal injury were investigated. Compared to vehicle-treated mice after total body irradiation (TBI), XH-105 treatment significantly enhanced survival rates under 7.5 Gy, 9.0 Gy, and 11.0 Gy TBI. XH-105 attenuated structural damage of the small intestine. XH-105-treated mice showed more survival crypts ( $p < 0.01$ ), more intact structure of villi and/or an increased villous height ( $p < 0.01$ ), as well as a significant increase in expression of enterocyte villi<sup>+</sup> compared to vehicle-treated mice. Furthermore, XH-105 decreased the rate of apoptosis, reduced DNA damage, maintained cell regeneration and promoted crypt proliferation and differentiation. XH-105 also reduced expression of Bax and p53 in the small intestine. These data suggest that XH-105 is beneficial for preventing radiation-induced intestinal injury by inhibiting the p53-dependent apoptotic signaling pathway.

Oxidative stress plays a central role in the common pathophysiology of neurodegenerative diseases. In Alzheimer's disease, the aggregation of A $\beta$  is thought to induce ROS. HL-008 is an aminothiol compound, and hence might be able to eliminate ROS in the cell microenvironment. In this study, HL-008 showed no toxicity to PC-12 cells and protected PC-12 cells against H<sub>2</sub>O<sub>2</sub>-induced cytotoxicity. Moreover, this study showed that pretreatment with HL-008 could increase cell viability following exposure to A $\beta_{1-42}$ . Furthermore, HL-008, at all concentrations investigated, enhanced neurite outgrowth in a dose-dependent manner.

In conclusion, in this study we designed and biologically evaluated a novel MEK inhibitor KZ-001 for the treatment of RAS/RAF mutant cancers, which was shown to be superior to the commercial drug AZD6244. In order to mitigate side effects of radiotherapy, we designed and

---

biologically evaluated a novel radioprotector XH-105 for the mitigation of radiation-induced intestinal injury during radiotherapy of cancer patients. Furthermore, the neurodegenerative protection of HL-008 was biologically evaluated, and this compound had significant protective effects against H<sub>2</sub>O<sub>2</sub> and beta-amyloid-induced neurotoxicity.

## **8.2 Future directions**

Although much progress in the area of RAS/RAF mutated cancer has been achieved, there are still many challenges for some subtypes of cancers. The key findings from this study indicate that KZ-001 is a promising MEK inhibitor to be applied in clinic. Future research can seek therapeutic treatments to drug-resistant and refractory cancers caused by MAPK signalling pathway aberration by using KZ-001. In this study, XH-105 and HL-008 demonstrated promising radioprotection and neuroprotection. In the future studies, more studies could focus on the action mechanism of their protective effects. Taken together, the KZ-001 plus HL-008 combination treatment could be further investigated to explore the radiosensitization capacity of KZ-001 *in vitro* and *in vivo*, whilst XH-105 exerting the capability to mitigate the side effect of radiotherapy.

### **8.2.1 Combination of KZ-001 with CDK4/6 inhibitors for the treatment of RAS mutant colorectal cancers.**

KRAS mutation is detected in about 50% of all colorectal cancers (CRC). KRAS mutated CRC contributed to resistance to monoclonal antibody cetuximab in KRAS wild type CRC, leading to relapse in patients [1]. This unmet clinical need highlights the urgent need to develop more efficient therapeutic approaches to target KRAS-mutated CRC [2]. Cyclin-dependent protein kinases (CDKs) are key mediators of cell cycle progression. CDK4 and CDK6 form active complexes with cyclin D1 and drive cell proliferation [3]. Lee et al. reported that combined inhibition of MEK and CDK4/6 inhibits tumor growth *in vivo* in KRAS mutant CRC cell line xenograft and patient-derived xenografts (PDX). The MEK inhibitor MEK162 combined with CDK4/6 inhibitor Palbociclib synergistically inhibited cancer growth *in vitro* and caused tumor regression in xenografts and PDX models [4]. Pek M. reported that the dual inhibition of CDK 4/6 and MEK led to a robust therapeutic response in KRAS-dependent and BRAF-mutant

---

CRC, both *in vitro* and *in vivo* [2]. A phase I/II clinical study (NCT02022982) showed that lower dosages of the CDK4/6 inhibitor Palbociclib could limit toxicity [2].

Above studies provided a rational basis for combining MEK inhibitor with CDK4/6 inhibitor to treat RAS mutant mCRC and melanoma. In Chapter 3, the effective MEK inhibition has been validated and it indicates that KZ-001 has a potential to be applied for the treatment of KRAS/BRAF mutant mCRC and NRAS-mutated melanomas in combination with CDK4/6 inhibitor.

### **8.2.2 Triple therapy (KZ-001 + BRAF inhibitors + EGFR inhibitors) for the treatment of BRAF mutant colorectal cancers**

Colorectal cancer (CRC) is the third most common cancer and the fourth main cause of cancer death worldwide [5]. BRAF<sup>V600E</sup> mutations are present in 10% of colorectal cancers, and patients have poor prognosis with a median overall survival of 4 to 6 months after failure of initial therapy. However, only 5% of BRAF<sup>V600</sup> mutant colorectal cancers respond to BRAF inhibitors due to adaptive feedback reactivation of MAPK signalling mediated by EGFR. Corcoran et al. demonstrated that combined BRAF, EGFR, and MEK inhibition (Triplet-therapy) has a promising efficacy in BRAF<sup>V600</sup> mutant colorectal cancer. Their findings also highlighted that the MAPK pathway is a critical target in BRAF<sup>V600E</sup> colorectal cancer and optimizing strategies are needed to blocking this pathway to overcome both primary and acquired resistance [6]. A phase III study showed that the triplet-therapy (encorafenib + cetuximab + binimetinib) resulted in enhanced activity with a confirmed response rate 26% (*versus* 2% in control group) and longer survival with median overall survival 9.0 months (*versus* 5.4 months in the control group) [7]. Nonetheless, identification of new drugs for the treatment of BRAF<sup>V600E</sup> mutant mCRC remains a key issue [8]. However, the challenge of combination therapy is the possibility of non-tolerance caused by triplet-regimen toxicities. A MEK inhibitor with high potency but low toxicity is needed to overcome this issue.

As demonstrated in the presented research, KZ-001 is a potent MEK inhibitor, with superior inhibitory efficacy compared to binimetinib. Future studies could determine whether

---

combining KZ-001 with a BRAF inhibitor and an anti-EGFR antibody or EGFR inhibitor can overcome the low response rate and drug resistance and produce a superior outcome. This study can be conducted *in vitro* first and then validated in preclinical xenograft models.

### **8.2.3 Combination of KZ-001 with anti-PD-1 or anti-PD-L1 to improve tumor immunity**

In the last 5-10 years, immunotherapy, such as anti-CTLA4, anti-PD-1, and anti-PD-L1, has emerged as a promising therapeutic approach in a wide variety of types of malignant tumors since it harnesses the immune system against cancer. However, in many indications, such as lung cancer, bladder cancer, less than 15-25% of cancer patients exhibit clinical responses to check point antibodies when administered as single agents. Small molecule targeted therapy also plays a critical role in cancer treatment. For example, MEK inhibitor has a proven useful in BRAF mutant melanoma. Inhibition of MEK can induce tumor regression but rarely resulting in tumor eradication [9].

Recent study showed that inhibition of MEK could enhance the efficacy of anti-PD-L1 inhibitor by regulating antitumor immunity [10]. Combining immune therapeutic with pathway-targeted agents has attracted increasing interest and emerged as a promising therapeutic approach for cancer. Combining MEK inhibitor with anti-programmed death-ligand 1 (PD-L1) antibody led to synergistic and durable tumor regression [9]. Major histocompatibility (MHC) class I downregulation is the primary mechanism associated with failure in anti-PD-1/PD-L1 blockade therapies for cancer. MEK inhibition significantly enhanced MHC Class I and PD-L1 expression via STAT3 activation. Moreover, MEK inhibition further upregulated the increase in CXCL9 and CXCL10 expression, which is associated with T cell infiltration in tumor tissues [10]. A study conducted by Ebert et al. demonstrated that combining the MEK inhibitor G-38963 and anti-PD-L1 significantly suppressed tumor growth, including some complete tumor regressions in mice [9]. These researches provided a rational basis for the combination study. KZ-001 which has superior property in both potency and PK could probably expect a better treatment outcome. Future research can focus on the combination study with KZ-001 and anti-PD-L1 or anti-PD-1. The synergistical inhibition potential on tumor growth and eradication capacity could be investigated *in vivo*.

---

#### **8.2.4 KZ-001 for the inhibition of reperfusion injury**

Restoration of blood flow after ischemia produces free radicals such as reactive oxygen species which have been shown to contribute to oxidative injury to brain [11].

It is important to inhibit reperfusion injury caused by restoration of cerebral blood flow. Ischemia-reperfusion injury is a critical medical condition and it is a therapeutic challenge for physicians. It was reported that oxidative stress activates mitogen-activated protein kinases (MAPKs) and contributes to brain reperfusion injury. Inhibition of the MAPK pathway could be a potential therapeutic approach to inhibit reperfusion injury after brain ischemia. Namuru et al. demonstrated that intravenous administration of the MEK inhibitor U0126 protected the brain from forebrain ischemia [11].

In this study, KZ-001 was demonstrated to be a potent and selective MEK inhibitor, and HL-008 has potential capability to decrease the ROS level. Hence, whether MEK inhibitor KZ-001 can mitigate reperfusion injury could be investigated *in vivo*. Moreover, whether combining KZ-001 with HL-008 could exhibit synergistic effects for brain reperfusion injury caused by restoration of cerebral blood flow can be further investigated.

#### **8.2.5 Apoptosis-related and neuroinflammation-related mechanism study of HL-008**

A $\beta$  has been shown to induce ROS production in PC-12 cells and animal models [12]. Excessive ROS production could lead to neuronal apoptosis in neurodegenerative disorders, such as A $\beta$ -induced neuronal apoptosis [13]. HL-008 is ROS scavenger based on previous study. It is still unknown that whether HL-008 can prevent neurodegenerative disease caused by oxidative stress via anti-apoptotic pathway. In the future study, the expression level of apoptosis-related gene, such as caspase 3, caspase 8, caspase 9, Bcl2, Bax could be evaluated by qRT-PCR and then the related protein expression level can be further detected by western blot.

Aggregated A $\beta$  interacts with neuronal and glial cells, causing the activation of inflammatory responses, production of oxidative stress, hyperphosphorylation of tau protein, and neuronal

---

apoptosis. Oxidative stress-damaged cells produce larger amounts of inflammatory mediators to promote microglia ageing [30]. In the future study, the gene expression level of Akt, JNK, tau, NF-KB could be investigated using qRT-PCR, and TNF- $\alpha$ , IL1 $\beta$  level could be analyzed using ELISA.

#### **8.2.6 Combination of KZ-001 with XH-105 to enhance tumor cell radiosensitivity**

Enhancing radiation damage to tumor tissue while reducing adverse effects on healthy tissue is challenging. Till now, no radiosensitizers that can be administered in combination with neo-chemoradiotherapy are approved for use in the clinic [14]. Chung demonstrated that the MEK inhibitor AZD6244 can enhance tumor cell radiosensitivity *in vitro* and *in vivo* [15]. The research presented here demonstrated that XH-005 could protect the small intestine against radiation-induced injury. It has also been reported that ROS also dynamically influence tumor microenvironments and initiate tumor angiogenesis, metastasis, and survival at varied concentration [16]. Therefore, radiosensitization capacity of KZ-001 *in vitro* and *in vivo* can be further investigated, whilst using XH-105 in combination to mitigate the side effect of radiotherapy.

---

### 8.3 References

1. Misale, S.; Yaeger, R.; Hobor, S.; Scala, E.; Janakiraman, M.; Liska, D.; Valtorta, E.; Schiavo, R.; Buscarino, M.; Siravegna, G.; Bencardino, K.; Cercek, A.; Chen, C. T.; Veronese, S.; Zanon, C.; Sartore-Bianchi, A.; Gambacorta, M.; Gallicchio, M.; Vakiani, E.; Boscaro, V.; Medico, E.; Weiser, M.; Siena, S.; Di Nicolantonio, F.; Solit, D.; Bardelli, A., Emergence of KRAS mutations and acquired resistance to anti-EGFR therapy in colorectal cancer. *Nature* 2012, 486, (7404), 532-6.
2. Pek, M.; Yatim, S.; Chen, Y.; Li, J.; Gong, M.; Jiang, X.; Zhang, F.; Zheng, J.; Wu, X.; Yu, Q., Oncogenic KRAS-associated gene signature defines co-targeting of CDK4/6 and MEK as a viable therapeutic strategy in colorectal cancer. *Oncogene* 2017, 36, (35), 4975-4986.
3. Ding, L.; Cao, J.; Lin, W.; Chen, H.; Xiong, X.; Ao, H.; Yu, M.; Lin, J.; Cui, Q., The roles of cyclin-dependent kinases in cell-cycle progression and therapeutic strategies in human breast cancer. *Int J Mol Sci* 2020, 21, (6).
4. Lee, M. S.; Helms, T. L.; Feng, N.; Gay, J.; Chang, Q. E.; Tian, F.; Wu, J. Y.; Toniatti, C.; Heffernan, T. P.; Powis, G.; Kwong, L. N.; Kopetz, S., Efficacy of the combination of MEK and CDK4/6 inhibitors in vitro and in vivo in KRAS mutant colorectal cancer models. *Oncotarget* 2016, 7, (26), 39595-39608.
5. Araghi, M.; Soerjomataram, I.; Jenkins, M.; Brierley, J.; Morris, E.; Bray, F.; Arnold, M., Global trends in colorectal cancer mortality: projections to the year 2035. *Int J Cancer* 2019, 144, (12), 2992-3000.
6. Corcoran, R. B.; Andre, T.; Atreya, C. E.; Schellens, J. H. M.; Yoshino, T.; Bendell, J. C.; Hollebecque, A.; McRee, A. J.; Siena, S.; Middleton, G.; Muro, K.; Gordon, M. S.; Tabernero, J.; Yaeger, R.; O'Dwyer, P. J.; Humblet, Y.; De Vos, F.; Jung, A. S.; Brase, J. C.; Jaeger, S.; Bettinger, S.; Mookerjee, B.; Rangwala, F.; Van Cutsem, E., Combined BRAF, EGFR, and MEK inhibition in patients with BRAF(V600E)-mutant colorectal cancer. *Cancer Discov* 2018, 8, (4), 428-443.
7. Kopetz, S.; Grothey, A.; Yaeger, R.; Van Cutsem, E.; Desai, J.; Yoshino, T.; Wasan, H.; Ciardiello, F.; Loupakis, F.; Hong, Y. S.; Steeghs, N.; Guren, T. K.; Arkenau, H. T.;

- 
- Garcia-Alfonso, P.; Pfeiffer, P.; Orlov, S.; Lonardi, S.; Elez, E.; Kim, T. W.; Schellens, J. H. M.; Guo, C.; Krishnan, A.; Dekervel, J.; Morris, V.; Calvo Ferrandiz, A.; Tarpgaard, L. S.; Braun, M.; Gollerkeri, A.; Keir, C.; Maharry, K.; Pickard, M.; Christy-Bittel, J.; Anderson, L.; Sandor, V.; Taberner, J., Encorafenib, Binimetinib, and Cetuximab in BRAF V600E-mutated colorectal cancer. *N Engl J Med* 2019, 381, (17), 1632-1643.
8. Pfeiffer, P.; Kohne, C. H.; Qvortrup, C., The changing face of treatment for metastatic colorectal cancer. *Expert Rev Anticancer Ther* 2019, 19, (1), 61-70.
  9. Ebert, P. J. R.; Cheung, J.; Yang, Y.; McNamara, E.; Hong, R.; Moskalenko, M.; Gould, S. E.; Maecker, H.; Irving, B. A.; Kim, J. M.; Belvin, M.; Mellman, I., MAP kinase inhibition promotes T cell and anti-tumor activity in combination with PD-L1 checkpoint blockade. *Immunity* 2016, 44, (3), 609-621.
  10. Kang, S. H.; Keam, B.; Ahn, Y. O.; Park, H. R.; Kim, M.; Kim, T. M.; Kim, D. W.; Heo, D. S., Inhibition of MEK with trametinib enhances the efficacy of anti-PD-L1 inhibitor by regulating anti-tumor immunity in head and neck squamous cell carcinoma. *Oncoimmunology* 2019, 8, (1), e1515057.
  11. Namura, S.; Iihara, K.; Takami, S.; Nagata, I.; Kikuchi, H.; Matsushita, K.; Moskowitz, M. A.; Bonventre, J. V.; Alessandrini, A., Intravenous administration of MEK inhibitor U0126 affords brain protection against forebrain ischemia and focal cerebral ischemia. *Proc Natl Acad Sci U S A* 2001, 98, (20), 11569-74.
  12. Li, G.; Ma, R.; Huang, C.; Tang, Q.; Fu, Q.; Liu, H.; Hu, B.; Xiang, J., Protective effect of erythropoietin on beta-amyloid-induced PC12 cell death through antioxidant mechanisms. *Neurosci Lett* 2008, 442, (2), 143-7.
  13. Peng, Y.; Xing, C.; Xu, S.; Lemere, C. A.; Chen, G.; Liu, B.; Wang, L.; Feng, Y.; Wang, X., L-3-n-butylphthalide improves cognitive impairment induced by intracerebroventricular infusion of amyloid-beta peptide in rats. *Eur J Pharmacol* 2009, 621, (1-3), 38-45.
  14. Buckley, A. M.; Lynam-Lennon, N.; O'Neill, H.; O'Sullivan, J., Targeting hallmarks of cancer to enhance radiosensitivity in gastrointestinal cancers. *Nat Rev Gastroenterol Hepatol* 2020, 17, (5), 298-313.
  15. Pan, J.; He, H.; Su, Y.; Zheng, G.; Wu, J.; Liu, S.; Rao, P., In vivo radioprotective

- 
- activity of cell-permeable bifunctional antioxidant enzyme GST-TAT-SOD against whole-body ionizing irradiation in mice. *Oxid Med Cell Longev* 2017, 2017, 2689051.
16. Aggarwal, V.; Tuli, H. S.; Varol, A.; Thakral, F.; Yerer, M. B.; Sak, K.; Varol, M.; Jain, A.; Khan, M. A.; Sethi, G., Role of reactive oxygen species in cancer progression: Molecular mechanisms and recent advancements. *Biomolecules* 2019, 9, (11).

---

## APPENDICES

The first pages of the published articles and supplementary information.